School of Engineering and Science

Numerical and Experimental Study of Hydrodynamics in a Compartmented Fluidized Bed Oil Palm Shell Biomass Gasifier

Wee Siaw Khur

This thesis is presented for the Degree of
Doctor of Philosophy
of
Curtin University

December 2011

DECLARATION

To the best of my knowledge and belief this thesis contains no material previously published by any other person except where due acknowledgement has been made.

This thesis contains no material which has been accepted for the award of any other degree or diploma in any university.

Signature:…….

Date:……...

To my beloved family

ABSTRACT

Numerical and experimental studies of hydrodynamic parameters of fluidized beds formed by either a single component system or a binary mixture in a pilot plant scale model of a Compartmented Fluidized Bed Gasifier (CFBG) have been performed. The numerical study is carried out with an Eulerian-Eulerian description of both gas and particle phases and a standard drag law for multiphase interaction. The numerically simulated results are then compared with the experimental results.

The 2D and 3D flow patterns of the combustor and the gasifier are first generated from the numerical study to observe the bubble formation, possible channeling behavior and the binary mixing patterns in the bed.

For a single component system, detailed 3D numerical analyses and experimental studies are done to investigate the bed expansion ratio, bubble diameter, bed pressure drop, and fluidization quality in CFBG. Two types of Geldart B inert particles namely river sand and alumina are used in the study.
All trends of the aforementioned studies are well-predicted with the numerical values not greater than 15% of the recorded experimental values. Good fluidization is attainable in the combustor side, while the pressure drop behaviour seen for the gasifier with river sand shows that channelling occurs in the bed. The channelling behaviour becomes more severe with alumina bed.

The solid circulation rate (SCR) is numerically simulated in this study as well. Solid circulation rate (SCR) increases with the increase in bed height while the main bed aeration does not affect the SCR which is consistent with the experimental data.

For a binary mixture system with palm shell and river sand as the second fluidizing material, detailed 3D numerical analysis of the bed expansion ratio is done in parallel with the experimental study. The results of numerical predictions of overall mixing quality and local mixing index are verified by comparing with the experimental results. The actual trends of the studies are modestly captured by the numerical model with under-predicted values of less than 20%. The overall binary mixing quality is enhanced with the smaller palm shell size and larger palm shell weight percent. In addition, increasing the superficial gas velocity increases the local binary mixing index in the experiment.

From the studies on bed expansion, bubble formation, steady equilibrium state and overall binary mixing quality, the 2D model provides well over-predicted values compared to the 3D flow model. Also, the local mixing index of the binary system is not captured by the 2D model. The numerical values predicted by 3D model are closer to the actual values.

The key findings from the aforementioned studies are used as a guide to develop and operate the pilot plant scale CFBG with 0.5 ton/day of palm shell feed for fuel gas production.

ACKNOWLEDGEMENTS

This research program has benefited from the input of many people without which this project could never have been as successful. I gratefully acknowledge the support, assistance and advice and extend my thanks to the following people who helped make this project both successful and enjoyable.

Firstly, I would like to show my sincere gratitude to God for sustaining me throughout this PhD study. Thank God for His inspirations and great help in various ways during the research study and thesis writing, as well as the abundant blessings from Him.

I gratefully acknowledge the financial and other support received for this research project from Curtin Sarawak Malaysia (CSM), Ministry of Science, Technology and Innovative Malaysia (MOSTI) and Malaysian Palm Oil Board (MPOB).

I would like to express my deep gratitude to my supervisor, Professor Dr. Alexander Gorin, for providing me the opportunity for this research and for his continuous unfailing advice, guidance, support, patience, seemingly never-ending positive encouragement and constructive ideas, inspiration as well as devotion in supervision during the course of this research.

I am deeply grateful to my co-supervisor, Associate Professor Dr. Hanbing Chua who has given me further invaluable technical and other advice, administrative assistance, guidance, inspiration, and invariable help. Also I would like to extend my gratitude to another co-supervisor, Associate Professor Dr. Hongming Yan, who has been very dedicated in supervision even though he is overseas and who has further shed light to me on important research skills and attitudes throughout this research, leading me to the accomplishment of this study.

I would like to thank my research partner, Mr. Vuisoon Chok, without him, the project would not have completed with the construction of pilot plant. Great thanks for his highly dedicated spirit on the project, motivation, encouragement, advice and guidance.

I also would like to thank Dr. Fangzi Chen, from CAD Singapore for his useful information on CFD geometry creation and simulation, his never failing virtual assistance, ideas and professionalism on CFD. Also, my gratitude is extended to those undergraduate students who have assisted in experiments and CFD simulations.

I am most indebted to my parents, their strong unfailing support in many ways, encouragement, understanding and immeasurable love during my 4 years of PhD study.

Last but not least, I would like to express my special thank to my husband, Kongheng Liau, who always knew I could do it. He always believed in me, especially when I had lost my faith. His patience, strength, support, assistance and thoughtfulness carried me through. I could not have done this without him.

LIST OF PUBLICATIONS

Journal

1. **Wee, S.K.**, Chok, V.S., Srinivasakannan, C., Chua, H.B. & Yan, H.M. 2008. "Fluidization Quality Study in Compartmented Fluidized Bed Gasifier (CFBG)." *Journal of Energy and Fuels* 22: 61-66.
2. **Wee, S. K.**, Chok, V.S., Gorin, A., Chua, H.B. & Yan, H.M. 2009. "The Effect of Effective Diameter on Fluidization Quality in Compartmented Fluidized Bed Gasifier." *Pertanika Journal of Science & Technology* 17 (2): 343-350.
3. **Wee, S.K.**, Gorin, A., Chua, H.B. & Yan, H.M. 2011. "Hydrodynamic Modeling of Single Particle and Binary Component System in Compartmented Fluidized Bed Gasifier." *American J Appl. Sciences* 7(6). (In press)

International Conference

1. **Wee, S. K.**, Lim, S.S., Chok, V.S., Srinivasakannan, C., Chua, H.B. & Yan, H.M. 2006."CFD Modelling on Hydrodynamics of Compartmented Fluidized Bed Gasifier (CFBG) Riser using Steam." *4th Technical Postgraduate Symposium*, Malaysia, 16-17 May.
2. **Wee, S.K.**, Chok, V.S., Srinivasakannan, C., Chua, H.B. & Yan, H.M. 2007, "The Study of Fluidization Quality in Compartmented Fluidized Bed Gasifier (CFBG)." *Heat-SET 2007*, France, 18-20 Apr.
3. **Wee, S.K.**, Chok, V.S., Srinivasakannan, C., Chua, H.B. & Yan, H.M. 2007. "Fluidization Quality Study in Compartmented Fluidized Bed Gasifier (CFBG)." *Bioenergy Outlook 2007*, Singapore, 26-27 April.
4. Chok, V. S., **Wee, S. K.**, Srinivasakannan, C., Chua, H. B. & Yan, H. M. 2007. "Fluidized Bed Biomass Gasification Technology: Review." *Proceeding in BIOENERGY Outlook 2007*, Singapore.

5. Chok, V. S., Chin, L. F. B., **Wee, S. K.**, Tang, W. W. & Gorin, A. 2007. "Hydrodynamics studies of sand/palm shells binary mixtures in Compartmented Fluidized Bed Gasifier (CFBG)." *Proceeding of the 1st Engineering Conference on Energy and Environment, UNIMAS,* Kuching, Malaysia, 301-306.
6. **Wee, S.K.**, Chok, V.S., Gorin, A. Chua, H.B. & Yan, H.M. 2008. "Experimental and Computational Study of Compartmented Fluidized Bed Gasifier (CFBG)." *HiTACG 2008*, Thailand, January.
7. Chok, V. S., **Wee, S. K.**, Mohd Ariffin, M. Z., Gorin, A., Chua, H. B. & Yan, H. M. 2008. "Optimization of Solid Circulation Rate in Compartmented Fluidized Bed Gasifier for Power Generation." *International Conference on Power Control and Optimization: Innovation in Power Control for Optimal Industry. AIP Conference Proceedings*, 1052, 301-304, Chiang Mai, Thailand.
8. Gorin, A., Chok, V. S., **Wee, S. K.**, Chua, H. B. & Yan, H. M. 2008. "Hydrodynamics of binary mixture fluidization in a compartmented fluidized bed." *18th International Congress of Chemical and Process Engineering: CHISA 2008*, Prague, Czech Republic.
9. **Wee, S.K.**, Chang, H.W., Gorin, A. Chua, H.B. & Yan, H.M. 2008. "Computational Modeling of Compartmented Fluidized Bed Gasifier (CFBG)." *ENCON 2008*, Malaysia, December.
10. **Wee, S.K.**, Gorin, A. Chua, H.B. & Yan, H.M. 2009. "Hydrodynamics Modeling of Single Component and Binary Mixture Compartmented Fluidized Bed Gasifier (CFBG)." *CUTSE 2009*, Malaysia, 24 – 26th November.
11. Chok, V. S., **Wee, S. K.**, M. Z., Gorin, A. & Chua, H. B. (2009). Effect of Particle and Bed Diameter on Characteristic Velocities in Compartmented Fluidized Bed Gasifier, *2nd CUTSE International Conference: Progress in Science & Engineering for Sustainable Development*, Miri, Malaysia.

TABLE OF CONTENTS

NOMENCLATURES

Symbols

A	Constant in Syamlal O'Brien drag model	-
A	Area	m^2
a	Weighting coefficient	-
B	Constant in Syamlal O'Brien drag model	-
C	Coefficient of friction	
C_d	Drag Coefficient	-
D, d	Diameter	m
e	Coefficient of restitution	-
Fr	Constant in Johnson et al. friction model	N/m^2
f	Drag function	-
F	Force vector	N
g	Gravitational acceleration	m/s^2
g_o	Radial distribution function	-
H	Height	m
h	Height of the bubble above the distributor	m
I	Unit tensor, identity matrix	-
I_{2D}	Second invariant of the deviatoric stress tensor	s^{-2}
J	Granular energy transfer, mass flux	kg/ms^3
k	Granular energy diffusion coefficient	kg/ms
K, k	constant	-
K	Solid-solid transfer coefficient	-
m	Mass, local mixing index	kg
n	Constant in Johnson et al. friction model	-
n	Number of sampling point	-
p	Constant in Johnson et al. friction model	-
P	Pressure	Pa
p^*	Pressure field	Pa

q	Diffusion of fluctuating energy	kg/s^3
Q	Flowrate	m^3/s
Q	Fluidization quality	-
R	Distributor pressure drop to the bed pressure drop ratio	-
Re	Reynold number	-
S	Scalar Transport	-
t	Time	s
U, u, v	Velocity	m/s
V	Volume	m^3
X	Mixture composition	-
X	Palm shell loaded in weight percent	wt%
x	Local palm shell mass concentration	kg
β	Phase change coefficient	-
γ	Collision dissipation	kg/ms
ε , α	Volume fraction	-
Θ	Granular temperature	m^2/s^2
μ	Viscosity	kg/ms
ξ	Bulk viscosity	kg/ms
ρ	Density	kg/m^3
τ	Stress tensor	Pa
ϕ	Angle of internal friction	-
ψ	Flow variable	m^3/s

Subscripts

b	bed
b	bubble
c	critical
col	Collisional
c_o, c_1	Cell
e	Effective
d	Distributor
f	Frictional
f	Face f
fr	friction
g	Gas phase
g	shear
int	Initial
kin	kinetic
KTGF	Kinetic Theory of Granular Flow
m	0 for gas phase, 1 for solid phase
max	Maximum
mf	Minimum fluidization
min	Minimum
o	initial
op	operating
p	particle
ps	Palm shell
r	riser
s	Solid phase
sl	Slip
t	terminal
t	total
rp	Phase r and phase p
v	v-valve

Abbreviation

2D	Two-dimensional
3D	Three-dimensional
CFB	Circulating Fluidized Bed
CFBG	Compartmented Fluidized Bed Gasifier
CFD	Computational Fluid Dynamic
CSM	Curtin Sarawak Malaysia
CVM	Constant Viscosity Model
DEM	Discrete Element Method
DPM	Discrete Particle Method
FCC	Fluid Catalytic Cracking
FVM	Finite Volumes Method
ICFB	Internally Circulating Fluidized Bed
MOSTI	Ministry of Science, Technology and Innovative Malaysia
MPOB	Malaysian Palm Oil Board
PDE	Partial Differential Equations
SCR	Solid Circulation Rate
TFM	Two-fluid model

LIST OF FIGURES

LIST OF TABLES

CHAPTER 1 INTRODUCTION

1.1 FLUIDIZED BED

Gas-solid fluidized beds are widely used in the petroleum, chemical, pharmaceutical, metallurgical and energy industries. A bed of particles is said to be fluidized when the drag exerted on the particles by up flowing gas balances the weight of the particles when correcting for buoyancy. The superficial gas velocity at which this occurs is called the minimum fluidization velocity. When the particles are fluidized, the mixture of particles and gas in many ways behave like a fluid, hence the term fluidization.

Biomass is a renewable energy resource derived from the carbonaceous waste of various human and natural activities, including by products from the timber industry, agricultural crops, major parts of household waste and wood. It is also an important source of energy and the most important fuel worldwide after coal, oil and natural gas. In order to convert biomass into fuel, fluidized bed biomass gasification is one of the convincing technologies. In current work, palm shell is selected as feedstock due to its indigenously abundance in Malaysia.

Nowadays, the process industries require governed circulation of solids persistently between two or more fluidized beds where the solids play the role as reactants. Separate reactors with external transfer lines have been used conventionally for this purposes; this type of set up induces high equipment cost and increase mechanical complexity. Until recently, attention has been put to pursue interconnected dual reactors (single compartmented vessel) for gasification where it is compact and incurs low equipment cost. This concept is adopted in present study, namely the Compartmented Fluidized Bed Gasifer (CFBG).

The hydrodynamic behavior of single component system and binary mixture system gas-solid fluidized bed is a complex subject and one of the most important areas for basic understanding of ambient-mode fluidization. Fluidization is affected prevalently by bed pressure drop, bubble properties, and different sizes and densities of solids mixing. Mixing/segregation behavior of binary mixture system is of practical importance because particle distributions influence bed expansion, mass and heat transfer as well as the chemical reaction in the fluidized beds. To date, limited studies were done to study the ambient-mode hydrodynamic characteristic in CFBG. In present work, pilot plant scale experimental work and numerical modeling is performed for this purpose.

1.2 NUMERICAL MODELING OF FLUIDIZED BED

A technology known as Computational Fluid Dynamics (CFD) is now providing an alternative to traditional physical modeling for predicting behavior and understanding fluid flows in engineering system. Limitations in the available methods and computational power restricted early CFD models to gas or liquid flows with simple physics in very simple geometries.

For many engineering applications involving the flow of a single fluid, CFD techniques can successfully predict both simple and complex flow phenomena. Application of CFD to multiphase flows (gas-solid, gas-liquid, liquid-solid or gas-liquid-solid) is not as wide spread because of greater complexity and computational requirement. The primary interest of this work is in palm shell, river sand and air mixtures vicinity, hence the major focus shall be on gas-solid multiphase flows.

There are two approaches commonly used in modeling the hydrodynamics of multiphase flows, namely the Eulerian-Lagrangian approach and the Eulerian-Eulerian approach. Until recently most of the reported models use specialized codes and are either constrained to small, simple rectangular or cylindrical geometries, or further restricted to modeling the structure in two dimensions. More and more authors are performing 3D numerical analysis of gas/particle flows, acknowledging that this highly complex type of

flow should be studied in three dimensions in order to capture the characteristics of the flow.

To date, there is no analogous CFD numerical simulation for compartmented type fluidized bed with v-valve and riser as interconnecting parts between two beds. The current study would be the first time ever in literature using CFD to model CFBG. Work reported in this thesis is based on Eulerian-Eulerian model and further discussion on previous researches and details of this technique will be discussed.

1.3 SCOPE OF STUDY

The scope of present study is to carry out the numerical modeling and experimental study on investigating the hydrodynamics of single component (river sand) and binary mixture (palm shell and river sand) system in a cold flow pilot plant scale CFBG.

Numerical results are to be validated with experimental data to evaluate the accuracy and predictability, also to point out the area which needs further improvement and come up with constructive recommendations for improvements.

1.4 THESIS OUTLINE

The thesis has been structured and the claims are explained in its extensive elucidatory level. The research claims are presented as per the following contents and the thesis is schematically shown in the thesis map (Figure 1.1):

Chapter 1 presents the very fundamental views of all the peripheral information to develop a research idea according to the recent status of the field of attention and objectives of the study;

Chapter 2 reviews the existing understandings in the literature on numerical analysis (CFD) in gas-solid multiphase fluidization using the Eulerian-Lagrangian approach and the Eulerian-Eulerian approach as well as the effect of the influencing modeling

parameters on the fluidization behavior, finally leading to the identification of gaps and determination of specific objectives for the current research;

Chapter 3 outlines the multiphase numerical models to be used, giving a brief summary of the constitutive equations;

Chapter 4 provides a summary of solution procedure set for numerical simulation;

Chapter 5 summarizes the experimental study methodology employed to attain the research objectives, along with explanations of the experimental and analytical techniques used in this study;

Chapter 6 presents the numerical visualization in two- and three-dimensions of fluidization hydrodynamics in single component system and binary mixture system in CFBG. Comparisons are made between 2D and 3D and the observed behaviors are discussed as well in the chapter;

Chapter 7 addresses the numerical and experimental studies of hydrodynamics for single component system in CFBG, and comparison of numerical results with results generated from experiment in this study. The variation between the numerical and experimental data is also discussed;

Chapter 8 addresses the numerical and experimental studies of hydrodynamics for binary mixture system in CFBG. It includes the verification of numerical results with results generated from experiment. The variation in numerical results and suggestion to result improvement is also discussed;

Chapter 9 draws conclusion for present study and recommendations in several areas/ aspects for further research in the future.

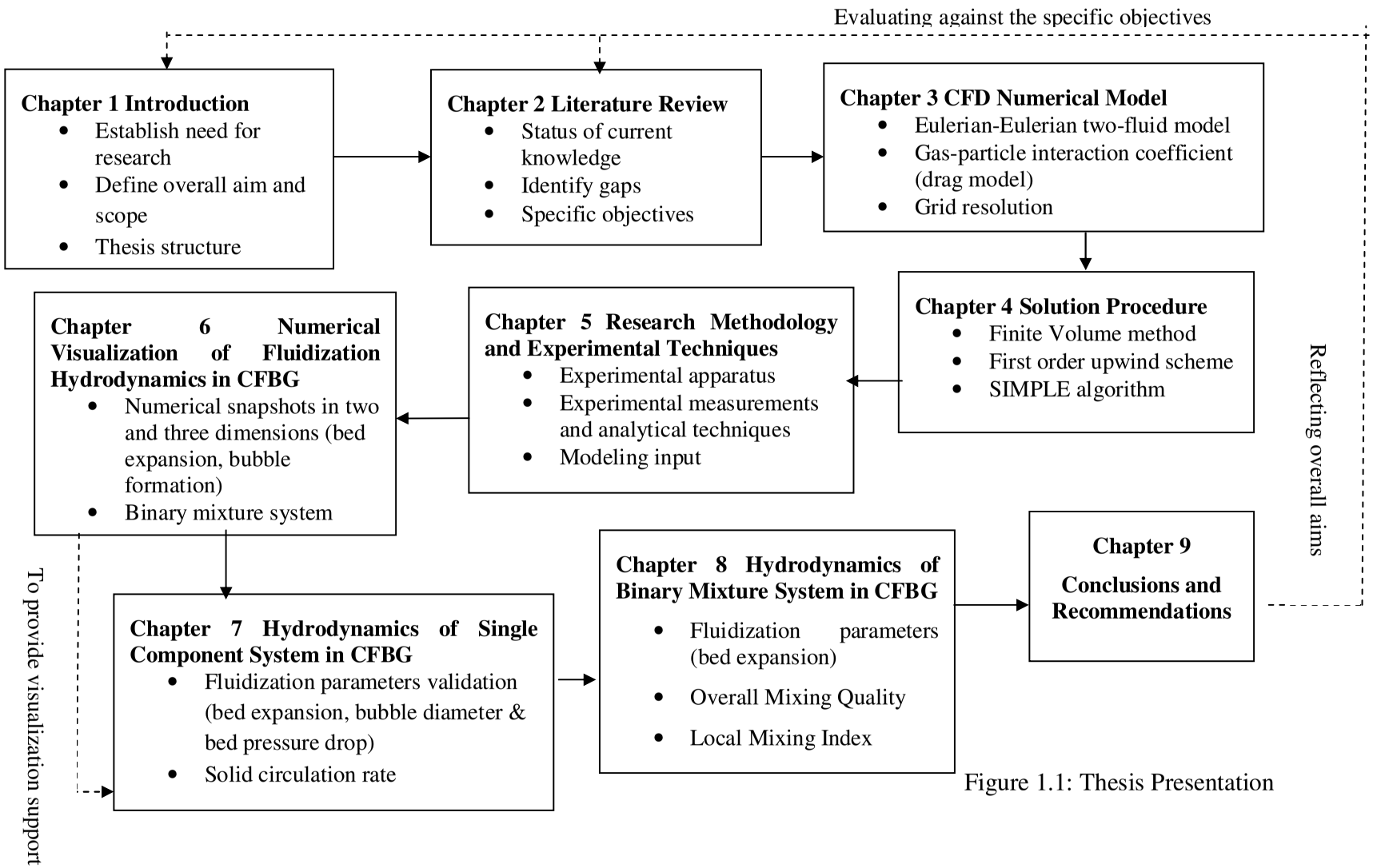

Figure 1.1: Thesis Presentation

CHAPTER 2 LITERATURE REVIEW

2.1 INTRODUCTION

The operating conditions and performance of fluidized bed are strongly tied to the hydrodynamics of the system. Hydrodynamics is governed by a set of nonlinear partial differential equations. In fact, engineers rely on the empirical models, dimensional analysis or on one-dimensional phenomenological model to design as well as to scale the fluidized beds.

The complexities in solution of flow problems are now dealt in personal desktop computers due to the invention of advance microprocessor based high computing technology. Recently computational fluid dynamics (CFD) has turned into an integral part in development of any engineering designs that satisfies all the criteria of constitutive equations by numerical analysis.

The core idea of CFD numerical simulation is based on the capacity of dealing a volume region dividing into a set of interconnected arrayed small cells (control volumes) and the application of continuity equations which govern the fluid flow are solved for each control volume by exchanging required information among the contiguous cells itself. CFD techniques are not only applied to solve the continuity equations but also to perform the process dynamics analysis, to help in reducing the design development time thus saving both the capital cost and establishing the same reliability as real prototyping which are obtained from the effective solutions. It is a very sophisticated tool for single phase modeling; however it still requires data validations for multiphase modeling.

This chapter first covers the two different approaches used in the numerical model, namely the Eulerian-Eulerian approach and the Eulerian-Lagrangian approach. Then the effects of different influencing parameters (mesh resolution, time step size, drag models, coefficient of restitution and convergence criterion) on fluidized bed are discussed. By using the recommended standard drag law, fluidization parameters studies (bed expansion, bubble diameter, bed pressure drop and solid circulation rate) of gas-solid fluidized bed in numerical solution is subsequently reviewed. In addition, the application of CFD to binary mixture system is included in the review. Application of CFD in two-dimensional simulations and three-dimensional simulations are also being discussed in this chapter.

2.2 GAS-SOLID MULTIPHASE SYSTEM APPROACHES

In order to simulate gas-solid fluidized bed system, there are two common types of multiphase models used in the CFD numerical solution, namely the Eulerian-Lagrangian approach and the Eulerian-Eulerian approach. The differences between the two approaches as well as the selection of the model to be used in current study will be discussed in the following section of the chapter.

2.2.1 Eulerian-Lagrangian Approach

Eulerian-Lagrangian is a discrete method, also known as discrete particle method (DPM) or discrete element method (DEM) that is based on molecular dynamics and is extensively employed to analyze the hydrodynamic characteristics of dense particles flow in a multi-phase fluid system. In this approach, the Eulerian framework is used to model the kinematics of the gas phase continuum, the Lagrangian framework is applied to build an explicit kinetic model of disseminated phase particles (trajectories). The forces exerted by the gas on the individual particles as well as the particle interplays are interpreted and solved with the help of Newtonian kinematic euqations.

Overall in a DEM model, the particles are screened individually to sort them in various particle size groups and generate assorted solid phase. Then the groups are treated in the

kinetic modeling of multi-phase systems by reckoning the individual paths of the particle trajectories that is designated as Eulerian-Lagrangian approach.

Particle-particle collisions in this approach can be modeled by either the hard sphere method (Gera et al., 1998; Hoomans et al., 1996) or the soft sphere method (Kobayashi et al., 2000). Hard sphere model approaches to sequential collisions (binary type and quasi-instantaneous) among particles with time and event variant strategy (i.e. collision between particles follows one after another not all at the same time) (Hoomans et al., 1996; Goldschmidt et al., 2004) and is important to define the characteristic equation of motion near the walls to forestall the volume fraction to transcend the limiting value of close-packing condition (Apte et al., 2003). On the other hand, the soft sphere approach (Cundall and Strack, 1979) demonstrates the transfer of energy between particles employing the multi-level particle-particle and particle–wall interactions (Kobayashi et al., 2000). Indeed, the soft-sphere approach (capable of handling extended time period of frictional contact among particle and handle multi-particle for collision) comes into action to resolve the malfunction occurred in hard sphere approach while handling the particle overlapping at a mass stage for numerical calculation and consumes more time period because of its proneness to inaccuracy due to presence of large amount of particle to interact (Goldschmidt et al., 2004).

Gera et al. (1998) compared the Eulerian-Lagrangian and Eulerian-Eulerian approach to study the hydrodynamics of a two-dimensional large-particle (diameter of 4mm) fluidized bed, where bubble rise velocity, voidage variations, averaged particle/particulate and fluid velocities are of prime interest. They concluded that, for simulation of small beds, the computational time required by Eulerian-Lagrangian and Eulerian-Eulerian approaches is comparable, but for simulations of millions of particles, Eulerian-Eulerian would be more feasible to be used (Ref. to section 2.2.2 for details of Eulerian-Eulerian approach) as Lagrangian approach is still limited to maximum of 10^6 number of cells even with the modern computational facilities (Hede).

Chiesa, et al. (2005) analyzed the bubble formation in a two-dimensional lab-scale gas-fluidized bed of particle diameter 1000 μm by employing both the Eulerian-Lagrangian and Eulerian-Eulerian approaches. The results from both approaches provide adequacy in microscopic point of view and the comparison between numerical and experimental analysis shows a sort of similarity. Eulerian-Lagrangian simulations show better accordance with the experimental results; however the CPU time necessary to perform the numerical simulation is four orders of magnitude higher than the time required to perform an Eulerian-Eulerian simulation.

Since the Eulerian-Lagrangian numerical analysis i.e. the discrete particle model (DPM)/ Discrete element model (DEM) is still limited of handling not more than a million of particles for a fluidized bed, the pilot scale or industrial fluidized beds are not possible to be simulated using this model as it consists of several times more particles than the maximum capacity of the model. Therefore, as the required CPU time is linearly proportional with the number of particles to be handled of pilot/industrial scale fluidized beds the DPM is not feasible for large scale hydrodynamic analysis until there is any facilitation of evolution in commercial availability of high performance computing machines (van der Hoef et al., 2004).

Eulerian-Lagrangian approach are powerful investigative tools which allow the direct feasibility studies of the effect of individual particles' physical properties such as its size, shape, and density on the resulting motion of a fluid in a fluidized bed. However, in current study, the detailed study of single particle trajectory (structural analysis) in fluidized bed is not of prime interest, rather the integral analysis is preferred for first hand numerical results on this type of reactor (CFBG). Hence, it is not advisable to use Eulerian-Lagrangian approach as the base model in CFD for the current research study.

2.2.2 Eulerian-Eulerian Model

Both the gas and solid phases are treated as diffusing continua in the Eulerian-Eulerian continuum modeling. These models consider all phases to be continuous and fully interpenetrating. A set of generalized equations from the Navier-Stokes equations are employed in the moving continuum. There are requirements of few closure laws to discern the physics of the fluidized particles in Eulerian models due to the continuum representation of the particulate phases. In order to describe the rheology of particulate phases, many authors used the kinetic theory of granular flow which had well validated with their experimental works to obtain the constitutive equations (Lu et al., 2002; Gelderbloom et al., 2003; Taghipour et al., 2005; Marschall et al., 1999). Therefore, an extension of the classical kinetic theory for dense particles, i.e. the hydrodynamic kinetic theory of granular flow (KTGF) has been integrated in the recent continuum of Eulerian-Eulerian model (a.k.a Two-Fluid Model). This kinetic theory is applied to analyze the effects of restitution coefficient on the hydrodynamics of dense gas-fluidized bed that is effectively dependent on the quantity of dissipated energy because of inelastic particle-particle interplays (Goldschmidt et al., 2001).

Two-fluid models are used in an extensive range of simulation analysis from laboratory scale to commercially large scale fluidized beds and the salient feature of this concept is the ability of predicting the flow behavior of large scale gas solid fluidized bed in reasonable computing time.

Lu et al. (2002) made the comparison for Eulerian-Eulerian simulation of bubble sizes and rise velocities in a two-dimensional laboratory scale bubbling fluidized bed with Geldart group B particles (diameter of 500 μm) using Gidaspow (1994) drag model at an asymmetrical flow condition. They concluded that the predicted values of bubble diameter and bubble rise velocities were in agreement with the empirically calculated data.

Gelderbloom et al. (2003) used the Eulerian-Eulerian approach incorporated with Syamlal O'Brien (1994) drag model to study the several hydrodynamics regimes including the bed expansion, bubbling, sedimentation, and consolidation of the two-dimensional laboratory scale bubbling/ collapsing rectangular fluidized bed for three Geldart groups, such as C, A, and B. Results showed that the two-fluid model was capable of predicting the hydrodynamics of these regimes. The simulated bubble sizes and bed collapse rates for all three Geldart groups were found to be within reported experimental error.

Taghipour et al. (2005) employed the Eulerian-Eulerian model integrating the kinetic theory to simulate the hydrodynamics (bed expansion ratio, solids volume fraction, bed pressure drop, local voidage profiles, and solid velocity) of a two-dimensional gas-solid fluidized bed reactor containing spherical glass beads of diameter 250 μm - 300 μm. The authors concluded the simulated results indicated reasonable agreement for most experimental operating conditions. Moreover, the assumptions of transient and time-average profiles of local void fraction showed similarity with the experimental results.

Marschall et al. (1999) also used the Eulerian-Eulerian approach with Gidaspow (1994) as the drag model to study the hydrodynamics (pressure drop, porosity, and velocity distribution) of a bench-scale internally circulating fluidized bed (ICFB). This type of reactor which consists of riser and annulus is an evolution from the spouted bed with a draft tube. The model was able to explain the effect of various reactor designs e.g. height of the surrounding annulus, length of the entrainment region on the flow fields. This paper was of the few that studied the effect of reactor design using CFD numerical solution. The model allowed the description of the complex pressure distribution between the spout and the annulus and to reproduce the experimentally observed influence of the annular bed height on the gas-bypass around the draft tube. This parameter was difficult to describe with empirical models.

From the reviews, CFD numerical modeling based on the Eulerian-Eulerian model approach has the privilege in employing it for investigating the hydrodynamic behaviors, and studying the effects of design towards the hydrodynamics of the bed. This model approach directly considers the dynamics of collisions and external forces acting on the particles which also balks the capability of handling more number of particles for the large fluidized beds of industrial applications that constitute of about a several degree of magnitude more particles than that of the capacity of the DPM (typically $<10^6$). It was asserted by Goldscmidt et al. (2001) that the feasible option to engineering scaling up of the hydrodynamic modeling could be the continuum models, while on the contrary, the discrete particle model is a good tool to render elaborate information of the basic hydrodynamic characterization which are sometimes difficult to obtain from the experimental observations. Comparisons between the Eulerian-Lagrangian and Eulerian-Eulerian approach are tabulated in Table 2.1.

Since the Eulerian simulations are capable to correctly reproduce the dynamic characteristics of laboratory-scale fluidized beds, the Eulerian CFD simulations could be useful as scale-up tools (van Wachem et al., 2001). Also Eulerian-Eulerian model approach can comfortably analyze the heat transfer phenomena in fluidized bed than that in the Eulerian-Lagrangian model (Wankhede and Adgulkar, 2008; Kuipers et al., 1992; Gustavasson and Almstedt, 2000). Therefore the Eulerian-Eulerian approach is selected as the multiphase base framework used to study the hydrodynamics (bed expansion, bubble diameter, pressure drop, and solid circulation rate) of a single component and binary mixture system in gas-solid Compartmented Fluidized Bed Gasifier (CFBG).

Table 2.1: Summary of the salient features of Eulerian-Lagrangian and Eulerian-Eulerian Model (Gera et al., 1998)

No.	Eulerian-Lagrangian Approach	Eulerian-Eulerian Approach
1	It is possible to account for the individual particles' shape, size, and density.	Different sizes and densities of the particles are treated as the separate phases which would increase the number of conservation equations to solve.
2	Individual particle motion can be traced.	Only averaged particulate motion in a grid cell can be computed.
3	Computational time depends on the calculation of particle motion explicitly, and three sets of equations for fluid motion iteratively.	Computational time depends on the iterative solutions of six sets of simultaneous differential equations. For large number of particles, the CPU time would be very small than the CPU time required for Eulerian-Lagrangian.
4	Considers multiple collisions of particles, based on the soft sphere approach	No such considerations.
5	It is possible to allow the particles to fall under the gravity to simulate fixed bed condition. Voidage at minimum fluidization is calculated from the number of individual particle in a grid cell.	Voidage and gas phase volume fraction needs to be specified as an initial condition. Particle-particle interaction, which is empirically modeled through the solid elasticity, is a very strong function of gas phase volume fraction.
6	Visualization of the individual particle mixing is possible.	Mixing characterized by integrating the averaged particulate phase velocity to obtain the estimated position of the particles is possible.
7	Minimum grid size for is 1 x 1 cm. Smaller grid size affects the accuracy of computations.	The convergent solution is obtained with the grid height and width of at least five particles diameter.

2.3 EFFECTS OF MODELING PARAMETERS

The two modeling parameters that are considered here is the gas-solid drag models and the coefficient of restitution. A lot of studies have been done to investigate the effects of these parameters. There are the main parameters which characterize the fluidization behaviors.

In the two-fluid model, the two phases are coupled through the interphase momentum transfer, hence it is one of the most important and dominant forces in fluidized bed modeling. The drag laws to model inter phase momentum exchange are usually developed empirically. Therefore their applicability and validity to model fluidized beds with specific particle size and flow conditions need to be evaluated.

In addition, collision of particles plays a major role in the dissipative energy of particles. The restitution coefficient describes the variation in kinetic energy of particles due to inter-particle collisions. Higher values of restitution coefficient describe higher elasticity of collisions, which results in lower dissipation rates. Higher coefficients of restitution are often used for gas-solid fluidized beds.

2.3.1 Drag Models

Different types of drag law may lead to qualitative differences in fluidization dynamics (Loboreiro et al., 2008). There are a few standard drag models which are readily available in the commercial CFD software including the Syamlal O'Brien (1994), Gidaspow (1994), and Wen and Yu (1966).

The Syamlal O'Brien (1994) drag model was derived for a single spherical particle in a fluid. The main idea about this model is the assumption that the Archimedes number is the same in a single particle and a multiparticle system. The Archimedes number relates the gravitational forces to the viscous forces. The Gidaspow (1994) drag model is a combination of the Wen and Yu (1966) drag model and the Ergun (1952) equation. The Wen and Yu (1966) drag model uses a correlation from the experimental data of

Richardson and Zaki (1954). This correlation is valid when the internal forces are negligible which means that the viscous forces dominate the flow behaviour. The Ergun (1952) equation is derived for a dense bed and relates the drag to the pressure drop through porous media. These models are tested to evaluate the effect of interphase momentum exchange coefficient between gas and solid phases.

Comparison of the model predictions, suing the aforementioned three standard drag models and experimental measurements on the time-average bed pressure drop, bed expansion and qualitative gas-solid flow pattern were done by Taghipour et al. (2005) in a two-dimensional fluidized bed. The results indicated reasonable agreement for most operating conditions. Instantaneous and time-average local voidage profiles showed similarities between the model prediction and experimental results.

van Wachem et al. (1998) performed numerical simulations using the Eulerian-Eulerian framework in a two-dimensional fluidized bed of Geldart B particles. The effects of three drag models, namely the Wen and Yu (1966), Gidaspow (1994) and Syamlal and O'Brien (1994) were compared in terms of bed expansion, bubble diameter, and bubble rise velocity. The Syamlal O'brien (1994) drag predicted lower pressure drop and bed expansion than the other two drag models and thus also underpredicted the gas holdup in the fluidized bed. Overall, all the investigated drag models were in fairly good qualitative agreement with the experimental data and empirical correlation.

The study of bubble behaviour (bubble aspect ratio, bubble diameter and bubble rise velocity) in two-dimensional gas-solid fluidized beds of Geldart B particles with and without immersed horizontal tubes was investigated by Asegehegn et al. (2011) using two-fluid model as the framework. There was no significant difference in the bubble properties predicted by the three drag models. The bubble aspect ratio and diameter predicted by the three drag models were in very good agreement with the experimental results. The drag model from the Syamlal and O'Brien (1994) predicted slightly lower rise velocity and circular bubbles compared to the other two. Moreover it predicted

lower bed expansion. These results were similar to van Wachem et al. (1998). Because the bubble sizes predicted by the different drag models were all close, while the predicted bed expansion from Syamlal and O'Brien (1994) was lower, it predicted the highest solids volume fraction for the dense phase.

Zhao et al. (2010) investigated the fluidization characteristic of two-dimensional plexiglass laboratory scale fluidized bed of Geldart B particles. The effects of three standard drag models in bed pressure drop and bed density were analysed. Their results showed that by using the Syamlal O'Brien (1994) drag model, the pressure drop was more stable. In terms of bed density analysis, Syamlal O'Brien (1994) predicted the density with small density fluctuations and was in good agreement with the experimental values, while other drag models predicted the results with larger density fluctuations. As such, they concluded that the Syamlal O'Brien (1994) model is more applicable to the hydrodynamics of Geldart B particles bed.

The effects of drag models (Gidaspow (1994), Arastoopour et al., (1990) and Syamlal O'Brien (1994)) in solid volume fraction and particle velocity of high density circulating fluidized bed were studied by Almuttahar and Taghipour (2008). It was found that all drag models examined predicted quite similar results. However, the Syamlal O'Brien (1994) drag model showed a better prediction. Their result was supported by Zimmermann and Taghipour (2005) who reported that the Syamlal O'Brien (1994) drag law is able to provide good description of the hydrodynamics of fluidized bed reactors with FCC particles.

Numerical results for a gas fluidized bed using the two-dimensional Eulerian-Eulerian model including the kinetic theory for the particulate phase (Geldart B and D particles) were presented by Hosseini et al. (2010) They examined the drag models' effect in solid hold-up profile of the laboratory scale fluidized bed with a partial sparger as the distributor. They selected several models such as Syamlal O'Brien (1994), Gidaspow (1994) and Arastoopour et al., (1990) for sensitivity analysis. The results showed that

Arastoopour et al. (1990) model predicted the solid hold-up with highest deviation. Syamlal O'Brien (1994) predicted better results in comparison with the others.

The solids flow dynamics in a circulating fluidized bed riser with Geldart B particles were studied by Vaishali et al. (2007). This type of reactor is a 'short contact time' reactor, in which solids are fluidized at velocities higher than the characteristic 'transport velocity' so that they are entrained out of the bed. They compared the effect of drag models (Wen and Yu (1966), and Syamlal O'brien (1994)) on two fluidization regimes, namely the fast fluidization regime and dilute phase transport regime. The Wen and Yu's (1966) drag law underpredicted the mean solids velocity profile for both regimes. Syamlal O'Brien's (1994) drag model was determined to be acceptable and predictive for fast fluidization regime.

Sanyal and Cesmebasi (1994) compared the effects of drag models in bubble dynamics of a rectangular fluidized bed. They concluded that the three drag laws studied in their work showed quite different bubble behavior. A particular one of them gave the closest resemblance to the experimental observations investigated in their paper. These authors also showed that it was important for each gas-solid flow simulation case to choose a suitable drag model valid for the particular geometry, operating condition, particle size and shape, flow regime, etc. in question.

Previous works had shown the inconsistencies of drag model effects with respect to different studies. Some authors reported that the drag models play very crucial role in multiphase simulations in predicting the bed pressure drop, bed expansion, bubble sizes and bed density while some reported that different drag models predicted no difference in results. From most of the studies shown in this section, Syamlal O'Brien (1994) drag law is ahead of other drag model to show its ability in predicting better resemblance of results when compared to the experimental data. Therefore, it is chosen as the standard drag law in our numerical studies later.

2.3.2 Coefficient of Restitution

The value of restitution coefficient ranges from 0 for perfectly inelastic collisions with complete dissipation of kinetic energy, to unity for elastic collision with no dissipation of kinetic energy.

The effects of different values of restitution coefficients of 0.85, 0.9 and 0.99 on particle velocity and elutriation rate constant were investigated by Azadi (2011) It was found that varying the coefficient of restitution did not change the results significantly.

Wang et al. (2010) conducted a parametric study to investigate the effect of restitution coefficient on the hydrodynamics of industrial scale gas-solid fluidized bed. They found that the value of restitution coefficient had a negligible effect on the bubble characteristic as well as the bed expansion.

Taghipour et al. (2005) confirmed that the two-dimensional hydrodynamic regime and bubble activity were closely linked to restitution coefficient, particularly for gas velocities beyond the minimum fluidization. They reported that by decreasing the restitution coefficient, the bed expansion decreased. At last, they suggested that high values of restitution coefficient (e.g., 0.99) were required to simulate the dynamics of the fluidized bed for gas velocities above the minimum fluidization.

Reuge et al. (2008) used the Eulerian-Eulerian model with Syamlal O'Brien (1994) drag model to simulate the hydrodynamics of two and three-dimensional Geldart B fluidized bed. The effects of restitution coefficient were tested on bed fluctuation frequency and bed expansion ratio. They concluded that the effect of the restitution coefficient was dependent on the fluidization regime: in the bubbling regime, an increase in restitution coefficient led to larger bed expansions and lower height of fluctuations, whereas it led to unchanged or lower bed expansions and to a massive reduction in the height of fluctuations in slugging regime.

A three-dimensional CFD numerical model, using an Eulerian-Eulerian model which incorporates the kinetic theory of granular flow and Gidaspow (1994) as drag function, was developed by Shi et al. (2010) to describe the gas-solid flow in fluidized bed polymerization reactors. They reported that their pressure drop studies were not sensitive to the changes of the restitution coefficient. Thus they suggested that a value of 0.9 is sufficient to simulate their reactor.

Modeling of the hydrodynamic behaviors of two-dimensional high-flux circulating fluidized beds with Geldart group B particles had been performed by Jin et al. (2010) using an Eulerian multiphase model with the kinetic theory of granular flow and Syamlal O'Brien (1994) drag law. The effects of restitution coefficient on solid volume fraction, particle velocity and gas velocity with respect to the particle diameter were analysed. Their results showed that the value of restitution coefficient had remarkable dependence on the particle diameter. Larger particles result in a more sensitive effect of restitution coefficient on flow characteristic. As a result of the analysis, they used restitution coefficient of 0.99 for their subsequent studies.

A three-dimensional two-fluid modeling approach with the kinetic theory of granular flow was used by Wang et al. (2010) to simulate the hydrodynamic behaviors of a laboratory scale bubbling fluidized bed and a circulating fluidized bed of Geldart B particles. The effects of restitution coefficient were tested on the solid circulation pattern with respect to gas flowrate. They concluded that different values of restitution coefficient were required for each gas flowrates to reproduce the measured flow patterns. Lower gas flowrates required smallest value while higher gas flowrate required larger value.

Jenkins and Savage (1983) utilized the coefficient of restitution (scaling between 1 and 0, for fully elastic collisions and for fully inelastic collisions, respectively) to calculate the loss of energy due to the collision of particles, which was not conceived in the classical kinetic theory. The energy dissipated as a result of collisions of granular

inelastic particles had been used by Lun et al. (1984) to obtain the ratio of the velocity fluctuations to the mean flow as a function of the coefficient of restitution. The proportional relationship of coefficient of restitution (restoration) and elastic collisions begot more unsteady kinetic energy when the value of coefficient of restitution decreases (Goldschmidt et al., 2004).

Goldschmidt et al. (2004) demonstrated that the hydrodynamics of dense fluidized beds strongly depends on the values used for the coefficient restitution. They pointed out that it is of outmost importance to correctly account for the effect of the non-ideal particle-particle encountered and to accurately determine the particle collision characteristic parameters.

The aforementioned reviews have shown that higher value of restitution coefficient is preferable in gas-solid fluidized bed simulations. Therefore a value of 0.9 will be used in the numerical studies later.

2.4 EFFECTS OF NUMERICAL SOLUTION PARAMETERS

Although CFD models have a promising future and are anticipated to make valuable contributions to predicting the performance of fluidized bed reactors, however currently there are no systematic guidelines available to make appropriate selection of solution parameters to simulate gas-solid flow. Therefore, the sensitivity of the hydrodynamics of fluidized bed was tested against the effects of several numerical solution parameters, such as mesh resolution, time step size, and convergence criterion by several authors (to be discussed as follow) to determine the best configuration of the CFD numerical model.

2.4.1 Mesh Resolution

Grid resolution is very important in a numerical simulation. A finer mesh commonly gives better calculation results, however induces higher computational time. Therefore to choose an appropriate mesh size is relatively crucial for reasonably accurate results. The currently available Eulerian-Eulerian model is usually closed with constitutive laws

that are based on the assumption of homogeneity at the level of computational cells. This assumption implies that the grid size used in numerical simulations should be sufficiently small so that the meso-scale structures prevailing in the gas-fluidized beds can be captured explicitly, which demands that the grid size should be of the order of 2–4 particle diameters in bubbling fluidized beds (Wang, 2009) or of the order of 10 particle diameters in circulating fluidized beds (Agrawal et al., 2001; Andrews et al., 2005; Benyahia et al., 2007; De Wilde, 2005; Guenther et al., 2002; Igci et al., 2008; Wang, 2008a).

Azadi (2011), in his paper, investigated the grid dependency of the modelling results using Eulerian-Eulerian model with Syamlal O'brien (1994) as the drag law for Geldart A and Geldart B particles bed. They simulated the two-dimensional laboratory scale binary gas-solid fluidized bed in three types of grid, namely coarse grid (50 x 200), medium grid (70 x 300) and fine grid (90 x 400). The results showed that coarse grid predicted lower particle axial velocity. However the medium and fine grids showed no significant change in results. Increasing the grid resolution from medium grid to fine grid did not show important variation in the results quantitatively.

Coroneo et al. (2011) tested the effect of grid resolution on solid volume fraction in a two-dimensional laboratory scale bidisperse mixtures of particle fluidized bed by employing Eulerian-Eulerian framework incorporated with kinetic theory of granular flow. They used three structured computational grids with cells of 5mm x 5mm (coarse), 2.5mm x 2.5mm (medium), and 1.25mm x 1.25mm (fine). They also manifested that the simulation run on the coarser grid was out of the asymptotic range of grid convergence. Passing from coarse grid to medium grid, the accuracy of results was significantly improved by 30%.

The effect of grid size in estimating the minimum bubbling velocity was studied by Wang et al. (2010). They used two-fluid model to simulate the hydrodynamics of industrial scale bubbling fluidized bed of Geldart B and D particles. They found that the

use of coarse grid had resulted in 77% error in comparison with the experimental results. The improvement was done with using finer grid where eventually produced results were in reasonable agreement with the experimental ones.

Almuttahar and Taghipour (2008) utilised the two-dimensional Eulerian-Eulerian model with kinetic theory of granular flow to model the hydrodynamics of a FCC particles high density circulating fluidized bed. They carried out the sensitivity analysis on the effect of meshing resolution with 50 x 200 (coarse), 75 x 308 (medium), and 100 x 400 (fine) grids used. Their results showed the fine mesh case and medium mesh case predicted similar solid volume fraction distributions. This indicated that the medium mesh size is sufficiently fine for providing reasonably mesh independent results.

Follow from that, Hartge et al. (2009) also carried out the sensitivity analysis on the effect of grid resolution. They used three-dimensional Eulerian-Eulerian model to simulate the mechanics of riser in a circulating fluidized bed. The grid size used are 50mm x 30mm x 62.6mm (coarse), 35mm x 22.5mm x 55mm (medium), and 25mm x 15mm x 50mm (fine) grids. Their data indicated that the change in axial solid concentration results between medium and fine grids was much lower compared to that between the coarse and medium grids. The data of the medium and fine grids actually overlaped for most of the data range. Therefore, they used medium grid for their subsequent studies.

In general, the continuous increase in mesh density may lead to slightly better results that are more grid-dependent. However, the computational power currently available is still a significant restriction when using a finer mesh. Based on the previous studies, for two-dimensional and three-dimensional simulations, the reasonable grid size to be used in current study would be medium size grid (of 10 particles size and with gradual increment of 1.8 after riser height) as to reduce the computational time without much compromising in the results accuracy.

2.4.2 Time Step Size

The size of the time step influences two effects: the convergence of the iterations regarding the solution of the differential equations, and the computation time. Therefore it is important to choose an appropriate time step size for reasonably accurate results at cheap computational cost.

Effect of several time steps e.g. 0.001s, 0.0005s and 0.0001s on the simulation results were tested by Azadi (2011). The author concluded that time steps of 0.001s and 0.0005s led to more stable results and convergence was achieved sooner in comparison with the time step size of 0.0001s, for each set of iterations per time steps. Choosing a too small time step size may increase the relative error. Hence, 0.001s was recommended by the author as the base case. This was also supported by other authors (Gera et al., 1998; Hulme et al., 2005; Cornelissen et al., 2007).

Coroneo et al. (2011) carried out the sensitivity studies on the influence of the time step (0.01s, 0.001s and 0.0001s) on simulation results. Their results showed that time step size of 0.001s estimated a better result. This was also supported by Taghipour et al. (2005) and Goldschmidt et al. (2004) for their monodisperse gas-solid bed.

Analysis of bubble dynamics in a two-dimensional fluidized bed was performed by Mazzei and Lettieri (2006) using two-fluid model. The authors concluded that a time step of 0.001s was sufficient to obtain accurate results. Smaller time steps yielded the same results but consuming more computational power, whereas bigger time steps could either make the simulation crash or lead to inaccurate predictions.

Based on previous studies, a time step of 0.001s is a value which leads to convergence in reasonable amount of iterations and also sufficiently accurate. Furthermore, it is observed that the use of very small time step size may also lead to divergence as in the use of very large step sizes.

2.4.3 Convergence criterion

Convergence is a major issue with the use of CFD software. CFD problems in general are non-linear, and the solution techniques use an iterative process to successively improve a solution, until 'convergence' is reached. Convergence describes limiting behaviour, particularly of an infinite sequence or series toward some limit . To assert convergence is to claim the existence of a limit, which may be itself unknown. The exact solution to the iterative problem is unknown, but the solution needs to be sufficiently close to the required level of accuracy. Convergence therefore does need to be associated with a requirement for a particular level of accuracy.

Studies done by Azadi (2011) using 0.001 and 0.0001 had shown that convergence criterion of 0.0001 increased computational costs with taking more iteration per time step, but only minor deviation in results in comparison with predictions achieved by using convergence criterion of 0.001. Therefore, the author concluded that the value of 0.001 was applied in the model as the sufficient relative error between two successive iterations.

As suggested by Azadi (2011), a convergence criterion of 0.001 will be used as to reduce the computer power needed in simulating a pilot-scale size three-dimensional gas-solid fluidized bed.

2.5 STANDARD DRAG MODEL IN EULERIAN-EULERIAN APPROACH FOR 2D HYDRODYNAMIC STUDIES OF SINGLE COMPONENT FLUIDIZED BED

The aid of Computational Fluid Dynamics (CFD) modeling approach has improved intensely the understanding in the complex hydrodynamics behavior of gas-solid fluidization in recent years. However, the models vary in their level of complexity from strictly empirical to those based on the fundamental conservation equations of fluid dynamics available in commercial CFD software may sometimes over/under-estimate the system behavior. Therefore, the modification of certain properties, e.g. gas-solid drag coefficient, solid-solid drag coefficient and etc, in the model is needed dependent

on the objectives of study in order to better represent the hydrodynamics in a fluidized bed. Several authors (Cruz et al., 2006; Cruz et al., 2002; Sinclair and Jackson, 1989; Nieuwland et al., 1996; Wang and Li, 2001; Mathiesen et al., 2000; Krishna and van Baten, 2001; Patureaux and Barthod, 2000; McKeen and Pugsley, 2003) had modified the standard models for more accurate CFD prediction of their system in terms of hydrodynamic parameters such as solids mass fluxes, bubble properties, bed dynamics and etc.

Though there are still upcoming works done in studying the models in CFD or refining the models to provide more precise predictions of the hydrodynamics of multiphase system, however, it is not the scope of work of current study to further fine-tune the model as to minimize the gap of discrepancy in hydrodynamic predictions. In present work, CFD technique is being used for the first time in simulating the hydrodynamics of CFBG type of reactor. Therefore it is required to check the predictability/ performance of CFD in such kind of complex geometry to understand the effect of design operating parameters on fluidization behavior and eventually extended to the desired hot gasification process. Therefore, it has been decided to precede the experimental validation of the conceived CFBG model's hydrodynamic properties by using the Eulerian-Eulerian approach with well-verified commonly used standard Syamlal O'Brien (1994) drag law, which is readily available in the commercial software.

The review below summarizes the application of CFD and its predictability in simulating the hydrodynamics in terms of bed expansion, bubble diameter, bed pressure drop and solid circulation rate of monocomponent gas-solid fluidized bed.

2.5.1 Bed Expansion

Taghipour et al. (2005) employed the Eulerian-Eulerian model integrating the kinetic theory and a restitution coefficient of 0.9 to simulate the hydrodynamics (bed expansion ratio, solids volume fraction, bed pressure drop, local voidage profiles, and solid velocity) of a gas-solid fluidized bed reactor containing spherical glass beads of

diameter 250-300 μm. The authors concluded that the simulated results indicated reasonable agreement for most experimental operating conditions such as bed expansion ratio, gas–solid flow patterns and pressure drops, etc. at superficial gas velocities higher than the minimum fluidization velocity, U_{mf}.

Simulations using Eulerian-Eulerian multiphase model with the Syamlal O'Brien (1994) drag function and a restitution coefficient of 0.9 in a laboratory scale fluidized bed of Geldart B particles were conducted by Hulme et al. (2005). They examined the average fluidized bed height across a bubbling fluidized bed reactor. The experimental bed height was found to be 42cm, while the simulated bed height was closed to 46cm. CFD numerical results showed a deviation of less than 10%. However the authors did not give details on the reasons of the discrepancy.

Olumuyiwa Oweyemi et al. (2005) used the Eulerian-Eulerian approach as framework with modified kinetic theory of granular flow and Syamlal O'Brien (1994) drag law, a restitution coefficient of 0.97 to study the bed height, bubble diameter and bed voidage of small scale rectangular gas-solid fluidized bed of Geldart B particles. For bed expansion analysis, a very minor (2.5% and 11%) variation was seen between the experimental results and computational results. This might be that the actual powder has a wide particle-size distribution while the simulation was performed assuming a system of monosized particles. Grace and Sun (1991) also reported that the particle size distribution could have a major influence on the bed expansion.

Sau and Biswal (2011) employed the Eulerian-Eulerian approach with Gidaspow (1994) drag model and a restitution coefficient of 0.9 to simulate the hydrodynamics of small sized fluidized bed of Geldart D particles. In their bed expansion studies, the CFD simulated results were in reasonably good agreement with experimental ones. It was also observed that the difference between the results were clearly less in the case of non-spherical particles whereas the difference were more in the case of spherical particles at

higher gas velocities. However, CFD was capable to predict the correct trends of bed expansion for both types of particles.

Hamzehei et al. (2010) simulated the hydrodynamics (bed pressure drop, bed expansion, void fraction and solid volume fraction) of a laboratory scale non-reactive cylinder fluidized bed reactor of Geldart B particles using two-fluid model with Syamlal O'Brien (1994) as drag law and a restitution coefficient of 0.9. The model predicted the correct increasing trends of the bed height with increasing superficial gas velocities.

Eulerian-Eulerian model including the kinetic theory of granular flow with Syamlal O'Brien (1994) drag law and a restitution coefficient of 0.8 was used by Hosseini et al. (2010) to simulate the solid hold up distribution and circulation pattern in a small scale fluidized bed of Geldart B and D particles. Their results showed good agreement between the experimental and simulated averaged bed expansions with the simulated values lower than the experimentally measured bed height at the velocities investigated. The possible explanation might be that the actual powder has a wide particle size distribution, while the simulation was performed assuming a system of monosized particles.

2.5.2 Bubble Diameter

Hulme et al. (2005) carried out the CFD simulations in investigating the bubble diameter of a small sized fluidized bed of Geldart B particles. Their results showed that accurate prediction of bubble diameter was possible with the CFD numerical model. Slight deviation observed at higher bed height where bubble diameter was predicted to be larger. The authors explained that the slight discrepancy maybe caused by the choice of closing equations or a combination of selected model parameters. However, CFD was capable to predict the increasing trends of bubble diameter with respect to bed height, which is encouraging.

The bubbling flow in a laboratory scale pulsed fluidized bed of Geldart B particles was simulated using the Eulerian-Eulerian modeling approach with Wen and Yu (1966) as drag function and a restitution coefficient of 0.9 by Li et al. (2009). The bubble diameter of the bed was determined qualitatively using computational snapshots. The authors concluded that the flow instabilities and bed pressure drop inside fluidized bed were mainly caused by the formation and motion of air bubbles.

Lu et al. (2002) made the comparison for the Eulerian-Eulerian simulation of bubble sizes and rise velocities in a bubbling fluidized bed of Geldart B particles at an asymmetrical flow condition. They used Gidaspow (1994) drag law and a restitution coefficient of 0.999 for the simulations. The fluidization process is a totally unstable one that occurs along with substantial bubble interplays as well as fully active asymmetrical flow pattern though most of the simulation works have been conceived based on a symmetrical flow field and solving for half of the bed width to optimize the computational effectuality within a reasonable time of calculation. In validating the simulation results with the values of Darton bubble size equations (1977) for isolated bubbles, it was observed that the results were in close agreement with the empirical data.

Gelderbloom, et al. (2003) used the Eulerian-Eulerian approach incorporated with Syamlal O'Brien (1994) drag model and a restitution coefficient of 0.8 to study the bubbling/ collapsing fluidized beds for three Geldart groups, e.g. C, A, and B. The computed bubble sizes were in agreement with the empirical Darton expression (1977) within the reported experimental error. The code also computed the complete distribution of the bubble size for the three Geldart groups.

Chandrasekaran et al. (2005) used the Eulerian-Eulerian framework based on kinetic theory of granular flow and a restitution coefficient of 0.6 to study the bubble diameters of a bubbling fluidized bed of linear low density of polyethylene. It was observed that more smaller bubbles formed than larger bubbles. There was considerable deviation between the simulated bubble diameters and experimental results at lower heights.

However, at higher bed heights it appeared that the simulations were able to closely predict the experimentally observed results.

CFD simulations of Group B materials in a laboratory scale rectangular fluidized bed were done by Olumuyiwa et al. (2005). The simulated bubble diameter results were validated with the experimental results and prediction from the Darton's correlation (1977). The simulated values were always lower than the experimental ones, with the scatter between the experimental and simulated bubble size being greater at higher heights in the bed. On the other hand, the Darton's correlation (1977) always overpredicted the bubble size. The authors concluded that the two-dimensional simulations had contributed to the underestimation of bubble size in this case. This was supported by Cammarata et al. (2003) where in their studies also reported that bubble size calculated by two-dimensional simulation was smaller than the results from three-dimensional simulations.

In their paper, van Wachem et al. (2001) validated the Eulerian–Eulerian gas–solid model simulations of bubbling fluidized beds with the correlations for bubble size and bubble rise velocity available in the literature. A restitution coefficient of 0.9 was used. Based on the two-dimensional simulation results, they compared the bubble sizes obtained from simulations of a freely bubbling gas fluidized bed of a Geldart group B powder with predictions given by Darton et al. (1977) correlation. Their results showed that the simulated bubble diameters were slightly smaller in the higher part of the fluidized bed, which was attributed to the deficiency of the technique used by Darton (1977) to capture small bubbles diameters.

Asegehegn et al. (2011) performed the study of bubble diameter in two types of bed geometries (without immersed tube and with immersed tube) of a gas-solid fluidized bed using a restitution coefficient of 0.95 in Two-fluid model. For beds without immersed tubes the simulation and experimental results were in very good agreement until a certain height near the eruption zone. After this height the simulation predicted no

growth of bubbles while a continuous growth of bubbles was observed from the experiment. In the case of beds with horizontal tubes good qualitative agreement was achieved between the simulation and experimental results. The slight discrepancy was mainly due to the wall effect that was neglected in the numerical simulation.

2.5.3 Bed Pressure Drop

Taghipour et al. (2005) employed the Eulerian-Eulerian model incorporating the kinetic theory for solid particles to simulate the bed pressure drop of gas-solid fluidized bed reactor containing spherical glass beads of diameter 250-300 microns. They concluded that the simulated results indicated reasonable agreement for most experimental operating conditions. They later made a comparison of the time average bed pressure drop using different drag laws. The simulation and experimental results showed better agreement at velocities above minimum fluidization velocity. The discrepancy maybe attributed to the solids not being fluidized, thus being dominated by the interparticle frictional force, which was not predicted by the multifluid model for simulating gas-solid phases.

Hulme et al. (2005) examined the bed pressure drop across a bubbling fluidized bed reactor. The CFD simulated results predicted the values within 2% of error in comparison with the theoretical pressure drop calculated using the pressure drop correlation. Sau and Biswal (2011) simulated the pressure drop by considering different superficial velocities, both above and under minimum fluidization velocity, in a small scale fluidized bed of Geldart D particles. Qualitatively, good agreement was found from their plotted graphs. Their simulated results were able to reproduce the trends of experimental ones.

The hydrodynamics of fluidized bed were studied by Zhao et al. (2010) using the two-fluid modelling approach with Syamlal O'Brien (1994) drag model and a restitution coefficient of 0.9. The results showed that by using Syamlal O'Brien (1994) drag model

the simulated bed pressure drop was in good agreement with the experimental results and the deviations between the two was more stable.

2.5.4 Solid Circulation Rate

In CFBG, the solid circulation of the heat carrier (river sand) plays a critical role, since the heat carried by the solid material heated from the combustor is supplied to the gasification endothermic reactions. For the given system, an increase in the solid circulation rate will reduce the difference of temperatures between the gasification and combustion zone; as such, enhance the product yield. The solid circulation rate is affected by several operating parameters such as the gas velocities to the gasifier and combustor, v-valve and riser, bed inventory and etc. A stable circulation rate of heat carrying particles is required to enhance the performance of the CFBG. Therefore it is very important for CFD to be able to simulate the mechanisms of solid circulation within CFBG and predict an accurate solid circulation rate.

Marschall and Mleczko (1999) used the Eulerian-Eulerian approach with Gidaspow (1994) drag law to study the hydrodynamics of a bench scale internally circulating fluidized bed (ICFB). This type of reactor which consists of riser and annulus is an evolution from the spouted bed with a draft tube. It was found that the controlling of circulation of solids is typically governed by the height of the annulus. The CFD model was able to explain the effect of various reactor designs and several hydrodynamic parameters, e.g. height of the surrounding annulus, length of the entrainment region on the flow fields, i.e. porosity and velocity distributions. With the aid of CFD, it was solemnly considered that the geometrical parameters regulate hydrodynamic regimes of the reactor.

Seo et al. (2011) used the multiphase Eulerian model incorporating with Gidaspow (1994) drag law and a restitution coefficient of 0.9 to determine the hydrodynamics characteristic of a laboratory scale cold model dual circulating fluidized bed reactor. The solid circulation rate plays crucial role in this type of reactor. It is dependent on the gas

velocity in riser and with aeration rate in the recycle chamber and it is to be maintained up to a minimum level of loop-sealing where the upward gas flow is maintained for a stable operation. The CFD simulation results supported the behaviors observed experimentally in the reactor.

Nguyen et al. (2011) investigated the gas and particles hydrodynamics behaviors in a pilot-scale cold mode riser and a bubbling fluidized bed gasifier (dual circulating fluidized bed gasifier) experimentally and computationally. The authors studied the solid circulation rate and solid holdup in a CFD multiphase Eulerian model with Gidaspow (1994) drag law and a restitution coefficient of 0.9. The simulated results agreed well with the experimental data with only maximum error of 10% reported. The authors also made a conclusive remark that the cold bed simulation could be extended to predict the solid circulation rate for the hot bed operation of the gasifier.

Zhang et al. (2003) investigated experimentally and computationally in a cold model of jetting fluidized bed with a central jet in terms of solid circulation pattern. The solid circulation pattern indicates directly the solid mixing and the heat and mass transfer between different regions in the bed. In their studies, the particles were first entrained into the jetting region by the high velocity jet and then moved upward to the bubble street region. Then, the particles entered the annulus region. Finally the particles moved primarily downward in the annulus region. This process was considered one cycle of solid particles. CFD model using Eulerian-Eulerian framework with Gidaspow (1994) drag law calculated the same results.

Limited studies have been reported on CFD simulation investigating the solid circulation rate between two chambers of fluidized bed. As to conclude section 2.4, previous studies had shown that CFD is capable to reproduce the hydrodynamics of fluidized bed with promising results in comparison with the experimental data. However, the geometry discussed in the reviews was simple regular rectangular and cylindrical column. As such, it is very encouraging to utilise CFD model to investigate the integral

characteristic of CFBG. This would be the first hand study using CFD in this type of complex geometry reactor where the shape is irregular.

2.6 MODELING OF HYDRODYNAMICS IN 2D BINARY MIXTURE SYSTEM

The prime requirement of the biomass combustion and gasification is the quality of mixing of solids in the best possible limit. The good mixing of sand particles and biomass induces a uniform temperature within gasifier and thus improves the product yield. For mixing process, the motion of the particles is influenced by the wake and drift of the rising bubbles. Moreover, the bubbles in the fluidized bed in which the binary mixture is dealt are also responsible for the segregation. Mixing or segregation behavior of mixture particles is of practical importance because particle distributions in the fluidized bed influence the chemical reaction, bed expansion, erosion and various mass and heat transfer properties in the fluidized beds (Zhang et al., 2003).

In such design complexities, CFD numerical analysis provides efficient and effective approaches to predict the mixing and segregation demeanor of the binary system, particularly in catering the resolution of few parametric determinations which are difficult to measure directly from experiments. There is limited amount of research publications available concerning the hydrodynamic analysis of multi-component based fluidized beds, whereas, most of the reliable CFD studies are available for the mono-component based fluidized bed hydrodynamic parameterization in benchmark forms.

Some previous studies on hydrodynamics of binary system in terms of bed expansion and mixing quality are discussed as follow.

2.6.1 Bed Expansion

Cooper and Coronella (2005) utilized the two-dimensional Eulerian-Eulerian multiphase model with Syamlal O'Brien (1994) drag model to reproduce the important hydrodynamic aspects of a laboratory scale rectangular binary bubbling fluidized bed with coke and rutile used. Simulation parameters, e.g. solution technique, grid,

maximum packing fraction, drag law and operating conditions, e.g. gas velocity, bed makeup, nozzle location were inquired the proportional effects on bubbling, particle mixing and segregation. The simulations presumed realistic bubbles, rate of bubbling, bubble wakes and bed expansion. It provided the options of investigating segregation mechanism too.

Gao et al. (2009) used the three-dimensional Eulerian-Eulerian model with Syamlal O'Brien (1994) as drag function and a restitution coefficient of 0.9 to investigate the hydrodynamics characteristic of the binary particles such as pressure drop, bed expansion and bed density profile in a bench scale fluidized bed. The bed expansion coefficient increased with the increased in superficial gas velocity. However, as the superficial gas velocity increased; more small particles were entrained into the dilute phase where eventually the solids inventory of the dense phase decreased causing the height of dense phase to decrease and the bed expansion coefficient was likely to reduce. The computational results were able to predict this particular characteristic.

Mazzei et al. (2010) applied two-dimensional two-fluid model with the modified drag model to investigate numerically the dynamics of segregating bidisperse mixtures fluidized bed. In terms of bed expansion, the model was able to correctly capture the trend qualitatively. The average percent error in the predictions was of 11%.

2.6.2 Mixing Quality

A Two-Fluid Method computational code using the Di Felice (1994) drag model and a restitution coefficient of 0.9 was utilized to investigate the equilibrium degree of mixing of two-component beds of particles with equal size and different density in a laboratory scale fluidized bed by Renzo et al. (2008) The simulated mixing behavior was validated with the experimental data at various superficial gas velocities. It was found that the computational results were capable to reproduce the phenomena occurring in real apparatuses.

Zhang et al. (2003; 2004) presented an Eulerian-Eulerian model with Gidaspow (1994) drag function describing gas-solid fluid dynamics in a binary rectangular fluidized bed. They focused to analyze the solid circulation pattern, the time-averaged voidage profile, and time-averaged gas velocity in the fluidized bed which was composed of a binary mixture of sand and resin. The mixing pattern of the mixture was simulated and validated with the experimental data. The results showed good agreement with the experimental data.

The bed density profile that was done computationally and experimentally by Gao et al. (2009) achieved reasonable agreement. A well-mixed pattern of small particles and large particles could be achieved at the moderate gas velocity. Further increased in velocity resulted in conversion of fluidized bed into entrained bed. Low superficial velocity caused the bed to segregate where small particles fluidized in the upper regime of the bed and large particles remained stagnant at the bottom. The authors concluded that decreasing the diameter and density of the large particles tended to improve the mixing behaviours of the two particles.

Lu et al. (2003; 2007) used the Two-Fluid Eulerian CFD model with kinetic theory of granular flow and a restitution coefficient of 0.9 to study the segregation behavior of a binary mixture bed. When the fluidization velocity slightly exceeded minimum fluidization velocity, the simulation results predicted a complete segregation bed. The finer particles tended to move up into the upper regime in the bed, the big particles settled down in the bottom. The higher the superficial gas velocity, the more uniform the distribution of solids. Compared with their earlier experimentally measured mass fractions and mean particle diameter distributions, the computed results well agreed with the measured data.

The studies done by Lu et al. (2003) were supported by Sun et al. (2005) who also used the Eulerian-Eulerian framework with kinetic theory of granular flow and coefficient restitution of 0.9. Their simulated results indicated that the superficial gas velocity,

particle size, and mass fraction of sand particles had considerable impact on segregating and mixing behavior of binary mixture fluidized bed. They concluded that the model was able to capture the key features of binary mixture fluidization of biomass.

As to conclude section 2.4, extensive researches have been done on studying the hydrodynamics of mono-component fluidized bed by using CFD model but the study for binary system is rather limited. Scarce reviews on hand show that CFD is indeed a powerful and helpful tool to determine the hydrodynamics of binary mixture system fluidized bed. Hence, CFD will be tested on its predictability on the mixing characteristic of CFBG binary system.

2.7 SIGNIFICANCE OF 3D MODELING OF GAS-SOLID FLUIDIZED BED

There are many CFD simulations literature found which are based on two-dimensional computational approaches. Limitation of computing power is one of the key baffles there to opt for the two-dimensional CFD analysis in lieu of three-dimensional CFD analysis. Two-dimensional analysis normally assumes a symmetrical flow field in the bed and solve only for half of the bed width in order to save computational time. In reality, fluidization is a chaotic process with strong bubble interaction and a highly asymmetrical flow pattern. Thus realistic benchmarking of CFD simulation results require the three-dimensional analysis on a model though two-dimensional analysis may be able to provide some local information which can be input into the three-dimensional simulations. Three-dimensional computation is time consuming and its application in a single stand computing facility is very sparse for the case of fluidization beds till recent years. But reportedly, there are a number of three-dimensional analyses based on single particle fluidization bed hydrodynamic analysis. Three-dimensional analysis for binary component system fluidization in industrial scale is still in demand for exploring.

Peirano et al. (2001) investigated the importance of three-dimensionality in the Eulerian approach with Syamlal O'Brien (1994) drag model and a restitution coefficient of 0.9 simulations of stationary rectangular bubbling fluidized beds. The results of their

simulations showed that the two-dimensional simulations should be used with caution and only for sensitivity analysis, whereas the three-dimensional simulations were able to reproduce both the statics (bed height and spatial distribution of particles) and the dynamics (power spectrum of pressure fluctuations) of the bed. In addition, they showed that the accurate prediction of the drag force (the force exerted by the gas on a single particle in a suspension) was of little importance when dealing with bubbling beds.

Cammarata et al. (2003) also studied the bubbling behavior predicted by two-dimensional and three-dimensional Two-Fluid model simulations with 0.95 as the restitution coefficient for a rectangular fluidized bed. The bed expansion, bubble hold-up and bubble size calculated from two-dimensional and three-dimensional simulations were compared with the predictions obtained from the Darton equation (1977). A more realistic physical behavior of fluidization was obtained using three-dimensional simulations. Both Peirano et al. (2001) and Cammarata et al. (2003) concluded that three-dimensional simulations should be preferably performed except maybe in cases where the flow was by nature two dimensional. However, these authors indicated that the two-dimensional simulations could be used to conduct sensitivity analyses. For a cylindrical fluidized bed, there were no studies comparing two-dimensional and three-dimensional simulations.

Briongos and Guardiola (2005) presented a new method to scale hydrodynamic data obtained from a two-dimensional gas–solid fluidized bed, establishing links between two-dimensional and three-dimensional geometries by applying the chaos scale-up methodology. They tested the methodology for two-dimensional fluidized beds and three-dimensional cylindrical fluidized beds. The findings suggested that the two-dimensional and three-dimensional fluidized beds were dynamically similar if the fluidized beds had the same flow properties, which was represented by the Kolmogorov entropy under the same fluidization conditions. However, the results presented were limited to small ranges of gas velocities and particle properties.

Xie et al. (2008) employed the Eulerian-Eulerian model with kinetic theory of granular flow and Syamlal O'Brien (1994) as drag law to show the range of validity for simulations based on a two-dimensional cartesian coordinate system for both laboratory scale cylindrical and rectangular fluidized beds under three regimes which was bubbling, slugging and turbulent regimes. Comparison of two versus three-dimensional simulations was also determined. Their results showed that there was a significant difference between the two-dimensional and three-dimensional simulations, and only three-dimensional simulations could predict the correct bed height and pressure spectra.

Reuge et al. (2008) simulated the hydrodynamics of two- and three-dimensional Geldart B fluidized bed using Eulerian-Eulerian as framework incorporated with Syamlal O'Brien (1994) drag law and a restitution coefficient of 0.8. They reported that the three-dimensional simulations were necessary for correctly reproducing the experimental bed expansions and heights of fluctuation; the two-dimensional simulations widely overestimated both the quantities.

Almuttahar and Taghipour (2008) utilised the two-dimensional Eulerian-Eulerian model with Syamlal O'Brien (1994) drag function and a restitution coefficient of 0.99 to model the hydrodynamics of a FCC particles high density circulating fluidized bed. They found that the solid fraction near the wall predicted by the CFD numerical model was less than the experimental values. This discrepancy could be attributed to the simplication used to reduce the computational difficulties of handling such complex and large system. Hence it was suggested by the authors that real three-dimensional geometry should be modeled in order to get accurate model predictions.

The gas and particles hydrodynamics behaviors in a pilot-scale cold mode riser and a bubbling fluidized bed gasifier (dual circulating fluidized bed gasifier) were investigated by Nguyen et al. (2011) experimentally and numerically. They used the Eulerian-Eulerian approach with Gidaspow (1994) drag function and a restitution coefficient of 0.9 in the CFD analysis. The two-dimensional simulations overpredicted the axial solid

holdup distribution in riser. The main reason was due to the limitation in two-dimensional simulation to capture down flow of particles. Hence, the authors suggested that a three-dimensional study would be useful to enhance the prediction accuracy of the solid holdup in the fast fluidization regime of the riser.

Two- and three-dimensional Eulerian-Eulerian models for numerical simulations of two dimensional jetting fluidized beds were compared by Kawaguchi et al. (1998). Qualitative differences in solid motion were reported at the beginning of the fluidization process and near the corners of the column.

Busciglio et al. (2009) conducted the three-dimensional Two-Fluid model simulations of a bubbling fluidized bed with Gidaspow (1994) drag law to assess the suitability of assuming perfectly two-dimensional behavior (the experimental set up is almost two-dimensional). According to their investigation, there was no significant difference between three-dimensional and two-dimensional simulations, as the choice of two-dimensional simulation only gave rise to random differences of less than 2% in the simulated bubble properties. However, no quantitative comparison with respect to the solid velocity and local voidage was reported in this paper.

Esmaili and Mahinpey (2011) employed the Eulerian-Eulerian approach and a restitution coefficient of 0.92 to study the hydrodynamics of a three-dimensional small scale rectangular shape fluidized bed of Geldart B particles. Their results indicated that the pressure drop for both two-dimensional and three-dimensional simulation showed a declining trend by increasing the superficial gas velocity which was in good qualitative agreement with the experimental data. However, three-dimensional simulations showed their superiority in predicting the pressure drop inside the bed compared to the two-dimensional simulations. The reason could be the effect of participating governing equations of the z direction (depth of the bed) in Navier Stokes equation of multiphase flow.

Li et al. (2010) simulated the solids holdup, bed pressure drop and bubble diameter in two-dimensional and three-dimensional simulation for laboratory scale fluidized bed using Eulerian-Eulerian model. In their study of solids holdup, there was little difference in bed heights for corresponding two-dimensional and three-dimensional simulations. This may be attributed to the thin column thickness (in three dimensions) so that the flow was essentially two-dimensional. Pressure drop across the bed for two superficial gas velocities predicted by two-dimensional and three-dimensional simulations indicating +/- 1 standard deviation in comparison with theoretical values. This deviation could be ascribed to the wall effect. In two-dimensional simulations, pressure drops were slightly lower than the theoretical value due to the wall shear caused by downward solids flow along the side walls. The bubble diameter predicted by the two-dimensional and three-dimensional simulations was somehow quite similar.

The bubble diameter comparison done by Asegehegn et al. (2011) in two types of bed geometries (without immersed tube and with immersed tube) of a gas-solid fluidized bed showed that the simulation slightly underpredicted bubble diameter in the tube bank region. This was mainly due to the wall effect that was neglected in the numerical simulation while the experiments were performed using the two-dimensional beds. Preliminary studies using two-dimensional and three-dimensional simulations showed that the three-dimensional simulations predicted bigger bubbles than the two-dimensional simulations and were in better agreement with the experimental data. The discrepancy observed between the two-dimensional simulations and experimental measurements at the upper part of the bed were not observed when simulations were performed in three-dimension. This clearly indicated that neglecting the front and back walls in two-dimensional simulations significantly altered the bubble hydrodynamics.

Shi et al. (2010) ran a numerical simulation of fluidized bed polymerization reactor by using the three-dimensional Eulerian-Eulerian model with kinetic theory of granular flow and Wen and Yu (1966) drag law and a restitution coefficient of 0.9. The simulated pressure drop done was verified by the calculated data based on bed pressure drop

classical calculation. The predicted pressure drop results were found to agree well with the calculated data. The slight difference may result from neglect of the pressure drop caused by friction and particle collision in the classical calculation.

Zhang et al. (2008) used an Eulerian granular multiphase model incorporated with energy-minimizaion multi-scale (EMMS) drag model to simulate a three-dimensional circulating fluidized bed (CFB) gasifier. Simulation was carried out to investigate the distribution of solids vertical velocity in the gasifier. Their work was the first ever work done based on full loop, three-dimensional transient simulation of a semi-industrial scale CFB unit. Their results agreed generally well with experimental data.

Owoyemi and Lettieri (2008) used Eulerian-Eulerian approach as framework with extended modified monocomponent Syamlal O'Brien (1994) drag model and a restitution coefficient of 0.97 to bidisperse system. The simulations were carried out in three-dimensional laboratory scale rectangular column. Their work was mainly focus on the investigation of mixing and segregation pattern of bidisperse system, bed expansion and bubble dynamics. Quantitatively, around 2% - 4% of error was observed in bed height analysis between the experimental results and computational results. The slight deviation might be due to the experimental error which can be considered negligible.

In addition, they also tested the mixing quality of bidisperse system at different average composition through experiment and CFD. They found that the CFD results showed good agreement with the experimental data and the semi-theoretical expression with slight discrepancy of 8%. This difference may be due to the pervasiveness of the mixing and solids recirculation mechanisms over the antagonistic effect of segregation in the CFD simulations, highlighting present gaps in current computer models to describe correctly the particle-particle interactions and, in turn, incorrectly predicting the mixing and segregation dynamics of these systems.

A short summary has been presented in Table 2.2 to make a distinct realization on two-dimensional and three-dimensional analysis from the literatures (Li et al., 2010; Peirano et al., 2001; Busciglio et al., 2009; Esmaili and Mahinpey, 2011; Laverman et al., 2008; Reuge et al., 2008).

Table 2.2: Comparison of Two-dimensional (2D) and Three-dimensional (3D) Simulations

Parameter	**2D**	**3D**
Computational Load	Low	High
Bed Expansion (comparison with experimental data)	Relatively higher	Well agreement
Dependence of bubble diameter on specularity coefficient	Sensitive	Sensitive
Dependence of bubble diameter on bed height (comparison with experimental data)	Larger diameter	Well agreement
Dependence of bubble diameter on bubble rise velocity (comparison with experimental data)	Weakly explained	Well agreement
Mesh size sensitivity	Computational time relatively increases with decreasing of element size	Computational time increases drastically with decreasing of element size

Based on the table, it shows that the three-dimensional simulations provide more precise solitude of hydrodynamic characteristic. To understand the CFBG fluidization behavior,

detailed information is needed in terms of fluidization pattern of single component and binary mixture system, solid circulation between two compartments (combustor and gasifier), dynamic mixing of binary system, and the effects of various non-uniform geometries. All these considerations necessitate three-dimensional CFD numerical simulations, which may even be viewed as "virtual experimentation" if with reliable CFD numerical model.

2.8 EXPERIMENTAL STUDIES ON HYDRODYNAMIC PARAMETERS

The fluidization study in unique CFBG has limited review to be compared with. The detailed analysis of papers published on experimental studies of hydrodynamic parameter for dual compartmented gasifier of laboratory scale is represented in the Ph.D thesis by Chok (2011). The methodological aspects of experimental studies are included in corresponding relevant chapters with respective referencing.

2.9 SUMMARY

Based on the literature survey presented in this chapter, it can be summarized as per the followings:

- There are two different approaches used in multiphase numerical simulations of gas-solid fluidized bed systems. These are remarkably known as Eulerian-Lagrangian approach and the Eulerian-Eulerian approach.
- Eulerian-Lagrangian framework is a discrete method that formulated relying on the molecular dynamics of individual particle-particle interplays. Eulerian-Eulerian continuum framework deals the gas phase and solid phase or gas-solid multiphase where anyone of the components may considered as the diffusing continua.
- Although, Eulerian-Lagrangian approach predicts better resemblance to the experimental results; however, it is limited to handling not more than a million of particles and consuming high computational time. On the contrary, the Eulerian-Eulerian approach is able to predict the dynamic characteristics of dense fluidized bed (more particles) with lower computational power.

- As a result, Eulerian-Eulerian continuum models comprise a more obvious choice for hydrodynamic modeling of present work.
- The standard multiphase models available in computational fluid dynamics software can be modified according to one's interest in gas-solid fluidized bed operation. The mostly being modified parameters in literature are the inter-particle drag correlations, the solid viscosity and etc. However, some authors also claimed that with the standard model available, it is sufficient to predict the hydrodynamics of multiphase system. Also, higher value of restitution coefficient is more favoured in CFD analysis considering the result accuracy.
- The effects of numerical solution parameters (time step sizes, mesh resolution and convergence criterion) are also reviewed and they do affect the computational time as well as accuracy of results.
- CFD numerical model have been useful to predict the hydrodynamic of two-dimensional single component and binary mixture system small scale, simple rectangular or cylindrical gas-solid fluidized bed, however very limited reviews have been reported for three-dimensional large scale fluidized bed studies particularly in binary mixture system, where specific biomass - palm shell is used. Moreover, compartmented type fluidized bed has never been studied before.
- Therefore, it is concluded that the hydrodynamic of single component and binary mixture system CFBG will be performed using standard three-dimensional Eulerian-Eulerian framework incorporated with Kinetic Theory of Granular Flow, standard Syamlal O'Brien as drag function and restitution coefficient of 0.9. Medium mesh size, a time step of 0.001s and convergence criterion of 0.001 will be adopted in the solution procedure for reasonable computational time without compromising result accuracy. This work occupying CFD technique will be the first step in virtual experimentation based on three-dimensional transient simulation of a pilot plant scale unit.

2.10 SPECIFIC RESEARCH OBJECTIVES

Based on the literature review and the research gaps identified, the main objectives of the current study have been discerned as follows:

- To use Computational Fluid Dynamics (CFD) numerical technique for investigating the hydrodynamic behaviour and underlying relationship between gas and solid flows within the single component and binary mixture system gas-solid bubbling fluidized bed at ambient mode in a pilot plant scale Compartmented Fluidized Bed Gasifier (CFBG) by using three-dimensional simulations.
- To use CFD for studying the dynamic mixing and possible segregation in binary mixture system in CFBG using specific biomass (palm shell).
- To numerically simulate the solid circulation process between combustor and gasifier compartments.
- To perform fluidization experiments in a cold flow model (prototype) with identical dimension as the pilot-scale unit used for fuel gas production.
- To validate the CFD simulated results with experimentally obtained data.
- Finally, to provide the research findings and outcomes from studies above as a preliminary guide for designing and operating the demonstration unit – pilot plant scale CFBG with 0.5 ton/day of palm shell feed for fuel gas production.

CHAPTER 3 CFD NUMERICAL MODEL

3.1 INTRODUCTION

In this section, a brief insight in the physically and mathematically complex field of multiphase flows in fluidized beds will be given. A synthetic presentation of the Eulerian-Eulerian two-fluid model based on granular kinetic theory, analyzing the steps required to formulate the associated set of partial differential equations will be provided.

The first step of any flow modeling project is to identify key controlling processes and relate these controlling processes to underlying fluid dynamics. This analysis will allow one to formulate clear objective for the flow modeling exercise. Detailed knowledge of fluid dynamics, analysis of space and time scales of the specific problem at hand and analysis of the available resources, are required to develop an appropriate modeling approach. The modeling approach devises ways of dividing the complex problems into tractable sub-problems and ways of achieving the project objectives within the allocated resources. The basic elements of mapping a computational flow model on a computer are shown in Figure 3.1.

3.2 GOVERNING EQUATIONS

The governing equations of the system include the conservation of mass and momentum Equations of solid and gas phases were developed based on Eulerian-Eulerian model, using the averaging approach. The kinetic theory of granular flow, which considers the conservation of solid fluctuation energy, was used for closure of the solids stress terms. The governing equations can be summarized as follows:

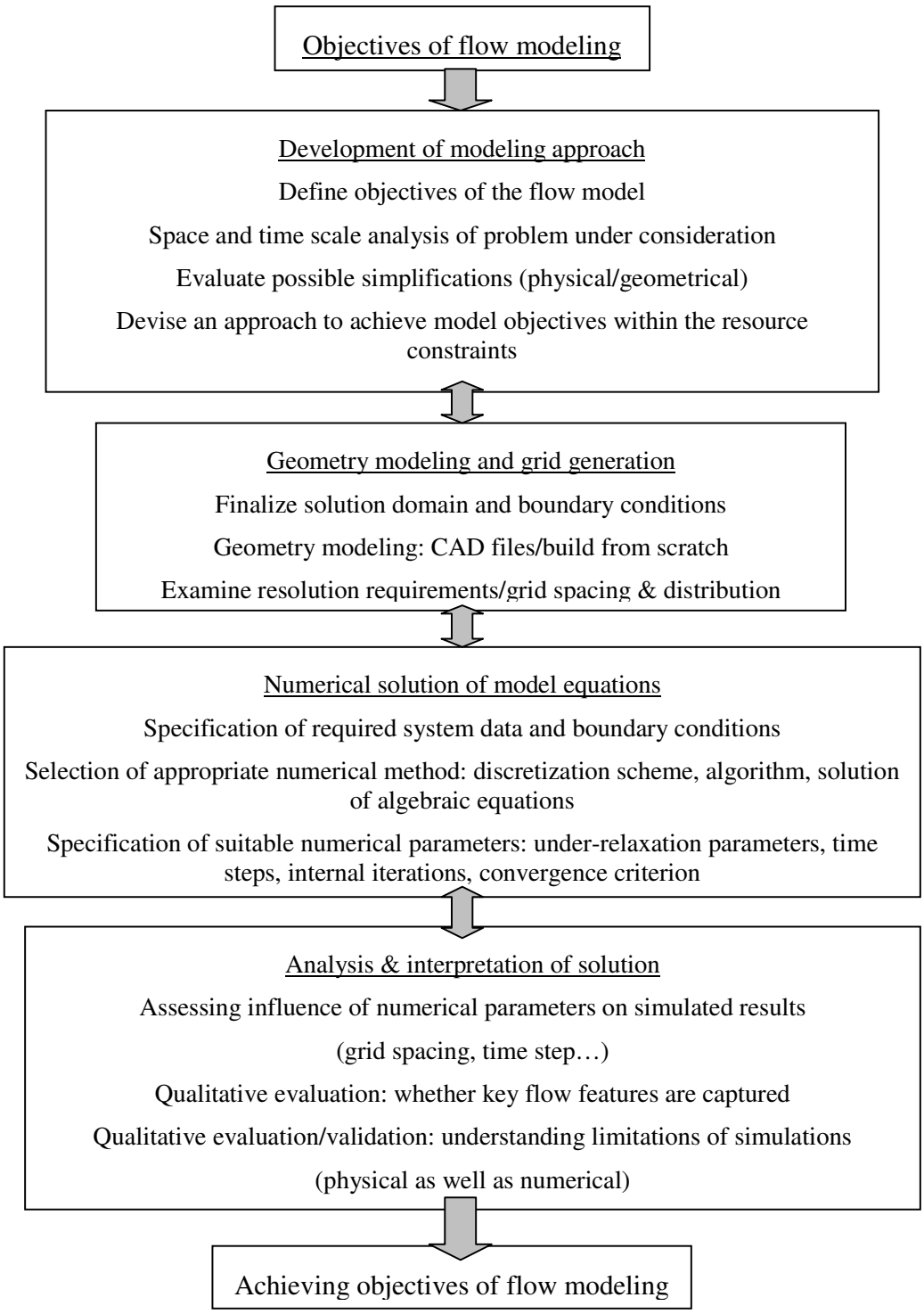

Figure 3.1: Mapping computational models onto CFD tools

By definition, the volume fractions of the phases must sum to one:

$$\varepsilon_g + \varepsilon_s = 1 \tag{3.1}$$

The continuity equation for gas and solid phases without mass transfer between the phases respectively are:

$$\frac{\partial(\varepsilon_g \rho_g)}{\partial t} + \nabla \cdot (\varepsilon_g \rho_g u_g) = 0 \tag{3.2}$$

$$\frac{\partial(\varepsilon_s \rho_s)}{\partial t} + \nabla \cdot (\varepsilon_s \rho_s u_s) = 0 \tag{3.3}$$

The conservation of momentum for the gas and the solids phase are described by

$$\frac{\partial(\varepsilon_g \rho_g u_g)}{\partial t} + \nabla \cdot (\varepsilon_g \rho_g u_g u_g) = \nabla \cdot (\tau_g) - \varepsilon_g \nabla P - \beta(u_g - u_s) + \varepsilon_g \rho_g g \tag{3.4}$$

$$\frac{\partial(\varepsilon_s \rho_s u_s)}{\partial t} + \nabla \cdot (\varepsilon_s \rho_s u_s u_s) = \nabla \cdot (\tau_s) - \varepsilon_s \nabla P - \nabla P_s + \beta(u_g - u_s) + \varepsilon_s \rho_s g \tag{3.5}$$

$[-\varepsilon_g \nabla P - \beta(u_g - u_s)]$ is an interaction force (drag and buoyancy forces) representing the momentum transfer between gas and solid phases (Taghipour et al., 2005; Zimmermann and Taghipour, 2005; Zhong et al., 2007; Zhong et al., 2006; Syamlal and O'Brien, 1989; Syamlal and O'Brien, 2003).

3.2.1 Lift Forces

For multiphase flows, the effect of lift forces on the secondary phase particles (or droplets or bubbles) is included. These lift forces act on a particle mainly due to velocity gradients in the primary phase flow field. The lift force will be more significant for larger particles, but the model assumes that the particle diameter is much smaller than the interparticle spacing. In most cases, the lift force is insignificant compared to the drag force, so there is no reason to include this extra term.

3.3 INTERPHASE MOMENTUM TRANSFER COEFFICIENT

The interphase momentum transfer is an important term in the modeling of gas-particle interactions, since particle fluidization results from the drag exerted by the interstitial gas on the particulate phase. One of the requirements of the drag coefficient is to properly predict the minimum fluidization velocity.

3.3.1 Gas-gas Momentum Transfer Coefficient

For fluid-fluid flows, each secondary phase is assumed to form droplets or bubbles. This has an impact on how each of the fluids is assigned to a particular phase. The exchange coefficient in general form:

$$K_g = \frac{\alpha_g \alpha_s \rho_g f}{\tau_g} \tag{3.6}$$

where f, the drag function, is defined differently for the different exchange coefficient models and τ_g, the "particulate relaxation time", is defined as

$$\tau_g = \frac{\rho_g d_g^2}{18\mu_g} \tag{3.7}$$

where d_g is the diameter of the bubble.

Nearly all definitions of f include a drag coefficient (C_D) that is based on the relative Reynold number (Re). It is this drag function that differs among the exchange coefficient models. For all these situations, Kpq should tend to zero whenever the primary phase is absent within the domain, to enforce this, the drag function f is always multiplied by the volume fraction of the primary phase q.

For the model of Schiller and Naumann

$$f = \frac{C_D \,\mathrm{Re}}{24} \tag{3.8}$$

where

$$C_d = \begin{cases} \dfrac{24}{\varepsilon_g \,\mathrm{Re}_p}\left[1 + 0.15\left(\varepsilon_g \,\mathrm{Re}_p\right)^{0.687}\right] & \text{For } \mathrm{Re_p} \le 1000 \\ 0.44 & \text{For } \mathrm{Re_p} > 1000 \end{cases}$$

And *Re* is the relative Reynolds number. The relative Reynolds number for the primary phase q and secondary phase p is obtained from

$$\mathrm{Re} = \frac{\rho_q \left|\vec{v}_p - \vec{v}_q\right| d_p}{\mu_q} \tag{3.9}$$

The relative Reynolds number for secondary phases p and r is obtained from

$$\mathrm{Re} = \frac{\rho_{rp} \left|\vec{v}_r - \vec{v}_p\right| d_{rp}}{\mu_{rp}} \tag{3.10}$$

where $\mu_{rp} = \alpha_p \mu_p + \alpha_r \mu_r$ is the mixture viscosity of the phases p and r.

3.3.2 Gas-solid Momentum Transfer Coefficient

Several drag models exist for the Gas-Solid inter phase exchange coefficient (β). Taghipour et al. (2005) have compared three drag coefficients viz. Syamlal-O'Brien (1994), Gidaspow (1994) and Wen-Yu (1966) and found them "qualitatively similar". Also, they suggested that the Syamlal- O'Brien drag function gives a somewhat better prediction when compared with the other models and it is more suitable for predicting the hydrodynamics of Gas-Solid flows. Also, this drag coefficient can be adjusted easily to match the minimum fluidization velocity. Therefore in the present work, Syamlal O'Brien's (1994) drag coefficient was used.

This drag law is based on the measurements of the terminal velocities of particles in fluidized or settling beds (Syamlal and O'Brien, 1989; Syamlal and O'Brien, 2003). These correlations give exchange coefficients in terms of the volume fraction and relative Reynolds number as

$$\beta = \frac{3}{4} C_D \frac{\varepsilon_g \left(1 - \varepsilon_g\right)}{u_t^2 d_p} \rho_g \left|u_g - u_s\right| \tag{3.11}$$

Where C_D, the drag coefficient, is given by

$$C_d = \left(0.63 + \frac{4.8}{\sqrt{\mathrm{Re}_p / u_t}} \right)^2 \tag{3.12}$$

And u_t, a terminal velocity correlation, is expressed as

$$u_t = 0.5\left(A - 0.06\,\mathrm{Re}_p + \sqrt{(0.06\,\mathrm{Re}_p)^2 + 0.12\,\mathrm{Re}_p\left(2B - A + A^2\right)} \right) \tag{3.13}$$

$A = \varepsilon_g^{4.14}$, $B = 0.8\varepsilon_g^{1.28}$ for $\varepsilon_g \le 0.85$

$A = \varepsilon_g^{4.14}$, $B = \varepsilon_g^{2.65}$ for $\varepsilon_g > 0.85$

$$\mathrm{Re}_s = \frac{\rho_g d_s \left| u_g - u_s \right|}{\mu_g} \tag{3.14}$$

3.3.3 Solid-solid Momentum Transfer Coefficient

The solid-solid exchange coefficient K_{sl} has the following term:

$$K_{sl} = \frac{3(1+e_{ls})\left(\frac{\pi}{2} + C_{fr,ls}\frac{\pi^2}{8}\right)\alpha_s \alpha_s \alpha_l \rho_l (d_l + d_s)^2 g_{0,ls} \left| \vec{v}_l - \vec{v}_s \right|}{2\pi(\rho_l d_l^3 + \rho_s d_s^3)} \tag{3.15}$$

Where

e_{ls} = the coefficient of restitution

$C_{fr,ls}$ = the coefficient of friction between the l^{th} and s^{th} solid phase particle ($C_{fr,ls} = 0$)

d_l = the diameter of the particles of solid l

$g_{o,ls}$ = the radial distribution coefficient

3.4 KINETIC THEORY OF GRANULAR FLOW (KTGF)

The two-fluid model also requires constitutive equations to describe the rheology of the particulate phase that appeared in the momentum equation, i.e., the particulate phase viscosity and the particulate phase pressure gradient. These solids rheologies are very important but difficult to describe in modeling gas–solid flows using the TFM. Two approaches are usually used for treating these parameters. The first approach is commonly known as the Constant Viscosity Model (CVM) and was applied by several authors (Tsuo and Gidaspow, 1990; Kuipers et al., 1992; Gidaspow and Ettehadieh, 1983; Nieuwland et al., 1996; Enwald et al., 1996). This approach treats solids phase viscosity as constant and solids pressure as a function of the modulus of elasticity of the powder, which in turn is assumed to be a function of local porosity only. The advantage of this model is its simplicity but it does not take into account the effect of non-uniform characteristics of the particle phase viscosity. The second approach models solids stress using the Kinetic Theory of Granular Flow (KTGF) principle, which is based on kinetic theories of non-uniform gases as described by Chapman and Cowling (1970). The KTGF was first applied to granular flows by Jenkins and Savage (1983) and Lun et al. (1984). Later Sinclair and Jackson (1989) applied this theory to model gas–solid flow in a pipe. The model was further developed and applied to dense gas–solid fluidized beds by Gidaspow (1994). As a result of shearing of the particulate phase, particles collide resulting in a random granular motion. This fluctuation in particle velocity generates an effective pressure in the particulate phase together with an effective viscosity that resists shearing of the particle assembly. KTGF uses this non-ideal particle–particle collision to describe the dependence of the rheologic properties of the fluidized particles on local particle concentration and the fluctuating motion of the particles. Analogous to the thermodynamic temperature for gases, the model introduced a granular temperature as a measure of particle velocity fluctuations. It then assumes the solids stresses to be functions of this granular temperature, which in turn vary with time and position in the fluidized bed.

Thus an additional conservation equation for fluctuating energy is solved in addition to the conservation of mass and momentum equations. The granular temperature Θ of solid phase as an order of solid fluctuation is defined as one-third of the mean square velocity of particles random motion. Granular temperature is different from solid phase temperature and proportional to the granular energy. Therefore granular energy is defined as the specific energy of solid particles fluctuation. The granular temperature Θ is defined based on solids fluctuating velocity u' as

$$\Theta = \frac{1}{3}u'^2 \tag{3.16}$$

The variation of the particle velocity fluctuations is described by a separate conservation equation, the so-called granular temperature equation:

$$\frac{3}{2}\left(\frac{\partial(\varepsilon_s \rho_s \Theta)}{\partial t}\right) + \nabla \cdot (\varepsilon_s \rho_s u_s \Theta) = (-P_s I + \tau_s) : \nabla u_s - \nabla \cdot q - \gamma_s - J_s \tag{3.17}$$

Where $(-P_s I + \tau_s) : \nabla u_s$ is the generation of energy by the solid stress tensor, $\nabla \cdot q$ is the diffusion of energy (Gamwo et al., 1999; Syamlal and O'Brien, 1989, 2003; Hamzehei and Rahimzadeh, 2009).

Instead of solving the complete granular temperature equation Syamlal et al. (1994) proposed an algebraic form of the equation. They assumed a local equilibrium between generation and dissipation of the granular energy as these terms are the most dominant terms in dense regions. Thus the convection and diffusion terms can be neglected. Boemer et al. (1997) and van Wachem et al. (2001) showed that using the algebraic form instead of the full partial differential equation hardly affects simulation results while significant computational time can be saved. By neglecting the convection and diffusion terms and retaining only the generation and the dissipation terms, Eq. 3.17 is reduced to

$$0 = (-P_s I + \tau_s) : \nabla u_s - \gamma_s \tag{3.18}$$

3.4.1 Gas Phase Stress Tensor

Following Gidaspow (1994) it is assumed that the gas and solid phases are Newtonian fluids. Thus the stress tensor is modeled using the Newtonian stress–strain relation as

$$\tau_g = -\varepsilon_g\left[\left(\xi_g - \frac{2}{3}\mu_g\right)(\nabla\cdot u_g)I + \mu_g\left((\nabla u_g) + (\nabla u_g)^T\right)\right] \tag{3.19}$$

The gas phase bulk viscosity ξ_g is a measure of the difference between the thermodynamic and mechanical pressures and for a Newtonian fluid (e.g. air), the bulk viscosity is usually set to zero in what is referred to as the Stokes' assumption [8,9] while the shear viscosity μ_g is assumed to be constant.

3.4.2 Solids Phase Shear Stress Tensor

The solids phase is also assumed to be Newtonian and the stress tensor is given by

$$\tau_s = -\varepsilon_s\left[\left(\xi_s - \frac{2}{3}\mu_s\right)(\nabla\cdot u_s)I + \mu_s\left((\nabla u_s) + (\nabla u_s)^T\right)\right] \tag{3.20}$$

In fluidized beds the bulk and shear viscosities of the particulate phase are of the same order and thus bulk viscosity is not neglected.

3.4.3 Solids Bulk Viscosity

The solid bulk viscosity accounts for the resistance of the granular particles to compression and expansion. It is obvious that the importance of the bulk viscosity depends strongly on the velocity gradients. Solids bulk viscosity describes the resistance of particle suspension against compression. In the literature there is general agreement on the form of the solids' bulk viscosity, which is given by Lun et al. (1984)

$$\xi_s = \frac{4}{3}\varepsilon_s\rho_s d_p g_o(1+e)\sqrt{\frac{\Theta}{\pi}} \tag{3.21}$$

3.4.4 Solids Shear Viscosity

Shear viscosity represents the tangential forces due to translational and collisional interaction of particles. In general it is written as the sum of a collisional and a kinetic part

$$\mu_{s,KTGF} = \mu_{s,col} + \mu_{s,kin} \tag{3.22}$$

There are several models for the shear viscosity expression that are present in literature. Basically all use a similar expression for the collision contribution; however, their expression for the kinetic contribution of the solids shear viscosity differs. It is difficult to discriminate between the different models available since few detailed measurements exist. The models differ mainly in the dilute region (eso0.3), which is of minor importance in bubbling fluidized beds. In dense solid systems there is no difference in the predicted solids viscosity of the models (van Wachem et al., 2001). Therefore in this work the model proposed by Gidaspow (1994) was used and is given below.

$$\mu_{s,col} = \frac{4}{5}\varepsilon_s \rho_s d_p g_o (1+e)\sqrt{\frac{\Theta}{\pi}} \tag{3.23}$$

$$\mu_{s,kin} = \frac{1}{15}\sqrt{\Theta\pi}\rho_s d_p g_o \varepsilon_s^2 (1+e) + \frac{1}{16}\sqrt{\Theta\pi}\rho_s d_p \varepsilon_s + \frac{10}{96}\sqrt{\Theta\pi}\frac{\rho_s d_p}{g_o(1+e)} \tag{3.24}$$

3.4.5 Dissipation of Granular Energy

The dissipation term in the fluctuating granular energy equation (Eq. 3.17) represents the dissipation of granular energy due to inelastic particle–particle collisions and is usually expressed by the model of Lun et al. (1984) as

$$\gamma_s = 12(1-e^2)\frac{\varepsilon_s^2 \rho_s g_o}{d_p\sqrt{\pi}}\Theta^{3/2} \tag{3.25}$$

This dissipation term is usually taken into account by the magnitude of the particle–particle coefficient of restitution. The coefficient of restitution represents the fraction of energy dissipated due to the inelastic collision of particles. It varies between 1 for fully

elastic collisions without a loss of kinetic energy, hence the dissipation becomes zero, and 0 for fully inelastic collisions, and hence the dissipation tends to infinity. For glass beads many investigators used different values ranging from 0.9 to 0.99 (Taghipour et al., 2005) with 0.9 preferred by many who claimed that it provided better agreement with experimental results (e.g. Taghipour et al., 2005; Patil et al., 2005b; Hulme et al., 2005). Therefore in this work a coefficient of restitution of 0.9 was used.

3.4.6 Radial Distribution Function

The radial distribution function can be interpreted as the probability of a single particle touching another particle (probability of particle collision) in the solids phase. Thus its value increases with increasing solids volume fraction. The value of the radial distribution function varies from one at zero solids volume fractions and tends to infinity when the solids volume fraction reaches the maximum packing limit, due to constant contact of the particles. The function allows a tight control of the solids volume fraction, so that maximum packing is not exceeded and more accurate flow characteristics can be achieved. There are several models proposed for the radial distribution function and are compared by van Wachem et al. (2001). In this work the model from Ma and Ahmadi (1986) was used and is written as

$$g_o = 1 + 4\varepsilon_s \left\{ \frac{1 + 2.5\varepsilon_s + 4.5904\varepsilon_s^2 + 4.515439\varepsilon_s^3}{\left[1 - \left(\varepsilon_s / \varepsilon_{s,\max}\right)^3\right]^{0.67802}} \right\} \tag{3.26}$$

3.4.7 Solids Pressure

Difficulties are encountered in preventing the solid volume fraction from exceeding the maximum particle packing, i.e. the fixed bed value for randomly packed spheres. This is resolved by means of adding solid phase pressure in the solid momentum equation. The solid phase pressure, relationed to the interaction among particles, plays an important role for both a physical and numerical point of view. It prevents the solid fraction from reaching impossibly high values, and helps to make the system numerically stable by converting imaginary characteristics into real ones.

The solids pressure represents the normal forces due to particle–particle interactions and it prevents the solids phase from reaching unrealistic high solids volume fractions. It also helps to make the system numerically stable by converting imaginary characteristics into real ones (Kuipers et al., 1992). It is written as the sum of the kinetic and collisional term as given by Lun et al. (1984)

$$P_{s,KTCGF} = \varepsilon_s \rho_s \Theta + 2 g_o \varepsilon_s^2 \rho_s \Theta (1+e) \tag{3.27}$$

3.4.8 Frictional Stresses

At a packed state, the bed is crammed with particles, and hence the frictional force prevails over the other forces, while at a fluidized state, lasting contact gives way to free flight and brief collisions among particles. The competition and transformation of dominating forces lead to flow transition from the packed bed to fluidization. Subsequently, three mechanisms of the particle-phase transport result in two types of flow states, as shown in Figure 3.1. When particles are closely packed, as in the case of dense fluidized beds, the behavior of the granular flow is not adequately described by kinetic theory, which assumes collisions to be binary and quasi-instantaneous. In regions with high particle volume fractions multi-particle contacts (frictional stresses) dominate the stress generation mechanism. Hence it is necessary to include these stresses in the model. Similar to shear stress, frictional stress is composed of the frictional shear viscosity and frictional solids pressure, which includes tangential and normal frictional forces. The frictional stresses are simply added to the solids stresses from KTGF when the solids volume fraction exceeds a certain value $\varepsilon_{s,\min}$, which is usually set to 0.5 (Johnson et al., 1990)

$$\mu_s = \mu_{s,KTGF} + \mu_{s,f} \tag{3.28}$$

$$P_s = P_{s,KTGF} + P_{s,f} \tag{3.29}$$

In this work the Schaeffer (1987) model for frictional shear viscosity and the Johnson et al. (1990) model for frictional pressure were used

$$\mu_{s,f} = \frac{P_s \sin\phi}{2\sqrt{I_{2D}}} \tag{3.30}$$

$$I_{2D} = \frac{1}{6}\left[\left(\frac{\partial u_s}{\partial x} - \frac{\partial v_s}{\partial y}\right) + \left(\frac{\partial v_s}{\partial y}\right)^2 + \left(\frac{\partial u_s}{\partial x}\right)^2\right] + \left[\frac{1}{2}\left(\frac{\partial u_s}{\partial y} + \frac{\partial v_s}{\partial x}\right)\right]^2 \tag{3.31}$$

$$P_{s,f} = Fr\frac{\left(\varepsilon_s - \varepsilon_{s,\min}\right)^n}{\left(\varepsilon_{s,\max} - \varepsilon_s\right)^P} \tag{3.32}$$

where the values for Fr = 0.05, n = 2 and p = 5 are used (Johnson et al.,1990).

3.5 MAXIMUM PACKING LIMIT IN BINARY MIXTURES

The packing limit is not a fixed quantity and may change according to the number of particles present within a given volume and the diameter of the particles. Small particles accumulate in between larger particles increasing the packing limit.

For a binary mixture with diameter $d_1 > d_2$, the mixture composition is defined as

$$X_1 = \frac{\alpha_1}{\alpha_1 + \alpha_2} \tag{3.33}$$

Where

$$X_1 <= \frac{\alpha_{1,\max}}{(\alpha_{1,\max} + (1\_\alpha_{1,\max})\alpha_{2,\max})} \tag{3.34}$$

The maximum packing limit for the mixture is given by

$$\begin{aligned}\alpha_{s,\max} &= (\alpha_{1,\max} - \alpha_{2,\max} + [1 - \sqrt{\frac{d2}{d1}}](1-\alpha_{1,\max})\alpha_{2,\max}) \\ &*(\alpha_{1,\max} + (1-\alpha_{1,\max})\alpha_{2,\max})\frac{X_1}{\alpha_{1,\max}} + \alpha_{2,\max}\end{aligned} \tag{3.35}$$

The packing limit is used for the calculation of the radial distribution function.

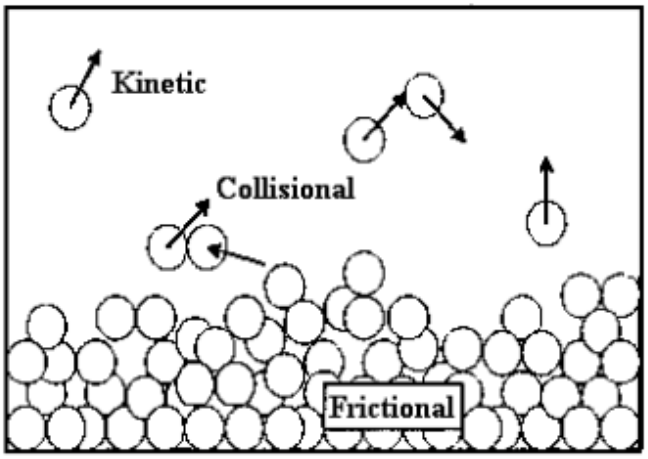

Figure 3.2: Three particle transport mechanism, Kinetic, Collisional, and frictional transport

CHAPTER 4 MODEL SOLUTION PROCEDURE

4.1 INTRODUCTION

Numerical solution of problem for a two-phase fluid motion lies in application of methods for space-time discretization. Its purpose is to reduce the partial differential equations (PDE), describing the hydrodynamics behavior of the system, to a finite dimension.

4.1.1 Finite Volume Method (FVM)

The numerical method that is most widely used is the finite volumes method (FVM), which arises from finite difference technique. Mathematical domain under investigation is fulfilled with a control volumes mesh called cells which are usually of cubic shape. Integration of balance equations on each control volume leads to an algebraic set of non-linear equations expressed in a way similar to models differential equations. Discretization procedure includes the following steps:

- Integration of fundamental balance equations on each control volume of the computational domain
- Discretization
- Solution of the resulting algebraic equations through iterative methods

A finite volume method distinguishes from any other because the conservation of all flow variables on each cell of the computational domain is imposed. This condition establishes a direct connection between algorithm structure and physical behavior of the system.

4.1.2 Discretization

The discrete values of scalar ψ (generic flow variable) is stored at the cell centers, however the face value of ψ are required for the convection terms and must be interpolated from the cell center values. This is accomplished using an upwind scheme. Upwinding means that the face value of ψ is derived from quantities in the cell upstream or "upwind", relative to the direction of the normal velocity.

4.1.3 First-order Upwind Scheme

When first-order accuracy is desired, quantities at cell faces are determined by assuming that the cell center values of any field variable represent a cell-average value and hold throughout the entire cell; the face quantities are identical to the cell quantities. Thus when first-order upwinding is selected, the face value of ψ is set equal to the cell-center value of ψ in the upstream cell.

4.1.4 Pressure-Based Solver

In this section, special practice related to the discretization of the momentum and continuity equations and their solution by means of the pressure-based solver are addressed. These practices are most easily described by considering the steady-state continuity and momentum equations in integral form:

$$\oint \rho \vec{v} \cdot d\vec{A} = 0 \tag{4.1}$$

$$\oint \rho \vec{v}\vec{v} \cdot d\vec{A} = -\oint p\mathrm{I} \cdot d\vec{A} + \oint \bar{\bar{\tau}} \cdot d\vec{A} + \int_V \vec{F} dV \tag{4.2}$$

Where I is the identity matrix, $\bar{\bar{\tau}}$ is the stress tensor, and $\vec{F}$ is the force vector.

4.1.4.1 Discretization of the Momentum Equation

The scalar transport equation is also used to discretize the momentum equations. For example, the *x*-momentum equation can be obtained by setting ϕ = u:

$$apu = \sum_{nb} a_{nb} u_{nb} + \sum p_f A \cdot \hat{t} + S \tag{4.3}$$

Co-located scheme is used, whereby pressure and velocity are both stored at cell centers. However, Equation 4.3 requires the value of the pressure at the face between cells c_0 and c_1, shown in Figure 5.1. Therefore an interpolation scheme is required to compute the face values of pressure from the cell values.

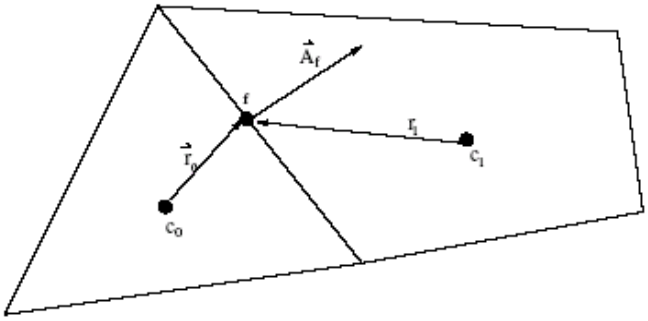

Figure 4.1: Control Volume Used to Illustrate Discretization of a Scalar Transport Equation

4.1.4.2 Pressure Interpolation Scheme

Pressure interpolation scheme is used to interpolate the pressure values at the faces using momentum equation coefficient:

$$P_f = \frac{\frac{P_{c_0}}{a_{p,c_0}} + \frac{P_{c_1}}{a_{p,c_1}}}{\frac{1}{a_{p,c_0}} + \frac{1}{a_{p,c_1}}} \tag{4.4}$$

This procedure works well as long as the pressure variation between cell centers is smooth. When there are jumps or large gradients in the momentum source terms between control volumes, the pressure profile has a high gradient at the cell face, and cannot be interpolated using this scheme. If this scheme is used, the discrepancy shows up in overshoots/ undershoots of cell velocity.

Flows for which the standard pressure interpolation scheme will have trouble include flows with large body forces such as in strongly swirling flows, in high-Rayleigh number natural convection and the like. In such cases, it is necessary to pack the mesh in regions of high gradient to resolve the pressure variation adequately.

Assumption of normal pressure gradient at the wall is zero has contributed to error. This is valid for boundary layers but not in the presence of body forces or curvature. Again, the failure to correctly account for the wall pressure gradient is manifested in velocity vectors pointing in/ out of walls.

4.1.4.3 Discretization of the Continuity Equation

Equation 4.1 can be integrated over the control volume to yield the following discrete equation:

$$\sum_{f}^{N_{faces}} J_f A_f = 0 \tag{4.5}$$

where J_f is the mass flux through face f, ρv_n.

It is necessary to relate the face values of velocity, $\vec{v_n}$, to the stored values of velocity at the cell centers. Linear interpolation of cell-centered velocities to the face results in unphysical checker-boarding of pressure. The face value of velocity is not averaged linearly; instead, momentum-weighted averaging, using weighting factors based on the a_p coefficient from Equation 4.3 is performed. Using this procedure, the face flux, J_f, may be written as

$$\begin{aligned} J_f &= \rho_f \frac{a_{p,c_0} v_{n,c_0} + a_{p,c_1} v_{n,c_1}}{a_{p,c_0} + a_{p,c_1}} + d_f((p_{c_0} + (\nabla p)_{c_0} \cdot \vec{r_0}) - (p_{c_1} + (\nabla p)_{c_1} \cdot \vec{r_1})) \\ &= \hat{J}_f + d_f(p_{c_0} - p_{c_1}) \end{aligned} \tag{4.6}$$

where p_{c_0}, p_{c_1} and v_{n,c_0}, v_{n,c_1} are the pressures and normal velocities, respectively, within the two cells on either side of the face, and $\hat{J}_f$ contains the influence of velocities in these cells. The term d_f is a function of $\bar{a}_p$, the average of the momentum equation a_p coefficients for the cells on either side of face *f*.

4.1.5 Pressure-Velocity Coupling

Pressure-velocity coupling is achieved by using Equation 4.7 to derive an additional condition for pressure by reformatting the continuity equation. The pressure-based solver solves the flow problem in either a segregated or coupled manner.

$$\int_A n \cdot (\rho u \psi) dA - \int_A n \cdot \left(\Gamma \frac{d\psi}{dx} \right) dA = \int_{CV} \varphi dV \tag{4.7}$$

where A is the area of control volume surfaces, while n is the outwardly directed normal unit vector.

4.1.6 SIMPLE Algorithm

The SIMPLE algorithm uses a relationship between velocity and pressure corrections to enforce mass conservation and to obtain the pressure field.

If the momentum equation is solved with a guessed pressure field *p**, the resulting dace flux, J_f^*, computed from Equation 4.7

$$J_f^* = \hat{J}_f^* + d_f \left(p_{c0}^* - p_{c1}^* \right) \tag{4.8}$$

does not satisfy the continuity equation. Consequently, a correction $J_f^{'}$ is added to the face flux J_f^* so that the corrected face flux, Jf

$$J_f = J_f^* + J_f^{'} \tag{4.9}$$

satisfies the continuity equation. The SIMPLE algorithm postulates that $J_f^{'}$ be written as

$$J_f^{'} = d_f (p_{c0}^{'} - p_{c1}^{'}) \tag{4.10}$$

where p' is the cell pressure correction.

The SIMPLE algorithm substitutes the flux correction into the discrete continuity equation to obtain the pressure correction p' in the cell:

$$app' = \sum_{nb} a_{nb} p_{nb}^{'} + b \tag{4.11}$$

where the source term b is the net flow rate into the cell:

$$b = \sum_{f}^{N_{faces}} j_f^* A_f \tag{4.12}$$

The pressure-correction equation may be solved using the algebraic multidrig method. The cell pressure and the face flux are corrected using

$$P = p^* + \alpha p \, p' \tag{4.13}$$

$$J_f = J_f^* + d_f (p_{c0}^{'} - p_{c1}^{'}) \tag{4.14}$$

Here αp is the under-relaxation factor for pressure. The corrected face flux, J_f, satisfies the discrete continuity equation identically during each iteration.

4.2 DOMAIN DISCRETIZATION

The computational domain for the CFBG is shown in Figure 4.2. The heights of the domains are 1.8m for all the simulations. The diameter of CFBG is 0.66m. Geometry and grids are created in a CAD program called GAMBIT 2.2.30 and exported into FLUENT 6.2.16. In order to capture all the flow characteristics it is decided to use a three- dimensional structure to represent the CFBG. This gives rise to an increase in computational effort/time, but it is recommended (Benyahia, 1999; van Wachem, 2000) to do this in order to get feasible simulation results when working with gas-particle flows. The resulting grid is shown on Figure 4.2. The tetrahedral grid with medium size grid (of 10 particles size and with gradual increment of 1.8 after riser height) has been constructed over a period of 2 weeks, and consists of 1, 441,056 cells. The grid spacing

was distributed non-uniformly; more cells were placed for an overall bed height of 0.5m to capture the complex flow behavior of that part. For two-dimensional simulations, a two-dimensional tetrahedral grid with medium size grid (of 10 particles size) which consists of around 5120 cells was employed.

The governing equations are solved using the finite volume method, where the partial differential equations are defined in volume integral form. The SIMPLE algorithm of multiphase flows by Patankar (1980) was used for pressure-velocity coupling and correction. Typically, a time step of 0.001s with 100 iterations per time step was also used. This number of iterations was found to be adequate to achieve convergence for the majority of time steps. During the first 3.5s, the flow behavior in CFBG was recovering from chaotic transient condition until quasi-steady-state conditions were reached. Therefore, the time averaged distributions of flow variables were computed after reaching the steady state conditions, which is 4s onwards. A convergence criterion of 0.001 was specified for the relative error between two successive iterations. 3D simulations are performed as they are prone to provide more realizable continuum characteristics of the fluidization. Moreover, 3D simulations are preferable with the condition of availabilities of high computing facilities as well as in the cases where the flow itself is not mainly governing as a two dimensional flow.

In this paper an approximate calculation of the normal velocity at the interfaces (defined by a small threshold value for the phase volume fraction) was used. Gas-Solid flows are inherently unstable, so, for vast majority of Gas-Solid flows, a transient simulation analysis was conducted and the results were time-averaged. Transient simulations diverge if a large time-step is used. Using a very small time step makes the computations very slow. Therefore, the time step was automatically adjusted to reduce the computational time.

The first order upwind scheme was used for discretization of the governing equations. The computational domain was divided into a finite number of control volumes. Volume

fraction and density were stored at the main grid points that were placed in the center of each control volume. A staggered grid arrangement was used, and the velocity components were solved at the control volume surfaces. The conservation equations were integrated in the space and time. The sets of resulting algebraic equations were solved iteratively (Gidaspow, 1994; Kunii and Levenspiel, 1991; Ranade, 2002; Patankar, 1980; Grace and Taghipour, 2004; Bird et al., 2002)

The following steps were followed in the simulations:

1. Initially the physical properties and exchange coefficients are calculated.
2. Velocity fields based on the current pressure field and the corresponding u_m^* , v_m^* (m = 0, 1 for solid and gas phases) are evaluated.
3. The fluid pressure correction $P_g^{'}$ is calculated.
4. The fluid velocity corrections from $P_g^{'}$ are evaluated, and the fluid velocity fields are updated using $u_m = u_m^* + u_m^{'}$.
5. The pressure gradients $\partial P_m / \partial \varepsilon_m$ are evaluated for use in the solid volume fraction correction equation.
6. The solid volume fraction correction $\varepsilon_m^{'}$ is evaluated.
7. The solid volume fraction is updated.
8. The velocity corrections for the solid phase are estimated and the solid velocity fields are updated. That is $u_s = u_s^* + u_s^{'}$.
9. The solid pressure is evaluated.

The normalized residuals calculated in Steps 2, 3, 4, and 8 are used to check for convergence. If the convergence criterion is not satisfied, then the iterations starting with Step 2 are repeated.

4.3 INITIAL BOUNDARY CONDITIONS

At the inlet the velocity inlet boundary condition with uniform superficial velocity of the gas phase was set. At the outlet the pressure outlet boundary condition was set for the

mixture phase and the height of the free board was made long enough so that fully developed flow was achieved for the gas phase. Zero-gradient boundary conditions (Neumann boundary conditions) are applied to the outlet velocities.

$$\frac{\partial u}{\partial x}(x,t) = \beta(t) \tag{4.15}$$

where $\beta(t)$ = 0. The bottom of the reactor is a velocity inlet and follows the Dirichlet boundary conditions:

$$u(x, t) = a(t) \tag{4.16}$$

where a(t) equals a constant. While the superficial velocity of the gas is specified as uniform across the inlet, the solid volume fraction at the inlet is specified as 0, where the solids are impenetrable at the distributor.

At the walls the gas phase was assumed to have a no-slip boundary condition. The pressure in the mesh cells at the top of the bed are fixed at a specific value (1.01 x 10^5 Pa). At the bottom o the bed the gas inflow is specified.

The values used for the parameters needed in the simulations are shown in Table 4.1. Air at ambient temperature and pressure is used for the fluidizing gas. The gas is treated as compressible and thus the density is coupled to the pressure, according to the ideal gas law. Particles of uniform size which belongs to Geldart B as heat carrier were used in this work.

Table 4.1 Computational Model Parameters

Description	Type/ value	Comments
Inlet	Velocity-inlet	Uniform distribution for gas phase
		No particles enter for solid phase
Outlet	Pressure-outlet	Atmospheric
Wall	Stationary wall	No slip for gas phase
		Zero shear stress for solid phase
Coefficient of restitution	0.9	Fixed value
Time step	0.001s	Specified
Iterations per time step	100	Specified
Convergence criterion	0.001	Specified
Under-relaxation factors		
Pressure	0.6	Specified
Momentum	0.7	Specified
Volume fraction	0.3	Specified
Granular temperature	0.2	Specified

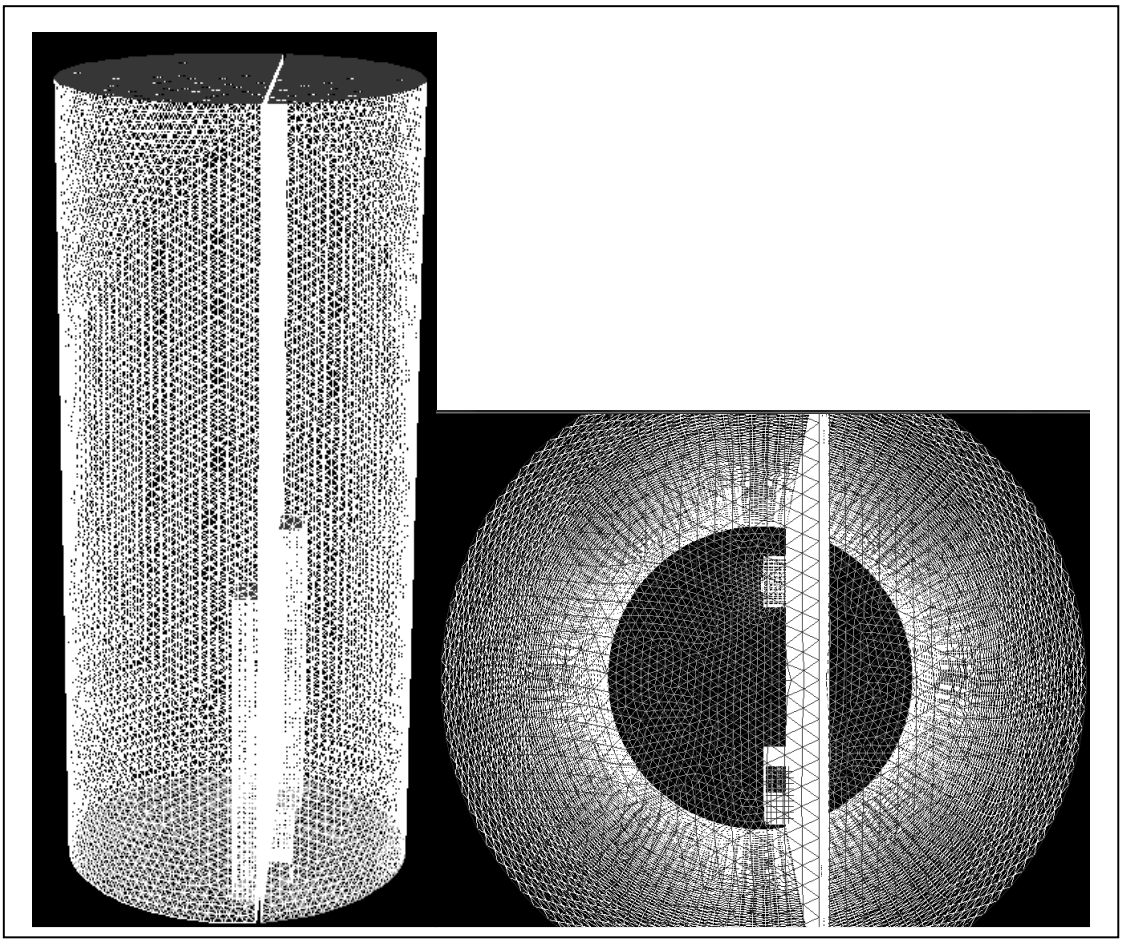

Figure 4.2: Three-Dimensional Grid Used for the Simulations

CHAPTER 5
METHODOLOGY AND EXPERIMENTAL TECHNIQUE

5.1 INTRODUCTION

This chapter details the research methodology employed to achieve the objectives as outlined in Chapter 2, along with explanations on the experimental and modeling techniques used. An overview for the overall research methodology for the present study as well as the general methodology for achieving each of the specific objectives proposed in Chapter 2 is presented here.

5.2 WORKING PRINCIPLE OF CFBG WITH REACTIONS

CFBG as proposed by Rudolph et al. (1985) is divided into two discrete compartments, which is the combustor and gasifier respectively, where the combustor is typically larger than the gasifier to ensure sufficient heat supply to the gasification reaction. During hot operation, combustion and gasification reactions take place in the combustor and gasifier accordingly. Both compartments in CFBG operate in bubbling fluidized mode and therefore can be further categorized as dense bubbling phase and lean dispersed phase. Dense bubbling phase is referred to the fluidizing solid zone where the axial bulk density remains virtually constant, contrary to the lean dispersed phase where the bulk density gradually decreases.

In CFBG, fluidized solid flows freely between the compartments but the gaseous streams are strictly separated. The solids in the combustion compartment burn with air to raise the solid temperature. The hot solids are then transferred into the gasification compartment and react with steam to produce high-energy syngas. This allows the flue gas from combustor consisting mainly the CO_2 and N_2 to be removed separately from

the gasification product gases such as H_2, CO and CO_2, and thereby avoids the difficulty of gas separation to obtain high quality product gas even from air-blown gasifier. The solid circulation between the compartments allows heat transfer between combustion and gasification process.

The solid circulation mechanism of CFBG depends on two v-valves and two risers, one in each compartment. An isometric view of this arrangement is given in Figure 5.1. V-valve is a type of non-mechanical valve that is typically used in conventional CFB system to transport solids (Liu, 1980). It uses aeration gas to control the solid flow. Riser, on the other hand is a long pipe where it functions coherently to pneumatically transport the solid to other compartment. Liu (1980) claims that a v-valve provides an exceptional sealing against back pressure surges. The details of solid circulation mechanism will be explained later.

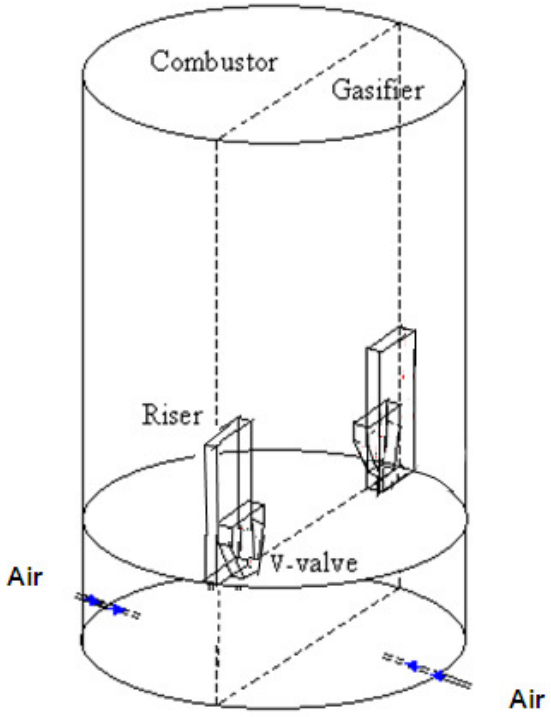

Figure 5.1: The isometric view of the CFBG

5.3 CFBG COLD FLOW MODEL

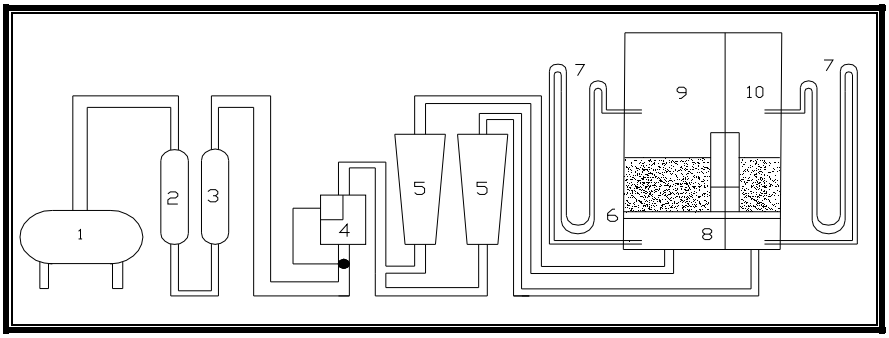

Figure 5.2: The schematic diagram of CFBG cold flow model
(1- Compressor; 2- Refrigeration; 3- Dryer; 4- Pressure regulator; 5- Rotameter; 6- Distributor; 7- Manometer, 8- Plenum; 9- Combustor; 10 – Gasifier)

The experimental set up is shown in Figure 5.2. The CFBG is custom-made by the mild steel as the body structure and Perspex material as the cover to ease the visual observation during the experiment. The overall diameter of the CFBG is 0.66m with a height of 1.8m and plenum height of 0.20m, partitioned into two compartments, namely the combustor and the gasifier by a vertical diving wall in a ratio of 65:35 respectively based roughly on the stoichiometric and energy balance requirements for biomass gasification and combustion. Both of the compartments were fluidized using air (air was not supplied to V-valve and riser). The maximum air supply was 3,500 l/min. Rotameters were used to regulate the air flowrates to maintain bubbling mode of fluidization. The accuracy of the flowrate measurement is of ±5%.

Combustor or gasifier compartment is neither a full cylindrical nor semi-cylindrical but rather a segment of a cylindrical. It is crucial to find the equivalent or effective diameter for this type of CFBG reactor with non-uniform and uncommon shape. Hence, the effective diameter, D_e as stated in Nicholas and Paul (1984), is representatively used in this study (Equation 5.1).

$$D_e = 4 \times \frac{mean\ cross\ \text{sec}tional\ area\ of\ \ flow\ channels\ through\ bed}{mean\ wetted\ \ perimeter\ of\ \ flow\ channels} \tag{5.1}$$

The effective diameter for combustor and gasifier is 0.413m and 0.257m correspondingly (refer Appendix A for detailed effective diameter calculations). The presence of v-valve and riser in both compartments has been addressed when considering the effective bed diameter.

Perforated plate distributor with orifice diameter of 3mm is used due to its simplicity and low cost to uniformly distribute the fluidizing agent, ambient air into the beds of particle at free area of 0.27% and 0.32% in triangular pitch arrangement for gasifier and combustor accordingly and to ensure good quality of fluidization. The ratio, R_c, the critical distributor pressure drop to the bed pressure drop, will be used as the minimum attainable and reliable ratio for counterchecking with the operating ratio, R_{op}, to ensure distributor satisfactory and acceptable performance. The values of R_c can be determined using an empirical correlation (Equation 5.2) that was developed by Qureshi and Creasy (1979).

$$R_c \geq 0.01 + 0.2[1 - \exp(-0.5 D_e / H_{mf})] \tag{5.2}$$

Distributor free area is the percentage of the area that is occupied by the orifices, which is defined in Equation 5.3.

$$\text{Free area} = \frac{Total\ Orifices\ Area}{Distributor\ Plate\ Area} \times 100\% \tag{5.3}$$

100 micron mesh is employed on top of the distributor to avoid particles weeping through the orifices.

5.4 EXPERIMENTS IN SINGLE COMPONENT SYSTEM

5.4.1 Bed Pressure Drop Measurement

The bed pressure drop (ΔP_b) of combustor and gasifier was measured by the water manometer with the accuracy of ±0.1 cmWg. Three water manometers are connected at each compartment, located at the plenum, 1cm above the distributor and 70cm above the distributor to measure the total pressure drop (ΔP_t), across the distributor (ΔP_d) and bed (ΔP_b) accordingly. The mesh disturbance to the fluidized bed system was examined by measuring the pressure drop between the plenum and position slightly above distributor simultaneously during experiment.

5.4.2 Minimum Fluidization Velocity (U_{mf}) Determination

The experiments were first conducted using pure sand only as the bed material. This is important in order to check whether the fluidization behavior, particularly the bed pressure drop profile in CFBG is distinctive from those usually observed in the fluidized bed of cylindrical shape using common bed material. Besides that, the characteristic velocities obtained in this condition provide the operating parameters for the CFBG when the presence of other bed material (e.g. biomass) is very small or negligible.

The procedures to attain U_{mf} are shown as below:

1. Check the water manometer level for empty compartment.
2. Load the sand (weigh the mass) to the desired bed height.
3. Start airflow to the system gradually.
4. Record the manometer level for each flowrate.
5. Increase the air flowrate further when constant pressure drop is obtained to include the extended constant pressure drop line in the pressure drop vs. velocity graph.
6. U_{mf} is attained at the interception between the increasing pressure drop line and the constant pressure drop line as shown in Figure 5.3.

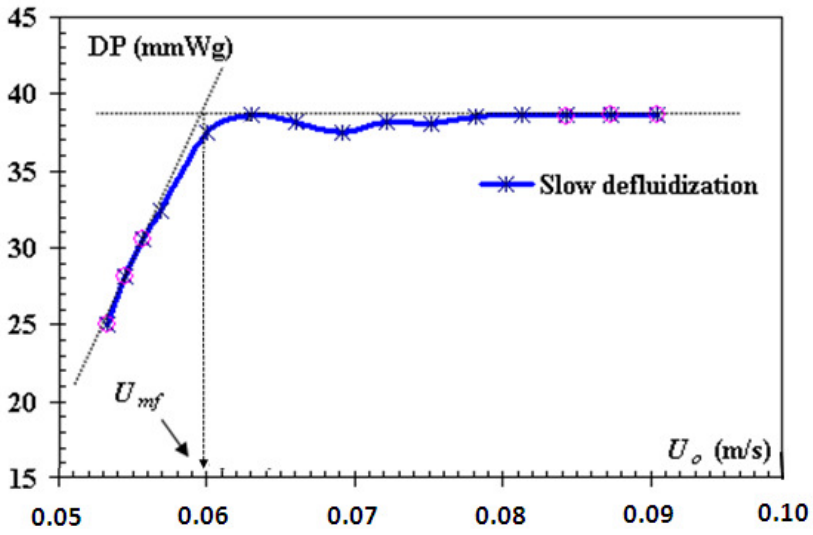

Figure 5.3: Typical sand bed pressure drop profile for U_{mf}

The typical bed pressure drop profile shown Figure 5.3 is obtained from river sand of mean size 272μm in the gasifier. Similar bed pressure drop profile is obtained for alumina for U_{mf} determination. Hence, it is confirmed that the bed pressure drop profile obtained from CFBG is very similar to those from a cylindrical column of laboratory scale. A summary of U_{mf} for river sand and alumina used in the study is shown in Table 5.1.

Table 5.1: Summary of U_{mf} for different sizes of particles

Type	**d_p (μm)**	**U_{mf} (m/s)**
River Sand	272	0.060
Alumina	360	0.154

5.4.3 Bed Expansion Measurement

The bed starts to expand when the gas supplied reached its minimum fluidization velocity. Further increasing the superficial gas velocity, it will reach a critical value at which the upward drag forces will exactly equal the downward gravitational forces,

causing the particles to become suspended within the fluid. The steps to measure the bed expansion are illustrated as follow:

1. The bed is loaded with sand to the desired bed height.
2. Start airflow to the system gradually.
3. Bed height is observed visually with the aid of measuring tapes situated at the side of the column wall of each compartment.
4. Bed height is recorded for each flowrate.

The accuracy of bed expansion is ±0.1cm.

5.4.4 CFBG Detailed Solid Circulation Working Mechanism

In this section, the two compartments are connected for the solid in the fluidized state to interchange internally via aeration to V-valve and riser pairs. The experimental setup used earlier (Figure 5.1) is equipped with four air rotameters for the aerations to the two pairs of V-valve and riser as shown in Figure 5.4.

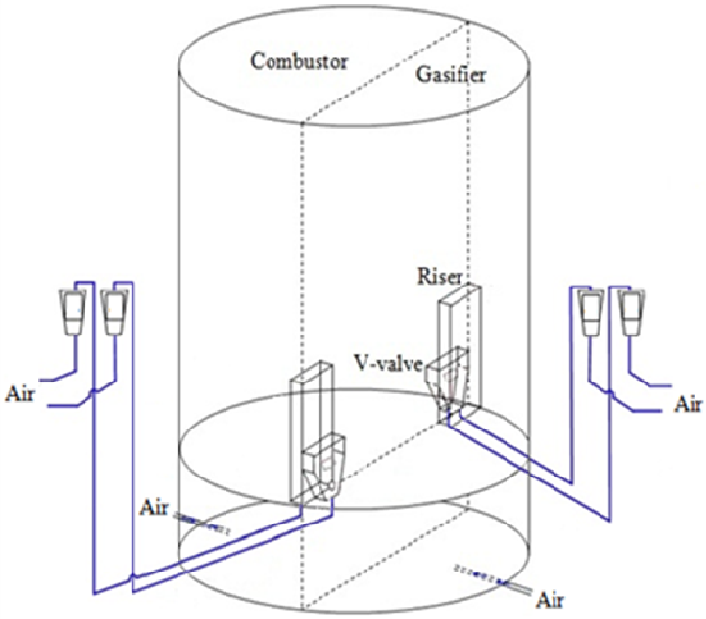

Figure 5.4: Isometric view of CFBG; the addition of air rotameters to V-valves and Risers

The geometrical details of the cold flow model are given in Table 5.2. It is expected that four operating variables, namely static bed height (H_b), aeration to the bed (Q_b), V-valve (Q_v) and riser (Q_r), to mainly affect the solid circulation rate in the CFBG.

As shown in Figure 5.5, V-valve and riser operates synergically according to this sequence:

1. V-valve pumps solid from the dense bubbling phase of one compartment (e.g. combustor).
2. Solid is then transport pneumatically through the riser.
3. It is finally discharged on the lean disperse phase of the other compartment (e.g. gasifier).
4. Similarly, the other set of v-valve and riser works simultaneously at the same time in the same way.

Table 5.2: Geometrical details of the CFBG cold flow model

Descriptions		
Reactor cross section	mm^2	108900π
Gasifier cross section	mm^2	38115π
Combustor cross section	mm^2	70785π
V-valve orifice diameter	mm	30
V-valve bottom cross section	mm^2	50×50
V-valve to riser inlet cross section	mm^2	50×100
Riser outlet cross section	mm^2	50×100
Riser height	mm	600
V-valve location	mm	On distributor
Riser location	mm	On distributor

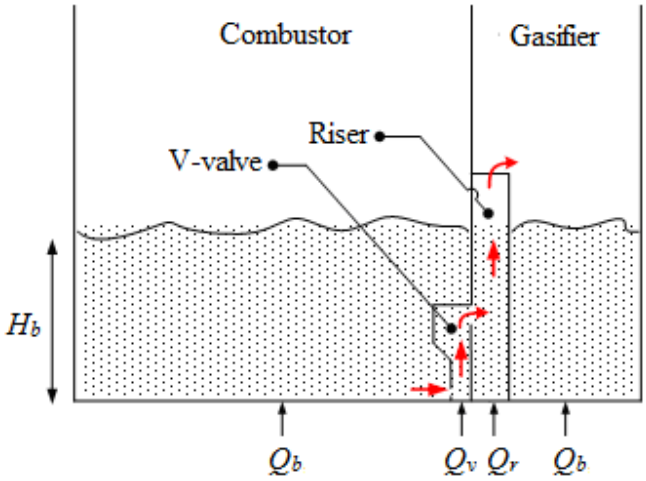

Figure 5.5: Schematic diagram of CFBG (red arrows showing the solid is transferred from the combustor to the gasifier)

5.4.5 Solid Circulation Rate Theory

In Sathiyamoorthy and Rudolph (1990) and He (1993) work, SCR measurements were conducted at visually observed constant bed height, what was regarded as the steady state condition i.e. The SCR is computed by direct collection of the entrained solids from the riser and taking the weight increased with time. It was Yan and Rudolph (1996) that highlighted the drawbacks on the approach above, namely (i) the bed height cannot be observed in high temperature reactor, (ii) direct collection of hot particles is extremely dangerous and difficult, and (iii) the bed temperature is also fluctuating significantly. Recognizing that the bed pressure drop is a function of bed inventory (hence bed height), and it is independent of the operating temperature, thus the author proposed the use of bed pressure drop and initial rate from the pressure response curve to measure SCR. Their empirical correlation predicted well for the SCR in both hot and cold conditions.

At the present work, both approaches (Sathiyamoorthy and Rudolph, 1990; He, 1993) are applied in cold experiments to evaluate the practicality in measuring SCR. For relatively high SCR, addition or collection of solids is difficult, as it requires an extremely large amount of solids and silo capacity even at the modest duration (e.g. for

SCR at 2,400 kg/hr, 10 minutes of solids collection is equivalent to 400 kg). Moreover, the difference in SCR between the two methods is less than 20%. Therefore, method in Yan and Rudolph (1996) is adopted to determine SCR.

Modification is made by introducing *K* value in Equation 5.4 on the pressure drop across the bed to a more generalized consideration of different geometrical parameters and/or particle properties effects. Besides that, the use of curve fitting is deployed to determine the initial rate of the pressure response curve.
In a bubbling fluidized bed, the bed pressure drop is given by

$$\Delta P_b = K\rho_s g H_b (1-\varepsilon_b) \tag{5.4}$$

where for compartmented reactor, experimental *K* values vary from 0.6 to 1.0 depending on the bed geometry and particle properties.

Given that $\rho_b = \rho_s(1-\varepsilon)$ and $\rho_b = \frac{m_s}{V_b}$, from Equation 5.4, it follows that

$$\Delta P_b = K\left(\frac{m_s g}{A_b}\right) \tag{5.5}$$

It is noted that the bed pressure drop functions in Equations 5.4 and 5.5 once established provide a convenient way to determine the bed mass or height in both cold and hot conditions.

Taking constant $k_1 = K\left(\frac{g}{A_b}\right)$, Equation 5.5 becomes

$$\Delta P_b = k_1(m_s) \tag{5.6}$$

where k_1 is the gradient of the curve of experimental bed pressure drop versus cumulative bed mass.

The differential form of the bed pressure drop defines the solid circulation rate

$$\frac{d(\Delta P_b)}{dt} = k_1\left(\frac{dm_s}{dt}\right) \tag{5.7}$$

where $\left(\frac{dm_s}{dt}\right)$ is the rate of solid transferred to or received from the other compartment.

When the solid circulation rate is at a steady state, there is no net change in ΔP_b while the solid is circulated between both compartments. By temporarily interrupting the solid transfers (i.e. shut off the V-valve and riser pair for one of the compartments), the differential bed pressure drop can be represented as

$$d(\Delta P_b) = -\Delta P_b\, dt \tag{5.8}$$

The negative sign represents the decrease of the differential bed pressure drop for the compartment that is transferring the solid. On the other hand, positive sign is used to characterize the pressure change in the compartment that is gaining the solid.

From Equation 5.8, the initial rate of the pressure response curve can be found by fitting the data in exponential function as

$$\Delta P_b = k_2 e^{-k_3 t} \tag{5.9}$$

This has been confirmed in all the experiments carried out in the present study where each set of the experimental data can produce a good linear fit ($R^2 \approx 1$) in

$$\ln(\Delta P_b) = -k_3 t + \ln k_2 \tag{5.10}$$

Then, differentiating the exponential function and setting $t \rightarrow 0$,

$$\left.\frac{d(\Delta P_b)}{dt}\right|_{t\rightarrow 0} = k_2 k_3 \tag{5.11}$$

where k_2 and k_3 are determined experimentally from the curve of natural logarithmic bed pressure drop versus time.

The initial value of solid circulation rate (SCR) just after the interruption is essentially the solid circulation rate at a steady state, or $SCR = \left(\frac{dm_s}{dt} \right)\Big|_{t \to 0}$.

Thus, by combining Equations 5.7 and 5.11, it follows that

$$SCR = \frac{k_2 k_3}{k_1} \tag{5.12}$$

5.4.6 Solid Circulation Rate Measurement

Solid circulation rate (SCR) is computed from the k values. To find k_1, k_2 and k_3 respectively, two different experimental plots are required, namely (i) bed pressure drop versus cumulative bed mass and (ii) pressure response curve. Both the experimental procedures are described here and can be implemented either on the combustor or gasifier to determine the solid circulation rate.

The plot of the bed pressure drop versus cumulative bed mass is obtained by measuring the bed pressure drop, ΔP_b when a known solid (sand) mass is added to the compartment in a fluidized state. The data is recorded until the bed inventory reaches the required bed height. Figure 5.6 shows the gradients, indicated as k_1 for the combustor and gasifier are 0.41 and 0.68 cmWg/kg respectively.

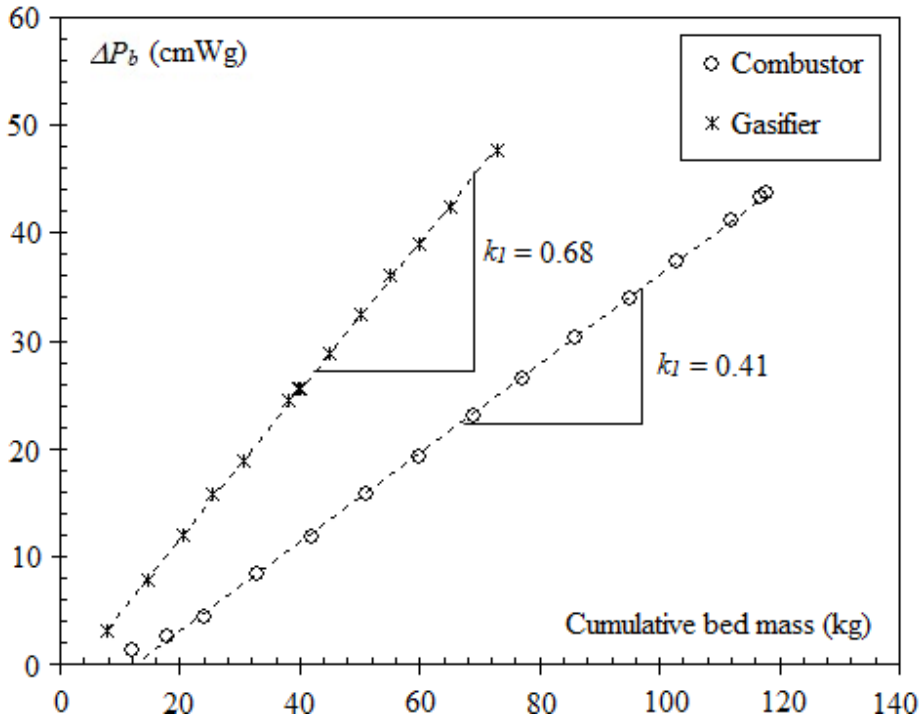

Figure 5.6: Typical bed pressure drop versus cumulative bed mass for river sand

On the other hand, the steps to obtain the pressure response curve are as follows:

(i) the solid of a known mass is filled to the same bed height in both of the compartments.

(ii) aerations to the bed, V-valve and riser pairs in both compartments are configured to the required settings as stated in Table 5.2.

(i) solid circulation between the compartments is allowed to occur until a steady state (no net change in bed pressure drop or expanded bed height in both compartments) is achieved.

(ii) solid circulation is then interrupted by shutting the aerations to a pair of the V-valve and riser only[1].

[1] The compartment without the V-valve and riser aerations will exhibit an upward trend on its pressure response curve since it is gaining solid. In contrast, the other compartment will show a downward trend since it is losing solid.

(iii) Once sufficient data is collected for the pressure response curve, aerations to the closed V-valve and riser are resumed to the required settings as in (ii) to restore the steady state solid circulation rate and bed pressure drop.

(iv) A new set of configurations is introduced and steps (i) to (v) are repeated.

The typical pressure response curve presented in natural logarithmic ΔP_b versus time function is shown in Figure 5.7. In this example, the product of k_2 and k_3 is equal to 0.197 cmWg/s. It can be seen that the pressure response curve has a good linear fit in the exponential form. This is found on all the experiments where $R^2 \approx 1$.

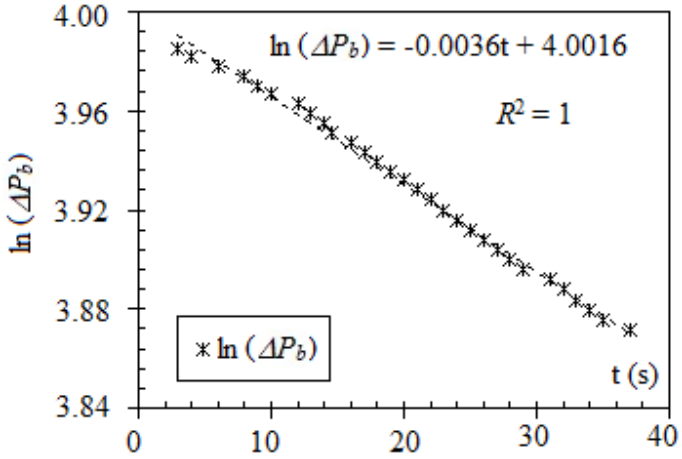

Figure 5.7: Typical pressure response curve in the gasifier

$H_b = 0.4$ m, $Q_b = 1.7\ U/U_{mf}$, $Q_v = 5\ U/U_{mf}$, $Q_r = 8\ U/U_{mf}$

5.5 EXPERIMENTS IN BINARY MIXTURE SYSTEM

The as-received palm shell size distribution is shown in Figure 5.8. The biomass residuals were obtained from a palm oil mill and underwent natural drying prior utilization. The final moisture content was found to be 8–10 wt%. The palm shell was then sieved to check its size distribution. It can be clearly seen that the biomass consists mostly larger particles of 3.56 and 7.13 mm. 3 different sieved sizes of palm shell (1.77mm, 3.56mm, 7.13mm) are used in this study, excluding the smallest palm shell that mostly consists of loose fiber. The physical properties of the sand and palm shell are given in Table 5.3.

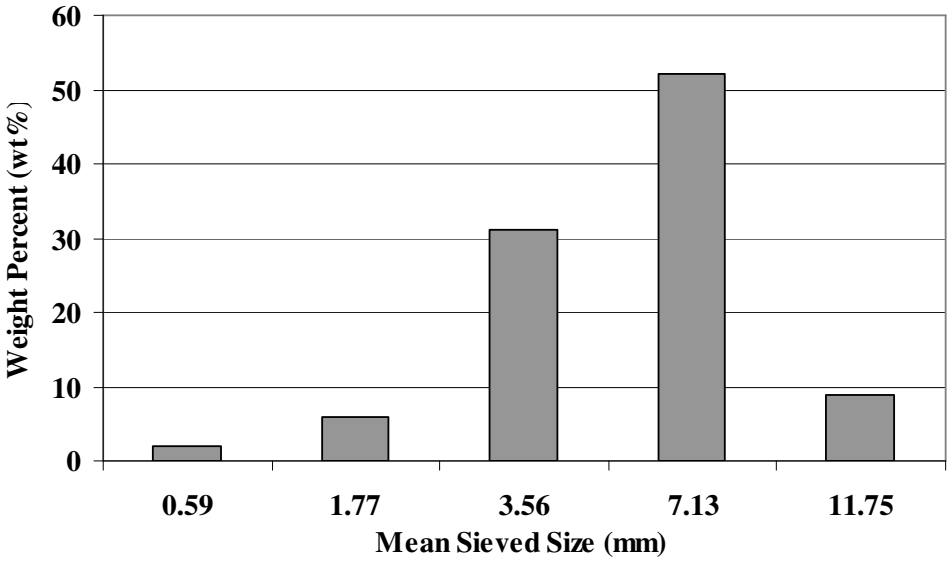

Figure 5.8: Palm shell size distribution

Table 5.3: Palm shell and sand properties

	Palm Shell	Sand
Particle Diameter /Sieved ranged (mm)	1.77/(+1.18-2.36)	0.196
	3.56/(+2.36-4.75)	0.272
	7.13/(+4.75-9.50)	0.341
		0.395
Density (kg/m3)	1500	2700
Moisture (%)	8-10%	-
Weight Percent (wt %)	5, 10, 15%	-

5.5.1 Binary Mixture Minimum Fluidization Velocity (U_{mf}) Determination

Palm shell is considered as Geldart D particle, a classification for spouting bed material. However, mixing palm shell with a second fluidizable material (sand) can facilitate proper fluidization, as observed by Fauziah et al. (2008). It has been confirmed in experiment that as-received palm shell cannot be fluidized solely. In the present study,

palm shell of various mean particle sizes and weight percent have been added to the river sand whose fluidization characteristics have been previously determined.

The U_{mf} of binary mixture system is determined using the same method as for single component system, i.e. using the bed pressure drop profile. The summary of binary U_{mf} for different wt% of palm shell and palm shell size and river sand is shown in Table 5.4.

Table 5.4: Binary U_{mf} at Different Binary Mixture System

Type	Binary U_{mf} (m/s)
River sand + 5 wt% palm shell (3.56mm)	0.078
River sand + 10 wt% palm shell (3.56mm)	0.082
River sand + 15 wt% palm shell (3.56mm)	0.084
River sand + 10 wt% palm shell (1.77mm)	0.084
River sand + 10 wt% palm shell (7.13mm)	0.079

5.5.2 Binary Mixture Mixing Measurement

The sand-palm shell mixing studies are performed using the experimental setup as described in the preceding section. The bed materials used are the sand mean particle size of 272 μm and palm shell of 3 mean sieve sizes namely 1.77, 3.56 and 7.13 mm comprising of 5, 10 and 15 wt%. All the experiments are conducted at constant total bed weight of 77 kg, except for the study on the effect of the bed height on the mixing quality.

Prior to the experiments, the sand is filled into the respective compartments to a desired weight/height. The compartments are tapped until the sand is compacted. Palm shells are then uniformly loaded on the top of the sand bed forming two segregated layers. This approach is selected to track palm shell migration and it also represents top-bed feeding. Starting from the fixed bed state, the experiments are initially performed by increasing

the superficial velocity in the specified range. Once the maximum superficial velocity is achieved, the experiments are then continued by decreasing the superficial velocity. These procedures allow samples to be taken in two directions i.e. at increasing and decreasing superficial velocities. It exemplifies the typical mode of operation in a bubbling fluidized bed combustor/gasifier where the operating superficial velocity is initially increased to promote fuel mixing during the plant startup; as the fluidized bed reaches a higher bed temperature e.g. 800°C - 900°C, the operating superficial velocity is reduced to about 1/3 of the requirement at the ambient condition (Yan, 1995). The flow rates are regulated between $1U_{mf}$ - $2.5U_{mf}$ by rotameters to maintain the bubbling mode of fluidization.

5.5.2.1 Sampling Method

"Thief" probe and sieving method is preferred due to the following advantages: (i) fast response (ii) able to collect sample while the bed is fluidized (iii) able to collect sample at different locations in the bed (iv) able to collect the sample in a number of time under various operating conditions.

"Thief" probe operates by imbedding it vertically in the fluidized bed at a set location. A sampling container (commonly known as the end-cup sampler), located at the end of the probe, is initially at closed position during the insertion into the fluidized bed. Once insertion is complete, its enclosure cap is opened allowing solids to flow into the end-cup sampler. It is then closed and the probe is withdrawn from the bed. The collected mixtures are sieved and weighed to determine the component weight fraction. Once measured, the mixtures are returned to the fluidized bed for the subsequent sampling exercise.

The thief probe and the end-cup sampler sizes are kept to the minimum to minimize the interference with the flow pattern. Here, the thief probe is made of a thin rectangular plate of 25 mm wide and 2 mm thick. The cylindrical end-cup sampler is of 50 x 50 mm in diameter and length respectively, i.e. large enough for the solid to enter but small

when compared to the compartment diameter. The enclosure cap of the end-cup sampler is maneuvered by a 2 mm ID rod.

Solid sample is collected using thief probe, from 3 different sections (v-valve, center and riser) in 3 different levels (L1-L3 indicating top, center, bottom), which constitutes 9 imaginary cells (*n*) shown in the Figure 5.9. Meanwhile, 3 repetitive data are collected from each cell, with the sampling interval of 5 minutes each, to allow for re-establishment of mixing state after the previous sampling. Shen et al. (2007) and Zhang (2008) observed that equilibrium mixing in fluidized bed is attained within 1 minute. The sampling weight measurement has the accuracy of ±0.005%.

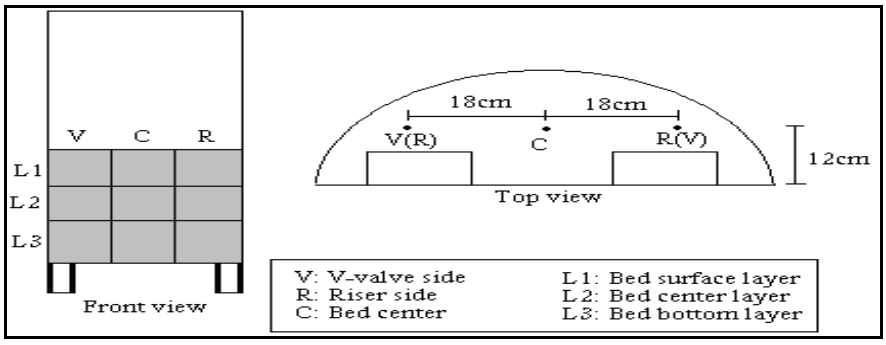

Figure 5.9: Sampling points in gasifier. Brackets "( )" represent combustor side

5.5.3 Binary Mixture Mixing Measurement in Numerical Simulation

In numerical simulation, the gasifier is also divided into 9 imaginary points for binary mixing data collection as described in Figure 5.9. Numerical simulation provides the information about the palm shell volume fraction at particular imaginary points, palm shell mass fraction is then determined from

$$\rho = \frac{m_{PS}}{V_{PS}} \tag{5.13}$$

where ρ is the density of palm shell, m is the mass fraction of palm shell and V is the volume fraction of palm shell.

CHAPTER 6 NUMERICAL VISUALIZATION OF FLUIDIZATION HYDRODYNAMICS IN CFBG

6.1 INTRODUCTION

This chapter presents the numerical visualization of fluidization behavior of single component (river sand only) and binary mixture system (palm shell + river sand) in CFBG. It is essential to provide information on flow pattern which are useful for understanding of the transfer processes and their peculiarities in terms of particle movement and bubble formation. The qualitative analysis of integral characteristic results are presented in two and three-dimensional visuals. Some common features of the flow are able to be captured by two-dimensional simulation; however the effects of riser and v-valve on fluidization can only be captured by three-dimensional simulation.

6.2 SINGLE COMPONENT SYSTEM SOLID VOLUME FRACTION FLOW PATTERN

6.2.1 Two-Dimensional Flow Pattern at Gasifier

Figure 6.1(a) & (b) shows the two-dimensional contour plots of solids fraction for the single component (river sand of mean particle size 272μm) gas-solid fluidized bed at the gasifier compartment. This sand size is selected due to the majority of sieved size in this range.

The static bed height is set at 0.35 m which is sufficient to observe the bubbling fluidization behaviour of the bed. The bed is impulsively fluidized at 2 U_{mf} at time 0.0 s. The U_{mf} of river sand is determined from our experiment to be 0.06 m/s. When palm shell is added to the bed, The U_{mf} of binary system will easily reach 1.5 U_{mf} – 3 U_{mf}

depends on the percentage of palm shell added. Therefore, fluidizing the bed at 2 U_{mf} is desirable.

The color contour starts to change at 0.25s showing that the bed starts loosening when the gas percolates through the solid interstitials. Pool of small bubbles start to form at 0.5 s. The small bubbles "randomly" develop near the gas distributor and then lift off. When bubbles slowly rise through the bed, the bed expanded mainly from the larger space between the interstitials due to all excess superficial gas velocity above the minimum fluidization velocity. It is observed that the bed continues to expand smoothly with bubble formation until it levels off at a steady state bed height at time around 1.75s to 2.00s. At this point, the bed has expanded 39% from its initial static height. Comparison of two versus three-dimensionally simulated bed height will be discussed in the following section.

To analyse the bubbles, a void fraction of solids has to be chosen as a cut off for determining the bubble boundaries. The computational cells having solid volume fraction less than the value of 0.4, are considered as bubbles, while the other ones are considered as the emulsion phase (Hulme et al., 2005).

From the plots, it can be seen that when these small bubbles move upwards, they tend to coalesce to form bigger bubbles. This is due to several reasons. As they travelled up the bed, the hydrostatic pressure on the bubbles decreases, therefore bubbles grow towards the bed surface. Also, bubbles may coalesce with bubbles which are side by side. Bubbles grow by depleting the continuous phase locally. Finally, the larger bubbles reach the freeboard and erupt at the bed surface. The chaotic bubble formation cease and steady bubbles form after 1.25s with steady profile.

Based on this analysis, the CFD results should be taken after 2 s of simulation. In all, 21 time step results have been presented for the solids volume fraction contour profile analysis in Figure 6.1.

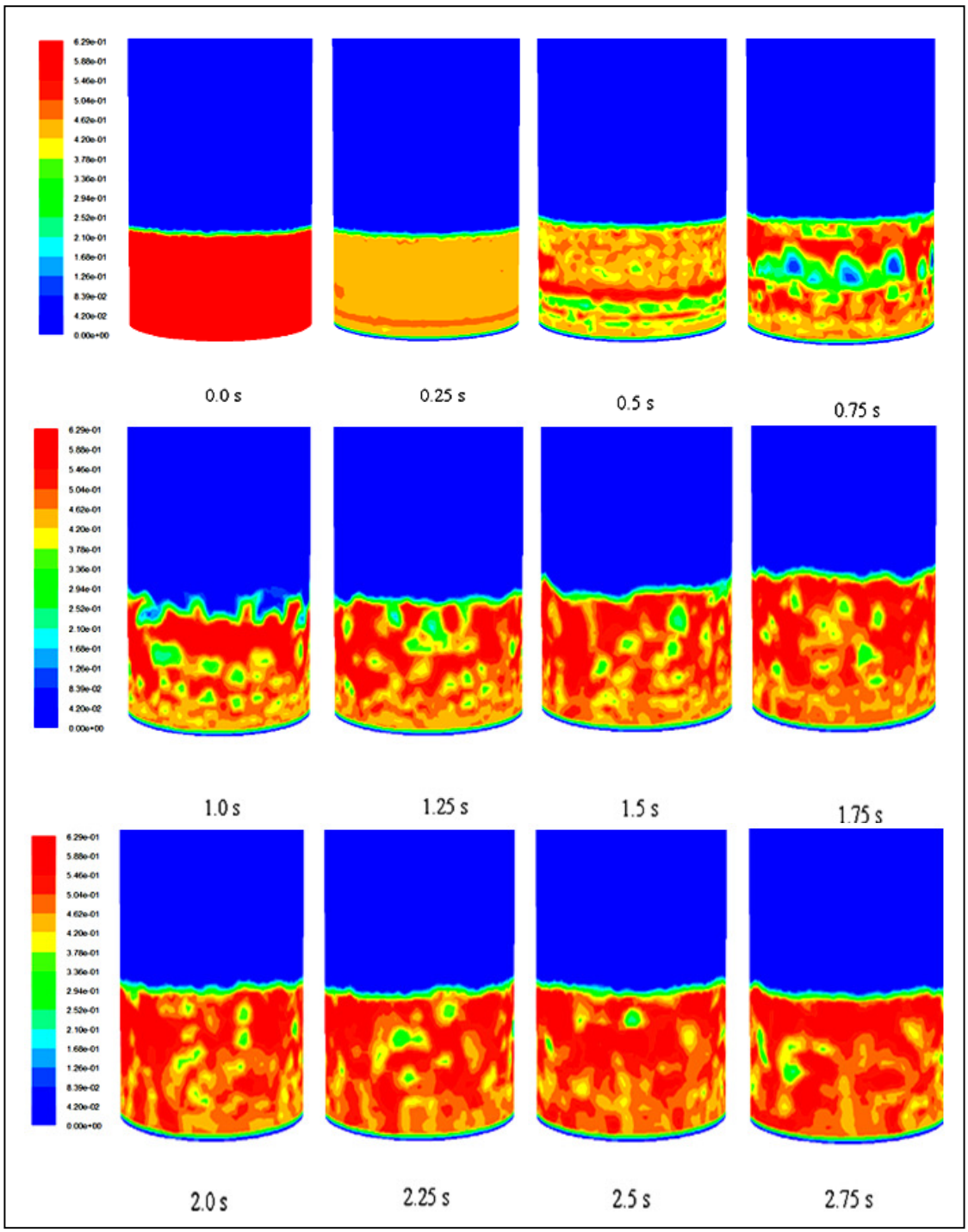

Figure 6.1(a): Simulated solids volume fraction flow pattern of two-dimensional bed at various times (U = 0.12 m/s, i.e. 2 U_{mf}, river sand 272 µm) (t= 0.0 s – 5.0 s with 0.25 s successive interval)

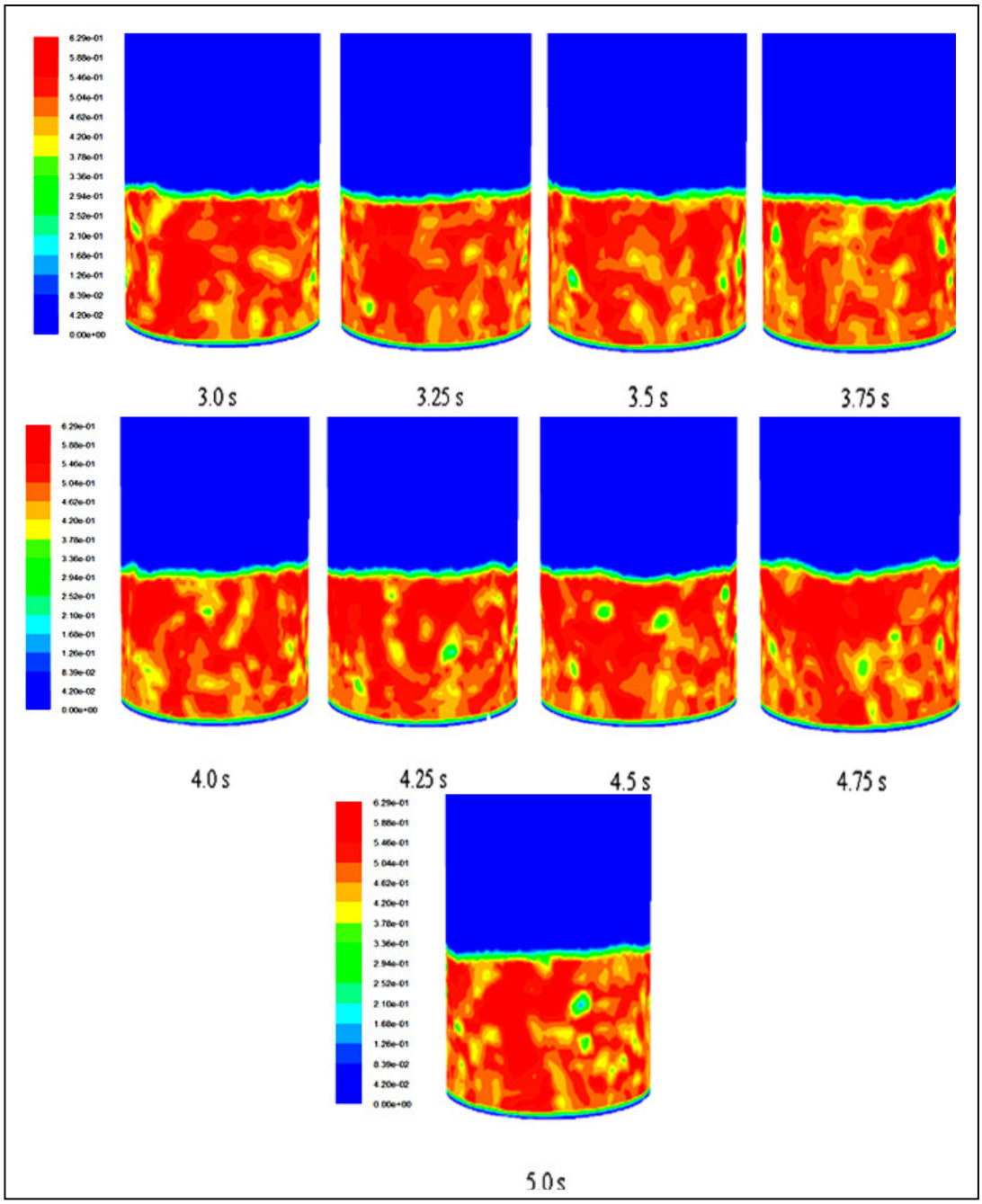

Figure 6.1(b): Simulated solids volume fraction flow pattern of two-dimensional bed at various times (U = 0.12 m/s, i.e. 2 U_{mf}, river sand 272 µm) (t= 0.0 s – 5.0 s with 0.25 s successive interval)

6.2.2 Three-Dimensional Flow Pattern at Gasifier

Figure 6.2 depicts the three-dimensional contour plots of solids fraction for the single component (river sand of size 272 μm) gas-solid fluidized bed at the gasifier compartment. The flow pattern shown will be used to compare with the two-dimensional analysis in Figure 6.1.

The initial static bed height is set at 0.35 m and fluidized at 2 U_{mf} at time 0.0 s. Small bubbles start to form at 0.5s. The bubbles grow as they rise with coalescence. Finally the larger bubbles erupted at the top of the bed, causing the surface disturbances and flow instabilities to form as can be observed at 1.0s. The bed as bulk is fully under bubbling mode at around 1.5s. However, localised dead zone is detected above the v-valve where the sand remains stagnant. The explanation will be given in the following section. This observation however is not captured by the two-dimensional profile in Figure 6.1 (a) & (b).

From the snapshots, the bed is suspended by upward flowing gas. The expansion stopped at 3.5s. At this point, the bed has expanded 29% from its initial static bed height. This indicates a deviation of 10% between the two-dimensional simulation (Figure 6.1) and the three-dimensional simulation. According to Table 2.2 in Chapter 2, the two-dimensional simulation predicted higher bed expansion when compared with the experimental data. More detailed quantitative comparison of results with the experimental data will be discussed in Chapter 7.

Based on this analysis, the numerical results should be taken after 3.5s of simulation where chaotic behavior stopped and steady state bed height is achieved. This is different from the two-dimensional study where results should be taken after 2s.

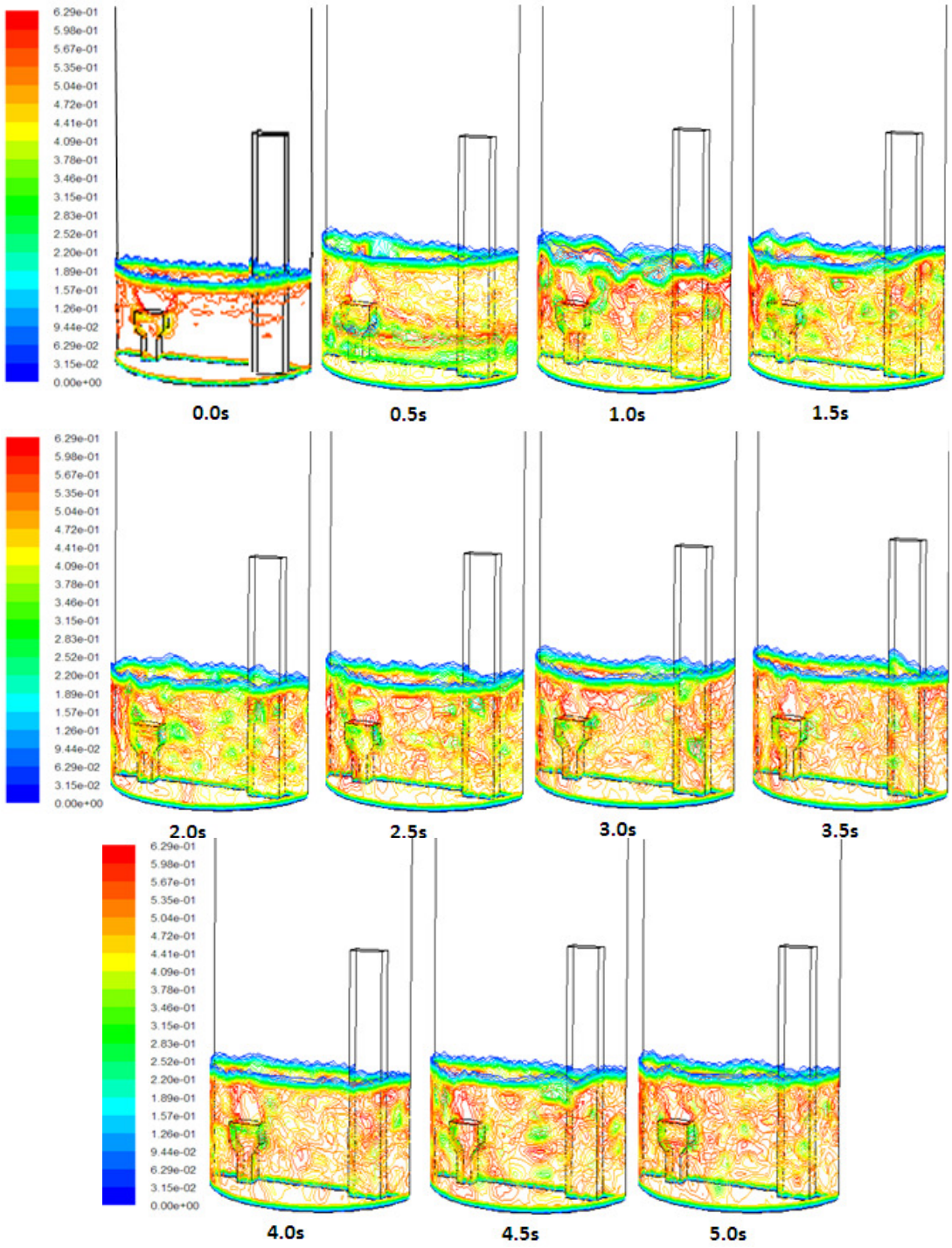

Figure 6.2: Simulated solids volume fraction profile of three-dimensional bed at various times (U = 0.12 m/s, i.e. 2 U_{mf}, river sand 272 mcirons) (t= 0.0 s – 5.0 s with 0.5 s successive interval)

6.2.3 Comparison between Two- and Three-Dimensional Analyses in Single Component System

Comparison between the two-dimensional (2D) and the three-dimensional (3D) analyses is made for single component system at the gasifier based on Figure 6.1 and Figure 6.2. Some common features are captured, however differences are also observed.

Initial formation of bubbles has been detected to be the same for both analyses, which is 0.5s. Small bubbles develop near the inlet and travel through the bed, forming larger bubbles by coalescence. This behaviour is also observed in both analyses. In addition, the bed expansion can be seen from both figures however they give totally different results, 39% expansion in 2D study and 29% expansion in 3D study. Quantitative comparison of the bed expansion will be given in Chapter 7. In 2D study, it is suggested that the steady equilibrium state reach at 2s; however 3.5s is suggested in 3D study. Steady state reached faster due to the simplification (the effect of 3rd dimension is ignored) used in 2D grid system.

3D analysis detects the localised dead zone at v-valve where the river sand is not able to fluidize but this phenomenon is not captured by 2D analysis. The effect of non-uniform shape to the fluidization behaviour is able to be identified in 3D simulation. This is a significant difference and important finding which can provide preliminary information on the degree of particles mixing and temperature distribution in the bed during the hot processes.

2D simulation should be used with caution and only for sensitivity analyses or where the flow is by nature two-dimensional. In this study, 3D simulation is still preferable when dealing with complex shape fluidized bed where effect of geometry is inevitable to the fluidization hydrodynamics.

6.2.4 Three-Dimensional Flow Pattern at Combustor

Figure 6.3 depicts the simulated three-dimensional distribution profile of river sand of size 272 μm (volume fraction) at the combustor compartment with superficial velocity of 2 U_{mf} at various times (t = 0s ~ t = 4.0s).

The static bed height is set at 0.35 m and impulsively fluidized at 2 U_{mf} at 0.0 s. The bubbles start to form at 0.5s. The same observation is attained in comparison with Figure 6.1 and Figure 6.2. The gas bubbles rise more rapidly than the rest of the gas and coalesce frequently as they rise through the bed. Bubbles grow in size; combine with bubbles which are side by side until the bed surface and eventually erupted.

The bed is fully under bubbling mode at around 2.5s. As one can see from the figure, the sand above the v-valve remains stagnant creating dead zones in the bed; the sand trapped at that region is unable to be fluidized. This is also detected at the gasifier side (Figure 6.2). This is due to the non-uniform shape of combustor and gasifier segment with the presence of v-valve and riser. This observance may lead to non-homogeneous temperature distribution and poor mixing quality in binary system during the hot combustion and gasification process.

It is also observable from Figure 6.3 that the bed expanded due to the excessive gas velocity needed to fluidize the bed. The bed has expanded 25% from its initial static height. More detailed quantitative comparison of results will be discussed in Chapter 7.

The expanded bed height at combustor is noticeably lower than that at the gasifier side (29%). 4% difference is significant when it comes to large scale fluidized bed. The flow behaviour of a gas-solid fluidized bed is very complex and highly sensitive to bed diameter (Nicholas and Paul, 1984). Gasifier is smaller than the combustor by 60%. The effect of internal parts (v-valve and riser) may attribute differently in the compartments. In addition, our visual observation also shows that gasifier always has more expanded

bed than that in the combustor. As compared to gasifier in Figure 6.2, combustor has fewer bubbles formed due to the aforementioned reason.

The expansion stopped at 3.5s when bubbles are fully developed through the bed. Based on this analysis, the CFD results discussed in Chapter 7 were taken after 3.5s (same observation from Figure 6.2) despite the 2s from the two-dimensional simulation in Figure 6.1.

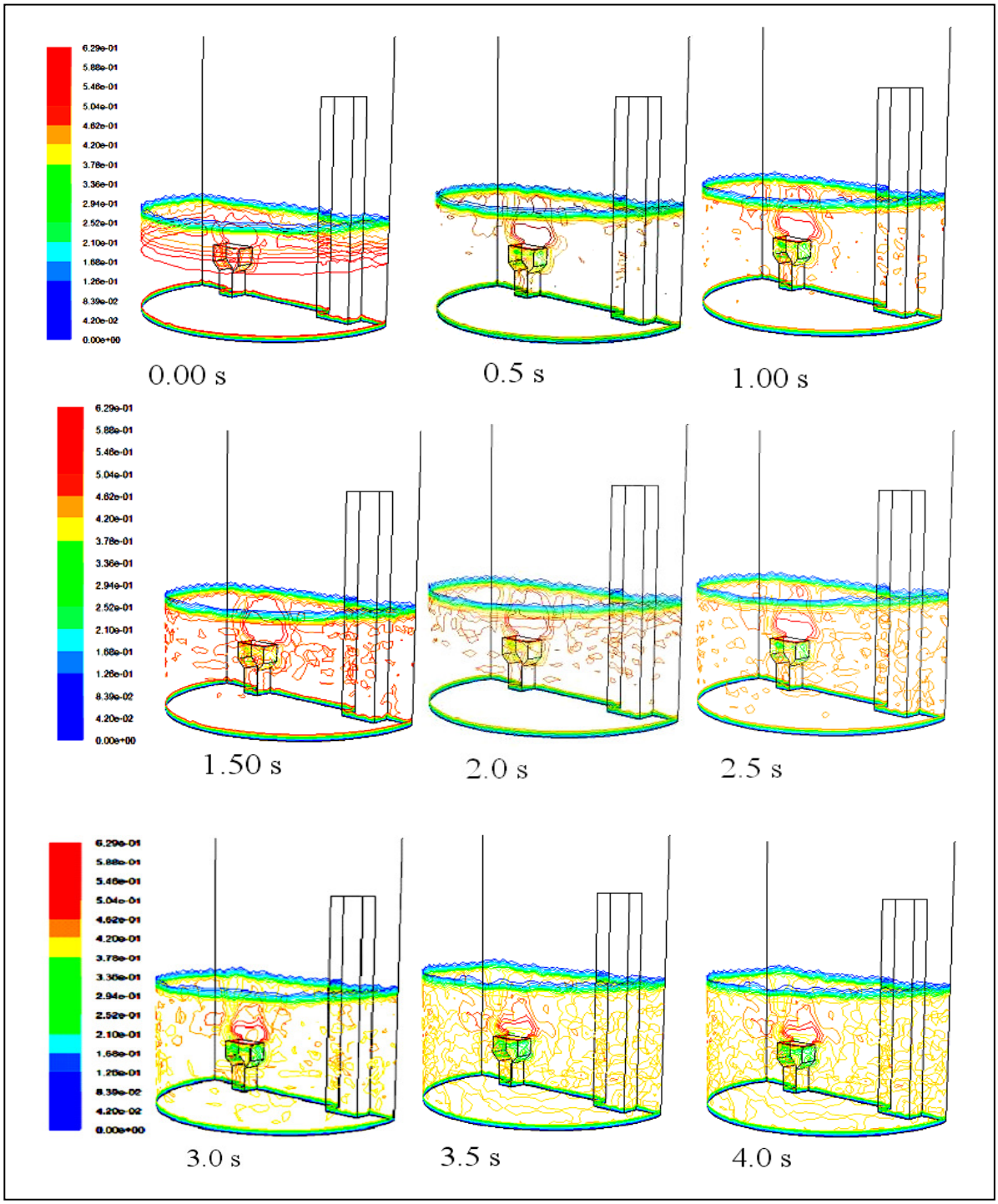

Figure 6.3: Simulated solids volume fraction flow pattern of three-dimensional bed of single component system in combustor compartment at various times (U = 0.12 m/s, i.e. 2 U_{mf}) and static bed height of 0.35m.

6.3 BINARY MIXTURE SOLID VOLUME FRACTION FLOW PATTERN

6.3.1 Two-Dimensional Flow Pattern

Figure 6.4 shows the simulated two-dimensional solid distribution pattern of binary mixture bed with 10 wt% of mean sieved size 3.56 mm palm shells (volume fraction) at increasing superficial gas velocities from 0 U_{mf} to 2.9 U_{mf} (8 sets of different superficial velocity profiles for the contour analysis of volume fraction) in the gasifier at total static bed height of 0. 375m. In Olumuyiwa Owoyemi et al. study, it shows that the binary system becomes uniform mixed around 4s. In addition, our single component system study shows that steady state reaches at 3.5s. Hence, in this work, the results are taken at t= 5s.

The U_{mf} of binary mixture system is obtained from our experiment, which is 0.08 m/s. The green color region shows the presence of palm shell whereas the region under the green region (blue color) consists of river sand. At first the river sand and palm shells was filled in two completely segregated layers, where palm shells were topped uniformly on the river sand before the simulation started.

One can observe from the figure that when the superficial gas velocity reaches the minimum fluidization velocity of the binary mixture, the palm shells start to move downwards allowing the river sand to move upwards, initiating the mixing of palm shell and river sand. Detailed discussion of binary mixing mechanism will be provided in the following section.

With increasing velocity, the palm shells segregates prevalently to the sides at 1.9 U_{mf}. However this observation is only seen at two-dimensional study. The binary mixing profile in three-dimensions will be discussed in the section later.

The overall bed expands steadily with increasing superficial gas velocity until 2 U_{mf}. At this point, the bed has expanded 57% from its initial static height.

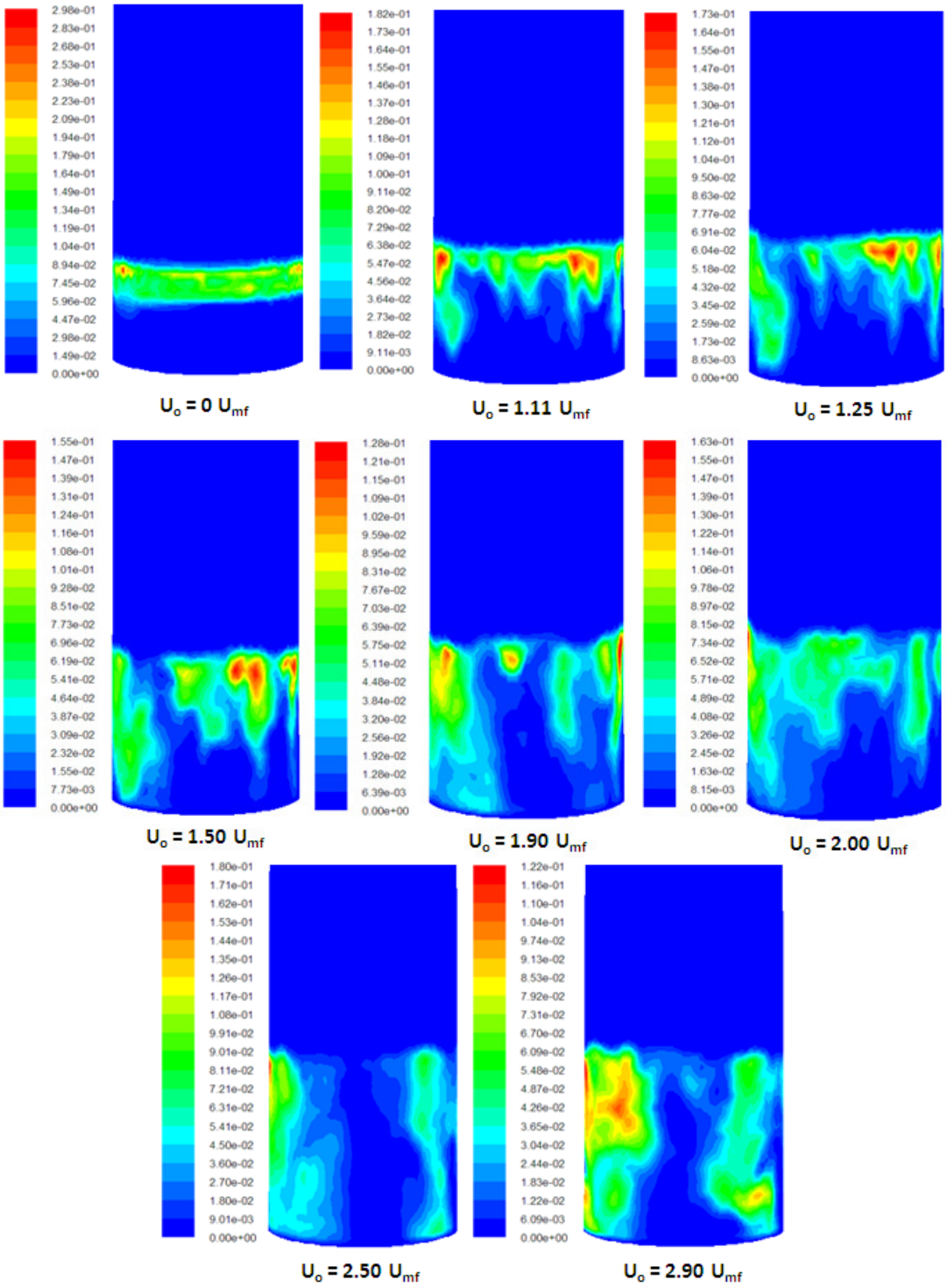

Figure 6.4: Simulated solids volume fraction flow pattern of two-dimensional binary mixture bed of 10wt% size 3.56mm palm shell at various superficial velocities and 0.375m static bed height (t = 5s)

6.3.2 Three-Dimensional Flow Pattern

Figure 6.5 shows the simulated solid distribution pattern of binary mixture bed with 10 wt% of mean sieved size 3.56 mm palm shells (volume fraction) at increasing superficial gas velocities from 0 U_{mf} to 2.9 U_{mf} (8 sets of different superficial velocity profiles for the contour analysis of volume fraction of a three-dimensional fluidized bed) in the gasifier at total static bed height of 0.375 m. Total static bed height means the sum of river sand static height and palm shell static height. River sand bed and palm shell bed is set at 0.33m and 0.045m respectively. The results are taken at t = 5s.

The colored region shows the presence of palm shell whereas the bottom part (without color region) consists of river sand. At first the river sand and palm shells was filled in two completely segregated layers, where palm shells were topped uniformly on the river sand.

The palm shells remain segregated at 0 U_{mf}. It distributes downward gradually at 1.11 U_{mf}, which initiates the mixing of palm shells and river sand. The mixing action is produced by the rising bubbles, whose wake and drift leads to the motion of particles. The palm shells tend to move to the bottom from both sides as well as in the wake of rising bubbles until evenly distributed. The bursting bubbles from centre of the column push the palm shells at the bed surface of centre region to the sides; hence the tendency of palm shells moving sideway is higher. The downward movement of palm shells also shows that the river sand at the bottom is transported upward by the rising bubbles. This mechanism of transport has also been observed by other researches (Nienow, 1980, 1985)

With increasing velocity, the mixing of palm shells becomes more vigorous. The palm shells propagate to the side way. At 1.90 U_{mf} and 2.00 U_{mf}, palm shell has already exhibiting well mixing behaviour. However, the palm shells propagate to the side again at 2.50 U_{mf}. This awkward behaviour is also observed in Figure 6.4 (palm shells start segregating prevalently to the sides at 1.9 U_{mf} onwards). The palm shells tend to spread to the front part of riser. The presence of large bubbles of different sizes at high U_{mf} in

the fluidized bed adds complexity to the mixing pattern observed. Also the actual complex shape of CFBG creates localised dead zones near the v-valve and riser, thus contributing to poor mixing around that region which is shown in Figure 6.2 and Figure 6.3. However, the bed becomes qualitatively well mixed again at 2.90 U_{mf}.

The observation of the solid volume fraction in these presented flow pattern implies that the palm shells tend to become uniformly mixed at 2.00 U_{mf} onwards despite the peculiar behaviour observed at 2.50 U_{mf}. The mixing behavior in the fluidized bed, depending on the competition between the mixing and segregation potentials, is mainly a function of superficial gas velocity as well as the density and size of the particles. Quantitative comparison of vertical and lateral mixing quality with the experimental results will be discussed in Chapter 7.

The expansion of binary mixture system bed can also be observed from these snapshots. At 0 U_{mf}, the bed height is higher than at 1.11 U_{mf}. This is however not observed in the two-dimensional study. The porosity of palm shell is bigger than that of the river sand. When the sand started to fluidize, it fills the interstitial between palm shells causing the bed height to drop. Our visual observation also shows the same phenomenon at the onset of fluidization. The bed height is expanding steadily with increasing superficial gas velocities until it levels off at 2.5 U_{mf}. At this point, the bed has expanded 15% from its initial static height. This indicates a deviation of 42% between two-dimensional simulation (Figure 6.4) and three-dimensional simulation. The detailed comparison of bed expansion with the experimental data will be discussed in chapter 7.

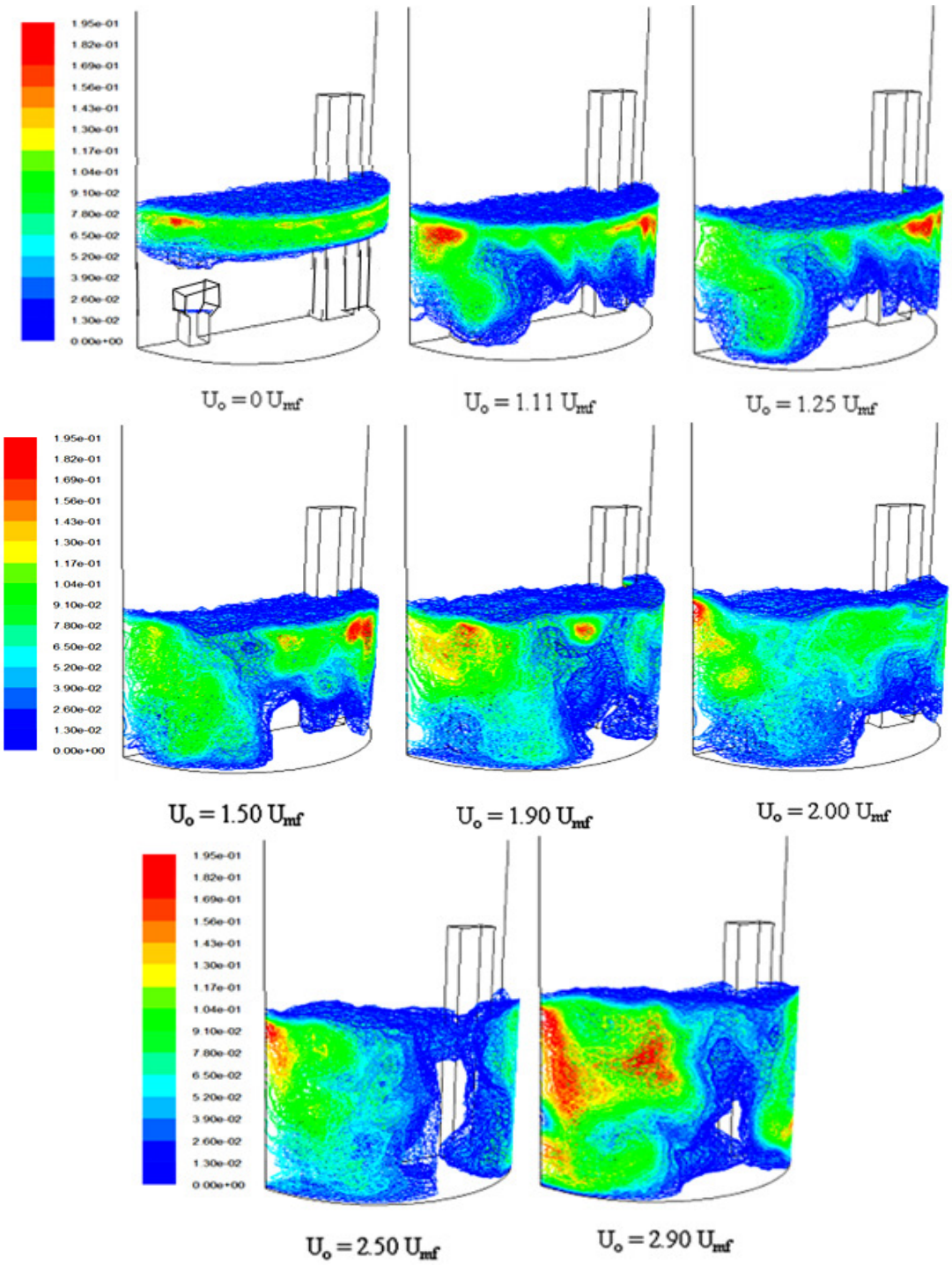

Figure 6.5: Simulated solids volume fraction flow pattern of three-dimensional binary mixture bed of 10wt% size 3.56mm palm shell at various superficial velocities and 0.375m static bed height (t = 5s)

6.3.3 Comparison between Two- and Three-Dimensional Analyses in Binary Mixture System

Comparison between two-dimensional (2D) and three-dimensional (3D) analyses is made for binary mixture at the gasifier based on Figure 6.4 and Figure 6.5.

The mixing pattern of palm shells can be observed in both figures. In 2D study, it shows only the plane mixing; the radial mixing of palm shell is not captured. As shown in 3D simulation, the palm shells tend to distribute downward from the side of gasifier. This is not able to be discerned from 2D study. Also, the actual experiment to determine the mixing of binary system is performed based on 9 imaginary points within the bed; thus only 3D simulation is appropriate to carry out such analysis.

In addition, bed expansion can be seen from both figures however they deviate from each other significantly. 57% expansion is detected in 2D study while 15% expansion is observed in 3D study at 2.5 U_{mf}. The initial drop in bed height at the onset of fluidization is also not captured by the 2D simulation.

The effect of riser shape on the binary mixing is shown in the 3D analysis. Palm shell segregates at that region and tend to gather in front of riser despite evenly distributing around riser. This phenomenon is however not observed in 2D study. Even distribution of temperature within the gasifier during hot processes is very crucial for product yield; hence this is a valuable finding which can be used to predict any non-homogeneous temperature distribution in the bed during gasification reaction.

2D analysis is useful when regular geometry is involved. With the concern of CFBG, 3D simulation is more practical to produce realistic results.

6.4 SUMMARY

The emphasis of this chapter has been given to the numerically simulated visualization results on the fluidization characteristic of single component system and binary mixture system in CFBG. The comparison of two- versus three-dimensional solid volume profile in terms of flow pattern and bed expansion with respect to various time and superficial gas velocities has been made.

In 2D analysis, the bubble formation/ growth and bed expansion is observed. The bed expansion predicted by the 2D study for single component and binary mixture system is always higher than that by the 3D study. The steady equilibrium state can also be identified by the 2D analysis. In addition, the overall binary mixing quality of palm shells and sand can be predicted; however, the local mixing within the bed is not able to be captured by the 2D study. In the contrary, among all that mentioned before, 3D simulations have the utmost capability to identify localized dead zone due to geometrical effect and also to provide radial view of flow pattern in the bed.

The fluidization characteristic at the gasifier and the combustor is compared. The expanded bed height at the combustor is noticeably lower than that at the gasifier side. The flow behaviour of a gas-solid fluidized bed is very complex and highly sensitive to bed diameter. The effect of internal parts (v-valve and riser) may attribute differently in the compartments.

To conclude, 2D simulation should be used with caution and only for sensitivity analyses or where the flow is by nature two-dimensional. In this study, 3D simulation is still preferable when dealing with complex shape fluidized bed where effect of geometry is inevitable to the fluidization hydrodynamics. In addition, the numerical results should be taken after 3.5s of simulation.

CHAPTER 7 HYDRODYNAMICS OF SINGLE COMPONENT SYSTEM IN CFBG

7.1 INTRODUCTION

This chapter addresses the 3D numerical simulation of hydrodynamic studies in CFBG, and comparison of numerical results with results of the experimental studies and where possible with results of semi-empirical correlation in single component system. The hydrodynamic parameter studies include bed expansion ratio, bubble diameter, bed pressure drop and solid circulation rate. The bed pressure drop results are further extended to study the fluidization quality in the CFBG. The bed expansion ratio, bubble diameter and bed pressure drop characterize the fluidization behaviour while the latter characterizes the CFBG performance. In addition, the variation between numerical and experimental data is discussed.

7.2 BED EXPANSION RATIO STUDY

The most common used expression of the bed expansion ratio is defined as the ratio of the fluidized bed height, H to the initial static bed height, H_o.

$$Bed\ Expansion\ Ratio = \frac{H}{H_o} \tag{7.1}$$

7.2.1 Combustor Compartment

Table 7.1 summarizes the model parameters/conditions applied for the numerical simulation of bed expansion ratio study at the combustor side. Air at ambient temperature and pressure is used as the fluidizing medium. Mono-sized river sand of 272

µm and density of 2620 kg/m^3 is specified in the numerical study. The compartment is filled with particles to the desired bed height with the initial solid packing specified.

Table 7.1: 3D Simulation model parameters for the bed expansion ratio study in the combustor

Description	Value	Unit	Comment
Diameter	0.413	m	Combustor
Particle density	2620	kg/m^3	River sand
Mean particle size	272	µm	Uniform distribution
U_{mf}	0.06	m/s	Determined experimentally
Initial solid packing	0.45	-	Fixed value
Gas density	1.2	kg/m^3	Ambient air
Superficial gas velocity	0.06 – 0.12	m/s	$1U_{mf} - 2U_{mf}$
Static bed height	0.35, 0.40, 0.45	m	Specified

7.2.1.1 River Sand as the Inert Particles

The 3D simulations are first performed to examine the bed expansion from onset of fluidization at the combustor side. Figures 7.1 – 7.3 show the comparison of numerically simulated results for bed expansion ratio study with the experimental results using river sand of mean particles size 272 µm as the fluidization medium at various static bed heights, i.e. 0.35m, 0.40m and 0.45m. The superficial gas velocities are in the range of $1U_{mf}$ – $2U_{mf}$. ±10% error bars are set in the figures to indicate with respect to the numerical simulation results, the degree of deviation between numerical and experimental values.

From the figures, it is observed that the bed increases linearly with increasing gas velocity. The bed of solids becomes more loosen (higher porosity) with the increase in superficial gas velocity due to excess gas velocity above the minimum fluidization velocity.

For numerical simulation, the predicted trends confirm well with the experimental ones. 3D numerical visualization of flow pattern at bed height of 0.35m and $2U_{mf}$ is also done to study the bed expansion (refer Chapter 6, Figure 6.3). The visualization clearly illustrates that the bed expanded due to higher porosity in the bed where bubbles formation can be seen. The deviations are less than 10% for the range of study. However, the simulated results demonstrate the tendency to over-predict the bed expansion ratio at $2U_{mf}$ onwards.

The bed expansion ratio is always under-predicted by the numerical solution at lower U_{mf} (less than $1.5U_{mf}$). At $1U_{mf}$, the predicted bed expansion ratio is generally 1.0 for all cases. This shows that minimum fluidization condition has not been attained. The U_{mf} of river sand is determined experimentally where the actual bed is loaded with wide spectrum of river sand size. However, mono-sized river sand is specified in the numerical simulation. Thus, the predicted bed expansion ratio possibly tells that the numerical U_{mf} can be higher than the experimentally determined U_{mf} for mono-sized river sand system. The numerically simulated bed expansion ratio breaks even with the experimental data at above $1.5U_{mf}$.

The effect of static bed height on the bed expansion ratio is shown in Table 7.2. It is noticed that the different static bed height does not have any significant impacts on bed expansion ratio experimentally and numerically.

On average, from Figures 7.1 – 7.3, the predicted bed expansion ratio ranges from 1.05 to 1.30 while for experimental sets of data, the bed expansion ratio ranges from 1.10 to 1.20 for the U_{mf} range studied.

Table 7.2: Effect of the static bed height on the bed expansion ratio at $2U_{mf}$

Static Bed Height (m)	Bed Expansion Ratio	
	Experiment	CFD
0.35	1.22	1.25
0.40	1.19	1.24
0.45	1.22	1.29

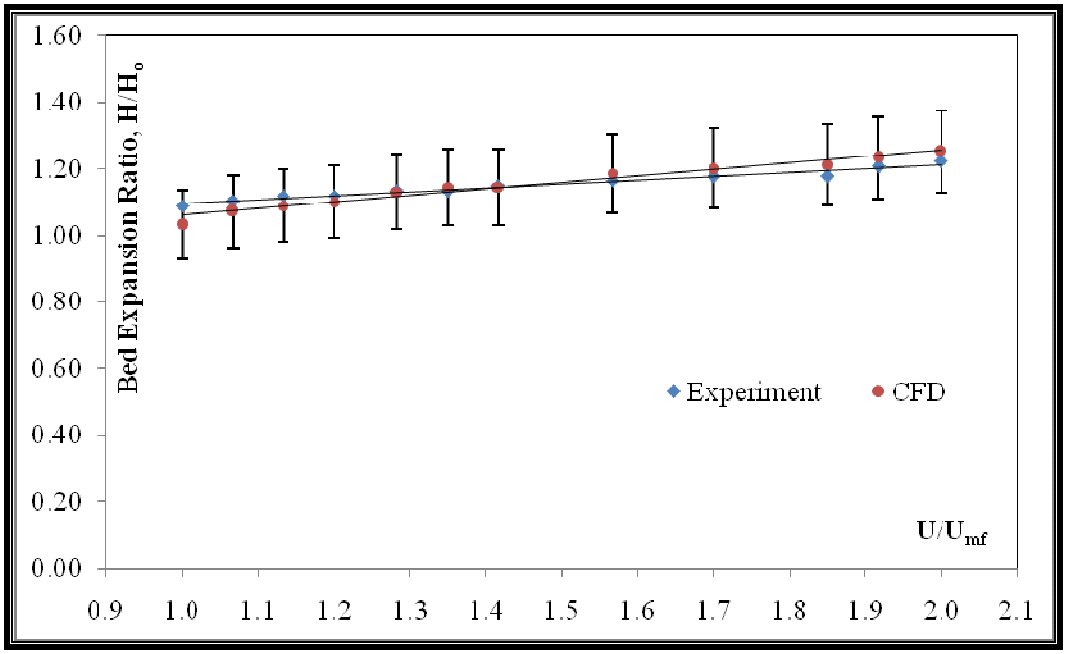

Figure 7.1: Comparison of the numerical results with the experimental results at static bed height of 0.35m for the bed expansion ratio in the combustor

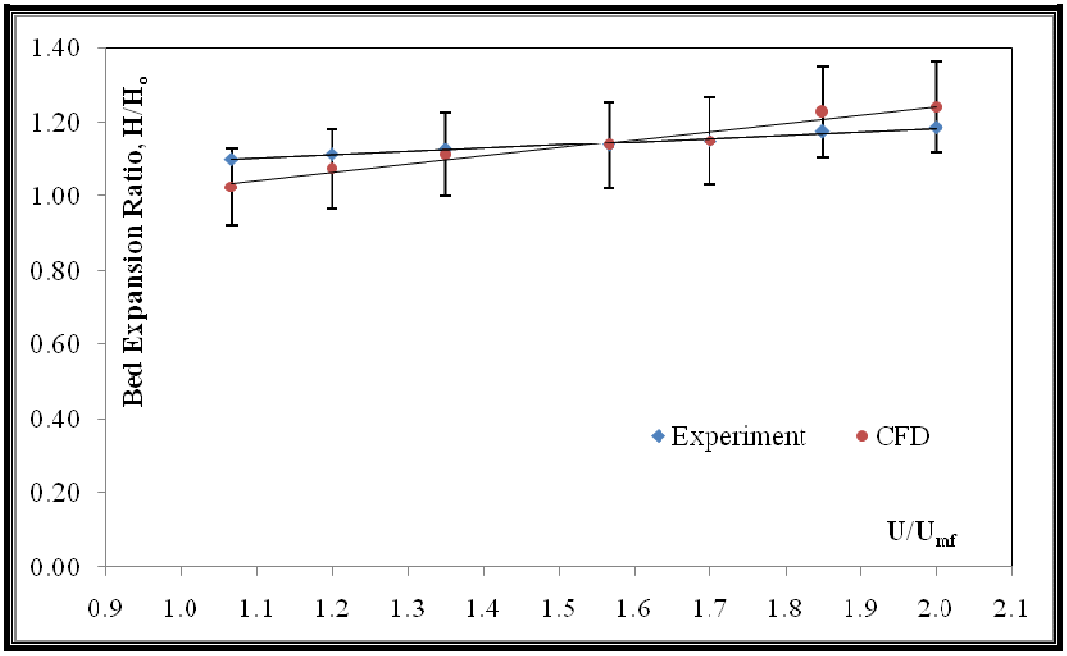

Figure 7.2: Comparison of the numerical results with the experimental results at static bed height of 0.40m for the bed expansion ratio in the combustor

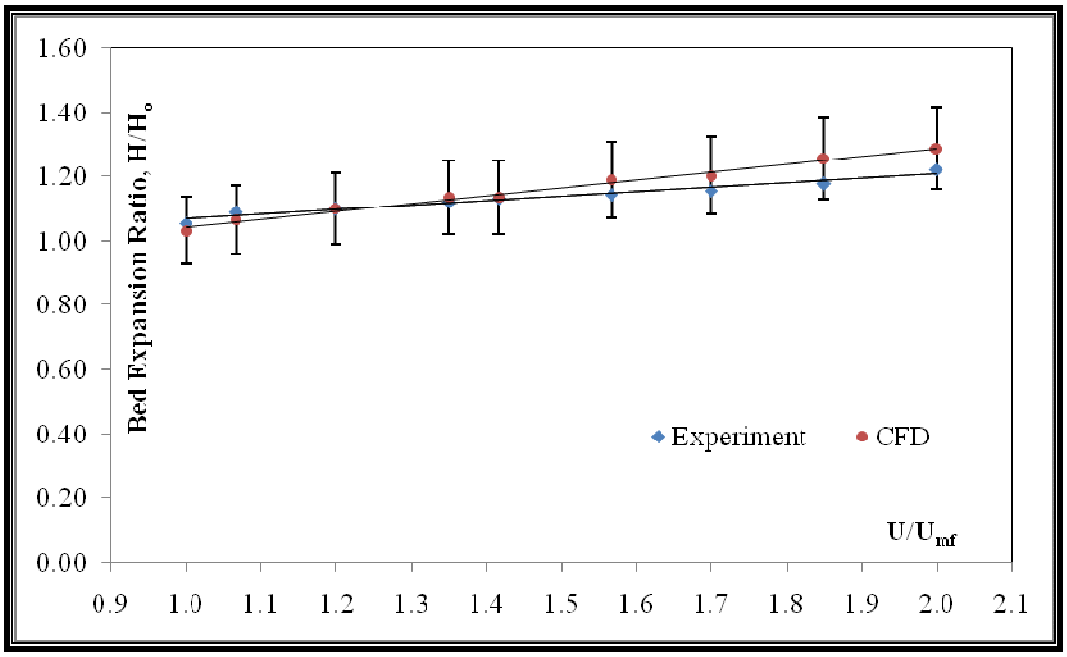

Figure 7.3: Comparison of the numerical results with the experimental results at static bed height of 0.45m for the bed expansion ratio in the combustor

7.2.2 Gasifier Compartment

Table 7.3 summarizes the model parameters/conditions applied for the numerical simulation of bed expansion ratio study at the gasifier side. Air at ambient temperature and pressure is used as the fluidizing medium. Mono-sized river sand of 272 µm and alumina of 360 µm is specified in the study.

Table 7.3: 3D Simulation model parameters for the bed expansion ratio study in the gasifier

Description	Value	Unit	Comment
Diameter	0.257	m	Gasifier
Particle density	2620	kg/m^3	River sand
	3992	kg/m^3	Alumina
Mean particle size			
River sand	272	µm	uniform size
Alumina	360	µm	uniform size
U_{mf}			
River sand	0.06	m/s	Determined (experiment)
Alumina	0.154	m/s	Determined (experiment)
Initial solid packing	0.45	-	Fixed value
Gas density	1.2	kg/m^3	Ambient air
Superficial gas velocity			
River sand	0.060 – 0.120	m/s	$1U_{mf} - 2U_{mf}$
Alumina	0.154 – 0.216	m/s	$1U_{mf} - 1.4U_{mf}$
Static bed height			
River sand	0.35, 0.40, 0.45	m	Specified
Alumina	0.14, 0.30, 0.35	m	Specified

7.2.2.1 River Sand as the Inert Particles

Figures 7.4, 7.5 and 7.6 show the comparison of results from the numerical simulation for bed expansion ratio study with the experimental results at the gasifier side where

river sand is used as the fluidization medium at various static bed heights, i.e. 0.35m, 0.40m and 0.45m. The superficial gas velocities range from $1U_{mf}$ to $2U_{mf}$. ±10% error bars are set in the figures to indicate with respect to numerical results, the degree of deviation between numerical and experimental values.

The experimental bed height increases with the increase in superficial gas velocity. The numerical results also demonstrate an increase in bed expansion ratio with slightly higher rate of increase but still within ±10%.

The same behaviour as seen in the combustor study is also observed here where the predicted bed expansion is always lower than experimental bed expansion ratio at lower U_{mf} (less than $1.5U_{mf}$) (refer section 7.2.1.1 for the discussion of variation).

From the study, different static bed height does not show any noticeable impacts on the bed expansion ratio as shown in Table 7.4.

2D and 3D numerical visualization of flow pattern with river sand at static bed height of 0.35m is compared for the fluidization behaviour in Chapter 6 (Figure 6.1 and 6.2). Quantitative analysis shows that the 3D simulation predicts more accurate results than 2D simulation. 2D simulation predicted a highly expanded bed with expansion ratio of 1.39 at $2U_{mf}$. In comparison with the experimental value in Table 7.4, 2D simulation has over-predicted the bed expansion by 13%. This is attributed to the simplication in 2D simulation. Hence, with respect to bed expansion ratio study, 3D simulation is opted for to obtain more realistic results.

Table 7.4: Effect of the static bed height on the bed expansion ratio at $2U_{mf}$

Static Bed Height (m)	Bed Expansion Ratio	
	Experiment	CFD
0.35	1.22	1.29
0.40	1.14	1.20
0.45	1.27	1.31

On average, from Figures 7.4 – 7.6, for experimental sets of data, the bed expansion ratio ranges from 1.05 to 1.20 while for the simulated data, the predicted bed expansion ratio ranges from 1.00 to 1.25 for $1U_{mf} - 2U_{mf}$.

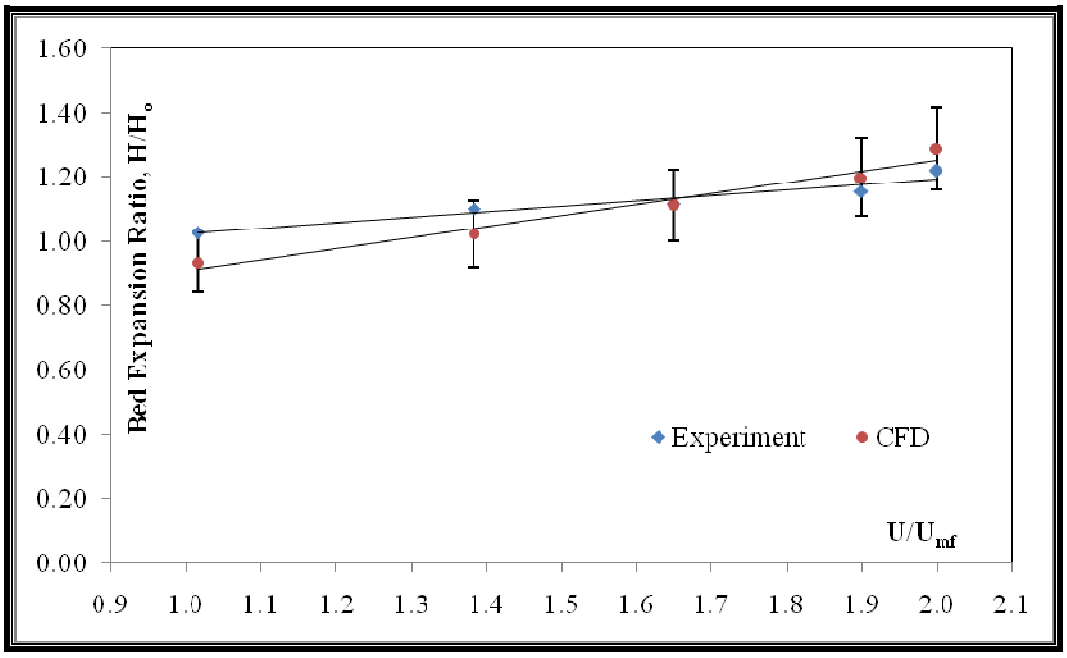

Figure 7.4: Comparison of the numerical results with the experimental results at static bed height of 0.35m for the bed expansion ratio in the gasifier

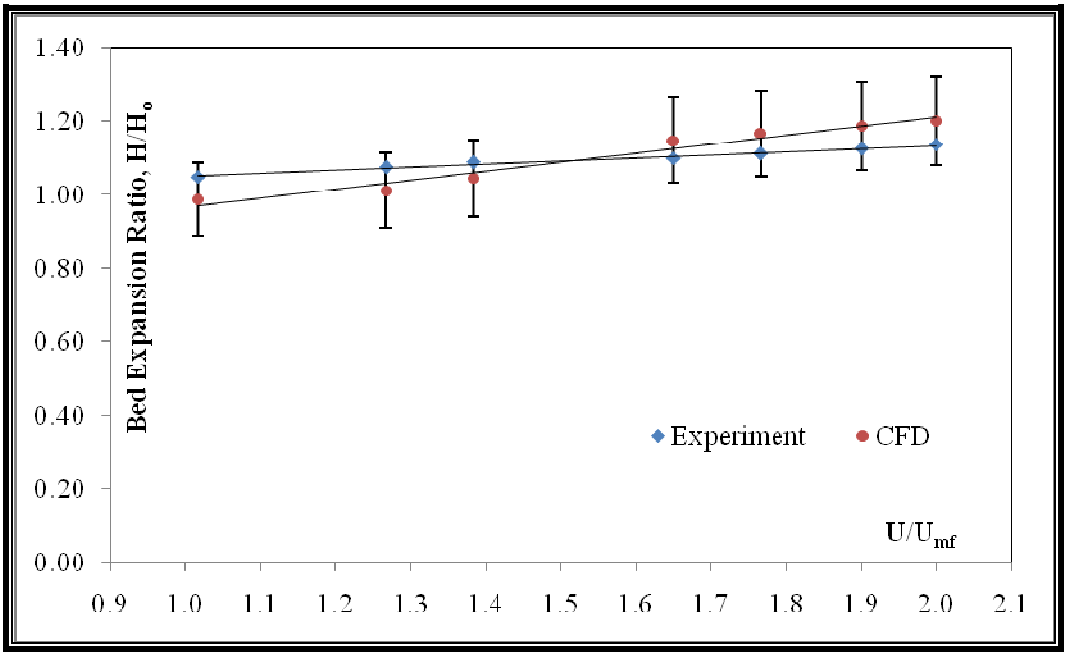

Figure 7.5: Comparison of the numerical results with the experimental results at static bed height of 0.40m for the bed expansion ratio in the gasifier

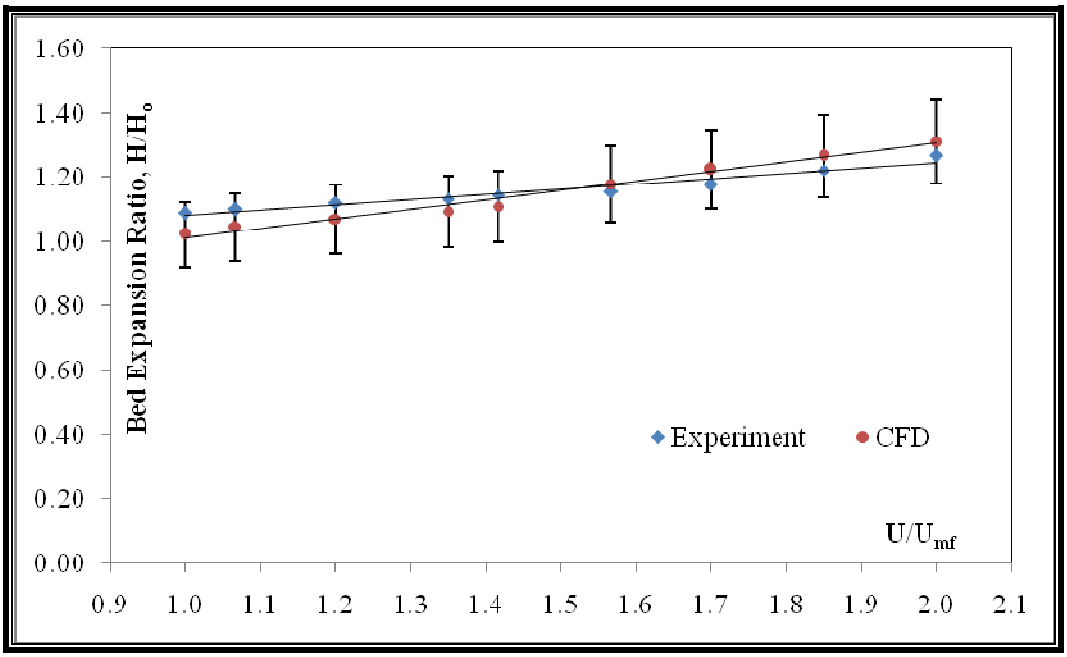

Figure 7.6: Comparison of the numerical results with the experimental results at static bed height of 0.45m for the bed expansion ratio in the gasifier

7.2.2.2 Alumina as the Inert Particles

Figures 7.7, 7.8 and 7.9 show the comparison of numerically simulated results for the bed expansion ratio study with the experimental results at the gasifier side where alumina is used as the fluidization medium at various static bed heights, i.e. 0.20m, 0.30m and 0.35m. The superficial gas velocities are in the range of $1.0U_{mf}$ – 1.4 U_{mf}. ±10% error bars are set in the figures to indicate with respect to numerical results, the degree of deviation between numerical and experimental values.

Alumina is heavier than river sand by 1.5 times. Therefore the bed expansion ratio study is carried out in shallow bed in order to cover a closer weight for comparison with river sand as shown in Table 7.5. Small range of fluidization is chosen because steady fluidization for these particles occurs within $1.0U_{mf}$ – 1.4 U_{mf}.

Table 7.5: Weight of the inert particles with respect to the bed height

Bed Height (m)	Weight (kg)	
	River Sand	Alumina
0.20	-	57
0.30	-	81
0.35	67	95
0.40	77	-
0.45	87	-

Similar to those observed before, the experimental bed expansion ratio increases with increasing superficial gas velocity. The effect of static bed height is shown in Table 7.6, where different static bed height does not impose any significant impacts on the bed expansion ratio.

The numerically simulated results predict increasing trends and agree well with experimental results with errors less than ± 5%. Mono-sized alumina is specified in the numerical simulation while in actual experiment, the bed is also loaded with mono-sized alumina, and thus the effect of wide spectrum of particle size on U_{mf}, eventually result in

higher deviation (10%) as seen in section 7.2.2.1 is discarded. Some common features of the alumina numerical visualization can be observed at Figure 6.1 and 6.2.

On average, the experimental bed expansion ratio changes from 1.02 to 1.10, while the predicted bed expansion ratio ranges from 1.02 to 1.10 for $1.0U_{mf} - 1.4U_{mf}$.

Table 7.6: Effect of the static bed height on the bed expansion ratio at $1.4U_{mf}$

Static Bed Height (m)	Bed Expansion Ratio	
	Experiment	CFD
0.20	1.13	1.11
0.30	1.12	1.10
0.35	1.11	1.09

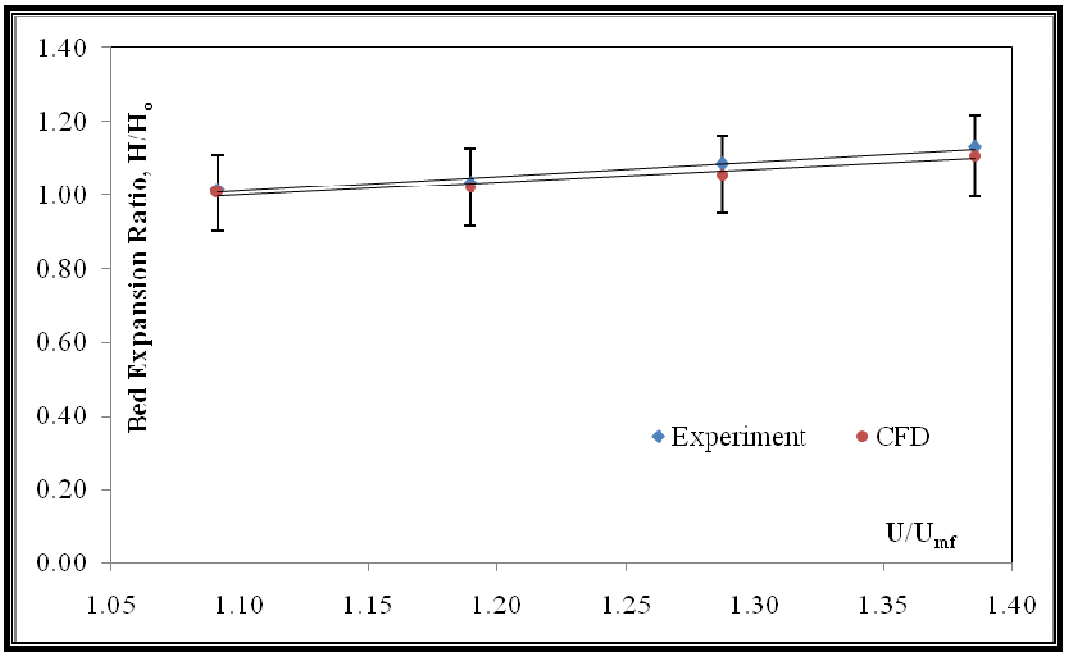

Figure 7.7: Comparison of the numerical results with the experimental results at static bed height of 0.20m for the bed expansion ratio in the gasifier

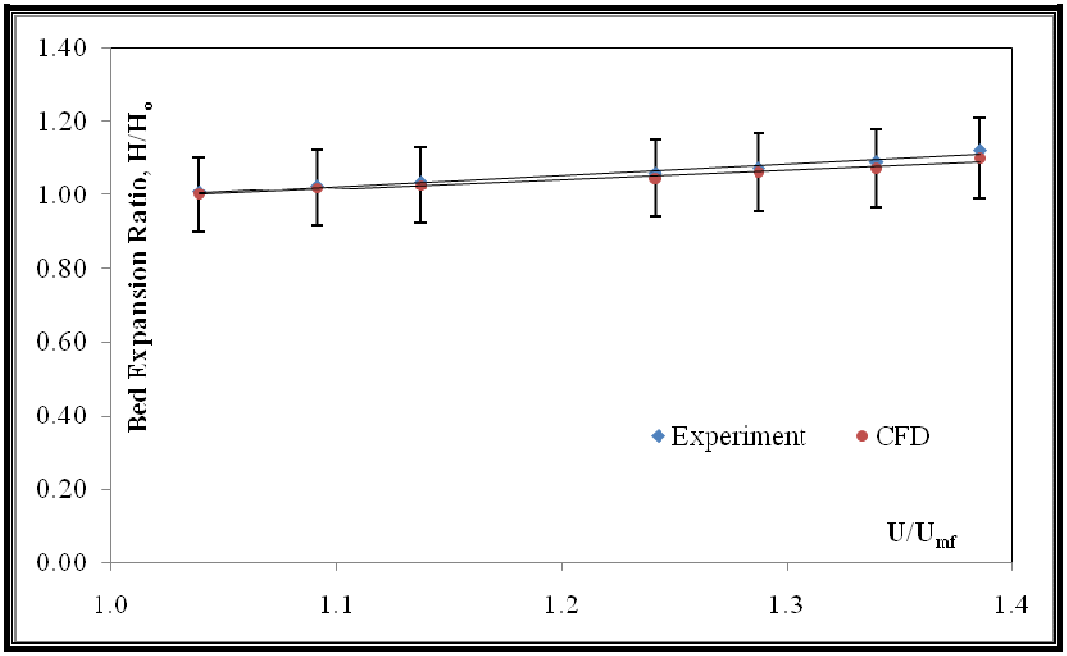

Figure 7.8: Comparison of the numerical results with the experimental results at static bed height of 0.30m for the bed expansion ratio in the gasifier

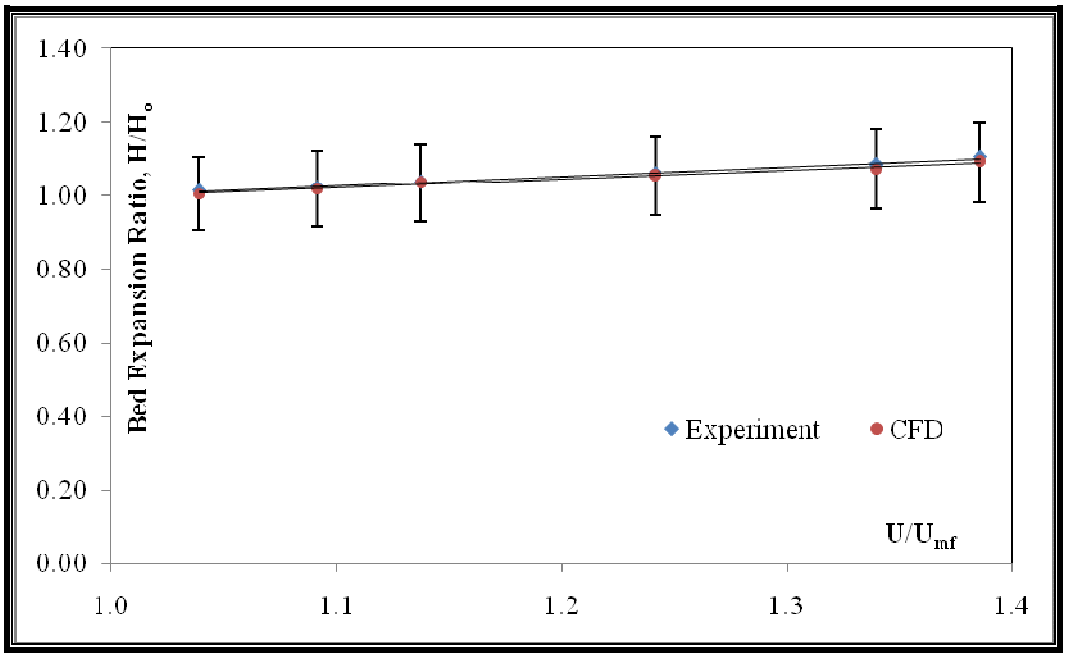

Figure 7.9: Comparison of the numerical results with the experimental results at static bed height of 0.35m for the bed expansion ratio in the gasifier

7.2.3 Effect of Effective Diameter on Bed Expansion Ratio

The effect of effective diameter on the bed expansion ratio is investigated at different bed heights, i.e. 0.35m, 0.40m and 0.45m as shown in Figure 7.10. The effective diameter of combustor and gasifier is 0.413m and 0.257m respectively. The effect of static bed height on the bed expansion ratio has been discussed separately in sections earlier; therefore the study will be focus solely on the effect of effective diameter in this section.

As seen in the figure, the experimental expanded bed in the gasifier is most of the time transcending the experimental expanded bed in the combustor. The relative expansion between gasifier and combustor is of great importance for pilot plant performance and operational economic. The flow behaviour of a gas-solid fluidized bed is very complex and highly sensitive to bed diameter (Nicholas and Paul, 1984). Combustor is larger than gasifier by 60%. The effect of internal parts (v-valve and riser) may attribute differently in the compartments. It is worth noting that in our previous study, the tendency shown in the gasifier is in fact an indicator of a channelling bed. In addition, our visual observation also shows that gasifier always has more expanded bed than combustor. As shown in the numerical visualization (refer Chapter 6, Figure 6.2 and 6.3), the flow pattern shows that more bubbles are formed in the gasifier, this may also be one of the reason contributing to more expanded bed in the gasifier.

The numerical results predict a similar trend as the experimental results; however it predicts a more expanded bed in the gasifier at higher U_{mf} (more than $1.5U_{mf}$). At lower U_{mf}, numerical model predicts a comparable bed expansion ratio at the gasifier and the combustor.

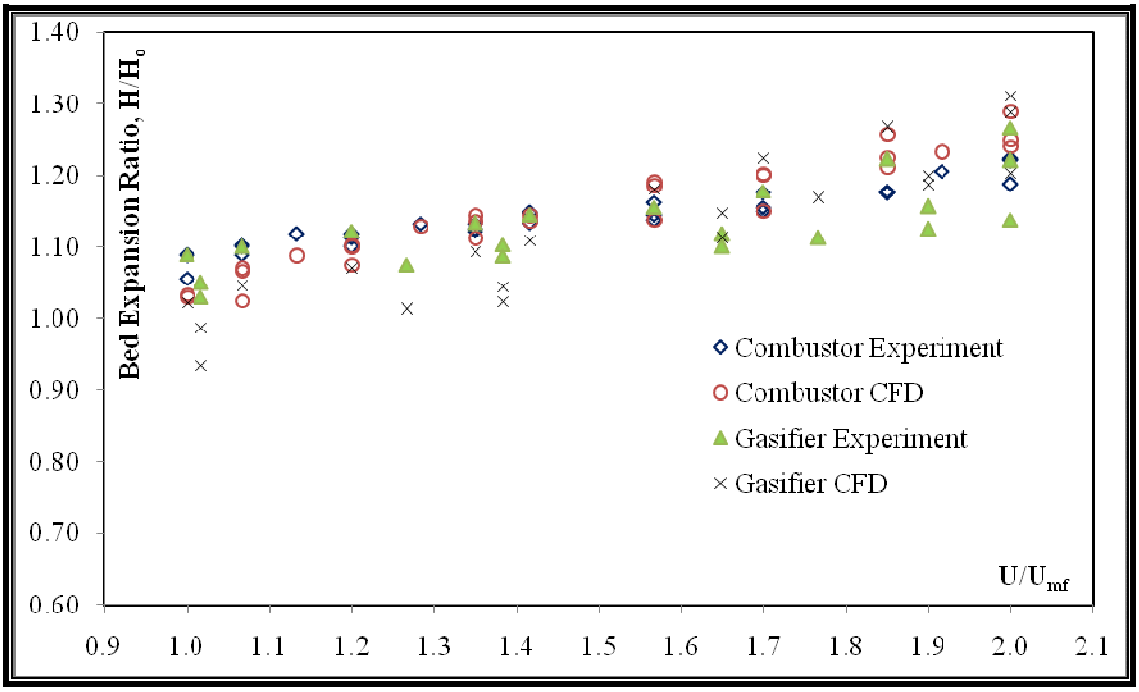

Figure 7.10: Effect of the effective diameter on the bed expansion ratio at the static bed height of 0.35m, 0.40m and 0.45m

7.2.4 Effect of Different Inert Particles on Bed Expansion Ratio

Figure 7.11 depicts the effect of different inert particles on the bed expansion ratio at static bed height of 0.20m, 0.30m, 0.35m, 0.40m and 0.45m. The fluidization regime ranges from $1.0U_{mf} - 1.4U_{mf}$. The study is conducted at the gasifier side.

The bed expands with increasing gas velocity for both materials. The bed expansion ratio is higher for river sand while the bed expansion ratio of alumina is lower by 6% experimentally and numerically for the range studied. Our visual observation shows that uneven bed expansion occurs in alumina bed; also alumina tends to stick on the wall of CFBG during fluidization. The bed seems to be cohesive and it forms channels through which the aeration gas will escape rather than being dispersed through the interstices supporting the particles. It is worth noting that in our previous study (Wee et al., 2007); the pressure drop profile shows that through-channelling occurs in alumina bed. The heavier and coarser alumina organizes itself differently because of monodispersed

characteristic as compared to river sand with a wide particle size distribution, making a portion of the bed less porous, which facilitates the air to flow through it; this eventually contributes to localized bed expansion. The shape of the reactor and the density of particles are also factors that affect channelling (Nicholas and Paul, 1984).

Based on this analysis, alumina is not selected as a fluidizing medium for palm shell in the binary mixture system; river sand (by default, it is cheaper and easily available) is therefore chosen to be used in the binary mixture system.

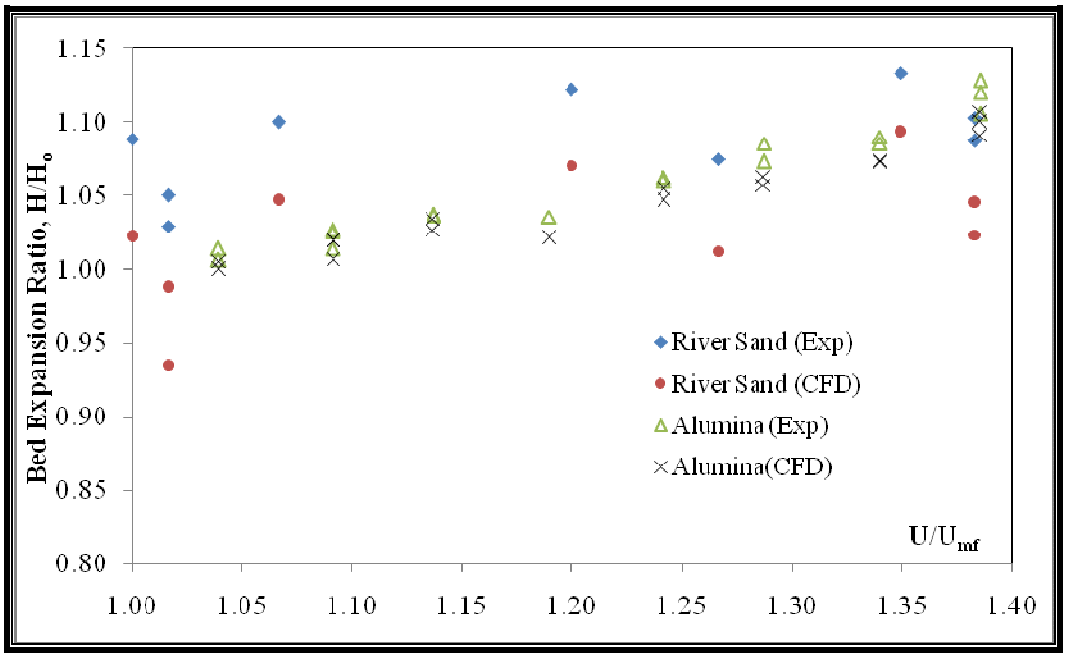

Figure 7.11: Effect of the different inert particles on the bed expansion ratio at the gasifier

7.3 BUBBLE DIAMETER STUDY

Bubble diameter study is carried out only in the numerical simulation. The common practice and the only approach to compare the simulated results is by using the Darton et al. (1977) correlation.

In the freely fluidized bed case, the gas flow is distributed uniformly across the inlet of the bed. Small bubbles form at the bottom of the fluidized bed that rise, coalesce and erupt as large bubbles at the fluidized bed surface as shown in numerical visualization of flow pattern in Chapter 6 (Figure 6.1, 6.2 and 6.3). The bubble model developed by Darton et al. (1977) is used to estimate the bubble size in freely bubbling fluidized bed. This model is based on the preferred paths of bubbles where the distance travelled by two neighbouring bubbles before coalescence is proportional to their lateral separation. Darton et al. (1977) have validated their model with measurements of many researchers. Their proposed bubble growth equation for Geldart B particles is

$$D_b = 0.54(U_o - U_{mf})^{0.4}(h + 4\sqrt{A_o})^{0.8} / g^{0.2} \tag{7.1}$$

where D_b is the bubble diameter, h is the height of the bubble above the distributor, and A_o is the 'catchment area' which characterizes the distributor; the constants are experimentally determined.

In numerical simulation, bubble size is determined from the void fraction of solids image produced by the CFD software (FLUENT). The diameter of the bubble is calculated as if its shape is circular. The equivalent bubble diameter, d_B, is calculated from the area equivalent of the bubble, A_B, as

$$d_B = \sqrt{4A_B/\pi} \tag{7.2}$$

where A_B, is the area equivalent of the bubble.

For the simulations comparing the model parameters, a void fraction cutoff of 0.4 recommended by literatures (Hulme et al., 2005) is used. The computational cells having solid volume fraction less than the value of 0.4, are considered as bubbles, while the other ones are considered as the emulsion phase.

7.3.1 Combustor Compartment

The numerical model settings can be found in Table 7.1.

7.3.1.1 River Sand as the Inert Particles

Figures 7.12, 7.13 and 7.14 illustrate the comparison of numerically simulated results with the Darton's (1977) correlation for bubble diameter estimation at various static bed heights, i.e. 0.34m, 0.40m, and 0.45m, with respect to superficial gas velocities of $1U_{mf}$ – $2U_{mf}$ in the combustor side where river sand is used as the fluidization medium.

By increasing the gas superficial velocities, the bubbles in the bed typically increase in size. The numerical results also show the increasing trend. As can be seen in Figure 7.12 and 7.14, at exactly $1U_{mf}$, bubble size is able to be simulated by the numerical solution; however the Darton's (1977) correlation predicts zero bubble size. From $1U_{mf}$ onwards, numerical simulation predicts smaller bubbles than that calculated by the Darton's (1977) correlation by around 15% deviation (±15% error bars are set for easy reading and comparison). Combustor compartment is not of exactly cylindrical shape; moreover it includes internal parts such as v-valve and riser, making its geometry more complex. Darton's (1977) bubble model in nature does not take into account the geometrical effect such as the effect of v-valve and riser on bubble size. As shown in our numerical visualization for combustor in Chapter 6 (Figure 6.3), in fact there is localized dead zone above v-valve where this may hinder the growth of bubbles. Hence, smaller bubbles are predicted by the numerical solution as compared to the Darton's (1977) correlation.

The effect of static bed height on the bubble size is presented in Table 7.7. The values are taken at $2U_{mf}$. The bubble diameter predicted by the Darton's (1977) bubble model is increasing for the range of static height studied, but numerical simulation does not predict similar trend. The static height has no obvious effect on the bubble size obtained from the numerical simulation. This shows that the effect of v-valve on hindering the bubble growth is still prevailing regardless of the increase in static bed height. This fact however requires physical data for validation.

Table 7.7: Effect of the static bed height on the bubble size at $2U_{mf}$

Static Bed Height (m)	Bubble Size (m)	
	Darton et al.	CFD
0.35	0.173	0.170
0.40	0.178	0.165
0.45	0.184	0.172

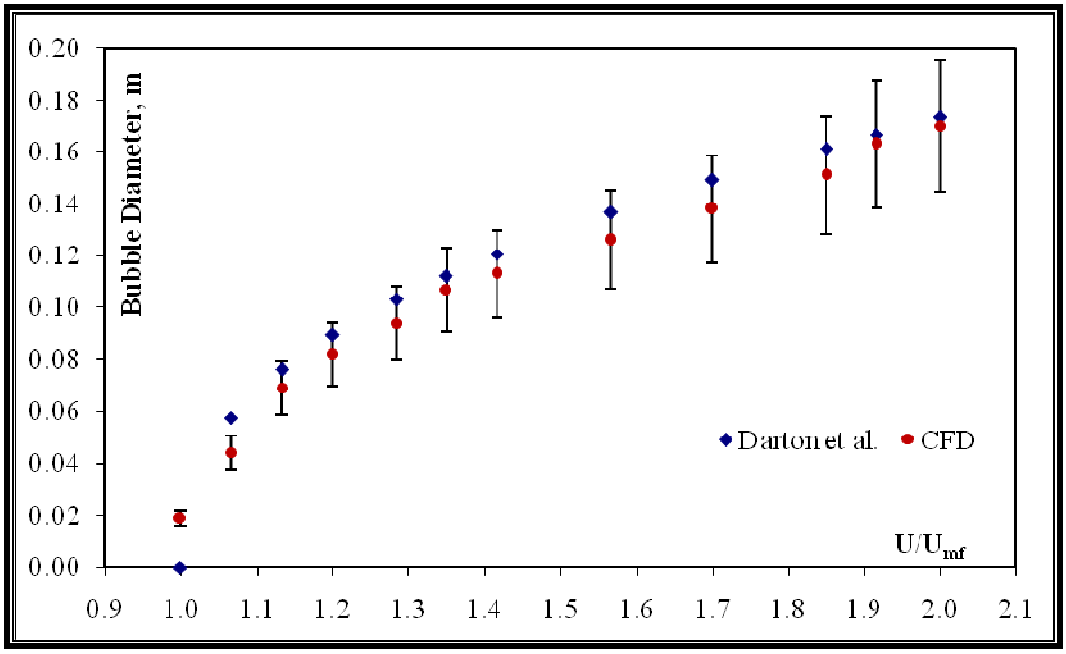

Figure 7.12: Comparison of the numerical results with the Darton's correlation at the static bed height of 0.35m for the bubble size in the combustor

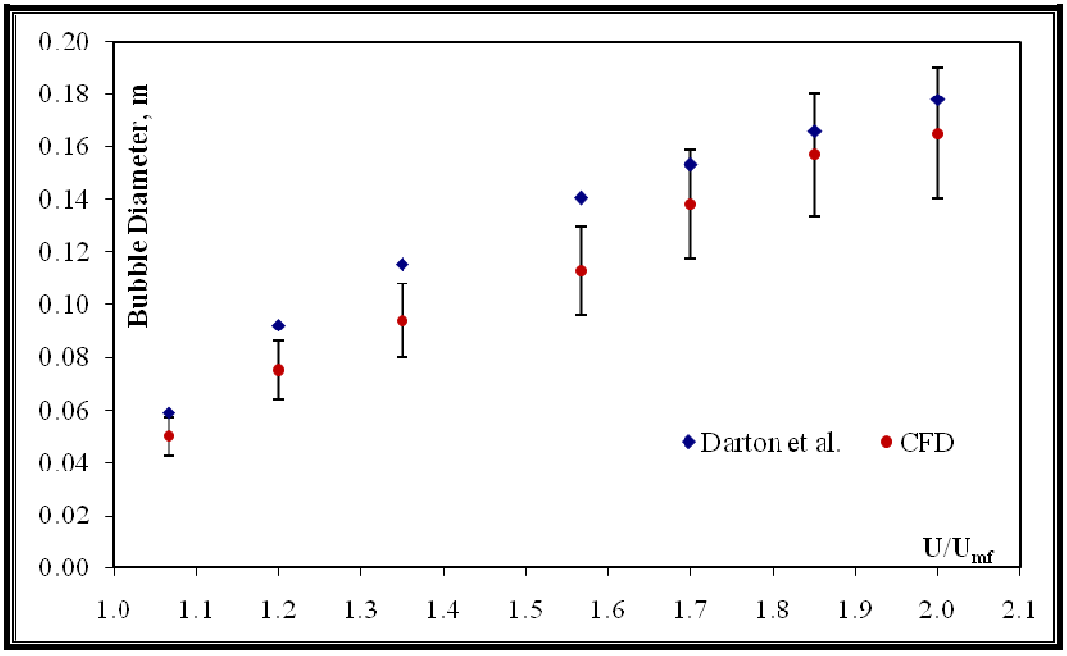

Figure 7.13: Comparison of the numerical results with the Darton's correlation at the static bed height of 0.40m for the bubble size in the combustor

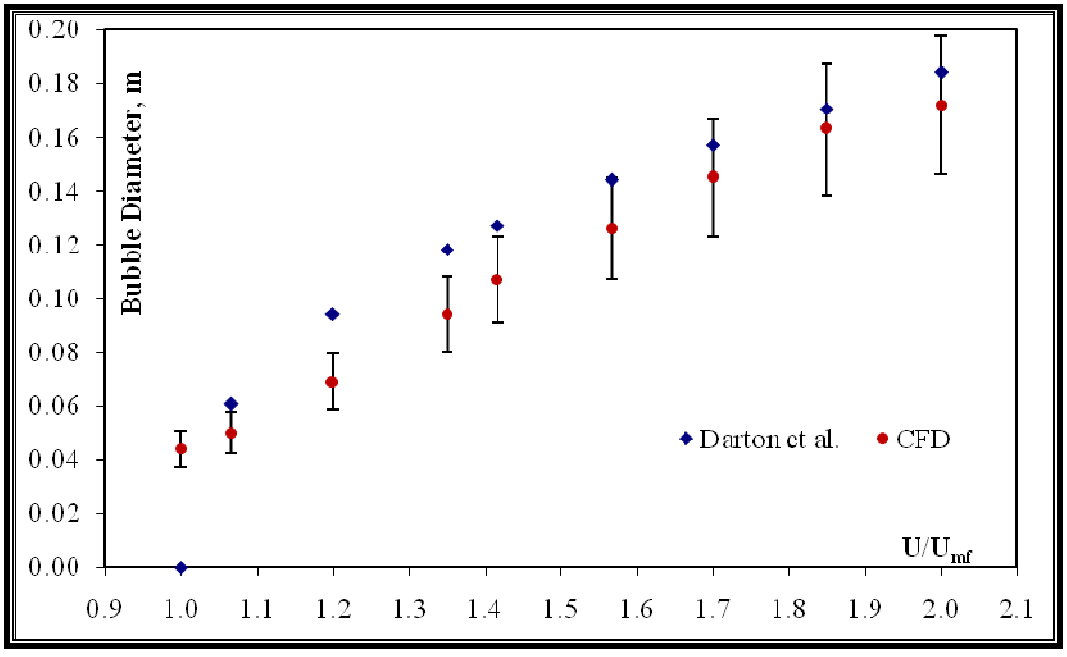

Figure 7.14: Comparison of the numerical results with the Darton's correlation at the static bed height of 0.45m for the bubble size in the combustor

7.3.2 Gasifier Compartment

The numerical model settings can be found in Table 7.3.

7.3.2.1 River Sand as the Inert Particles

Figures 7.15, 7.16 and 7.17 show the comparison of results obtained from the numerical simulation with the Darton's (1977) correlation for bubble diameter estimation at various static bed heights, i.e. 0.34m, 0.40m, and 0.45m, with respect to superficial gas velocities of $1U_{mf} - 2U_{mf}$ in the gasifier side where river sand is used as the fluidization medium.

Similar to those observed in the combustor side, the bubble size increases with increasing superficial gas velocities. This is because any gas in excess of that required for minimum fluidization should go through the bed as bubbles as shown in the numerical visualization in Chapter 6 (Figure 6.1 and 6.2). Therefore when more excess gas in the system due to higher superficial gas velocities, the bubble size increases.

Table 7.8 shows the effect of static bed height on the bubble size. The values are taken at $2U_{mf}$. Both Darton's (1977) and numerically simulated bubble size is increasing linearly with the increasing static height for the range studied.

As compared to the combustor side, the numerical results of the gasifier show higher deviation (around 20%) in comparison with the Darton's (1977) results. ± 20% error bars are set to ease comparison. Our numerical visualization of 3D flow pattern at the gasifier and combustor (refer Chapter 6, Figure 6.2 and 6.3) shows that more smaller bubbles (as seen in Table 7.8, numerically simulated bubbles in gasifier is smaller than that in the combustor) are formed at the gasifier side.

Table 7.8: Effect of the static bed height on the bubble size at $2U_{mf}$

Static Bed Height	Bubble Size (m)	
(m)	Darton et al.	CFD (gasifier)
0.35	0.173	0.144
0.40	0.176	0.150
0.45	0.185	0.157

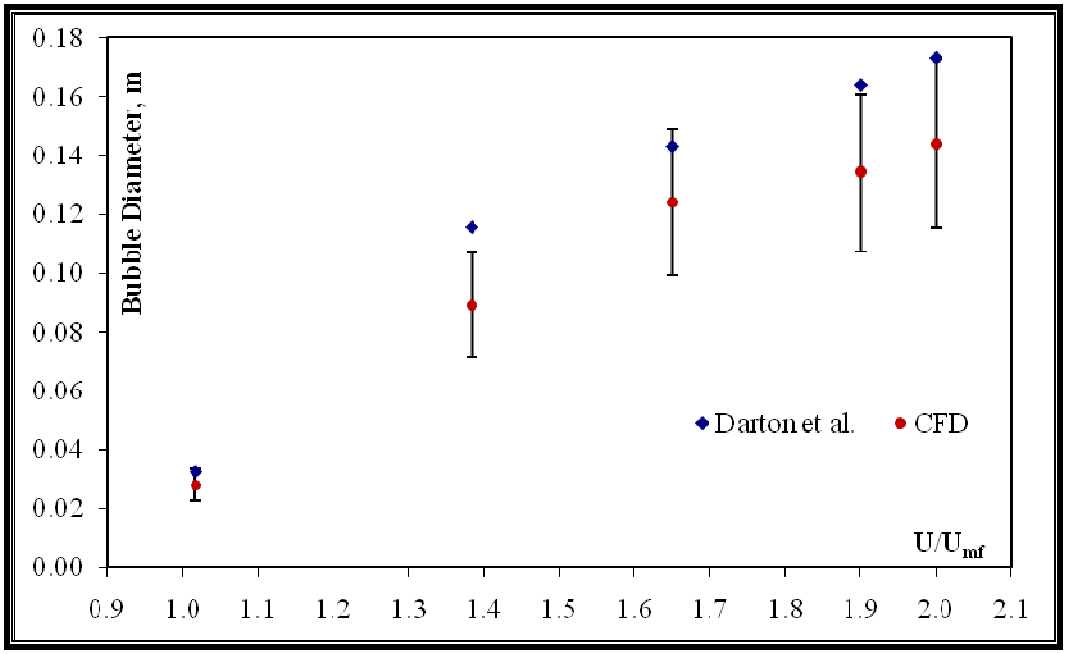

Figure 7.15: Comparison of the numerical results with the Darton's correlation at the static bed height of 0.35m for the bubble size in the gasifier

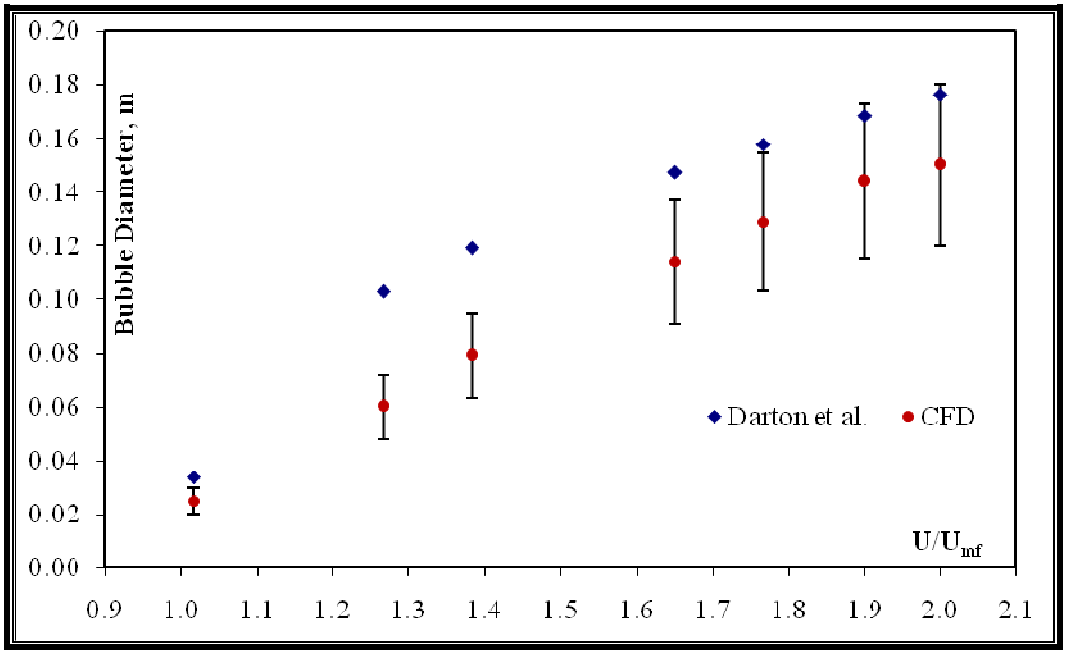

Figure 7.16: Comparison of the numerical results with the Darton's correlation at the static bed height of 0.40m for the bubble size in the gasifier

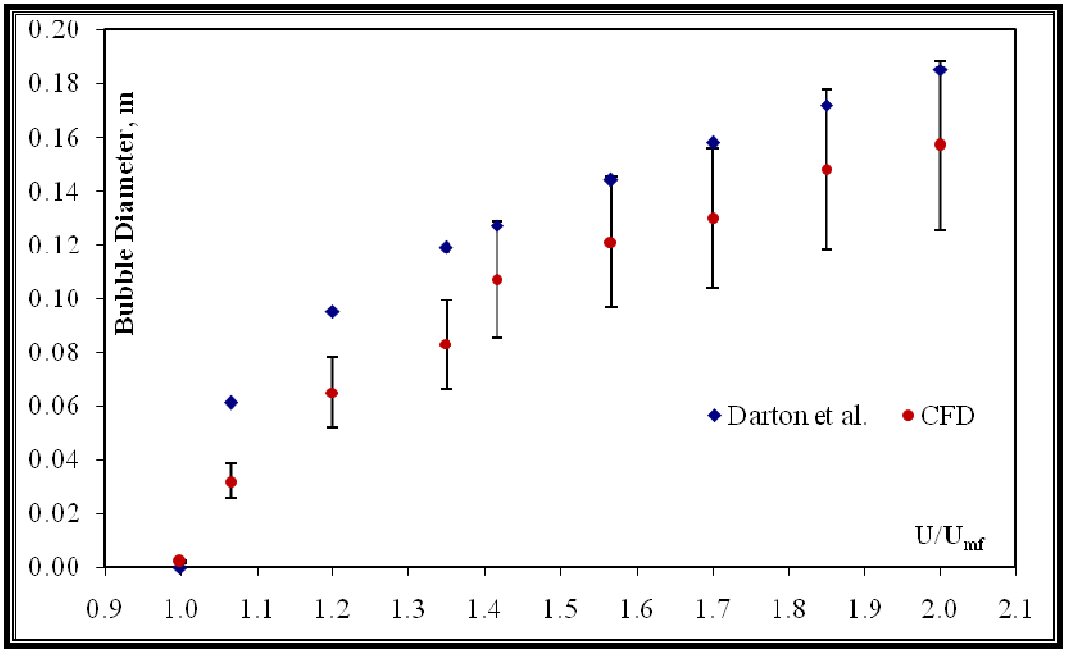

Figure 7.17: Comparison of the numerical results with the Darton's correlation at the static bed height of 0.45m for the bubble size in the gasifier

7.3.2.2 Alumina as the Inert Particles

Figures 7.18, 7.19 and 7.20 demonstrate the comparison of numerical simulated results with the Darton's (1977) correlation for bubble diameter estimation at various static bed heights, i.e. 0.20m, 0.30m, and 0.35m, with respect to superficial gas velocities of $1.0U_{mf}$ – $1.4U_{mf}$ in the gasifier side where alumina is used as the fluidization medium. ±20% error bars are set in the figure to indicate the degree of deviation between numerical and experimental values.

Bubble size increases with increasing gas velocities for both predictions. The deviation between bubble size estimated by the Darton's (1977) correlation and predicted by the numerical solution is large as shown in Figure 7.18. As has been discussed in previous section, intermediate- and through-channeling occurs in the alumina bed. When a shallow bed is used, the bubbles tend to form and erupt close to the wall because of the significant wall effect (Werther, 1968), resulting in higher porosity near the wall. There is a preferential path near the wall (lean phase), letting more flow through that portion, hence contributing to an intermediate channeling bed. Thus the large discrepancy is observed in Figure 7.18.

The effect of wall is inevitably weaker in a deep bed than in a shallow bed, because the bubbles have chances to coalesce with the adjacent bubbles, forming stronger forces to diminish the effect of wall and finally detach the bubbles from the wall. In a deeper bed as shown in Figure 7.19 and 7.20, the deviation decreases to around 25%. The Darton's bubble model is however dependent only on the superficial gas velocity and the bed height; other effects like the wall effect, actual geometrical flow behavior are not taken into consideration. To obtain more realistic comparison, physical experimental data should be made for bubble size at various heights. From this analysis, numerical solution is able to provide information on the channeling behavior of alumina at this point.

Table 7.9 shows the effect of static bed height on the bubble size. The values are taken at $2U_{mf}$. Both the Darton's (1977) bubble model and the numerical simulation of bubble

size are increasing linearly for the range studied. The similar linear relationship is obtained in river sand bed as well.

Table 7.9: Effect of the static bed height on the bubble size at $2U_{mf}$

Static Bed Height (m)	Bubble Size (m)	
	Darton et al.	CFD
0.35	0.151	0.117
0.40	0.166	0.145
0.45	0.170	0.150

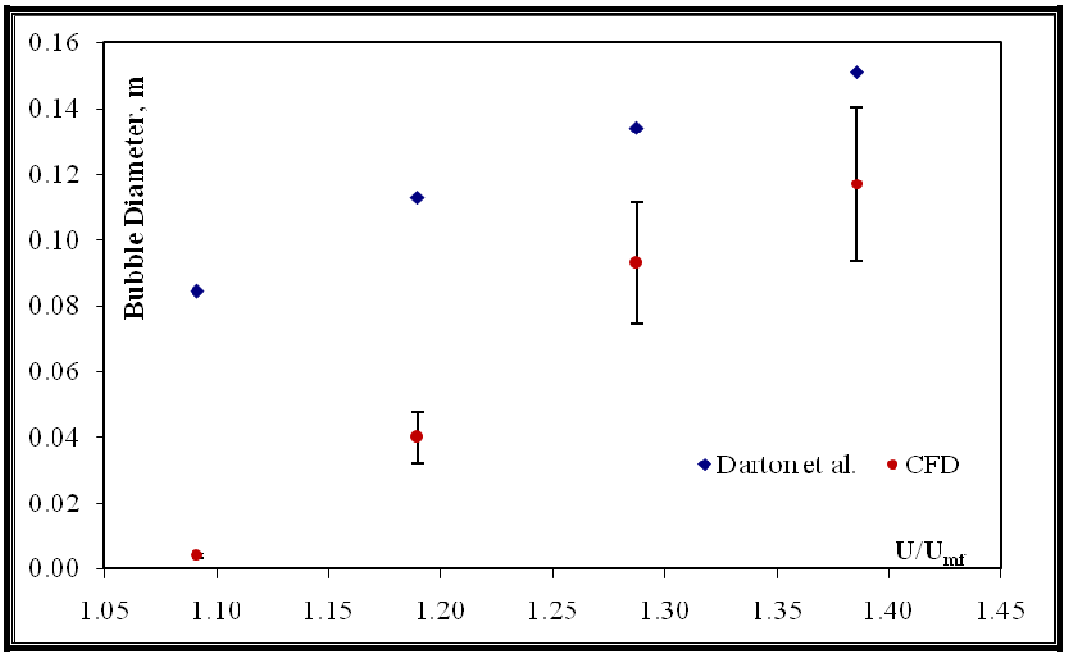

Figure 7.18: Comparison of the numerical results with the Darton's correlation at the static bed height of 0.20m for the bubble size in the gasifer

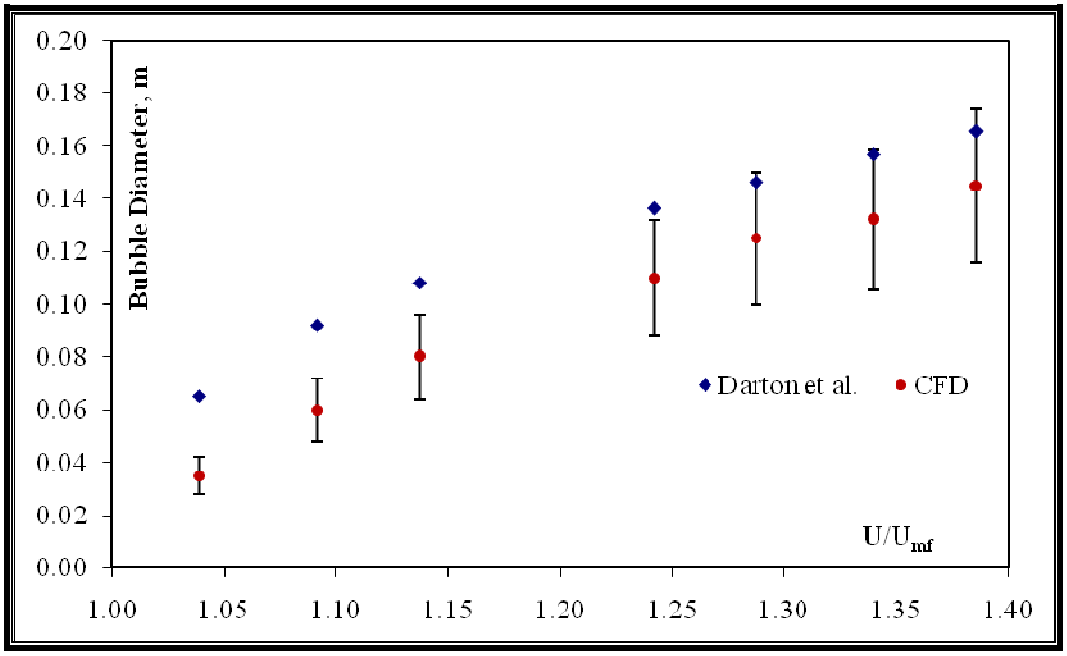

Figure 7.19: Comparison of the numerical results with the Darton's correlation at the static bed height of 0.30m for the bubble size in the gasifer

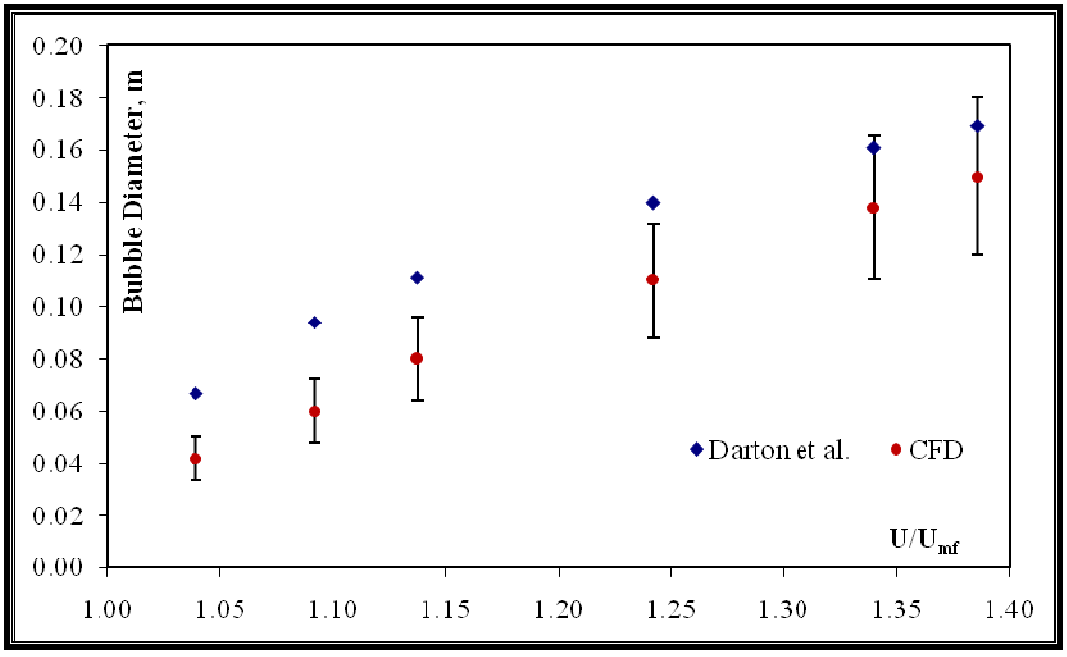

Figure 7.20: Comparison of the numerical results with the Darton's correlation at the static bed height of 0.35m for the bubble size in the gasifer

7.3.3 Effect of Effective Diameter on Bubble Size

The effect of effective diameter on the bubble size is investigated at different bed height, i.e. 0.35m, 0.40m and 0.45m as shown in Figure 7.21. The effective diameter of combustor and gasifier is 0.413m and 0.257m respectively.

As can be seen from the figure, the effective diameter has no significant effect on the Darton's (1977) prediction of bubble size. The bubble size is mostly in accordance for gasifier and combustor.

As for the numerical simulation, the effective diameter has observable effect on the bubble size. Larger bubble size is predicted at the combustor side. The bubble size predicted at the gasifier is always smaller by 5-10%. From our numerical visualization (refer Chapter 6, Figure 6.2 and 6.3), it also shows that more smaller bubbles are formed at the gasifier side. Though in the bed expansion ratio study in previous section, the bed expanded more at the gasifier side, and theoretically the bubble sizes should grow bigger in more expanded bed. However in this case, the effect of internals and wall with respect to effective diameter supersedes the effect of bed expansion. Gasifier is smaller than the combustor, thus smaller bubbles are expected due to more prevailing effects of internals and wall on fluidization behaviour.

Furthermore, it is worth noting that Darton et al. (1977) assumed that bubbles line up and grow as close together as possible, following specific paths, which is somewhat improbable in a chaotic system found in a fluidized bed, moreover a complex geometry CFBG. Hence, differences between simulated bubble size and those obtained from the correlation maybe due to the different bubble growth mechanisms that take place in simulated systems, i.e. the combination of the decrease in hydrostatic pressure toward the top of the fluidized bed as well as bubbles coalescing horizontally with neighbouring bubbles, respectively. The above leads to the perpetuation of bubbles, numerically, that might not necessarily line up and grow as close together as possible, as was assumed in the Darton's (1977) model.

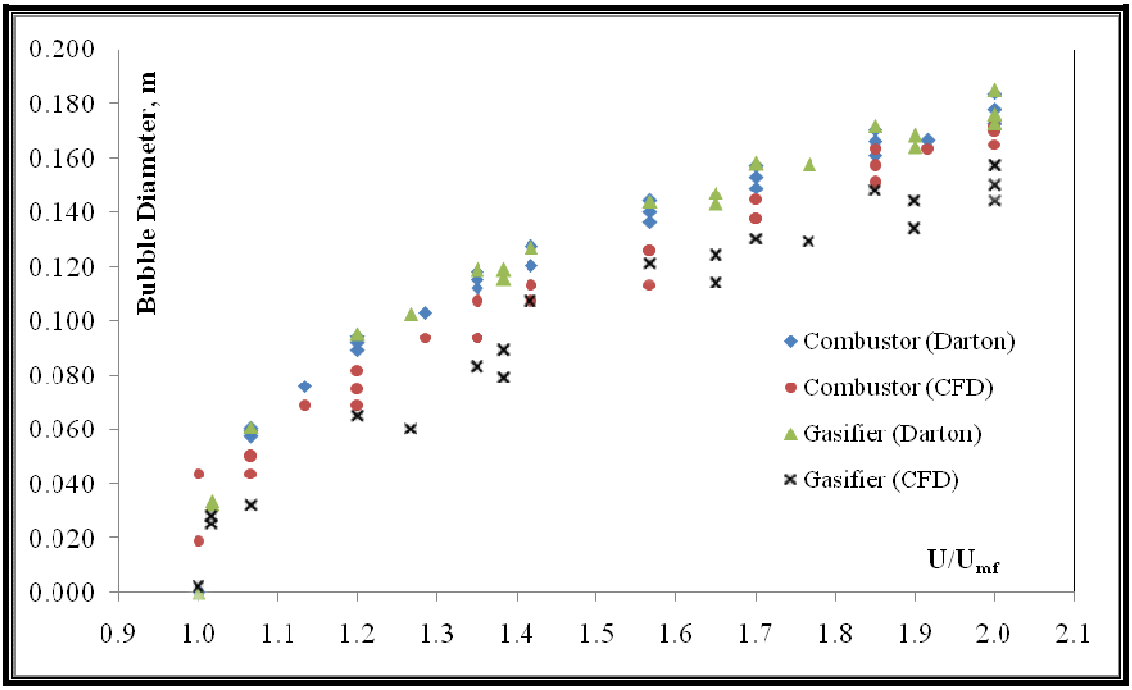

Figure 7.21: Effect of the effective diameter on the bubble size for the static bed height of 0.35m, 0.40m and 0.45m

7.3.4 Effect of Different Inert Particles on Bubble Size

Figure 7.22 shows the effect of different inert particles on the bubble size at static bed height of 0.35m. The fluidization regime ranges from $1.0U_{mf}$ to $1.4U_{mf}$. The study is conducted at the gasifier side.

In the figure, the bubble size in the alumina bed is bigger than that in the river sand bed. As discussed before, channelling occurs in alumina bed. Due to alumina's physical properties, portion of the bed becomes less porous, which creates a preferential path inside the bed. Bigger bubbles may grow along with the path. Unlike the river sand bed, bubble grows by depleting the continuous phase locally.

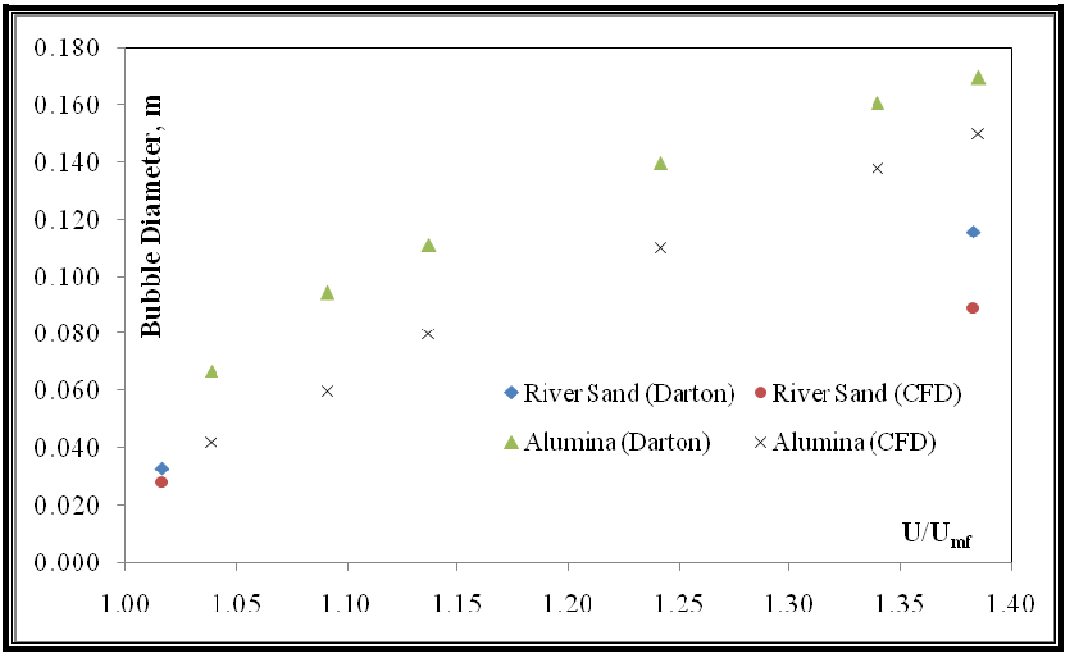

Figure 7.22: Effect of the different inert particles on the bubble size at the gasifier

7.4 BED PRESSURE DROP STUDY

The bed pressure drop is another important fluidization parameter in determining the hydrodynamics in CFBG. This parameter is preliminary investigated and then extended to check the fluidization quality in the combustor and gasifier compartments.

7.4.1 Combustor Compartment

The numerical model settings can be found in Table 7.1.

7.4.1.1 River Sand as the Inert Particles

Figures 7.23 – 7.25 depict the comparison of numerically simulated results for bed pressure drop study with the experimental results using river sand of mean particles size 272 µm as the fluidization medium at various static bed heights, i.e. 0.35m, 0.40m and 0.45m in the combustor. The superficial gas velocities are in the range of $1U_{mf} - 2U_{mf}$. ±10% error bars are set in the figures to indicate with respect to numerical results, the degree of deviation between numerical and experimental values.

As can be seen from the figures, the pressure drop profiles remain steady after the minimum fluidization velocity is reached. At this point the bed pressure drop should be equivalent to the pressure exerted by the weight of the suspended river sand. This will be verified in the fluidization quality section later.

The numerical results also predict similar trend but with under-predicted values at average less than 10% deviation. However, the deviation between experimental data and numerical data is larger (10%) at lower U_{mf} (less than $1.5U_{mf}$). As has been discussed in section 7.2.1.1, the U_{mf} from numerical simulation may be higher than the actual U_{mf} due to the setting of mono-sized distribution of river sand. Thus the numerical bed pressure drop profile at this point is still increasing to attain the static weight load (refer Chapter 5 section 5.4.2 for U_{mf} determination). The deviation decreases to less than 10% at above $1.5U_{mf}$. In Taghipour, et al. (2005) work, he stated that standard Syamlal O'Brien (1994) drag law generally underpredicts the bed pressure drop.

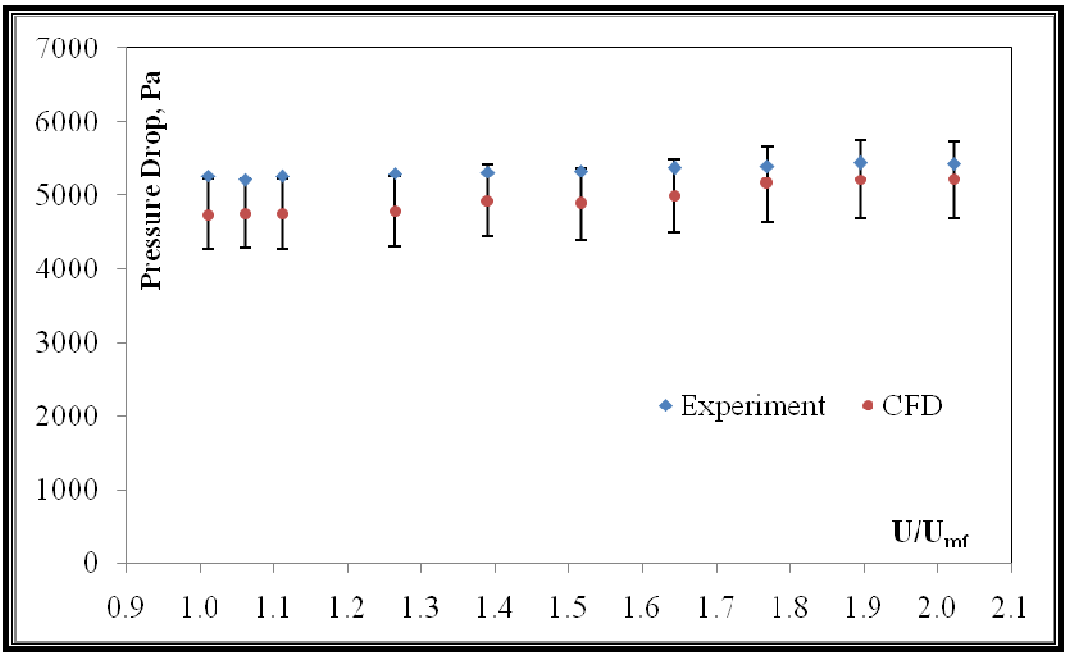

Figure 7.23: Comparison of the numerical results with the experimental results at the static bed height of 0.35m for the bed pressure drop in the combustor

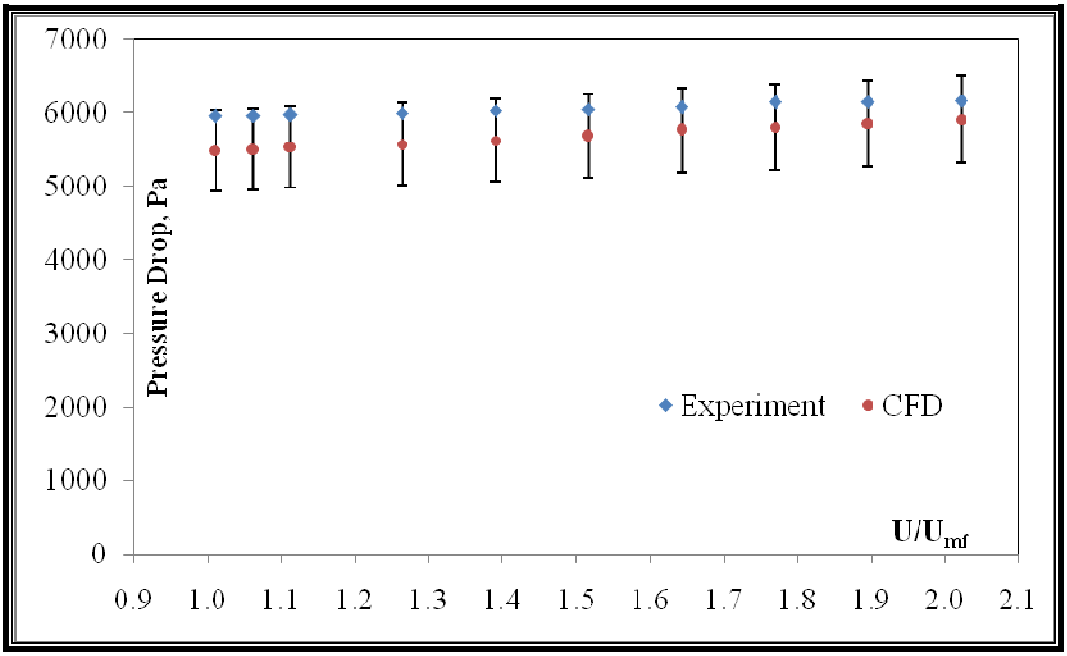

Figure 7.24: Comparison of the numerical results with the experimental results at the static bed height of 0.40m for the bed pressure drop in the combustor

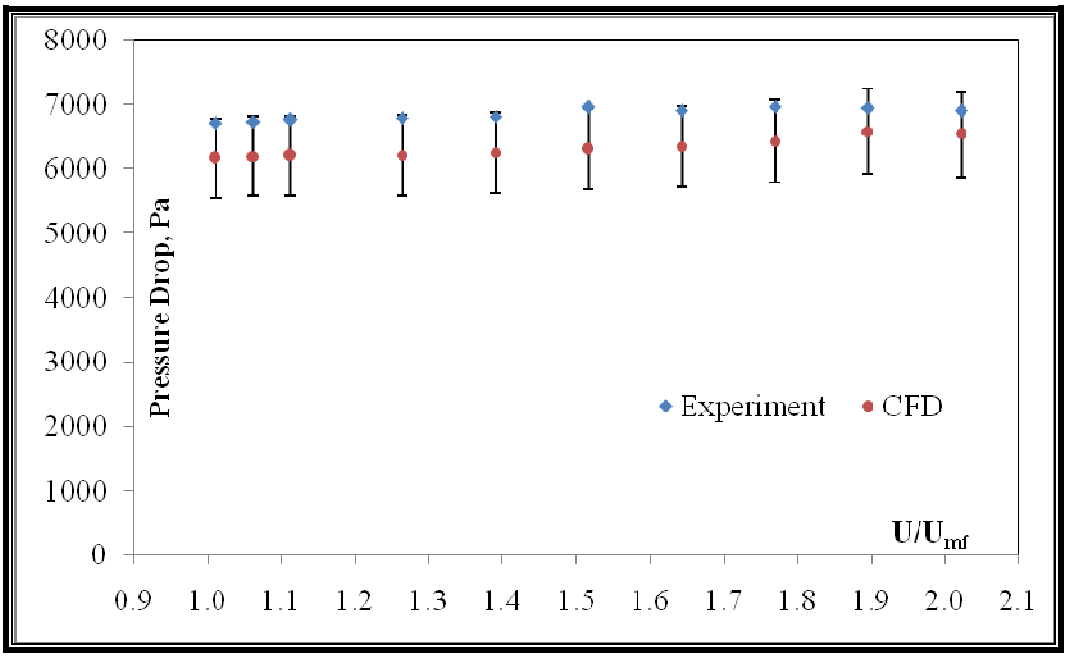

Figure 7.25: Comparison of the numerical results with the experimental results at the static bed height of 0.45m for the bed pressure drop in the combustor

7.4.2 Gasifier Compartment

The numerical model settings can be found in Table 7.3.

7.4.2.1 River Sand as the Inert Particles

Figures 7.26 – 7.28 show the comparison of numerically simulated results for bed pressure drop study with the experimental results using river sand of mean particles size 272 μm as the fluidization medium at various static bed heights, i.e. 0.35m, 0.40m and 0.45m in the gasifier. The superficial gas velocities are in the range of $1U_{mf}$ – $2U_{mf}$. ±10% error bars are set in the figures for comparison purposes between numerical values and experimental values.

As can be seen in the figures, the experimental bed pressure drop profile of the gasifier shows different tendency from that observed in the combustor side. The profiles seem to fluctuate around a fixed pressure drop line. This is also observed in numerically predicted values; however the level of fluctuation is not as severe as the experimental values. This behavior clearly shows that channeling happens in the gasifier compartment. Detailed discussion will be given in fluidization quality section for channeling behavior.

Based on this study, numerical simulation is able to capture the channeling behavior occurring in the gasifier side with deviation on average around ±10% which is quite satisfactory at this stage.

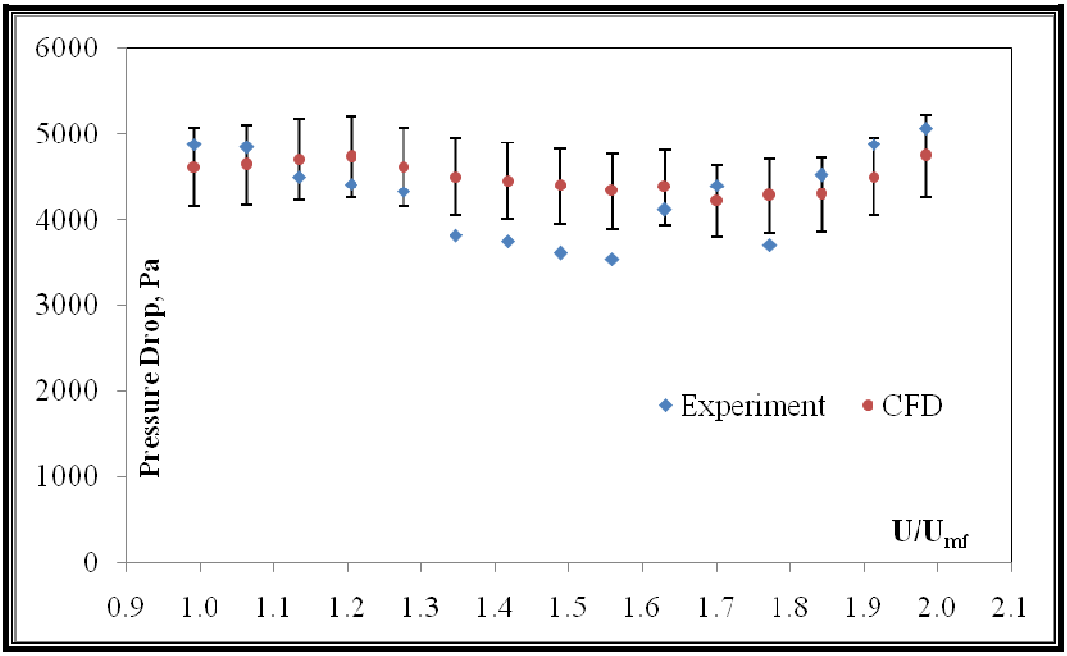

Figure 7.26: Comparison of the numerical results with the experimental results at the static bed height of 0.35m for the bed pressure drop in the gasifier

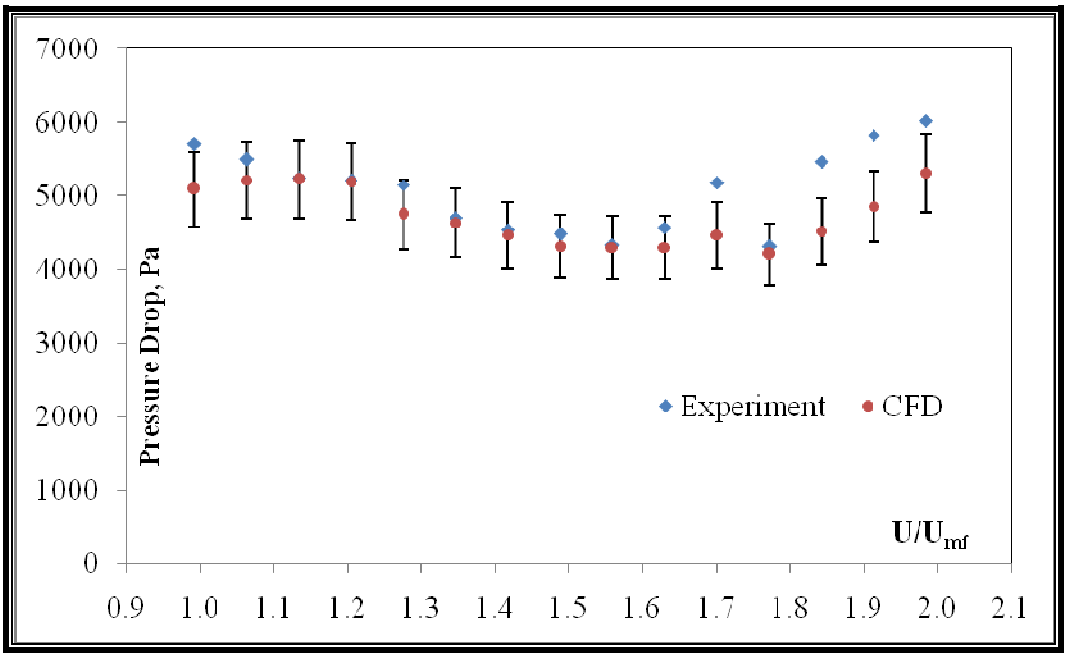

Figure 7.27: Comparison of the numerical results with the experimental results at the static bed height of 0.40m for the bed pressure drop in the gasifier

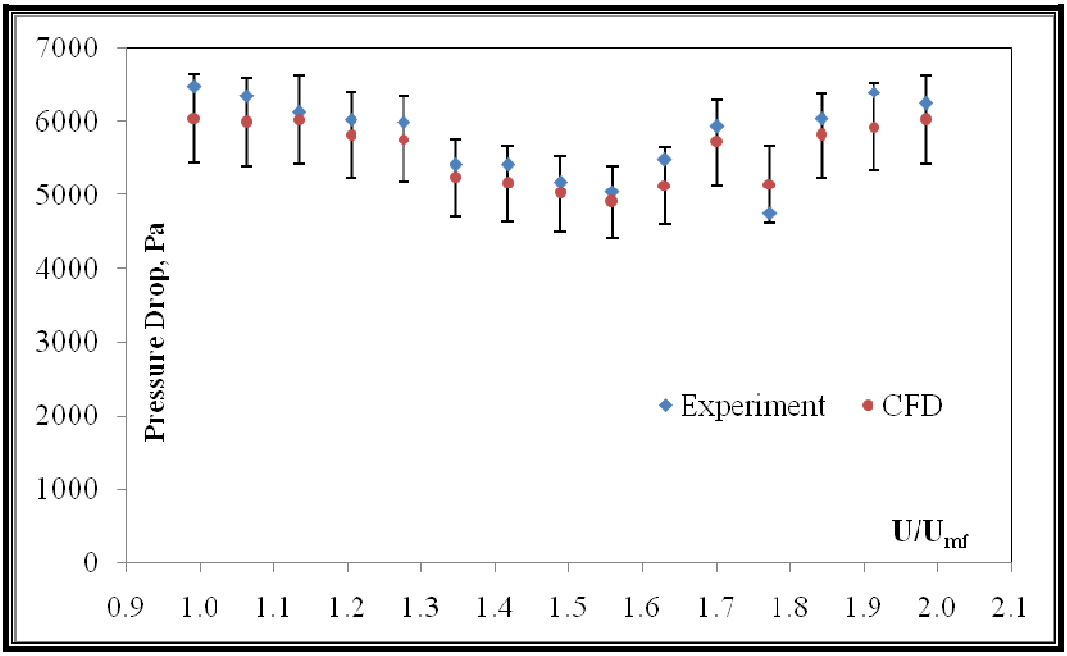

Figure 7.28: Comparison of the numerical results with the experimental results at the static bed height of 0.45m for the bed pressure drop in the gasifier

7.4.2.2 Alumina as the Inert Particles

Figures 7.29, 7.30 and 7.31 illustrate the comparison of results from numerical simulation for bed pressure drop study with the experimental results using alumina of particles size 360 µm as the fluidization medium at various static bed heights, i.e. 0.20m, 0.30m and 0.35m in the gasifier. The superficial gas velocities are in the range of $1.0U_{mf}$ – $1.4U_{mf}$. ±10% error bars are set in the figures for results comparison between the numerical simulation and experiment.

As can be seen in the figures, the experimental bed pressure drop profile fluctuates severely at shallow bed; the level of fluctuation becomes more subsided at deep bed. This is also observed in numerically predicted profile. This is similar to those that observed for the river sand bed. Follow from that, the fluctuating behavior shows that channeling occurs in the alumina bed as well. The profile demonstrates the tendency of increasing fluctuation at higher U_{mf}. Detailed discussion will be given in fluidization quality section for channeling behavior.

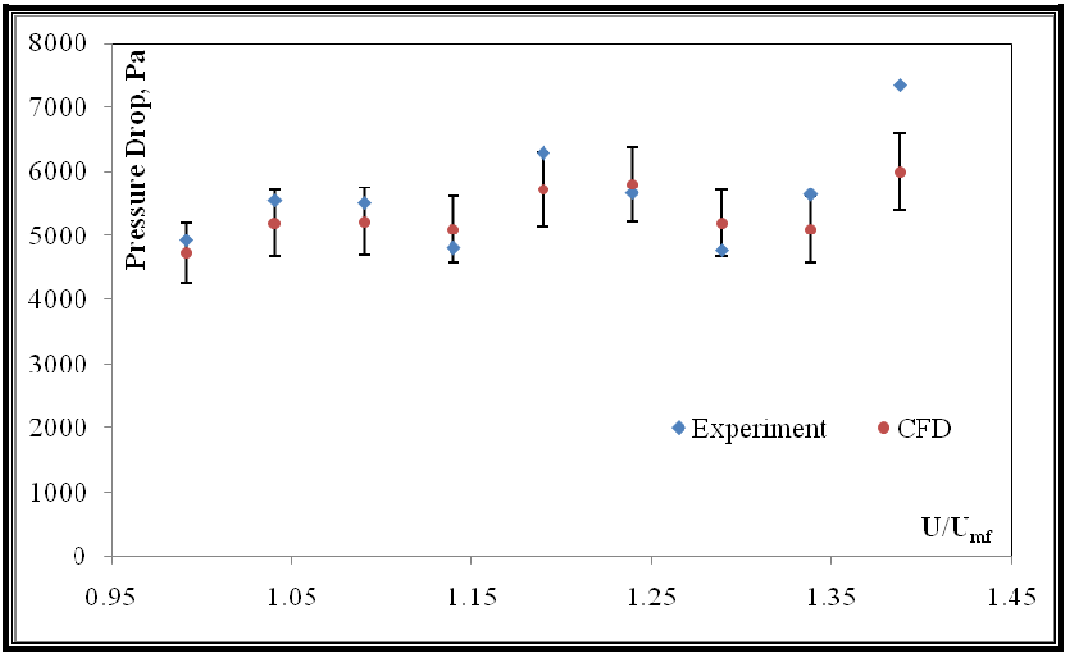

Figure 7.29: Comparison of the numerical results with the experimental results at the static bed height of 0.20m for the bed pressure drop in the gasifier

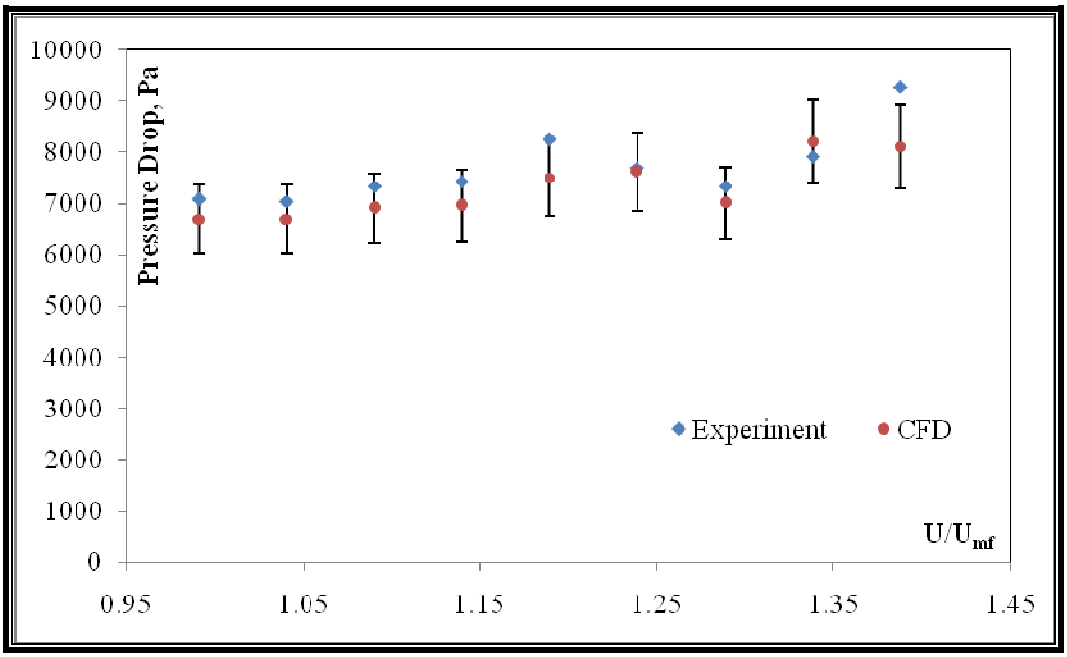

Figure 7.30: Comparison of the numerical results with the experimental results at the static bed height of 0.30m for the bed pressure drop in the gasifier

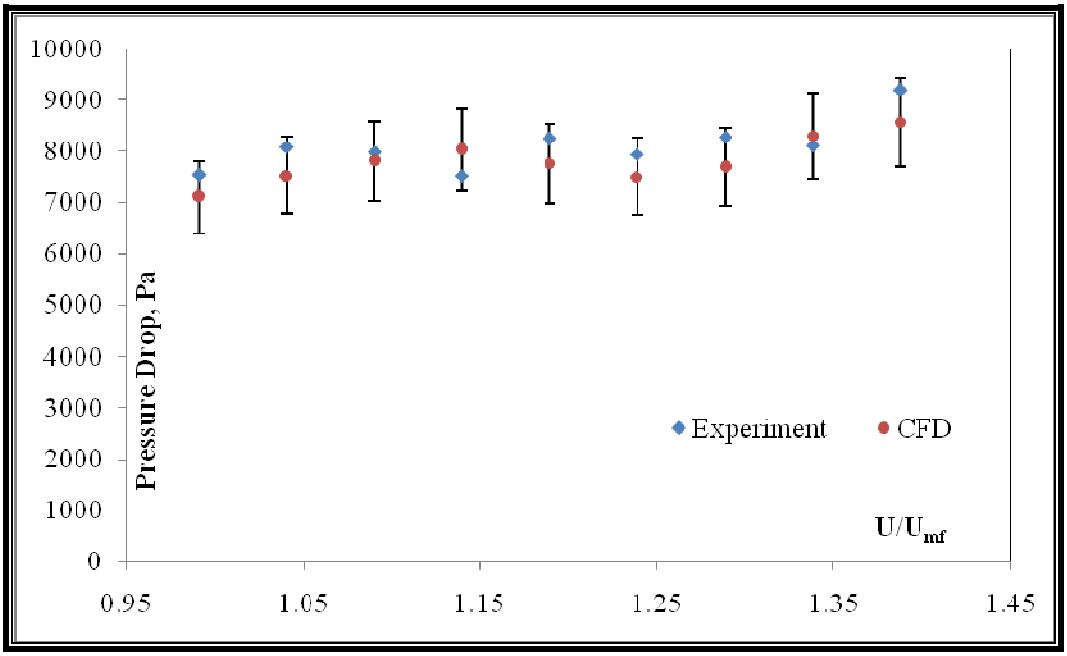

Figure 7.31: Comparison of the numerical results with the experimental results at the static bed height of 0.35m for the bed pressure drop in the gasifier

7.4.3 Fluidization Quality

Fluidization is defined as a process in which particles are transformed into a fluid-like state through contact with either a gas or a liquid. A good fluidization as shown in Figure 7.32 can be defined as the ratio, Q, of the experimental bed pressure drop to the pressure induced by the static bed weight (Sathiyamoorthy and Masayuki, 2003). Table 7.10 shows the static bed weight in the respective compartment at particular bed height.

Table 7.10: Static bed weight distribution in the combustor and gasifier

Static Bed Height (m)	Static Bed Weight (N)		
	Combustor	Gasifier	
	River Sand	River Sand	Alumina
0.20	-	-	570
0.30	-	-	810
0.35	1110	670	950
0.40	1290	770	-
0.45	1440	870	-

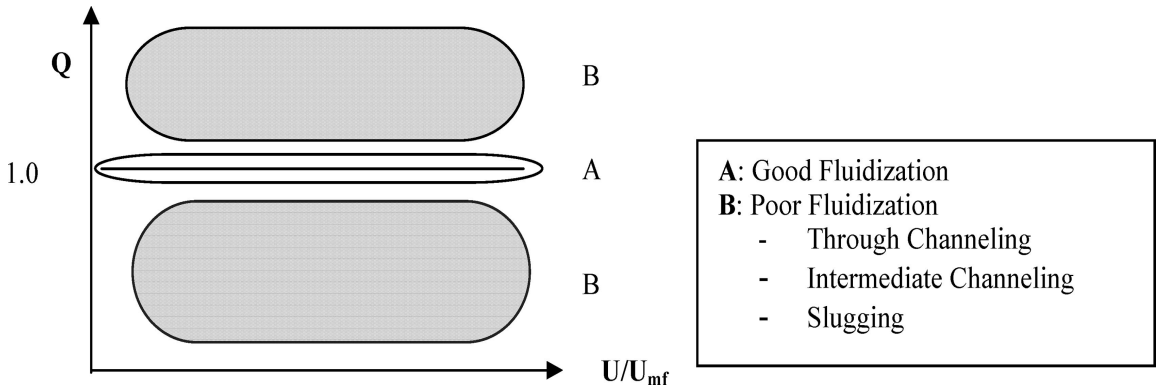

Figure 7.32: Fluidization quality

The region A in Figure 7.32 is the desired region for a well-lifted and well-mixed fluidization from minimum fluidization velocity, U_{mf} onwards, in other words this is the region of good fluidization. The value of Q in region A ranges from 0.95 to 1.05. The B regions are an indicative of a poor fluidization. There are considerably two reasons that lead to poor fluidization, i.e. channeling and slugging. Channeling can be further classified as through-channeling and intermediate channeling. In through channeling, the flow paths extend to the entire bed of particles, while the intermediate channeling involves only a portion of the bed, which results in higher bed pressure drop with increasing gas flowrates. The details of through channeling, intermediate channeling and

slugging can be found in Davidson et al. (1985), Kunii and Levenspiel (1991), and Nicholas and Paul (1984).

7.4.3.1 Effect of Effective Diameter and Static Bed Height on Fluidization Quality

The effect of the effective diameter on the experimental fluidization quality, Q, is investigated at different bed height, i.e. 0.35m, 0.40m and 0.45m as shown in Figure 7.33. River sand is used as the fluidizing medium. The effective diameter of the combustor and the gasifier is 0.413m and 0.257m respectively. Two dashed lines are in placed to indicate the good fluidization quality region.

As seen in figure, the combustor falls in the good-quality region, but the gasifier does not. As shown in Table 7.11, the values of R_{op} are greater than those of R_c (refer Chapter 5 section 5.3 for R_c determination) for both compartments in most cases. Moreover, the gasifier still yields poor fluidization quality. The flow behavior of a gas–solid fluidized bed is very complex and highly sensitive to bed diameter (Nicholas and Paul, 1984). The effect of wall on fluidization behavior, which has a strong relationship with effective diameter, D_e, is a determining factor that leads to the fluidization quality. Werther (1968) and other researchers showed that the wall effect becomes progressively more significant as the bed diameter decreases. Hence, the effective diameter, D_e, of each compartment has a pronounced effect on the Q value in terms of the wall effect. If D_e is sufficiently big, the Q is expected to maintain at around 1.0 within the practical operating range.

The profile of the gasifier is in fact an indicator of a channeling bed as per the definition earlier (Figure 7.32). When Q value is below 0.90, the bed is experiencing channeling.

Table 7.11: Comparison between the combustor and gasifier

	Combustor	Gasifier	
	River Sand	**River Sand**	**Alumina**
D_e (m)	0.413	0.257	0.257
H/D_e	0.85 – 1.09	1.36 – 1.75	0.78 – 1.36
R_{op}/R_c	1.0 – 3.3	1.4 – 5.6	3.6 – 18.6

It is observable from Figure 7.33 that the increment in static bed height does not have significant impact on the fluidization quality for both the combustor and the gasifier compartments.

Figure 7.34 shows the effect of the effective diameter on numerical fluidization quality, Q. Numerical simulation agrees well with the experimental data in terms of tendency, but the values are being under-estimated due to the reason as discussed earlier (refer bed expansion ratio study, section 7.2). Numerical modeling has been a sophisticated tool to predict the right trend as compare to the experimental results. In order to obtain more comparable results with the experimental data, numerical simulation needs to be fine-tuned so that wide spectrum of particles size can be set to cater for the actual experimental vicinity.

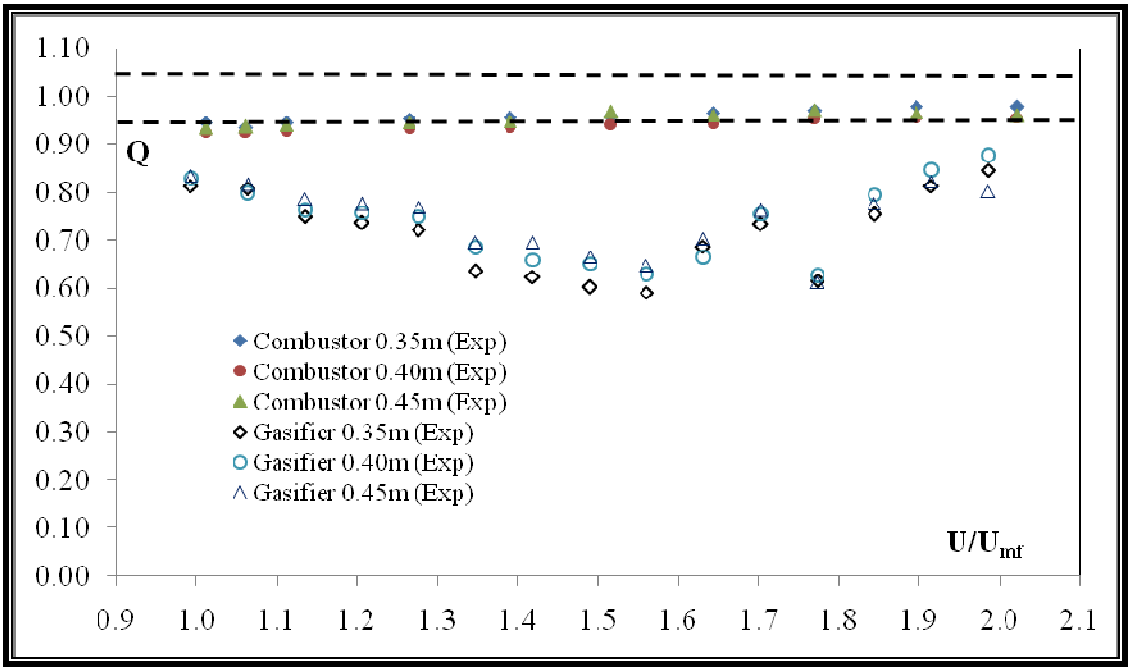

Figure 7.33: Effect of the effective diameter on the experimental fluidization quality, Q, at the static bed height of 0.35m, 0.40m and 0.45m

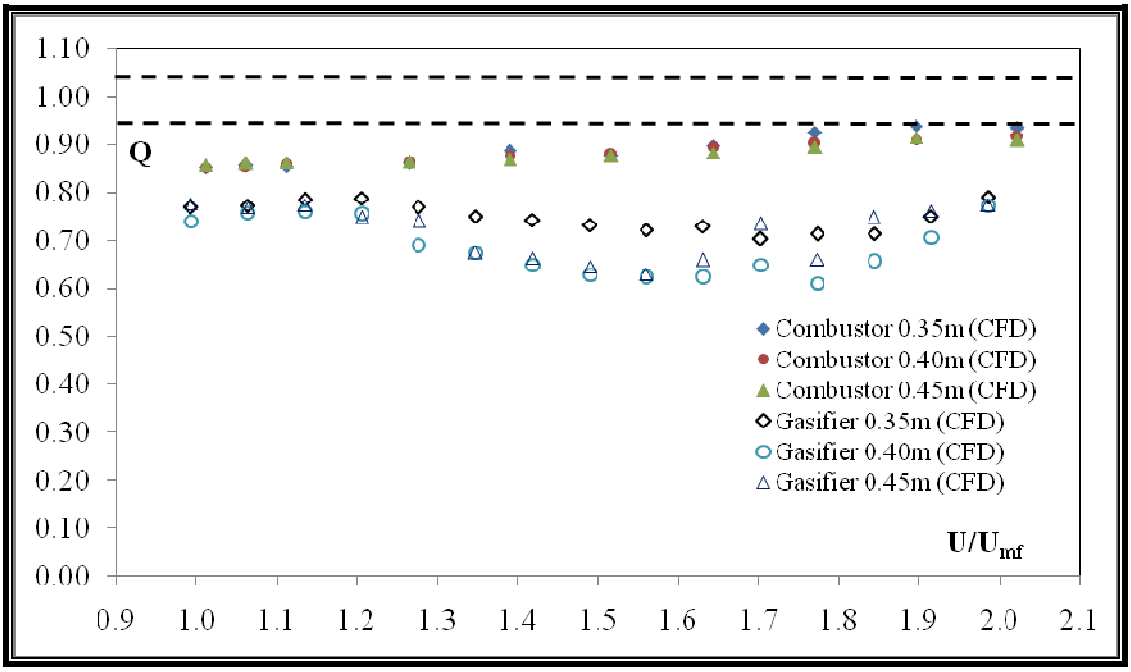

Figure 7.34: Effect of the effective diameter on the numerical fluidization quality, Q, at the static bed height of 0.35m, 0.40m and 0.45m

7.4.3.2 Effect of Different Inert Particles on Fluidization Quality

Figure 7.34 depicts the effect of the different inert particles used on the fluidization quality, Q, with respect to different static bed height, i.e. 0.35m, 0.40m and 0.45m at the gasifier. The fluidization regime ranges from $1.0U_{mf}$ to $1.4U_{mf}$. Two dashed lines are in placed to indicate the good fluidization quality region.

The fluidization quality remains poor because Q values are outside the boundary of good fluidization region. This again suggested that the D_e effect is prevailing. As mentioned above, the D_e has the leading effect on the Q if the basic distributor design requirement has been met; i.e., R_{op} is greater than the R_c. River sand bed has the Q value fluctuating around 0.7 – 0.8, this is an indication of through channeling. Through channeling can be detected when the Q value is always less than 0.90. Alumina bed also shows the channeling behavior. From the figure, the fluidization quality of alumina bed shows the continue increasing tendency with increasing of superficial gas velocities. This phenomenon indicates that the alumina bed experiences intermediate channeling. The intermediate channeling is more severe at shallow bed (refer Figure 7.29).

Numerical simulation predicts the similar trend for river sand used as compared to the experimental results. As for alumina bed, numerical simulation predicts a less fluctuating but similar trend of fluidization quality for the range studied. Numerical model is quite predictive at this stage.

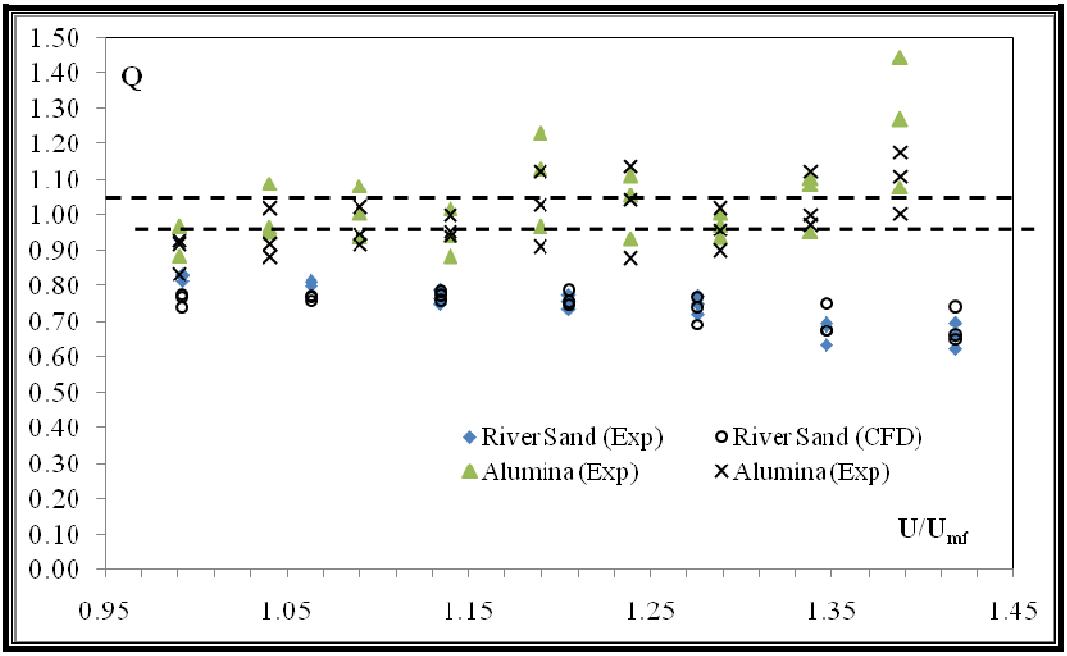

Figure 7.35: Effect of the different inert particles used on the fluidization quality in the gasifier

7.5 SOLID CIRCULATION RATE (SCR) STUDY

In CFBG, heat transfer between the two compartments, i.e. combustor and gasifier, is achieved via internal solid circulation. For steady state operation, right solid circulation rate (SCR) between the two compartments must be achieved and maintained. Hence, the determination of SCR is of great importance for the success of gasification and combustion reactions in their respective compartments. Solid circulation rate (SCR) profiles were analyzed for different bed heights, different main bed, v-valve and riser aeration.

The numerical simulation is carried out to depict the initial functional characteristics of the compartmented fluidization bed gasifier; indeed, the solid circulation rate (SCR) of the bed is affected by four distinct performance parameters like height of the fluidized bed, aeration rate of the main body, v-valve as well as the riser. The numerical simulation is used for the first attempt to predict the SCR of CFBG. To perform

experimental study with arbitrary settings for SCR is extremely time consuming; thus numerical solution plays important role in this aspect.

The fluidized bed consists mostly of inert particles whose properties dominate the fluidization characteristic. Hence, the SCR studies are conducted in single component system, using river sand. Table 7.12 summarizes the numerical model settings for SCR study in the gasifier and the combustor.

Table 7.12: 3D Simulation model parameters for the solid circulation rate study in the combustor and gasifier

Description	Value		Unit	Comment
	Combustor	Gasifier		
Particle density	2620	2620	kg/m^3	
Mean particle size	272	272	µm	
U_{mf}	0.06	0.06	m/s	Determined experimentally
Initial solid packing	0.45	0.45	-	
Gas density	1.2	1.2	kg/m^3	
Superficial gas velocity				
Main bed	0.078 – 0.102	0.078 – 0.102	m/s	$1.3U_{mf} – 1.7U_{mf}$
Riser	0.48 – 0.72	0.48 – 0.72	m/s	$8U_{mf} – 12U_{mf}$
V-valve	0.30 – 0.54	0.30 – 0.54	m/s	$5U_{mf} – 9U_{mf}$
Static bed height	0.20, 0.30, 0.40	0.20, 0.30, 0.40	m	

7.5.1 Effect of Static Bed Height on SCR

Figure 7.36 shows the effect of static bed height (0.20m – 0.40m) on the solid circulation rate (SCR). As seen in the figure, the SCR increases with the increase in bed height. The SCR is dependent on the hydraulic head (static bed weight) of the bed. The higher the static bed height, the larger the hydraulic force exerted, thus induces higher SCR. These trends are similar to those observed by other researchers in this type of reactor (He, 1993; Yan, 1995; Bhattacharya et al., 1999).

Numerical simulation under-predicts the SCR values, however the tendency of the profile is still following the experimental ones. As has been discussed earlier, the U_{mf} from the simulation can be higher than the actual U_{mf} due to mono-size distribution of river sand in numerical simulation. With the operation of riser and v-valve, the effect of dissimilar U_{mf} becomes more evident, thus all SCR values are under-predicted by around 15% for all case studies. Despite the aforementioned, numerical simulation is able to predict the tendency of SCR.

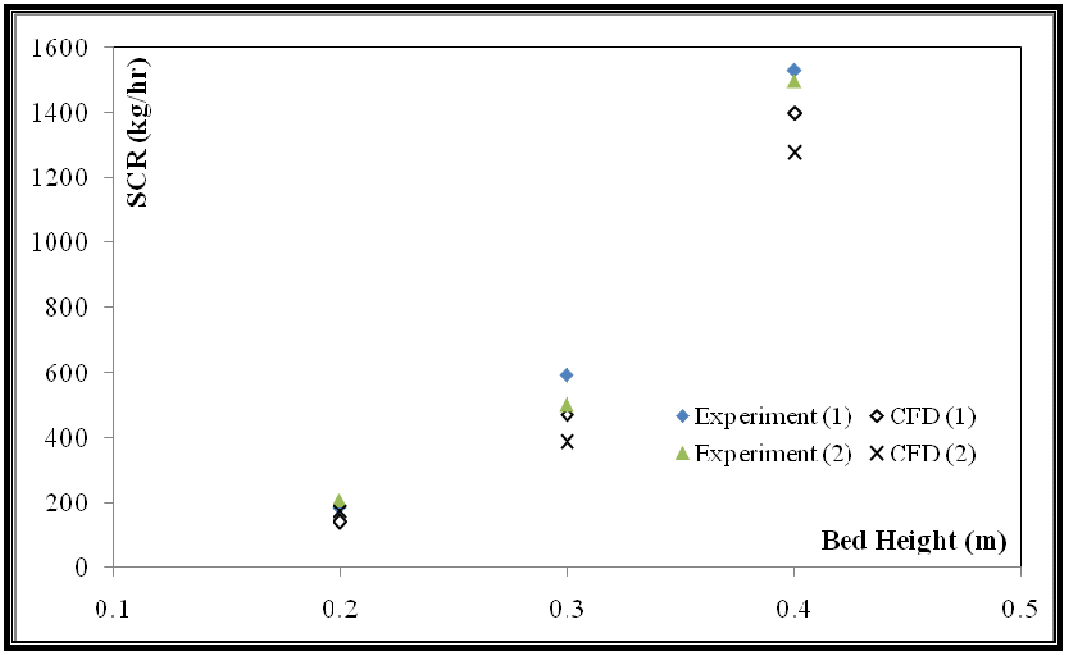

Figure 7.36: Effect of the static bed height on the solid circulation rate (SCR) (1)$Q_b = 1.3U_{mf}$, $Q_r = 12U_{mf}$, $Q_v = 5U_{mf}$; (2) $Q_b = 1.3U_{mf}$, $Q_r = 8U_{mf}$, $Q_v = 9U_{mf}$

7.5.2 Effect of Main Bed Aeration on SCR

The effect of the main bed aeration ($1.3U_{mf} - 1.7U_{mf}$) on the solid circulation rate (SCR) is illustrated in Figure 7.37. The different main bed aeration does not have any noticeable impacts on the experimental SCR. When the bed is fluidized, the bed pressure drop remains unchanged with further increase in the main bed aeration. As a result, one can expect the experimental SCR remains constant when the compartmented bed is fluidized within this range of superficial velocity.

However, the experimental findings are opposite to Bhattarcharya et al. (1997) and He (1993). According to Bhattarcharya et al. (1999), there are two opposing forces affecting SCR when the bed aeration increases. On one hand, increasing bed aeration leads to reduction of the driving force due to an increase in bed porosity. This contributes to a reduction of SCR. On the other hand, gas cross-flow from v-valve aperture to riser increases with the increase of bed aeration. The latter reduces the pressure drop across the v-valve and riser thus increasing SCR. This is also supported by He (1993) stated that bed aeration caused gas cross-flow, delivering more air to v-valve and riser, leading to higher SCR. It is worth noting that the main bed aeration operating range for Bhattacharya et al. (1997) and He (1993) is $1U_{mf} - 3U_{mf}$ and $1U_{mf} - 3.5U_{mf}$ respectively in small scale circulating fluidized bed experimental set up.

The numerical simulation predicts the similar behavior like those observed in experimental results. The SCR remains nearly constant with the variation in the main bed aeration from $1.3U_{mf}$ to $1.7U_{mf}$. The trend is well captured by the numerical solution. However, the SCR values are under-predicted by around 20%. In order to obtain more improved results, numerical simulation needs to be fine-tuned so that wide spectrum of particles size can be set to cater for the actual experimental vicinity. The numerically simulated operation of v-valve and riser for SCR is shown in Appendix B where the sand velocity and vortex within the v-valve and riser is studied.

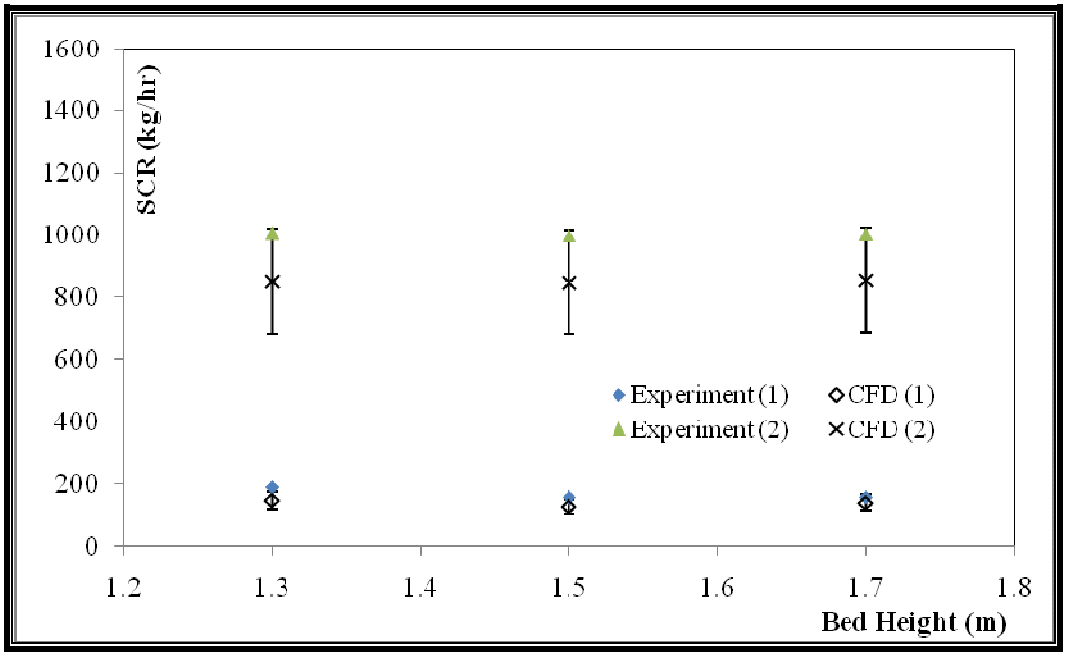

Figure 7.37: Effect of the main bed aeration on the solid circulation rate (SCR)
(1)H_b = 0.2m, $Q_r = 12U_{mf}$, $Q_v = 5U_{mf}$; (2) H_b = 0.4m, $Q_r = 8U_{mf}$, $Q_v = 5U_{mf}$

7.5.3 Effect of Riser Aeration on SCR

Figure 7.38 demonstrates the effect of the riser aeration ($8U_{mf}$ – $12U_{mf}$) on the solid circulation rate (SCR). It is observed that the SCR initially increases then decreases with increasing riser aeration. It is expected that the increase in riser aeration would increase the SCR due to higher entrainment rate. However, further increase of the riser aeration may increase the frictional and acceleration pressure drop in the riser. This may eventually result in a reduction in the SCR. This trend is consistent with the results reported by Bhattacharya et al. (1999).

This is however predicted differently by our numerical simulation. The SCR is linearly increased with the increment in riser aeration for the range of studies. The behaviour at higher riser aeration as discussed before is not captured by the numerical solution. This could be attributed to the higher U_{mf} from numerical simulation than actual U_{mf} as discussed earlier.

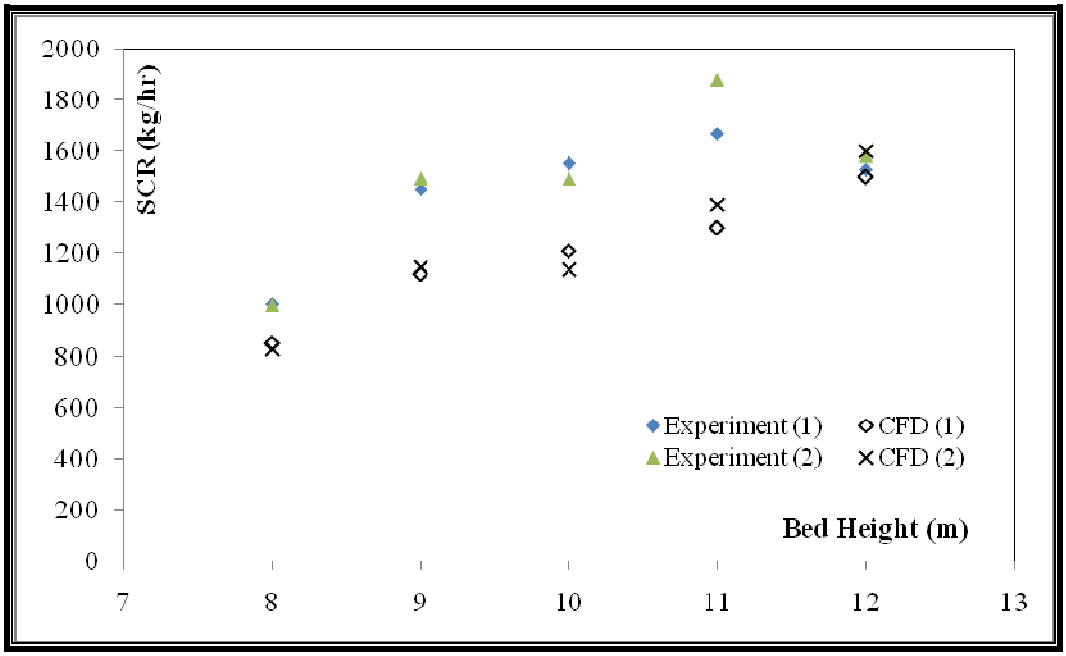

Figure 7.38: Effect of the riser aeration on the solid circulation rate (SCR)
(1)H_b = 0.4m, $Q_b = 1.3U_{mf}$, $Q_v = 5U_{mf}$; (2) H_b = 0.4m, $Q_b = 1.7U_{mf}$, $Q_v = 9U_{mf}$

7.5.4 Effect of V-valve Aeration on SCR

Figure 7.39 depicts the effect of the v-valve aeration ($5U_{mf}$ – $9U_{mf}$) on the solid circulation rate (SCR). For experiment (1), the SCR increases then decreases with increase in the v-valve aeration. Conversely, for experiment (2), the v-valve aeration has no obvious effect on the SCR. Ideally aeration through the v-valve creates a low pressure region that induces a pumping effect. Greater aeration through the v-valve will therefore lead to greater pumping effect, where more solids are being sucked thus contributing to higher SCR. However simultaneously, it also increases the resistance across the v-valve-to-riser orifice. Thus the two opposing effects explain the different SCR observed at experimental data.

The numerical simulation predicts dissimilar tendency of SCR. The SCR increases linearly with the increase in the v-valve aeration. The pumping effect is well predicted by the numerical simulation however the resistance across the v-valve-to-riser as discussed before is not captured.

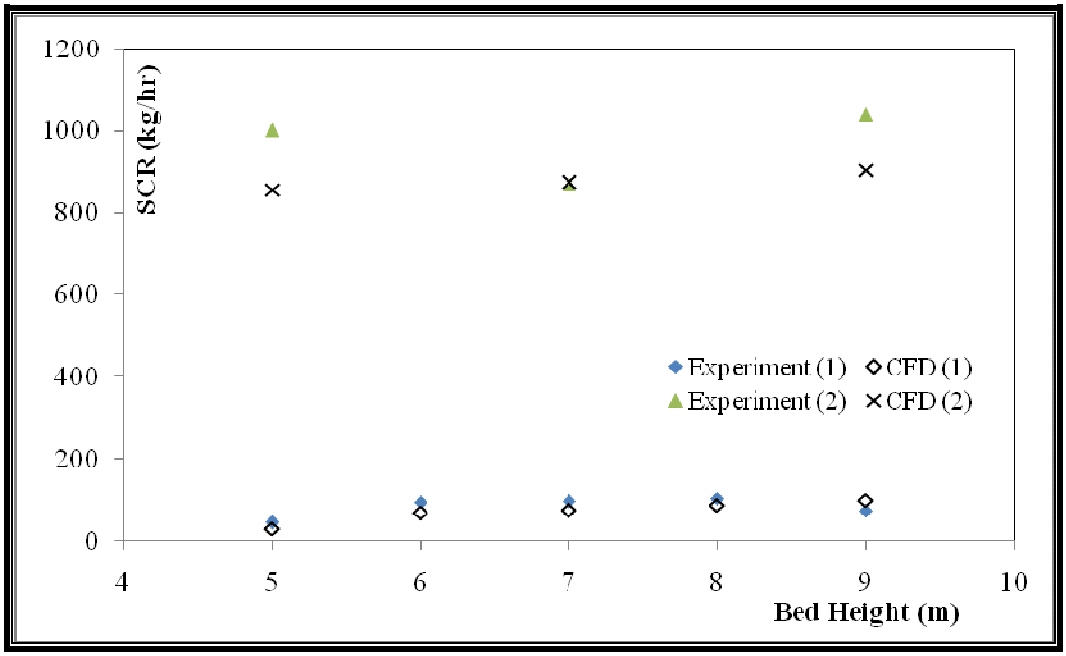

Figure 7.39: Effect of the v-valve aeration on the solid circulation rate (SCR) (1)H_b = 0.2m, $Q_b = 1.3U_{mf}$, $Q_r = 8U_{mf}$; (2) H_b = 0.4m, $Q_b = 1.7U_{mf}$, $Q_r = 8U_{mf}$

7.6 SUMMARY

The numerical analyses are done to study the bed expansion ratio, bubble diameter, bed pressure drop and the solid circulation rate in the single component system. The numerically simulated results are then compared with the experimental results.

The bed expansion ratio is well-predicted by the numerical solution. However it is advisable that either the U_{mf} of the inert particles could be determined numerically or inert particles of multi-sizes could be set in the numerical settings in the future for better results. It is found that the relative bed expanded more in the gasifier than that in the combustor at the same static bed height.

The numerically determined bubble size is compared with the Darton's (1977) bubble model in the current study. The bubble size predicted by the numerical simulation is always less than that calculated by the Darton's (1977) correlation. The Darton's (1977) bubble model is however dependent only on the superficial gas velocity and the bed

height; other effects like the wall effect, actual geometrical flow behavior are not taken into consideration. Physical data is required for more realistic comparison in this respect.

It is also found that the effective diameter has noticeable effect on the bubble size. Larger bubbles are predicted in the combustor. Though the bed expanded more at the gasifier side, however the effect of internals and wall with respect to effective diameter supersedes the effect of bed expansion, thus resulting in smaller bubbles at the gasifier.

The bed pressure drop study is extended to analyse the fluidization quality in CFBG. Good fluidization is achieved only in the combustor side, while the bed pressure drop behaviour in the gasifier with river sand shows that channelling occurs in the bed. The channeling behavior becomes more severe in alumina bed. At this point, the numerical solution captures the channeling behavior both in river sand and alumina bed fairly well. Generally the numerical results generally agree quantitatively well with the experimental results.

The solid circulation rate is all under-predicted by the numerical solution by around 15% - 20%. To improve, the U_{mf} should be determined numerically for mono-sized river sand. The trend of SCR is mostly captured fairly well for the operating range. The solid circulation rate (SCR) increases with the increase in the bed height in CFBG. This is consistent to the findings by other authors in compartmented reactor design. Hence, the direct route to maximize the SCR is the increase of the static bed height. However, in CFBG, the maximum operating bed height is limited by the riser height. Solid circulation rate remains almost unaffected by the main bed aeration since the bed pressure drop (the main driving force for the solid circulation) remains unchanged with further increase in the main bed aeration within the bubbling fluidization regime.

In addition, the bed expansion predicted by the 2D and 3D analysis is compared with the experimental values. 3D simulation predicts more accurate results than 2D simulation.

2D simulation predicted a highly expanded bed with expansion ratio of 1.39 at $2U_{mf}$, where the deviation is 13% while 3D analysis only predicts a deviation of 6%.

Overall, the current model is adequate to model the hydrodynamic of single component system in CFBG within the operating range. 3D simulation is typically more suitable for complex geometry CFBG.

CHAPTER 8 HYDRODYNAMICS OF BINARY MIXTURE SYSTEM IN CFBG

8.1 INTRODUCTION

This chapter addresses the numerical simulation of binary mixture system hydrodynamics in CFBG and the comparison of numerical results with the experimental results. The hydrodynamic parameter studies include bed expansion ratio, overall binary mixing quality and local binary mixing (lateral mixing and vertical mixing) index. The effects of different weight percent of palm shell, different palm shell size and different static bed height on the parameters are also investigated. In addition, the variation between numerical and experimental data is discussed. Improvement to better results is also suggested in this chapter.

8.2 BED EXPANSION RATIO STUDY

Table 8.1 summarizes the model parameters/conditions applied for the numerical simulation of hydrodynamic parameter study in gasifier. Air at ambient temperature and pressure is used as the fluidizing medium. Uniform size distribution of river sand is specified in the numerical study. Different palm shell size at different weight percent is used in current study. The minimum fluidization velocity considers here is the binary U_{mf}. Different weight percent of palm shell and size has different U_{mf}, these U_{mf} are determined experimentally and input into the numerical simulation (refer Chapter 3, section 3.x.x for binary U_{mf} determination). The compartment is filled with particles to the desired bed height with the initial solid packing specified. Palm shell is stacked segregated from river sand by specifying the static height. The static palm shell height is also determined experimentally. The fluidization ranges from $1U_{mf} - 3U_{mf}$.

Table 8.1: 3D Simulation model parameters for binary mixture system in gasifier

Description	Value	Unit	Comment
Diameter	0.257	m	Gasifier
Particle density	2620	kg/m^3	River sand
	1500	kg/m^3	Palm shell
Mean particle size			
River sand	272	μm	uniform size
Palm shell	1.77, 3.56, 7.13	mm	uniform size
Weight Percent			
Palm shell	5, 10, 15	%	Specified
Binary U_{mf}			
Size of 3.56mm			
5 wt% Palm shell	0.078	m/s	Determined (experiment)
10 wt% Palm shell	0.082	m/s	Determined (experiment)
15 wt% Palm shell	0.084	m/s	Determined (experiment)
Size of 1.77mm			
10 wt% Palm shell	0.084	m/s	Determined (experiment)
Size of 7.13mm			
10 wt% 7.13mm	0.079	m/s	Determined (experiment)
Initial solid packing			
River sand	0.45	-	Fixed value
Palm shell	0.20	-	Fixed value
Gas density	1.2	kg/m^3	Ambient air
Binary Superficial velocity			
Size of 3.56mm			
5 wt% Palm shell	0.078 – 0.234	m/s	1 U_{mf}– 3 U_{mf}
10 wt% Palm shell	0.082 – 0.246	m/s	1 U_{mf}– 3 U_{mf}
15 wt% Palm shell	0.084 – 0.252	m/s	1 U_{mf}– 3 U_{mf}
Size of 1.77mm			
10 wt% Palm shell	0.084 – 0.252	m/s	1 U_{mf}– 3 U_{mf}
Size of 7.13mm			
10 wt% 7.13mm	0.079 – 0.237	m/s	1 U_{mf}– 3 U_{mf}

Static bed height			
River sand	0.33	m	Specified
Palm shell			
Size of 3.56mm			
5 wt% Palm shell	0.02	m	Specified
10 wt% Palm shell	0.045	m	Specified
15 wt% Palm shell	0.065	m	Specified
Size of 1.77mm			
10 wt% Palm shell	0.05	m	Specified
Size of 7.13mm			
10 wt% 7.13mm	0.08	m	Specified

8.2.1 Palm Shell at Various Wt% and Size

Figures 8.1 – 8.5 show the comparison of numerically simulated results for bed expansion ratio study with the experimental results in binary system at the gasifier side where different mean particle sizes and weight percents (wt%) of palm shell (3.56mm at 5 wt%, 10 wt% and 15 wt%, 1.77mm at 10 wt%, and 7.13mm at 10 wt%) with river sand is used at various total static bed heights, i.e. 0.35m, 0.375m, 0.395m, 0.38m and 0.41m respectively. Total static bed height means the sum of river sand static height and palm shell static height.

From the figures, it is observed that the bed expansion ratio increases with increasing velocities. Numerical simulations predict the similar trend. However, the bed expansion ratio is under-estimated by numerical simulation by a discrepancy of around 20% (± 20% error bars are set for easy comparison between the numerical values and the experimental values). The binary U_{mf} is determined from experiment where the binary system is of wide distribution in sizes. In contrary, uniform size distribution has been set for river sand as well as palm shell in the numerical study, the experimentally determined binary U_{mf} can be smaller than the binary U_{mf} from numerical study, thus this may be attributed to under-estimation of bed expansion in the numerical solution. Another reason for this discrepancy could be due to the standard drag law – Syamlal

O'Brien (1994) drag model used. The inter-particle drag could be considered differently by the standard law for river sand and specific biomass (palm shell) system, moreover the gasifier includes internal parts such as v-valve and riser, making its geometry more complex. For more improved results, it might be instructive to use modified Syamlal O'Brien (1994) drag law specifically for river sand and palm shell in CFBG. In general, the numerical model is able to predict the trend of the bed expansion at the gasifier.

Comparing the Figure 8.1 – 8.3, it shows that the numerical simulations predict increasing deviation in bed expansion at the onset of fluidization for 5 wt% - 15 wt% palm shell in comparison to the experimental values. As discussed before, the numerical binary U_{mf} for monodispersed binary system can be higher than the experimentally determined binary U_{mf}. When higher wt% of palm shell is loaded in the system, the higher the numerical binary U_{mf} becomes. Thus, in Figure 8.3 where 15 wt% palm shell is used, the deviation is the largest at the onset of fluidization. The deviation decreases gradually with increasing gas velocities.

The 2D and 3D numerical visualization of binary with 10 wt% palm shell of 3.56mm is compared for fluidization behavior prediction in Chapter 6 (Figure 6.4 and 6.5). In term of bed expansion estimation, 2D analysis predicts well over-predicted results, i.e. 57% expansion is detected in 2D study while 15% expansion is observed in 3D study (see Figure 8.2) at 2.5 U_{mf}. 2D study is not appropriate for quantitative analysis due to its simplicity.

On average for Figure 8.1 – 8.5, the experimental bed expansion ratio has increased from 1.11 to 1.23 while the simulated bed expansion ratio has increased from 0.92 to 1.13 for 1 U_{mf}– 3 U_{mf}.

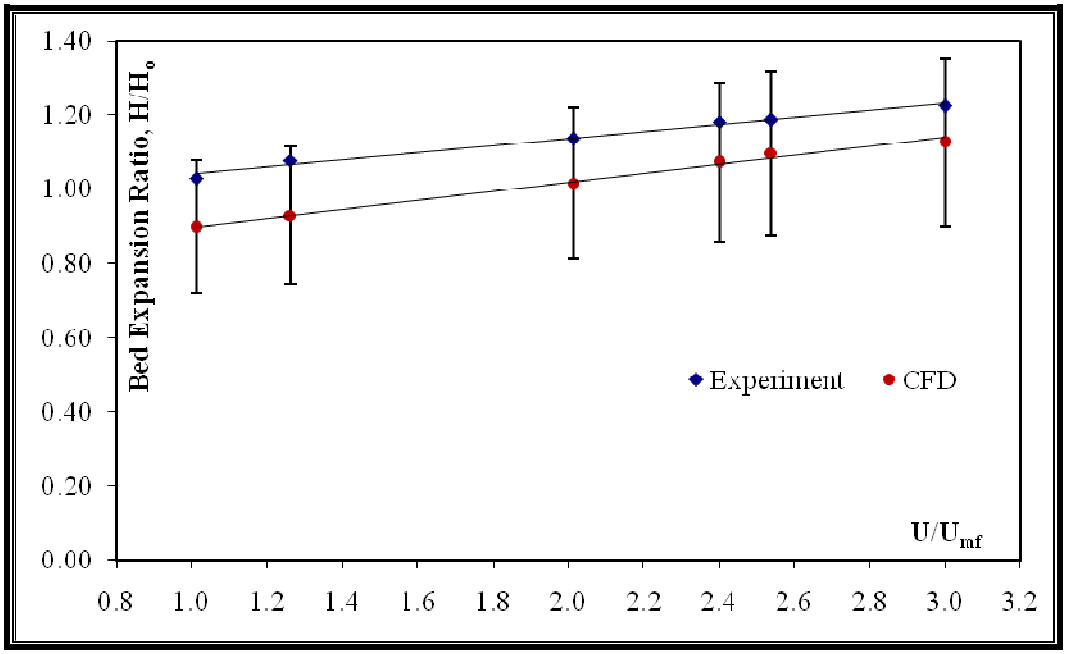

Figure 8.1: Comparison of the numerical results with the experimental results at total static bed height of 0.35m at the gasifier (5 wt% palm shell, size of 3.56 mm)

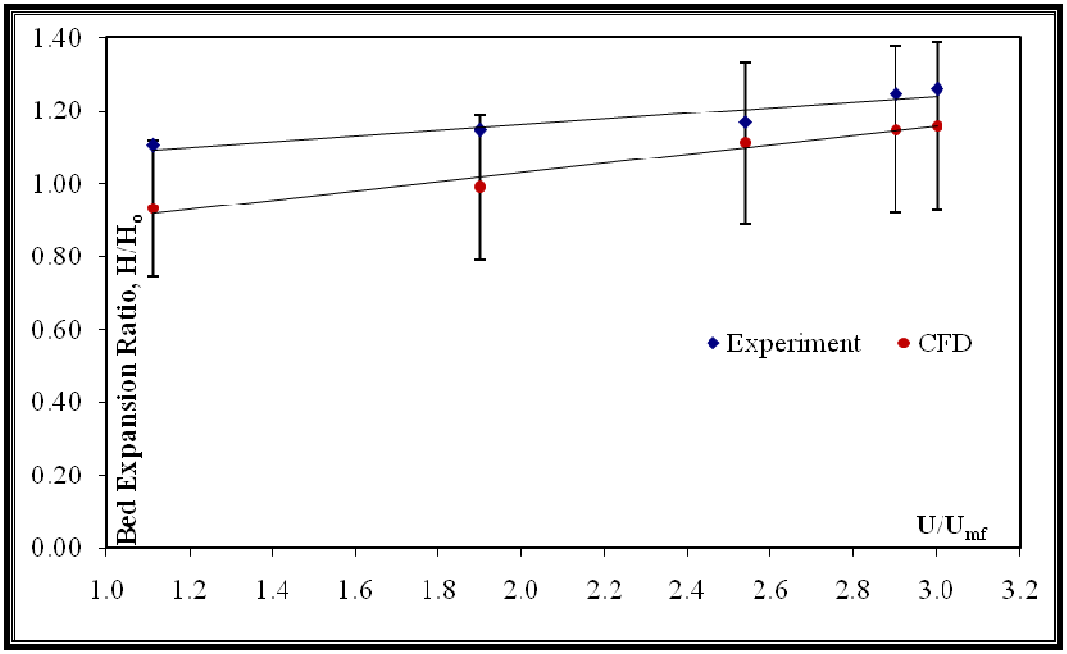

Figure 8.2: Comparison of the numerical results with the experimental results at total static bed height of 0.375m at the gasifier (10 wt% palm shell, size of 3.56 mm)

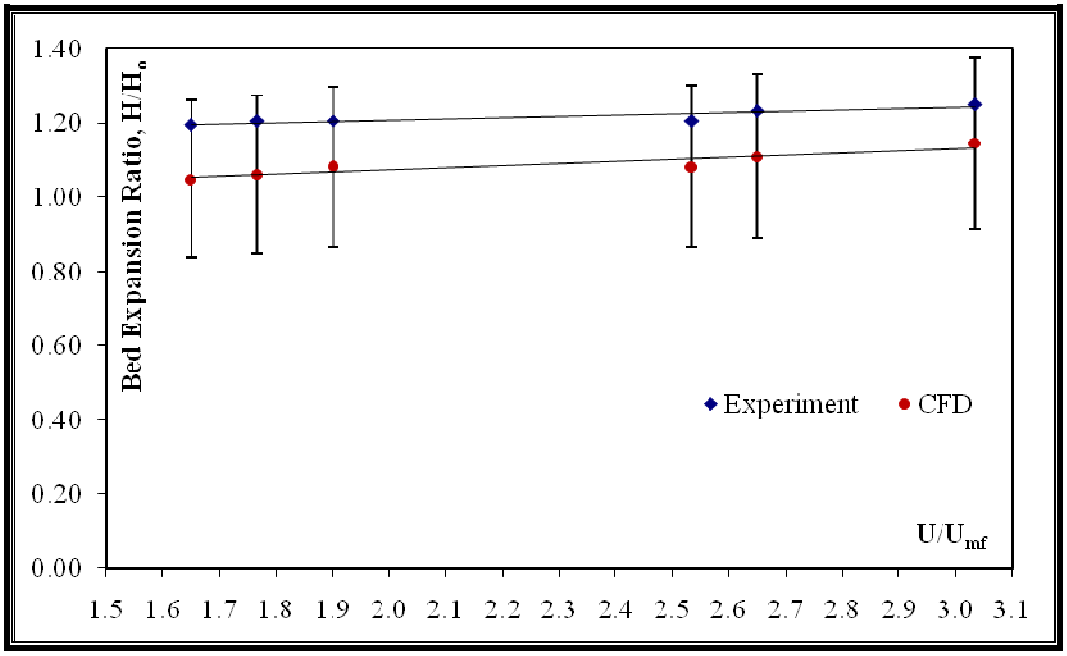

Figure 8.3: Comparison of the numerical results with the experimental results at static bed height of 0.395m at the gaisifer (15 wt% palm shell, size of 3.56mm)

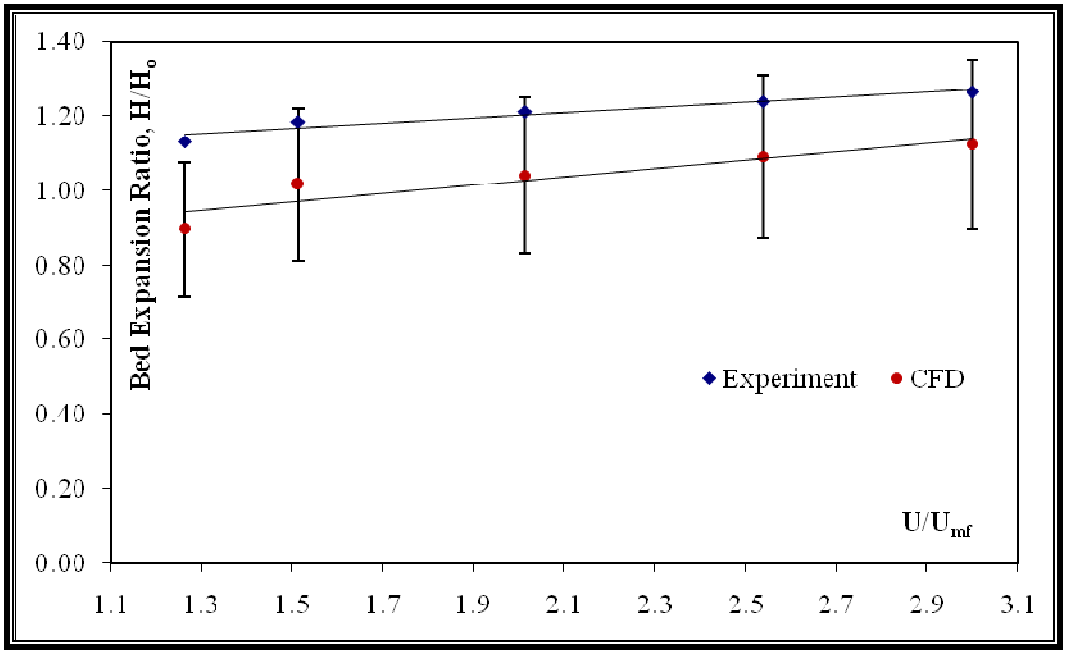

Figure 8.4: Comparison of the numerical results with the experimental results at total static bed height of 0.38m at the gasifier (10 wt% palm shell, size of 1.77 mm)

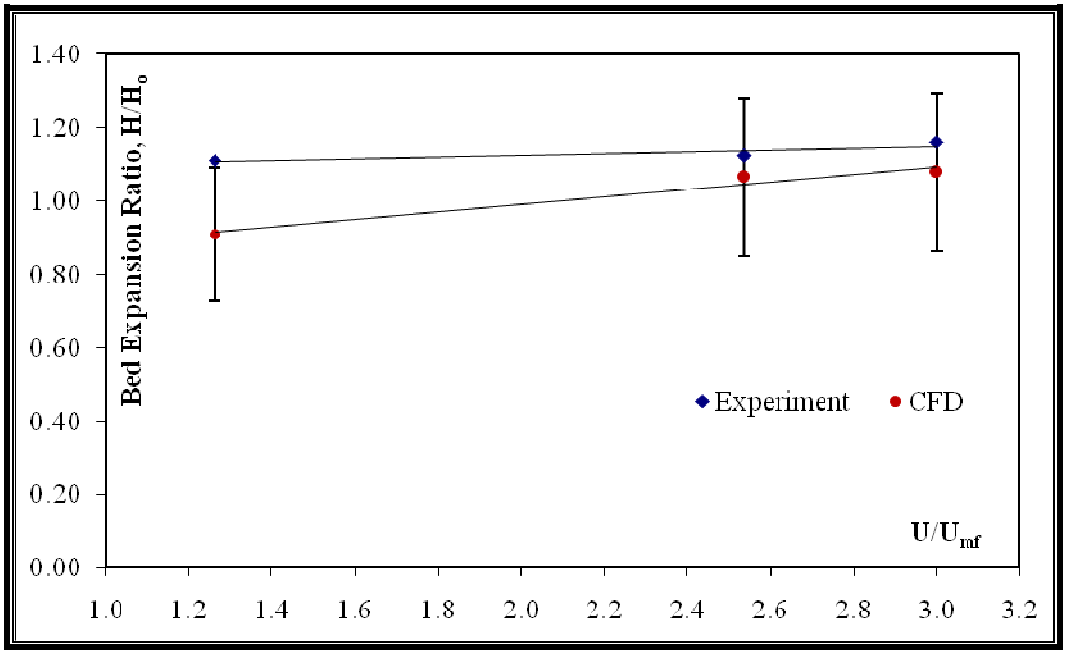

Figure 8.5: Comparison of the numerical results with the experimental results at total static bed height of 0.41m at the gasifier (10 wt% palm shell, 7.13 mm)

8.2.2 Effect of Palm Shell Wt% on Bed Expansion Ratio

Figure 8.6 shows the effect of the different palm shell weight percent (wt %) on the bed expansion ratio in the binary system at the gasifier side. The mean palm shell size used in this study is 3.56mm. The palm shell wt% ranges from 0 wt% to 15 wt% and the fluidization regime is from 1 U_{mf} to 3 U_{mf}, except for 0 wt% (single component system) where the fluidization regime ranges from 1 U_{mf} to 2 U_{mf}.

As can be seen from figure, the different palm shell wt% (5 wt%, 10 wt% and 15 wt%) has no noticeable effect on the binary bed expansion ratio. When it is to compare with no palm shell in the system (single component system), significant observation can be seen. The bed expanded more in single component system. This is because in binary mixture system, the porosity of palm shell and river sand is very dissimilar. When binary minimum fluidization is reached, palm shell and river sand is most likely to fill in the voidage of the opposite particles thus leading to lower expanded bed. This behavior can

be seen in our numerical visualization (Chapter 6, Figure 6.5) where the bed drops below the total static bed height at the onset of fluidization.

Generally, the numerical simulated values follow the trend of experimental results. Even though the deviation is considerably big (around 20%), but the tendency of the parameter can be predicted quite accurately for the operating range. For improved results, multi-size binary system should be modelled or modified standard drag law should be used specifically for the current system.

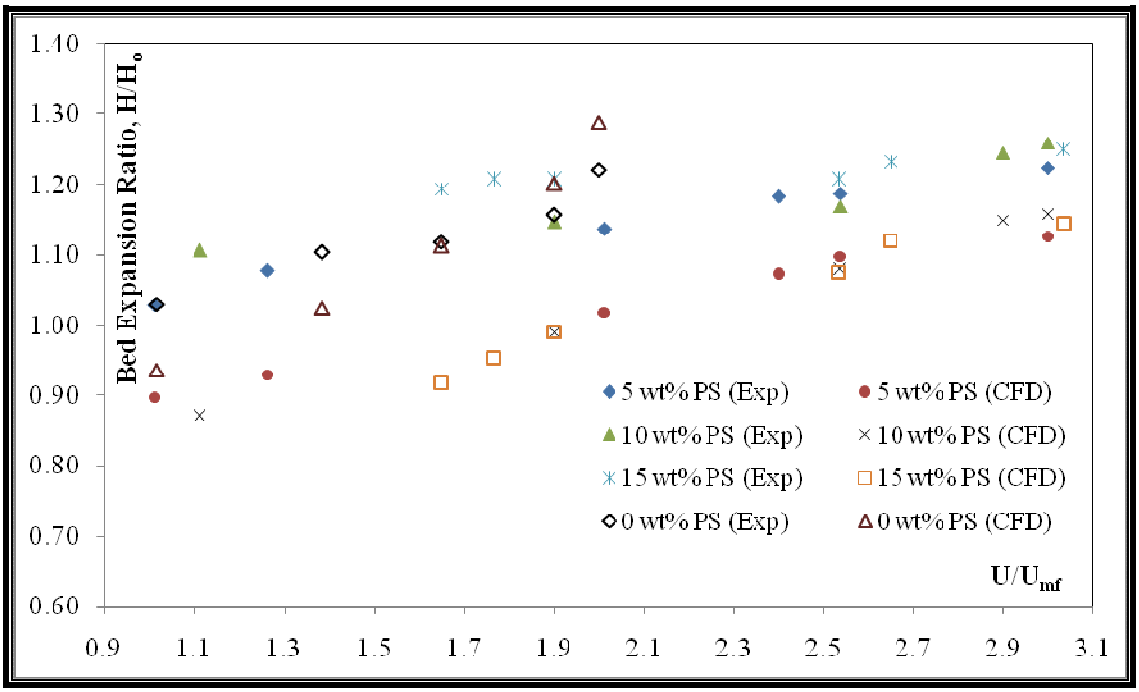

Figure 8.6: Effect of different palm shell wt% on the binary bed expansion ratio at the gasifier (mean palm shell size of 3.56mm)

8.2.3 Effect of Palm Shell Size on Bed Expansion Ratio

Figure 8.7 shows the effect of palm shell size on the bed expansion ratio in the binary system at the gasifier side. The mean palm shell size used in this study is 1.77mm, 3.56mm and 7.13mm at 10wt%. The fluidization regime is from 1 U_{mf} to 3 U_{mf}.

The bed becomes less expanded with increasing palm shell size. Different palm shell size in binary system has different porosity. Larger palm shell size induces higher porosity in the bed. More river sand required to fill the high voidage of larger palm shell size, thus leading to lower expanded bed.

However, this phenomenon is not observed in numerical simulation. The effect of palm shell size on the bed expansion ratio is trivial in the numerical results. This could be due to the restitution coefficient that accounts for the collision of particles, 0.9 may not be adequate to model the binary mixture system. Also, the estimation of inter-particle forces between palm shell and river sand by the standard Syamlal O'Brien (1994) drag law could be incorrect. For better results, it is suggested that modification of standard drag law should be done specially for binary mixture system in CFBG.

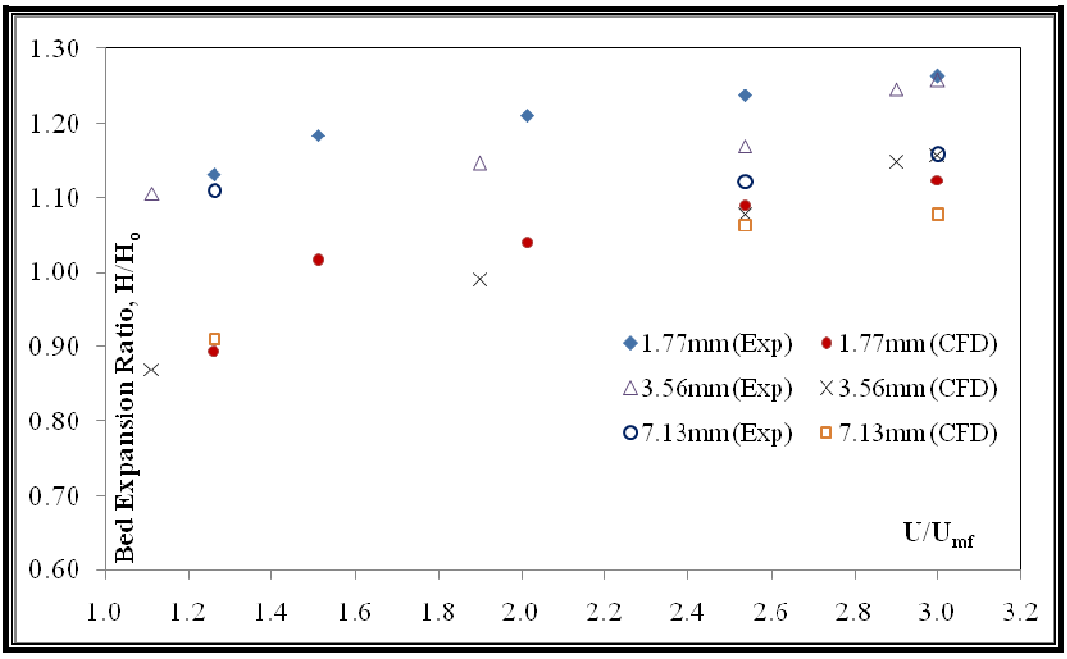

Figure 8.7: Effect of palm shell size on the bed expansion ratio at the gasifier (mean palm shell size of 1.77mm, 3.56mm, 7.13mm at 10 wt%)

8.3 OVERALL MIXING QUALITY STUDY

A binary system (e.g. sand-palm shell mixture) exhibits segregation tendency because of the difference in their particle properties, namely size and/or density. This is due to the variation of their respective drag forces when subjected to flowing gas, and the interaction forces between the particles. The degree of segregation/mixing depends on the operation and the geometrical parameters of the fluidized bed. Hence, it is the purpose of this section to study the mixing profiles of sand-palm shell binary mixture in different bed sections of the combustor and the gasifier, and also to determine the operational superficial velocity that produces good overall mixing quality and its dependency on particle properties and bed geometrical parameters.

Due to the complex CFBG geometry, it is reasonable to estimate the local mixing quality in terms of the local mixing index (m) in different locations throughout the compartments, i.e. combustor and gasifier.

The local mixing index (m) is defined as

$$m = x/X \tag{8.1}$$

where x is the local palm shell mass concentration (weight percent in the sample), and X is the palm shell loaded in weight percent. m = 1 represents perfect mixing, while segregation may lead to two conditions, either "dilution" (m < 1) or accumulation (m > 1).

The overall mixing quality (M) is determined as

$$M = 1 - \left(\frac{1}{n}\right)\sum_{i=1}^{n}\left|\left(\frac{x_i - X}{X}\right)\right| \tag{8.2}$$

where "n" is the number of sampling locations throughout the bed.

M = 1 and M < 1 correspond to perfect mixing and segregation respectively. It is assumed that a portion or the whole fluidized bed to be of good mixing quality when m =

1.00 ± 0.15 or M = 0.85 - 1.00 respectively.

8.3.1 Effect of Palm Shell wt% on Overall Mixing Quality

Figure 8.8 shows the comparison of numerically simulated effect of palm shell wt% on the overall mixing quality (M) with the experimentally determined results for mean palm shell size of 3.56mm and mean river sand size of 272 µm in the gasifier. The fluidization regime ranges from 1.0U_{mf} to2.5U_{mf}.

Mixing quality (M) can be near to zero especially at the onset of fluidization as can be seen for experimental result at 15 wt% palm shell. However, the M improves tremendously at 1.5U_{mf}. Generally, increasing the superficial gas velocity will improve mixing in segregated systems of mixtures with difference densities/ sizes (Wirsum et al., 2001). Shen et al. (2007) reported that wake exchange coefficient, which indicates vertical and lateral solid mixing intensity, reduces with the increase in U_{mf}. This corresponds to decreasing of M. Good overall mixing (0.85 – 0.95) is attainable at 1.5U_{mf} for palm shell ranged from 5wt% to 15 wt% and no significant changes of M from 1.5U_{mf} onwards.

Numerical simulation predicts qualitatively well-matched trends however lower values with the experimental results. The reason of under-predicted M could be attributed to the inaccurate estimation of inter-particles force between river sand and palm shell by the standard Syamlal O'Brien (1994) drag law. The deviation is larger at lower U_{mf} (less than 2U_{mf}); it reduces at higher U_{mf} (more than 2U_{mf}). Overall mixing quality of around 0.80 to 0.90 is attainable at 2.0U_{mf} from the numerical simulation.

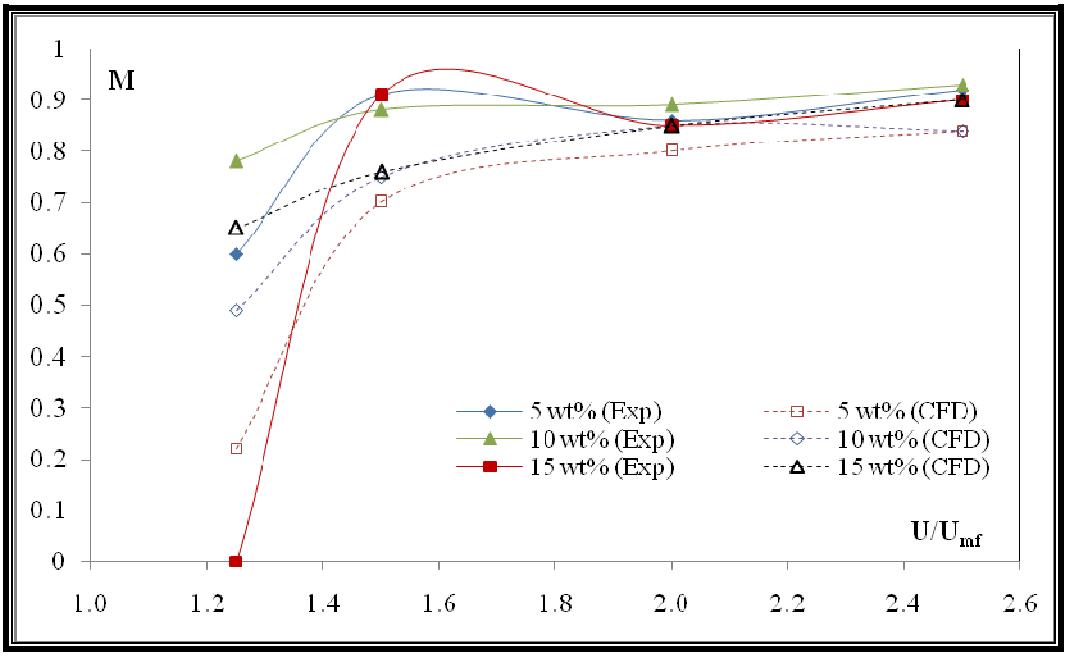

Figure 8.8: Effect of different palm shell weight% on the overall mixing quality (*M*) (mean palm shell size of 3.56mm in the gasifier)

8.3.2 Effect of Static Bed Height on Overall Mixing Quality

The comparison of the numerically simulated effect of the static bed height on the overall mixing quality (*M*) with the experimentally determined results for 10 wt% of mean palm shell size 3.56mm and mean river sand size of 272 µm in the gasifier is shown in Figure 8.9. The fluidization regime ranges from $1.0U_{mf}$ to $2.5U_{mf}$.

For experimental results, overall mixing quality of about 0.9 is achieved at $1.25U_{mf}$ for deep bed, whereas at shallow bed, the same degree of mixing is only achievable at higher superficial gas velocity ($1.5U_{mf}$). With increasing bed height, the bed pressure drop increased (see chapter 7, section 7.4.2.1) resulting in stable bubbling across bed distributor that uniformly mixed the fluidized bed. Conversely, in shallow beds; where the total bed pressure drop is reduced, then the bed is self aggravating and the local preferential channeling formed. The channeling behavior is captured in our numerical visualization (refer Chapter 6, Figure 6.5). This contributes to non-uniformity bubbling at the expense of the rest of the bed (Qureshi and Creasy, 1979). Therefore, at $1.25U_{mf}$,

poorer mixing is attained in the shallow beds and relatively good mixing in the deep beds. However, increasing the superficial gas velocity will improve the mixing in the shallow beds.

The numerical simulation predicts gradual increase in M with respect to the increase in U_{mf} for all heights. The tendency predicted at initial state of fluidization is different from that obtained for experiment. However, the simulated M is comparable with experimental value at higher U_{mf} ($2U_{mf}$ onwards). It is to be mentioned that the mixing quality is affected by the structure of the particle system of the mixture that is also related to the coordination number (Chandratilleke, 2011). Spot sampling of the particles may be a key factor for the large discrepancy of the analytical results in comparison to the experimental results.

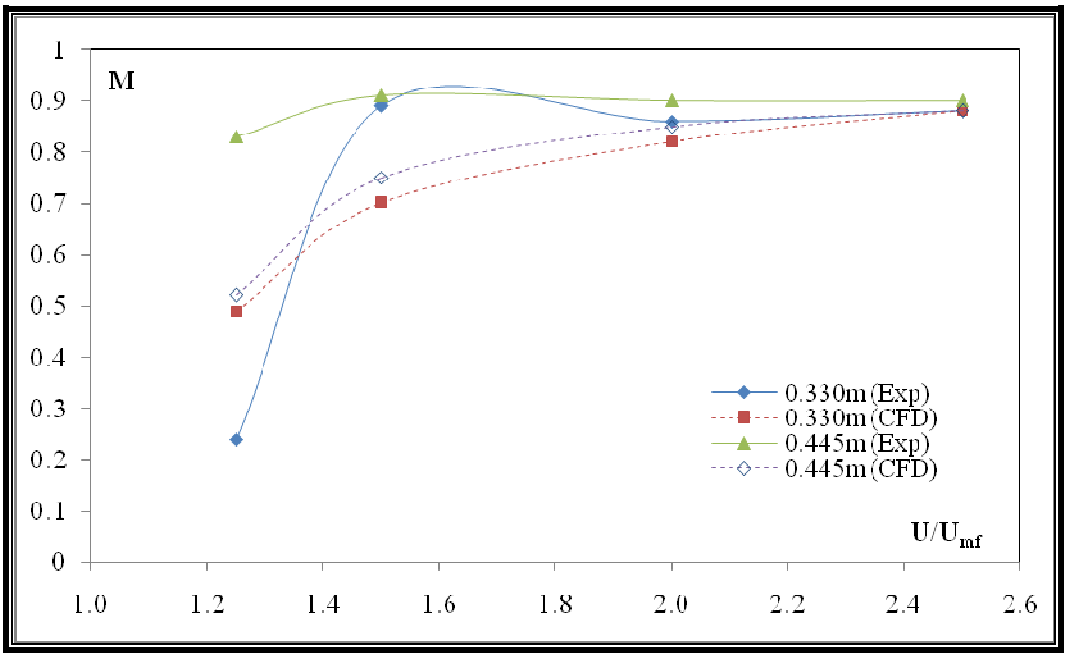

Figure 8.9: Effect of static bed height on the overall mixing quality (M) (10 wt% of mean palm shell size 3.56mm in the gasifier)

8.3.3 Effect of Palm Shell Size on Overall Mixing Quality

Figure 8.10 illustrates the comparison of the effect of palm shell size on the overall mixing quality obtained from the numerical simulation with the experimental results for 10 wt% palm shell in river sand of 272 μm in the gasifier. The fluidization regime ranges from $1.0U_{mf}$ to $2.5U_{mf}$.

At $1.25U_{mf}$, it is observed that the palm shell mean sieve size of 7.13 mm has the highest M value. This may be related to better percolation effect during the initial stage of fluidization. On the other hand, at $1.5U_{mf}$, the smallest palm shell mean sieve size of 1.77 mm has the highest overall mixing quality. With further increase in U_{mf}, the effect of palm shell size on M is not significantly discernable.

The numerical simulation predicts larger discrepancy in values as compared to the experimental one at lower U_{mf} (less than or equal to $1.5U_{mf}$). The peak as mentioned earlier for 1.77mm (experiment) is not captured by the numerical simulation. The deviation reduces with increasing superficial gas velocity. Overall, the numerical simulation predicts considerably well for M at higher U_{mf} (more than or equal to $2U_{mf}$).

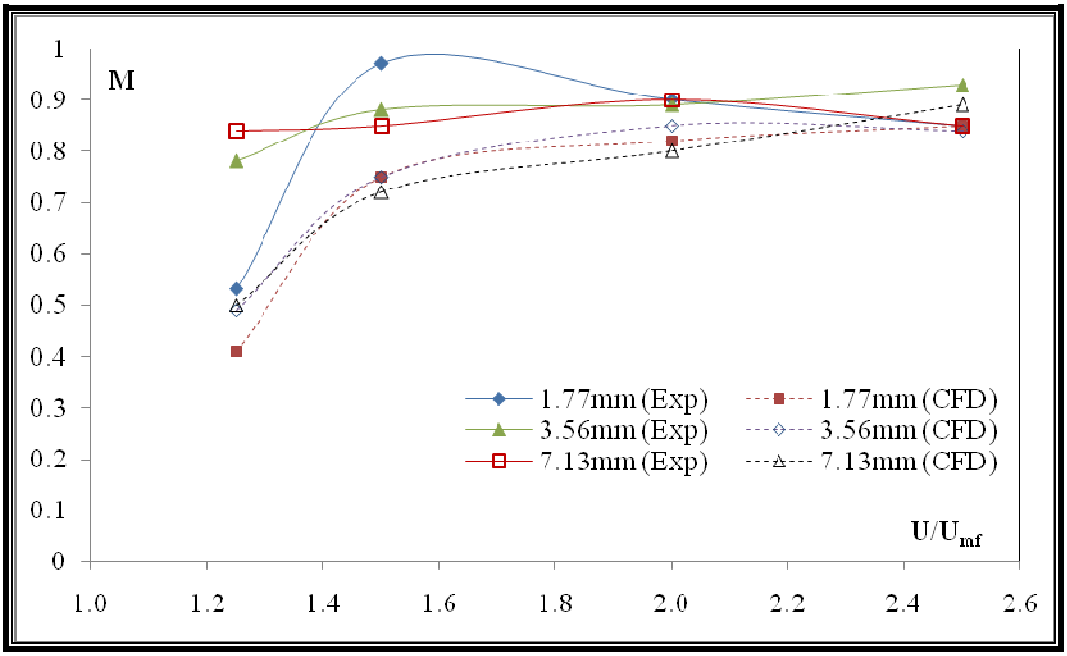

Figure 8.10: Effect of palm Shell size on the overall mixing quality (*M*) (10 wt% of palm shell in sand of mean size 272 µm)

8.4 MIXING AND SEGREGATION PATTERN (LOCAL MIXING INDEX)

8.4.1 Vertical Mixing

Figure 8.11 demonstrates the comparison between the numerically simulated and experimentally determined typical palm shell vertical distribution at various U_{mf}. The data is based on 10 wt% of palm shell and is therefore has a maximum accumulated value of m = 10 if collected sample is purely palm shell. The gray vertical line in the figure indicates the perfect mixing line of 1. The distribution analysis is divided into 3 parts, e.g. near the v-valve, at the bed center and near the riser. The fluidization regime ranges from $0U_{mf}$ to $2.5U_{mf}$.

Starting from packed bed condition where palm shells are initially stacked uniformly at the bed surface (segregated layer), with increasing superficial gas velocity, they gradually distribute to the lower region of the bed. At $1.25U_{mf}$, by visual observation, bubbles are more likely formed at the bed centre compared to the wall side. Consequently, palm shells at the center propagate to the downward regions of the bed

more rapidly compare to the wall side. This initiates the mixing process between the palm shell and river sand in the experiment.

Palm shells at the bed surface of the centre region are also dispersed to the wall side by bubbles bursting. At $1.5U_{mf}$, the concentration gradient on both the vertical wall sides getting closer due to the increasing bubbling rate that induces better mixing in the whole bed. However, palm shells with lower density, tends to migrate towards the bed surface due to the easiness of being swept away by the air flow from the distributor and carried up by the rising bubbles. At higher superficial gas velocity ($2.0U_{mf}$ -$2.5U_{mf}$), palm shells tend to become uniformly mixed, resulting in a smaller palm shells concentration gradient developed along the bed height. Hence, vertical mixing is enhanced. On average, local mixing index of 0.9 is attainable in the experiment.

The vertical distribution of palm shell is predicted differently by the numerical simulation. From the numerical visualization (Chapter 6, Figure 6.4 and 6.5), palm shells distribute downwards at $1.25U_{mf}$, which is different from that observed in the experiment. With increasing superficial gas velocity, the mixing becomes more vigorous at L1 and L2 of V-valve, bed centre and riser. However, at $2.5U_{mf}$, segregation occurs at the riser side, the local mixing index is affected drastically. This is not observed in the experimental data. This clearly shows that the current numerical model has some weaknesses in modelling the binary mixing of the binary mixture system. Attempt to modify the standard drag law in modelling the binary system of such complex geometry should be performed in order to obtain results with higher accuracy. Overall, reasonably good local mixing index is achieved only at the V-valve and the bed centre of L1 and L2 which is around 0.80.

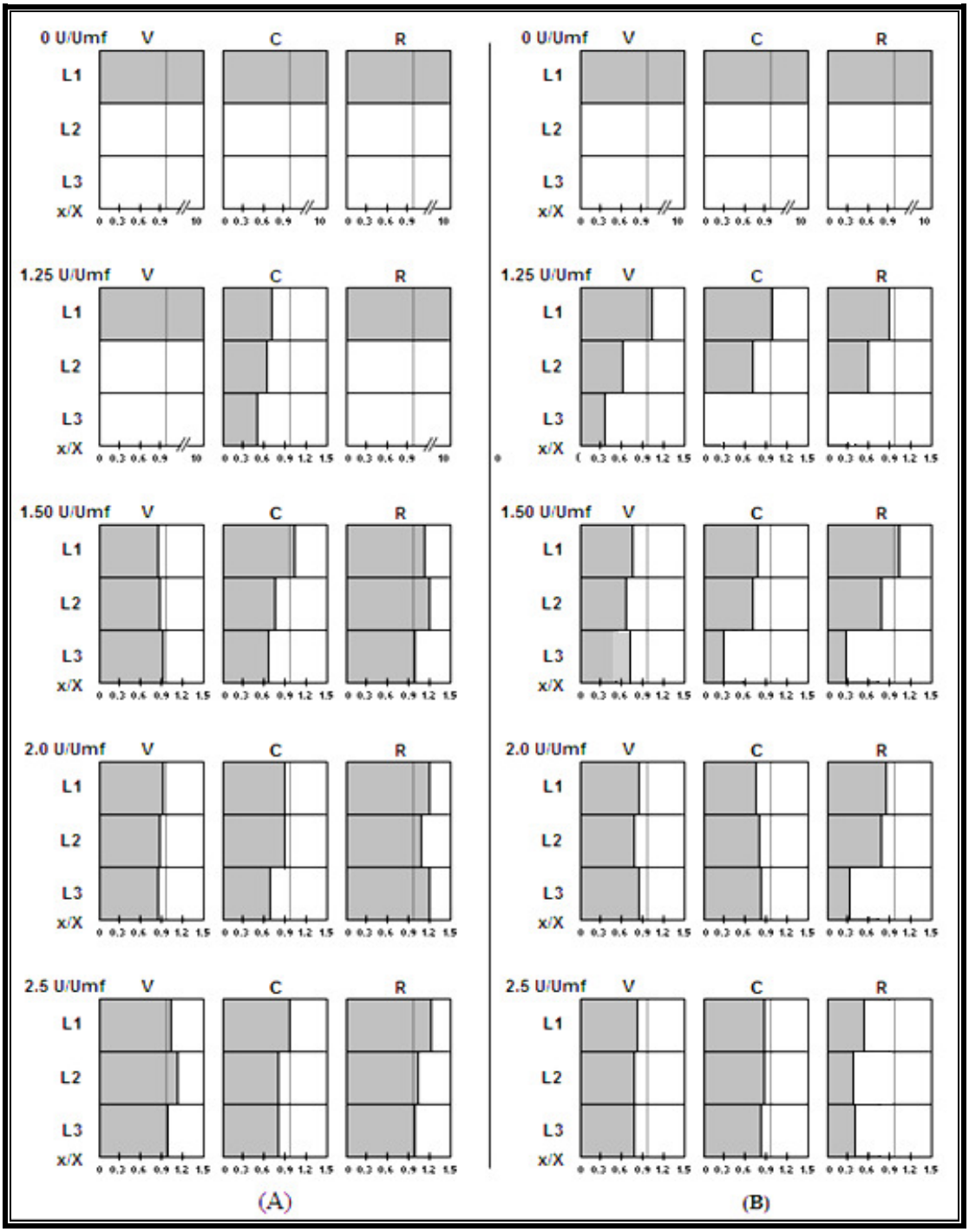

Figure 8.11: Comparison of the experimentally determined and the numerically simulated results of the effect of U_{mf} on the vertical mixing for 10 wt% palm shell with mean size 3.56mm in the gasifier

(A) Experiment, (B) Numerical simulation

8.4.2 Lateral Mixing

Figure 8.12 shows the comparison between the numerically simulated and the experimentally determined typical palm shell lateral distribution at various U_{mf}. The data is based on 10 wt% of palm shell and is therefore has a maximum accumulated value of m = 10 if collected sample is purely palm shell. The gray vertical line in the figure indicates the perfect mixing line of 1. The distribution analysis is divided into 3 parts, e.g. near the v-valve, at the bed center and near the riser. The fluidization regime ranges from $0U_{mf}$ to $2.5U_{mf}$.

Overall, for experimental data, the m of three layers improve with increasing superficial gas velocity. The lateral mixing of solids in a gas solid fluidized bed is caused by two mechanisms, which are the bursting bubbles at the bed surface and the bubbles displacement inside the bed (Kunii and Levenspiel, 1991). At 1.25 U_{mf}, lateral mixing is initiated by the bursting bubbles at the bed surface, where a large fraction of the palm shells at the centre are dispersed. At L2 and L3, local mixing induced by the bubbles displacement is insignificant. With increasing superficial gas velocity ($1.5U_{mf}$ - $2.5U_{mf}$), lateral palm shells distribution across the fluidized bed at L1, L2 and L3 approaches each other. This is due to the increasing bubbling rate, whereby lateral mixing induced by the bubbles displacement becomes more significant. Hence, lateral mixing is enhanced.

For the numerical simulation, as has been discussed earlier, with increasing superficial gas velocity, the lateral local mixing is enhanced only at the v-valve and bed centre of L1 and L2. With the increase in superficial gas velocity, segregation occurs near the riser side (refer numerical visualization in Chapter 6, Figure 6.5). The local mixing of each location is also under-predicted by the numerical simulation. The model needs to be improved in the future for more comparable results.

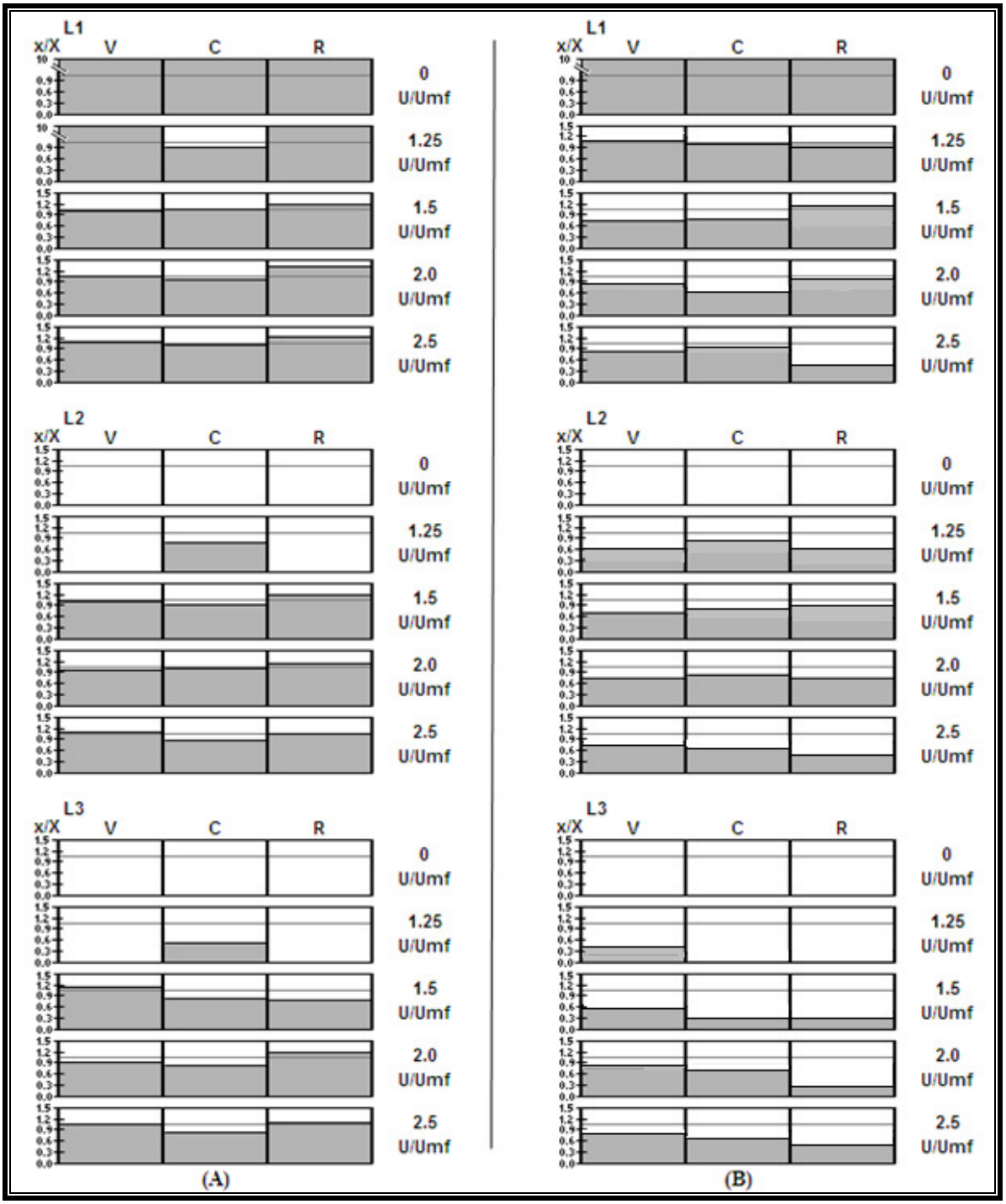

Figure 8.12: Comparison of the experimentally determined and the numerically simulated results of the effect of U_{mf} on the lateral mixing for 10 wt% palm shell with mean size 3.56mm in the gasifier

(A) Experiment, (B) Numerical simulation

8.5 SUMMARY

The numerical analyses are done to study the bed expansion ratio, overall binary mixing quality and local mixing index in the binary mixture system of CFBG. The numerically simulated results are then compared with the experimental results.

The numerical simulation under-predicts the bed expansion ratio by around 20%. There are few reasons that contribute to the deviation: (1) higher U_{mf} from the numerical simulation than the actual binary U_{mf}, (2) inter-particle forces may be calculated differently by the Standard Syamlal O'Brien drag law (3) the effect of internals in binary system is predicted differently by the numerical simulation. Despite the aforementioned, the tendency predicted by the numerical simulation agrees well with the experimental data.

The effect of different palm shell wt% and palm shell size on the binary bed expansion ratio is also investigated. Palm shell wt% (5 wt%, 10 wt% and 15 wt%) has no noticeable effect on the binary bed expansion ratio. On the other hand, the bed becomes less expanded with increasing palm shell size.

The overall mixing quality is under-predicted by the numerical simulation however the predicted trend follows the experimental one. It is found that the overall mixing quality (M) is enhanced for the smaller palm shell mean sieve size and larger palm shell weight percent. On the other hand, the bed height does not significantly affect the overall mixing quality, although it contributes to the fastest dispersion of palm shell during the initial stage of fluidization.

The local mixing index is also determined by the numerical simulation at the gasifier since the local composition may differ significantly from point-to-point in the bed. Increasing the superficial gas velocity, increases the local mixing index as observed in the experiment, however the mixing predicted by numerical simulation shows the tendency of segregation occurring at riser side from $2.0U_{mf}$ onwards. Generally fairly

good local mixing is achievable by the numerical solution only in the v-valve and bed center section, but for all sections by the experimental study at $2.0U_{mf}$ onwards.

In addition, the bed expansion predicted by the 2D and 3D analysis is compared with the experimental values. 3D simulation predicts more accurate results than 2D simulation. 2D simulation predicted the expansion ratio of discrepancy around +32% while 3D simulation only predicts a deviation of -4%.

Generally the current numerical model still has some weaknesses in modeling the binary mixture system. Though large deviation as compared to the physical data is predicted, but some tendency of the behavior is modestly captured. It is instructive to modify the Standard drag law and adjust the restitution coefficient suiting CFBG geometry in the future for better results.

CHAPTER 9
CONCLUSIONS AND RECOMMENDATIONS

9.1 INTRODUCTION

This chapter concludes the present study by highlighting the main research findings. It summarizes the key findings from the numerical modeling (CFD model) based on the Eulerian-Eulerian approach on hydrodynamic studies such as fluidization behavior, mixing quality and solid circulation rate in a complex geometry pilot plant scale cold flow CFBG used for the first attempt as well as the main operating parameters as a guide to develop and operate CFBG pilot plant. The conclusions and evaluations of the present research have also led to some recommendations for future study in this area of research.

9.2 CONCLUSIONS

9.2.1 Numerical Visualization

The 2D and 3D flow patterns of the combustor and the gasifier are first generated from the numerical study to observe the bubble formation, possible channeling behavior and the binary mixing patterns in the bed. From the studies on the bed expansion, bubble formation, steady equilibrium state and overall binary mixing quality, the 2D model provides well over-predicted values compared to the 3D flow model. Also, the local mixing index of the binary system is not captured by the 2D model. The numerical values predicted by 3D model are closer to the actual values.

The expanded bed height at combustor is noticeably lower than that at the gasifier side. The flow behaviour of a gas-solid fluidized bed is very complex and highly sensitive to bed diameter. The effect of internal parts (v-valve and riser) may attribute differently in the compartments.

2D model should be used with caution and only for sensitivity analyses or where the flow is by nature two-dimensional. In this study, 3D model is more suitable when dealing with complex shape fluidized bed. In addition, the CFD results should be taken after 3.5s of simulation.

9.2.2 Fluidization Behavior

- Bed expansion ratio study in single component system
  - The studies are conducted in two type of inert particles namely river sand of mean particle size 272μm and alumina of size 360μm in the combustor and the gasifier.
  - The bed expansion ratio is under-predicted by less than 10% however the tendency is well-captured by the numerical solution. It is found that the relative expansion in the gasifier is higher than that in the combustor at the same static bed height. The relative expansion between gasifier and combustor is of great importance for pilot plant performance and operational economic.
  - The cohesive nature of alumina making the alumina bed less expanded than the river sand bed.
  - The 2D and 3D analysis is compared for 0.35m bed at 2 U_{mf}. 3D simulation predicts more accurate results than the 2D simulation. 2D simulation predicted a highly expanded bed with a deviation of 13% while 3D analysis predicts a deviation of only 6%.

- Bed expansion ratio study in binary mixture system
  - The studies are performed at different weight percent (wt%) of palm shell at three different mean sieved sizes of d_{ps}, $2d_{ps}$ and $4d_{ps}$ where d_{ps} is 1.77mm with common inert particle, river sand in the gasifier. The effect of different palm shell wt% and palm shell size on the binary bed expansion ratio is also investigated.
  - The numerical simulation under-predicts the bed expansion ratio by around 20%. This discrepancy may be attributed to: (1) higher U_{mf} from the numerical

simulation than the actual binary U_{mf}, (2) inter-particle forces may be calculated differently by the Standard Syamlal O'Brien drag law (3) the effect of internals in binary system is predicted differently by the numerical simulation. Despite the aforementioned, the tendency predicted by the numerical simulation agrees well with the experimental data.

- Palm shell wt% (5 wt%, 10 wt% and 15 wt%) has no noticeable effect on the binary bed expansion ratio. On the other hand, the bed becomes less expanded with increasing palm shell size.
- From the 2D and 3D analysis 10wt% of palm shell at mean size 3.56mm, 3D simulation predicts more accurate results than 2D simulation. 2D simulation predicted the expansion ratio of discrepancy around +32% while 3D simulation only predicts a deviation of -4%.

- Bubble size study in single component system
  - The numerically determined bubble size for the combustor and the gasifier is compared with the Darton's bubble model in the current study. The bubble size predicted by the numerical simulation is always less than that calculated by the Darton's correlation.
  - The Darton's bubble model is however dependent only on the superficial gas velocity and the bed height; other effects like the wall effect, actual geometrical flow behaviour are not taken into consideration. Physical data is required for more realistic comparison in this respect.
  - The effective diameter has noticeable effect on the bubble size. Larger bubbles are predicted in the combustor. Though the bed expanded more at the gasifier side, however the effect of internals and wall with respect to effective diameter supersedes the effect of bed expansion, thus resulting in smaller bubbles at the gasifier.

- Bed pressure drop study in single component system
  - The bed pressure drop of the combustor and the gasifier is under-predicted by the numerical model with an average deviation of 10%.
  - The bed pressure drop profile in the combustor is rather stable compared to that at the gasifier with river sand and alumina which fluctuates severely. The severe fluctuation in profile is an indication of channeling bed.

- Fluidization Quality
  - Good fluidization is achieved in the combustor side, while the pressure drop behaviour seen for the gasifier with river sand shows that channelling occurs in the bed. The channelling behaviour becomes more severe with alumina bed.
  - At this point, the numerical solution captures the channelling behaviour both in river sand and alumina bed fairly well. Generally the numerical results agree quantitatively well with the experimental results.

- Solid Circulation Rate (SCR) study
  - The solid circulation rate is all under-predicted by the numerical solution by around 15%. The trend of SCR is mostly captured fairly well for the operating ranges.
  - The solid circulation rate (SCR) increases with the increase in the bed height in CFBG, which is consistent to the findings by other authors in compartmented reactor design. Hence, the direct route to maximize the SCR is the increase of the static bed height; however, the maximum operating bed height is limited by the riser height.
  - Solid circulation rate remains almost unaffected by the main bed aeration since the bed pressure drop (the main driving force for the solid circulation) remains unchanged with further increase in the main bed aeration within the bubbling fluidization regime.

- Overall binary mixing quality
  - The overall mixing quality in the gasifier is under-predicted by the numerical simulation by around 20%; however the predicted trend follows the experimental one.
  - It is found that the overall mixing quality is enhanced for the smaller palm shell size and larger palm shell weight percent. On the other hand, the bed height does not significantly affect the overall mixing quality, although it contributes to the fastest dispersion of palm shell during the initial stage of fluidization.

- Local binary mixing index
  - Increasing the superficial gas velocity, increases the local mixing index as observed in the experiment, however at 2.5 U_{mf}, the numerical simulation indicates the tendency of segregation occurring at the riser section of the gasifer.
  - Generally fairly good local mixing index (0.65 – 0.80) is achievable by the numerical solution in the v-valve and bed centre section and 0.85 – 0.95 is attainable from the experimental study at 2.0 U_{mf} onwards.

9.2.3 Operating Conditions for Pilot Plant CFBG

Table 9.1 summarizes the operating parameters as a guide recommended for testing of pilot plant CFBG for syngas production. Based on the hydrodynamic studies of cold flow CFBG, the SCR shown in the table is achieved to allow steady operation of particles transfer between the compartments with stable bed pressure drop. It also allows the particles to fall back to the main bed (no particles entrainment). With controlled and appropriate SCR, good fluidization quality and good overall binary mixing quality shall be achieved.

Table 9.1: Operating parameters recommended for pilot plant CFBG operation

To Maintain Fluidization Quality, Q	
Bed Height	0.40m
Effective Diameter	More than 0.40 m
Inert Particle	River sand of mean size 272 µm

To Maintain Overall Binary Mixing Quality, M	
Inert particle	River sand of mean size 272 µm
Palm shell	5 wt% - 15 wt% of 1.77mm, 3.56mm & 7.13mm
Main Bed Aeration	More than 1.5 binary U_{mf}
Total Static Bed Height	More than 0.40m

To Control Solid Circulation Rate, SCR

Main Bed Aeration	***Riser Aeration***	***V-valve Aeration***	***SCR***
Static bed height = 0.20m			
1.3 U_{mf}	8 U_{mf}	5 U_{mf}	50 kg/hr
		9 U_{mf}	180 kg/hr
	12 U_{mf}	5 U_{mf}	140 kg/hr
1.7 U_{mf}	12 U_{mf}	5 U_{mf}	140 kg/hr
Static bed height = 0.40m			
1.3 U_{mf}	8 U_{mf}	5 U_{mf}	845 kg/hr
		9 U_{mf}	1280 kg/hr
	12 U_{mf}	5 U_{mf}	1400 kg/hr
1.7 U_{mf}	8 U_{mf}	5 U_{mf}	860 kg/hr
		9 U_{mf}	900 kg/hr
	12 U_{mf}	9 U_{mf}	1600 kg/hr

9.3 RECOMMENDATIONS

Results presented in this thesis demonstrate the suitability of the numerical model for CFBG hydrodynamic studies however as part of the development and validation process a number of further areas of work have become apparent. Although the overall objectives of the present research have been achieved, various new gaps have also been identified following the evaluations of the findings from the present research, leading to the following recommendations for future research.

- Many fluidized bed systems operate with more than a single particle type and size. Extension of the model to allow for multiple particle sizes and densities would allow the model to be applied to more commercial applications.
- Though a large proportion of bubble formation is due to the equation of the gas-solid drag coefficient, a significant contribution falls onto the kinetic theory of granular flow. Kinetic theory used in this thesis, was originally derived by investigating the collisions between particles of like size and density. The current kinetic theory needs to be modified which applies to collisions between different size and density particles.
- The drag force between the gas and solid particles is one of the dominant forces in a fluidized bed. The drag laws to model the inter-phase momentum exchange are usually developed empirically. Therefore it is of necessity to modify the default constant values in the drag function chosen to predict the behavior of different inert solids suit for CFBG. Experimental determination of solid phase parameters such as the restitution coefficient for different particles in this study is also recommended.
- Although the mixing in a binary system fluidized bed is fairly well-predicted, the binary bubble formation is not being studied in this thesis. This may help to explain further in the mixing or segregation behavior. Also, physical data of bubble size in single component and binary mixture fluidized bed is required to enable a higher level of quantitative validation.

- Gas crossflow is an important phenomenon that may affect the CFBG hydrodynamics especially the SCR. Further work is recommended for gas crossflow study.
- All simulations and experiments in this research were carried out under ambient temperature. However it is of great importance to understand the hydrodynamics and reactions at high temperature, e.g. pyrolysis, devolatilization, gasification and combustion. Future work is required to conduct numerical modeling in the aforementioned areas. Further experimental works are also required to study the reaction kinetic for the gasification reaction.

REFERENCES

Agrawal, K., Loezos, P.N., Syamlal, M., and Sundaresan, S. 2001. "The Role of Meso-Scale Structures in Rapid Gas-Solid Flow." *Journal of Fluid Mechanics* 445: 151–185.

Almuttahar, A. and Taghipour, F. 2008. "Computational Fluid Dynamics of High Density Circulating Fluidized Bed Riser: Study of Modeling Parameters." *Powder Technology* 185: 11 – 23.

Andrews, A.T.I., Loezos, P.N. and Sundaresan, S. 2005. "Coarse-Grid Simulation of Gas-Particle Flows in Vertical Risers." *Industrial & Engineering Chemistry Research* 44: 6022–6037.

Apte, S. V., Mahesh, K. and Lundgren, T. 2003. "A Eulerlan-Lagrangian Model to Simulate Two-Phase/Particulate Flows." *Annual Research Briefs - 2003 [Center for Turbulence Research]*, Compilation Part Notice# ADP014800. 161-171.

Arastoopour, H., Pakdel, P. And Adewumi, M. 1990. "Hydrodynamics Analysis of Dilute Gas-Solid Flow in a Vertical Pipe." *Powder Technology* 62: 163 - 170.

Asegehegn, T. W., Schreiber, M and Krautz, H. J. 2011. "Numerical Simulation and Experimental Validation of Bubble Behavior in 2D Gas-Solid Fluidized Beds with Immersed Horizontal Tubes." *Chemical Engineering Science* 66: 5410 – 5427.

Azadi, Mehdi, 2011. "Multi-Fluid Eulerian Modeling of Limestone Particles' Elutriation from a Binary Mixture in a Gas-Solid Fluidized Bed." *Journal of Industrial and Engineering Chemistry* 17: 229 – 236

Benyahia S. 1999. "Analysis of Solid Flow Patterns and Mixing in Gas/Solid Flow Systems." *PhD Thesis*, Illinois Institute of Technology.

Benyahia, S., Syamlal, M. and O'Brien, T.J. 2007. "Study of the Ability of Multiphase Continuum Models to Predict Core-Annulus Flow." *A.I.Ch.E. Journal* 53: 2549–2568.

Bhattacharya, B., Sathiyamoorthy, D., Govardhana Rao, V. and Mahajan, S. P. 1997. "Intermixing of Fluidizing Gas Streams in a Compartmented Circulating Fluidized Bed." *Chemical Engineering Technology* 20: 522 - 532.

Bhattacharya, B., Sathiyamoorthy, D., Govardhana Rao, V. and Mahajan, S. P. 1999. "Solid Circulating in a Compartmented Gas Fluidized Bed." *Powder Technology* 101: 191 - 204.

Bird, R. B., Stewart, W. E. and Lightfoot, E. N. 2002. *Transport Phenomena*, 2nd Ed., Wiley, New York.

Boemer, A., Qi, H. and Renz, U. 1997. "Eulerian Simulation of Bubble Formation at a Jet in a Two-Dimensional Fluidized Bed." *International Journal of Multiphase Flow* 23: 927–944.

Briongos, J. V. and Guardiola, J. 2005. "New Methodology for Scaling Hydrodynamic data from a 2D- Fluidized Bed." *Chem. Eng. Sci.* 60: 5151.

Busciglio, A., Vella, G., Micale, G. and Rizzuti, L. 2009. "Analysis of the Bubbling Behaviour of 2D Gas-Solid Fluidized Beds Part II. Comparison between

Experiments and Numerical Simulations via Digital Image Analysis Technique." *Chemical Engineering Journal* 148: 145 – 163.

Cammarata, L., Micale, G. D. M., Lettieri, P. and Colman, D. 2003. "2D and 3D CFD Simulations of Bubbling Fluidized Beds Using Eulerian-Eulerian Models." *International Journal of Chemical Reactor Engineering* 1.

Chandrasekaran, B. K., van der Lee, L. Hulme, I. and Kantzas, A. 2005. "A Simulation and Experimental Study of the Hydrodynamics of a Bubbling Fluidized Bed of Linear Low Density Polyethylene Using Bubble Properties and Pressure Fluctuations." *Macromolecular Materials and Engineering* 290: 592 – 609.

Chandratilleke, G. R., Yu1, A. B., Bridgwater, J. and Shinohara, K. 2011. "A Particle-Scale Index in the Quantification of Mixing of Particles." *AIChE Journal*, doi: 10.1002/aic.12654

Chapman, S. and Cowling, T.G. 1970. "The Mathematical Theory of Non-uniform Gases." *Cambridge University Press*, Cambridge.

Chiesa, M., Mathiesen, V., Melheim, J. A. and Halvorsen, B. 2005. "Numerical Simulation of Particulate Flow by the Eulerian-Lagrangian and the Eulerian-Eulerian Approach with Application to a Fluidized Bed." *Computers and Chemical Engineering* 29: 291 – 304.

Chok, V.S. 2011. "Experimental Studies of a Compartmented Fluidized Bed Gasifier for Fuel Gas from Oil Palm Shell Biomass." *Ph.D Thesis*, Dept. of Chemical Engineering, Curtin University, Australia.

Cooper, S. and Coronella, C. J. 2005. "CFD Simulations of Particle Mixing in a Binary Fluidized Bed." *Powder Technology* 151: 27 – 36.

Cornelissen, J. T., Taghipour, F., Escudie, R., Ellis, N. and Grace, J. R. 2007. "CFD modelling of a liquid-solid fluidized bed." *Chem. Eng. Sci*. 62: 6334-6348.

Coroneo, M., Mazzei, L., Lettieri, P., Paglianti, A. and Montante, G. 2011. "CFD Prediction of Segregating Fluidized Bidisperse Mixtures of Particles Differeing in Size and Density in Gas-Solid Fluidized Beds." *Chemical Engineering Science* 66: 2317 – 2327.

Cruz, E., Steward, F.R. and Pugsley T.S. 2002. "Modelling CFB Riser Hydrodynamics Using Fluent, in: J.R. Grace, J. Zhu, H. de Lasa (Eds.), Circulating Fluidized Bed Technology." *Canadian Society of Chemical Engineers* VII: 435 – 442.

Cruz, E., Steward, F.R. and Pugsley, T. 2006. "New Closure Models for CFD Modeling of High-Density Circulating Fluidized Beds." *Powder Technology* 169: 115 – 122.

Cundall, P.A. and Strack, O.D.L. 1979. "A Discrete Numerical Model for Granular Assemblies." *Geotechniques* 29: 47–65.

Darton, R. C., Lanauze, R. D., Davidson, J. F. and Harrison, D. 1977. "Bubble Growth dur to Coalescence in Fluidized Beds." *Transaction of Institute of Chemical Engineers* 55: 274 – 280.

Davidson, J. S.; Clift, R. and Harrison, D. 1985. "Fluidization." 2nd ed.; *Academic Press*:London, U.K.

De Felice, R. 1994. "The Voidage Function for Fluid-Particle Interaction System." *International Journal of Multiphase Flow* 20: 153 – 159.

De Wilde, J. 2005. "Reformulating and Quantifying the Generalized Added Mass in Filtered Gas–Solid Flows Models." *Physics of Fluids* 17: 113 - 124.

Di Renzo, A., Di Maio, F. P., Girimonte, R. and Formisani, B. 2008. "DEM Simulation of the Mixing Equilibrium in Fluidized Beds of Two Solids Differing in Density." *Powder Technology* 184: 214 – 223.

Enwald, H., Peirano, E. and Almstedt, A.E. 1996. "Eulerian Two-Phase Flow Theory Applied to Fluidization." *International Journal of Multiphase Flow* 22: 21–66.

Ergun, S. 1952. "Fluid Flow through Packed Columns." *Chem. Eng. Prog.* 48 (2): 89 – 94.

Esmaili, E. and Mahinpey, N. 2011. "Adjustment of Drag Coefficient Correlations in Three Dimensional CFD Simulation of Gas-Solid Bubbling Fluidized Bed." *Advances in Engineering Software* 42: 375 – 386.

Fauziah, M., Norazah, A. R., Nornizar, A., Azli Bahari, A. and Tajuddin, M. J. 2008. "Cold Flow Binary Fluidization of Oil Palm Residues Mixture in a Gas-Solid Fluidized Bed System." *Pertanika Journal of Science & Technology* 16: 201 - 212.

Gamwo, I. K., Soong, Y. and Lyczkowski, R. W. 1999. "Numerical Simulation and Experimental Validation of Solids Flows in a Bubbling Fluidized Bed." *Powder Technology* 103: 117 – 129.

Gao, J.S., Lan, X. Y., Fan, Y. P., Chang, J., Wang, G., Lu, C. X. and Xu, C. M. 2009. "Hydrodynamics of Gas-Solid Fluidized Bed of Disparately Sized Binary Particles." *Chemical Engineering Science* 64: 4302 – 4316.

Gelderbloom, S. J., Gidaspow, D., and Lyczkowski, R. W. 2003. "CFD Simulations of Bubbling/Collapsing Fluidized Beds for Three Geldart Groups." *AIChE Journal* 49: 844 – 858.

Gera, D., Gautam, M., Tsuji, Y., Kawaguchi, T. and Tanaka, T. 1998. "Computer Simulation of Bubbles in Large-Particle Fluidized Beds." *Powder Technology* 98: 38 – 47.

Gidaspow, D. and Ettehadieh, B. 1983. "Fluidization in Two-Dimensional Beds with a Jet. 2. Hydrodynamic Modeling." *Industrial & Engineering Chemistry Fundamentals* 22: 193–201.

Gidaspow, D. 1994. "Multiphase Flow and Fluidization." *Academic Press*, San Diego.

Goldschmidt, M.J.V., Kuipers, J.A.M., and van Swaaij, W.P.M. 2001. "Hydrodynamic Modelling of Dense Gas- Fluidised Beds Using the Kinetic Theory of Granular Flow: Effect of Coefficient of Restitution on Bed Dynamics." *Chemical Engineering Science* 56: 571 – 578.

Goldschmidt, M.J.V., Beetstra, R. and Kuipers, J.A.M. 2004. "Hydrodynamic Modelling of Dense Gas-Fluidised Beds: Comparison and Validation of 3D Discrete Particle and Continuum Models." *Powder Technology* 142: 23– 47

Grace, J.R. and Sun, G. 1991. "Influence of Particle Size Distribution on the Performance of Fluidized Bed Reactors." *Canadian Journal of Chemical Engineering* 69: 1126 – 1134.

Grace, J. R. and Taghipour, F. 2004. "Verification and Validation of CFD Models and Dynamic Similarity for Fluidized Beds." *Powder Technology* 139: 99 – 110.

Guenther, C., Syamlal, M., Shadle, L. and Ludlow, C. 2002. "A Numerical Investigation of An Industrial Scale Gas–Solids CFB." *Presented at Proceedings of the Seventh International Conference on Circulating Fluidized Beds*, Ontario, Canada, pp. 483–488.

Gustavasson, M., and Almstedt, A. E. 2000. "Numerical Simulation of Fluid Dynamics in Fluidized Beds with Horizontal Heat Exchanger Tubes." *Chemical Engineering Science* 55 (4): 857-863.

Hamzehei, M. and Rahimzadeh, H. 2009. "Experimental and Numerical Study of Hydrodynamics with Heat Transfer in a Gas-Solid Fluidized bed Reactor at Different Particle Sizes*" Industrial Engineering Chemistry Research* 48: 3177 – 3186.

Hamzehei, M., Rahimzadeh, H. and Ahmadi, G. 2010. "Studies of Gas Velocity and Particles Size Effects on Fluidized Bed Hydrodynamics with CFD Modeling and Experimental Investigation."

Hartge, E. U., Ratschow, L., Wischnewski, R. and Werther J. 2009. "CFD-Simulation of a Circulating Fluidized Bed Riser." *Particuology* 7: 283 – 296.

He, Y. 1993. "Hydrodynamics of a Compartmented Dense Phase Circulating Fluidised Bed." *Ph.D. Dissertation*, Dept. of Chemical Engineering, The Univ. of Queensland, Australia.

Hede, P. D. "Hydrodynamic Modeling and Granular Dynamics", **ISBN** 87-7681-172-7, http://bookboon.com/uk/textbooks/chemical/hydrodynamic-modelling.

Hoomans, B.P.B., Kuipers, J.A.M., Briels, W.J. and van Swaaij, W.P.M. 1996. "Discrete Particle Simulation of Bubble and Slug Formation in a Two-Dimensional Gas-Fluidised Bed: A Hard-Sphere Approach." *Chemical Engineering Science* 51 (1): 99 – 118.

Hosseini, S. H., Ahmadi, G., Rahimi, R., Zivdar, M. and Esfahany, M. N. 2010. "CFD Studies of Solids Hold-up Distribution and Circulation Patterns in Gas-Solid Fluidized Beds." *Powder Technology* 200: 202 – 215.

Hulme, I., Clavelle, E., van der Lee, L. and Kantzas, A. 2005. "CFD Modelling and Validation of Bubble Properties for a Bubbling Fluidized Bed." *Ind. Eng. Chem. Res*. 44: 4254 – 4266.

Igci, Y., Andrews IV, A.T., Sundaresan, S., Pannala, S. and O'Brien, T. 2008. "Filtered Two-Fluid Models for Fluidized Gas-Particle Suspensions." *A.I.Ch.E. Journal* 54: 1431–1448.

Jenkins, J.T. and Savage, S.B. 1983. "A Theory for the Rapid Flow of Identical Smooth, Nearly Elastic, Spherical Particles." *Journal of Fluid Mechanics* 130: 187 – 202.

Jin, B. S., Wang, X. F., Zhong, W. Q., Tao, H., Ren, B. and Xiao, R. 2010. "Modeling on High-Flux Circulating Fluidized Bed with Gerdart Group B Particles by Kinetic Theory of Granular Flow." *Energy & Fuels* 24: 3159 – 3172.

Johnson, P.C., Nott, P. and Jackson, R. 1990. "Frictional-Collisional Equations of Motion for Particulate Flows and Their Application to Chutes." *Journal of Fluid Mechanics* 210: 501 – 535.

Kawaguchi, T., Tanaka, T. and Tsuji, Y. 1998. "Numerical Simulation of Two-Dimensional Fluidized Beds using the Discrete Element Method (Comparison between the Two and Three-Dimensional Models)." *Powder Technology* 96: 129 – 138.

Kobayashi, N., Yamazaki, R. and Mori, S. 2000. "A Study on the Behavior of Bubbles and Solids in Bubbling Fluidized Beds." *Powder Technology* 113: 327 – 344.

Krishna, R. and van Baten, J.M. 2001. "Using CFD for Scaling Up Gas-Solid Bubbling Fluidised Bed Reactors with Geldart A Powders." *Chemical Engineering Journal* 82: 247 – 257.

Kuipers, J.A.M., Prins, W. and van Swaaij, WPM 1992. "Numerical Calculation of Wall to Bed Heat Transfer Coefficients in Gas-Fluidized Beds." *AIChE Journal* 38 (7): 1079 - 1091

Kunii, D. and Levenspiel, O. 1991. "Fluidization Engineering." Second Ed., *Butterworth-Heinemann*, Boston.

Laverman, J.A., Roghair, I., Annaland, M. V. and Kuipers, H. 2008. "Investigation into the Hydrodynamics of Gas–Solid Fluidized Beds Using Particle Image Velocimetry Coupled with Digital Image Analysis." *Canadian Journal of Chemical Engineering* 86 (3): 523–535.

Li, T., Grace, J. and Bi, X. T. 2010. "Study of Wall Boundary Condition in Numerical Simulations of Bubbling Fluidized Beds*." Powder Technology* 203: 447 – 457.

Li, Z. Y., Su, W. G., Wu, Z. H., Wang, R. F. and Mujumdar, A. S. 2009. "Investigation of Flow Behaviours and Bubble Characteristics of a Pulse Fluidized Bed via CFD Modeling." *Drying Technology* 28-1: 78 – 93.

Liu, D. 1980. 'Pneumatically Controlled Multi-Stage Fluidized Beds." *Fluidization*, Plenum Press, 485 - 492.

Loboreiro, J., Gustavo G. J., Christine M. H., Dale M. S., Sibashis S. B., and Janine E. G. 2008. "The Influence of Binary Drag Laws on Simulations of Species Segregation in Gas-Fluidized Beds." *Powder Technology* 184: 275 – 290.

Lu, H. L., Liu, W. T., Li, F., Zhao, G. B. and He, Y. R. 2002. "Eulerian Simulations of Bubble Behavior in a Two-Dimensional Gas- Solid Bubbling Fluidized Bed." *International Journal of Energy Research* 26: 1285 – 1293.

Lu, H. L., He, Y. R. and Gidaspow, D. 2003. "Hydrodynamic Modelling of Binary Mixture in a Gas Bubbling Fluidized Bed Using the Kinetic Theory of Granular Flow." *Chemical Engineering Science* 58: 1197 – 1205.

Lu, H. L., Zhao, Y. H., Ding, J. M., Gidaspow, D. and Li, W. 2007. "Investigation of Mixing/Segregation of Mixture Particles in Gas-Solid Fluidized Beds." *Chemical Engineering Science* 62: 301 – 317.

Lun, C.K.K., Savage, S.B., Jeffrey, D.J. and Chepurniy, N. 1984. "Kinetic Theories for Granular Flow: Inelastic Particles in Couette Flow and Slightly Inelastic Particles in A General Flow Field." *Journal of Fluid Mechanics* 140: 223 – 256.

Ma, D. and Ahmadi, G. 1986. "An Equation of State for Dense Rigid Sphere Gases." *Journal of Chemical Physics* 84: 3449 – 3450.

Marschall, K. –J. and Mleczko, L.1999. "CFD Modeling of An Internally Circulating Fluidized-Bed Reactor." *Chemical Engineering Science* 54: 2085 – 2093.

Mathiesen, V., Solberg, T. and Hjertager B. H. 2000. "Predictions of Gas/Particle Flow with An Eulerian Model Including A Realistic Particle Size Distribution." *Powder Technology* 112: 34 – 45.

Mathiesen, V., Solberg, T. and Hjertager, B. H. "An Experimental and Computational Study of Multiphase Flow Behavior in A Circulating Fluidized Bed." *International Journal of Multiphase Flow* 26: 387 – 419.

Mazzei, L and Lettieri, P. 2006. "A Numerical Algorithm for the Analysis of the Bubble Dynamics in Two-Dimensional Fluidized Beds Simulated by Means of CFD Multiphase-Flow Codes." *International Journal of Chemical Reactor Engineering* 4: 1- 18.

Mazzei, L., Casillo, A., Lettieri, P and Salatino, P. 2010. "CFD Simulations of Segregating Fluidized Bidisperse Mixtures of Particles Differing in Size." *Chemical Engineering Journal* 156: 432 – 445.

McKeen, T. and Pugsley, T. 2003. "Simulation and Experimental Validation of A Freely Bubbling Bed of FCC Catalyst." *Powder Technology* 129: 139 – 152.

Nguyen, T. D. B., Seo, M. W., Lim, Y. I., Song, B. H. and Kim, S. D. 2011. "CFD Simulation with Experiments in a Dual Circulating Fluidized Bed Gasifier." Doi: 10.1016/i.compchemeng.2011.07.005.

Nicholas, P. C. and Paul, P. C. 1984. "Hydrodynamics of Gas–Solids Fluidization." *Gulf Publishing Co.*: Houston, TX.

Nienow. A.W. and Cheesman, D.J. 1980. "The Effect of Shape on the Mixing and Segregation of Large Particles in Gas-Fluidized Beds of Small Ones." Fluidization: *Plenum*: New York, 1: 373.

Nienow, A. and Chiba, T. 1985. "Fluidization of Dissimilar Materials." Fluidization, 2nd ed.; *Academic Press*; London, Chapter 10.

Nieuwland, J.J., van Sint Annaland, M., Kuipers, J.A.M. and van Swaaij, W.P.M. 1996. "Hydrodynamics Modeling of Gas/Particle Flows in Riser Reactors." *AIChE Journal* 42: 1569.

Owoyemi, O., Lettieri, P. and Place, R. 2005. "Experimental Validation of Eulerian-Eulerian Simulations of Rutile Industrial Powders." *Ind. Eng. Chem. Res*. 44: 9996 – 10004.

Owoyemi, O. and Lettieri, P. 2008. "Computational Fluid Dynamics Modeling and Validation of Bidisperse Fluidized Industrial Powders." *Ind. Eng. Chem. Res*. 47: 6316 – 6326.

Patankar, S. V. 1980. "Numerical Heat Transfer and Fluid Flow." First Ed., *Hemisphere Publishing,* Washington, DC.

Patil, D.J.,van Sint Annaland, M. and Kuipers, J.A.M. 2005b. "Critical Comparison of Hydrodynamic Models for Gas–Solid Fluidized Beds — part II: Freely Bubbling Gas–Solid Fluidized Beds." *Chemical Engineering Science* 60: 73 – 84.

Patureaux, T., and Barthod, D. 2000. "Usage of CFD Modeling for Improving and FCC Riser Operation." *Oil Gas Science Technology Review* IFP 55 (2): 219 – 225.

Peirano, E., Delloume, V. and Leckner, B. 2001. "Two- or Three-Dimensional Simulations of Turbulent Gas-Solid Flows Applied to Fluidization." *Chemical Engineering Science* 56: 4787 – 4799.

Qureshi, A. E. and Creasy, D. E. 1979. "Fluidized Bed Gas Distributors." *Powder Technology* 22: 113 – 119.

Ranade, V. V. 2002. "Computational Flow Modeling for Chemical Reactor Engineering." First Ed., *Academic press*, New York.

Reuge, N., Cadoret, L., Coufort-Saudejaud, C., Pannala, S., Syamlal, M. and Caussat, B. 2008. "Multifluid Eulerian Modeling of Dense Gas-Solids Fluidized Bed

Hydrodynamics: Influence of the Dissipation Parameters." *Chemical Engineering Science* 63: 5540 – 5551.

Richardson, J.F. and Zaki, W.N. 1954. "Sedimentation and Fluidization: Part I." *Trans. Inst. Chem. Eng*. 32: 35-53.

Rudolph, V., Rei, M.H. and Lin S.Y. 1985. "Horizontally Circulating Fluid Bed for Catalytic Reaction and Regeneration: Transport Phenomena in a Cold Test Model." *Proceedings of 4th R.O.C. Symposium on Catalysis and Reaction Engineering*, Kaohsiung, Taiwan, 100.

Sanyal, J. and Cesmebasi, E. 1994. "On the Effect of Various Momentum Transfer Coefficient Models on Bubble Dynamics in a Reactangular Gas fluidized Bed." *Chem. Eng. Sci*. 49: 3955 – 3966.

Sathiyamoorthy, D. and Rudolph, V. 1990. "Hydrodynamics of Compartmented Dense Phase Circulating Gas Fluidized Bed." *Proc. in Circulating Fluidized Bed Technology III*, 505 - 510.

Sathiyamoorthy, D. and Masayuki, H.2003. "On the Influence of Aspect Ratio and Distributor in Gas Fluidized Bed." Chem. Eng. J. 2003, 93, 151–161.

Sau, D.C. and Biswal, K. C. 2011. "Computational Fluid Dynamics and Experimental Study of the Hydrodynamics of a Gas-Solid Tapered Fluidized Bed." *Applied Mathematical Modeling* 35: 2265 – 2278.

Schaeffer, D.G. 1987. "Instability in the Evolution Equations Describing Incompressible Granular Flow." *Journal of Differential Equations* 66: 19 – 50.

Seo, M. W., Nguyen, T. D. B., Lim, Y. I., Kim, S. D., Park, S. W., Song, B. H., and Kim, Y. J. 2011. "Solid Circulation and Loop-Seal Characteristics of a Dual Circulating Fluidized Bed: Experiments and CFD Simulation." *Chemical Engineering Journal* 168: 803 – 811.

Shen, L. H., Xiao, J., Niklasson, F. and Johnsson, F. 2007. "Biomass Mixing in a Fluidized Bed Biomass Gasifier for Hydrogen Production." *Chemical Engineering Science* 62: 636–646.

Shi, D. P, Luo, Z. H. and Guo, A. Y. 2010. "Numerical Simulation of the Gas-Solid Flow in Fluidized-Bed Polymerization Reactors." *Ind. Eng. Chem. Res*. 49: 4070 – 4079.

Sinclair, J.L. and Jackson, R. 1989. "Gas Particle Flow in A Vertical Pipe with Particle-Particle Interactions." *AIChE Journal* 35: 1473.

Sun, Q. Q., Lu, H. L., Liu, W. T., He, Y. R. and Gidaspow, D. 2005. "Simulation and Experiment of Segregating/Mixing of Rice Husk-Sand Mixture in a Bubbling Fluidized Bed." *Fuel* 84: 1739 – 1748.

Syamlal, M. and O'Brien, T. J. 1989. "Computer Simulation of Bubbles in a Fluidized Bed." *A.I.Ch.E. Symposium Series* 85: 22 - 31.

Syamlal, M. and T.J. O'Brien. 1994. "The Derivation of a Drag Coefficient Formula from Velocity-Voidage Correlations." *A Technical Report under U.S. Department of Energy, Office of Fossil Energy*.

Syamlal, M. and O'Brien, T. J. 2003. "Fluid Dynamic Simulation of O_3 Decomposition in a Bubbling Fluidized Bed." *A.I.Ch.E. Journal* 49: 2793 – 2801.

Taghipour, F., Ellis, N. and Wong, C. 2005. "Experimental and Computational Study of Gas-Solid Fluidized Bed Hydrodynamics." *Chemical Engineering Science* 60: 6857 – 6867.

Tsuji, Y., Kawaguchi, T. and Tanaka, T. 1993. "Discrete Particle Simulation of Two-Dimensional Fluidized Bed." *Powder Technology* 77: 79–87

Tsuo, Y. and Gidaspow, D. 1990. "Computation of Flow Patterns in Circulating Fluidized Beds." *AIChE Journal* 36: 885–896.

Vaishali, S., Roy, S., Bhusarapu, S., Al-Dahhan, M. H. And Dudukovic M. P. 2007. "Numerical Simulation of Gas-Solid Dynamics in a Circulating Fluidized-Bed Riser with Geldart Group B Particles." *Ind. Eng. Chem. Res*. 46: 8620 – 8628.

van der Hoef, M.A., van Sint Annaland, M. and Kuipers, J.A.M. 2004. "Computational Fluid Dynamics for Dense Gas-Solid Fluidized Beds: A Multi-Scale Modeling Strategy." *Chemical Engineering Science* 59: 5157 – 5165.

van Wachem, B. G. M., Schouten, J. C., Krishna, R., and van den Bleek, C. M. 1998. "Eulerian Simulation of Bubbling Behaviour in Gas-Solid Fluidized Beds." *Computers and Chemical Engineering* 22: 299 – 306.

van Wachem B.G.M. 2000. "Derivation, Implementation and Validation of Computer Simulation Models for Gas-Solid Fluidized Beds." *PhD Thesis*, Technical University, Delft.

van Wachem, B.G., Schouten, J.C., van den Bleek, C.M., Krishna, R. and Sinclair, J.L. 2001. "Comparative Analysis of CFD Models of Dense Gas-Solid Systems." *AIChE Journal* 47: 1035 – 1051.

Wang, J. 2008a. "High-Resolution Eulerian Simulation of RMS of Solid Volume Fraction Fluctuation and Particle Clustering Characteristics in a CFB Riser." *Chemical Engineering Science* 63: 3341–3347.

Wang, J. W. 2009. "A Review of Eulerian Simulation of Gerdart A Particles in Gas-Fluidized Beds." Industrial & Engineering Chemistry Research 48: 5567–5577.

Wang, J. W., van der Hoef, M. A. and Kuipers, J. A. M. 2010. "Coarse Grid Simulation of Bed Expansion Characteristics of Industrial-Scale Gas-Solid Bubbling Fluidized Beds." *Chemical Engineering Science* 65: 2125 – 2131.

Wang, W., and Li, Y.C. 2001. "Hydrodynamic Simulation of Fluidization by Using a Modified Kinetic Theory." *Industrial Engineering Chemistry* 40: 5066 – 5073.

Wang, Y. F., Chao, Z. X. and Jakobsen, H. A. 2010. "A Sensitivity Study of the Two-Fluid Model Closure Parameters (β, e) Determining the Main Gas-Solid Flow Pattern Characteristics." *Ind. Eng. Chem. Res*. 49: 3433 – 3441.

Wankhede, U. S. and Adgulkar, D.D., 2008, "CFD Simulations of Heat Transfer in a Bubbling Fluidized Bed for Different Materials," First International Conference on Emerging Trends in Engineering and Technology, IEEE computer society, DOI: 10.1109/ICETET.2008.96

Wen, C.Y. and Yu, Y.H. 1966. "Mechanics of Fluidization." *Chem. Eng. Prog. Symp.* 62: 100 – 110.

Werther, J. 1968. "Influence of the Bed Diameter on the Hydrodynamics of Gas Fluidized Beds." *AIChE Symp. Ser*. 141 (70): 53 – 62.

Wirsum, M., Fett, F., Iwanowa, N. and Lukjanow, G. 2001. "Particle Mixing in Bubbling Fluidized Beds of Binary Particle Systems." *Powder Technology* 120: 63 – 39.

Xie, N., Battaglia, F. and Pannala, S. 2008. "Effects of Using Two- versus Three-Dimensional Computational Modeling of Fluidized Beds Part I, Hydrodynamics." *Powder Technology* 182: 1 – 13.

Yan, H. M. 1995. "Development and Modelling of Coal Combustion and Gasification in a Compartmented Fluidised Bed Gasifier." *Doctoral dissertation*, Department of Chemical Engineering, The University of Queensland, Australia.

Yan, H.M. and Rudolph, V. 1996. "A New Method for Measuring Solid Circulation Rate in Compartmented Fluidized Bed Gasifier." *Chemical Engineering Community* 147: 133 – 144.

Zhang, K., Zhang, J., and Zhang, B. J. 2003. "Experimental and Numerical Study of Fluid Dynamic Parameters in a Jetting Fluidized Bed of a Binary Mixture." *Powder Technology* 132: 30 – 38.

Zhang, K., Zhang, J. and Zhang, B. 2004. "CFD Simulation of Jet Behavior and Voidage Profile in a Gas-Solid Fluidized Bed." *International Journal of Energy Research* 28: 1065 – 1974.

Zhang, N., Lu, B. N., Wang, W. and Li, J. H. 2008. "Virtual Experimentation through 3D Full-Loop Simulation of a Circulating Fluidized Bed." *Particuology* 6: 529 – 539.

Zhang, Y., Jin, B. and Zhong, W. 2008. "Fluidization, Mixing and Segregation of a Biomass-Sand Mixture in a Fluidized Bed." *International Journal of Chemical Reactor Engineering* 6: 1 - 29.

Zhao, Yuemin, Tang, L. G., Luo, Z. F., Liang, C.C., Xing, H. B., Wu, W. C., and Duan, C. L. 2010. "Experimental and Numerical Simulation Studies of the Fluidization Characteristic of a Separating Gas-Solid Fluidized Bed." *Fuel Processing Technology* 91: 1819 – 1825.

Zhong, W., Zhang, M. and Jin, B. 2006. "Maximum Spoutable Bed Height of Spout-Fluid Bed." *Chemical Engineering Journal* 124: 55 – 62.

Zhong, W., Zhang, M., Jin, B., Zhang, Y., Xiao, R. and Huang, Y. 2007. "Experimental Investigation of Particle Mixing Behavior in a Large Spout-Fluid Bed." *Chemical Engineering and Processing*.

Zimmermann, S. and Taghipour, F. 2005. "CFD Modeling of the Hydrodynamics and Reaction Kinetics of FCC Fluidized-Bed Reactors." *Ind. Eng. Chem. Res.* 44: 9818 – 9827.

APPENDIX A EFFECTIVE DIAMETER, D_e CALCULATIONS

CFBG Diameter = 0.66m

Total Area = 0.3421m^2

A.1 D_e FOR COMBUSTOR

Area = 0.3421 x 0.65

= 0.2224m^2

mean cross-sectional area = 0.2224 – 0.1 x 0.05 (area of riser bottom) – 0.05 x 0.05 (area of v-valve bottom)

= 0.2149m^2

mean wetted perimeter = the perimeter of combustor

= 1.3475 + (0.1 + 0.05 + 0.05) (riser perimeter) + 0.05 x 3 (v-valve bottom perimeter) + 0.438 (remaining of the length of dividing wall)

= 2.1355m

Thus, effective diameter,

$$D_e = 4 \times \frac{mean\ cross\ \text{sec}tional\ area\ of\ \ flow\ channels\ through\ bed}{mean\ wetted\ \ perimeter\ of\ \ flow\ channels}$$

= 4 x 0.2149 / 2.1355

= 0.413 m

A.2 D_e FOR GASIFIER

Area = 0.3421 x 0.35

= 0.1197m^2

mean cross-sectional area = 0.1197– 0.1 x 0.05 (area of riser bottom) – 0.05 x 0.05

(area of v-valve bottom)

$= 0.1122 m^2$

mean wetted perimeter = the perimeter of combustor

= 0.7255 + (0.1 + 0.05 + 0.05) (riser perimeter) + 0.05 x 3 (v-Valve bottom perimeter) + 0.438 (remaining of the length of dividing wall)

= 1.3685m

Thus, effective diameter,

$$D_e = 4 \times \frac{mean\ cross\ sectional\ area\ of\ \ flow\ channels\ through\ bed}{mean\ wetted\ \ perimeter\ of\ \ flow\ channels}$$

= 4 x 0.1122 / 1.3685

= 0.257 m

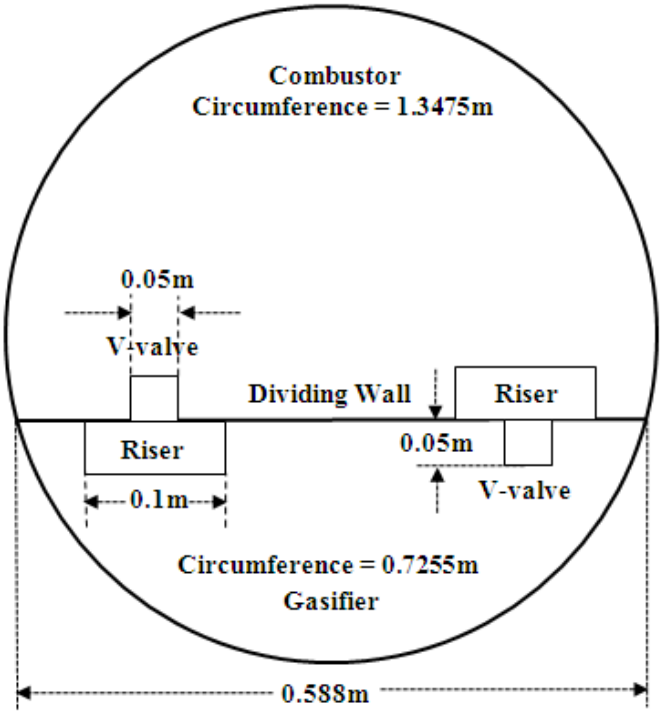

Figure A.1: Top view of CFBG reactor

APPENDIX B NUMERICAL STUDY ON FLOW BEHAVIOUR IN V-VALVE AND RISER OF DIFFERENT DESIGNS

Two different designs of riser are attempted, which are addressed as Design 1 (with lower part of riser) and Design 2 (without lower part of riser) as shown in Figure B.1 and B.2 with the purpose to choose the best design for smooth transportation of solids within the CFBG. This simulation is the preliminary analysis to support the CFBG pilot plant construction. Comparisons of these two designs with the aim of improving the CFBG hydrodynamics are performed.

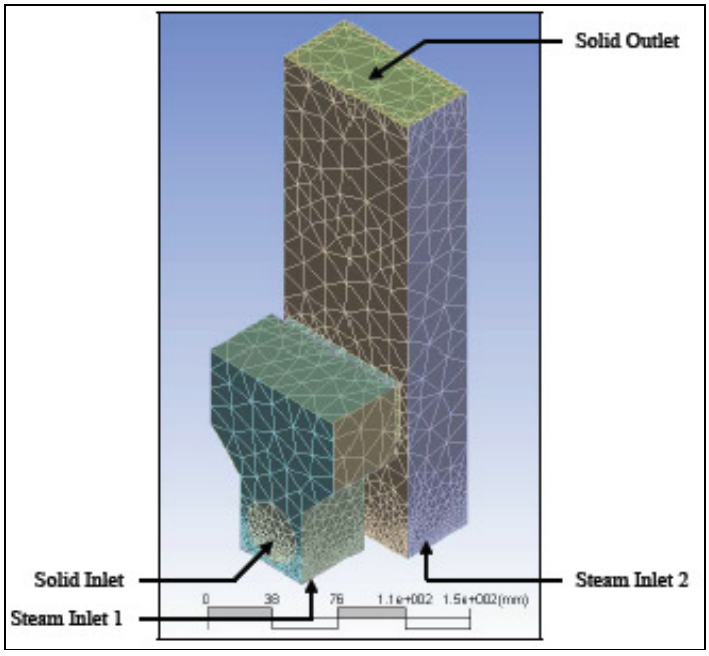

Figure B.1: Geometry of design 1 for CFBG internal parts

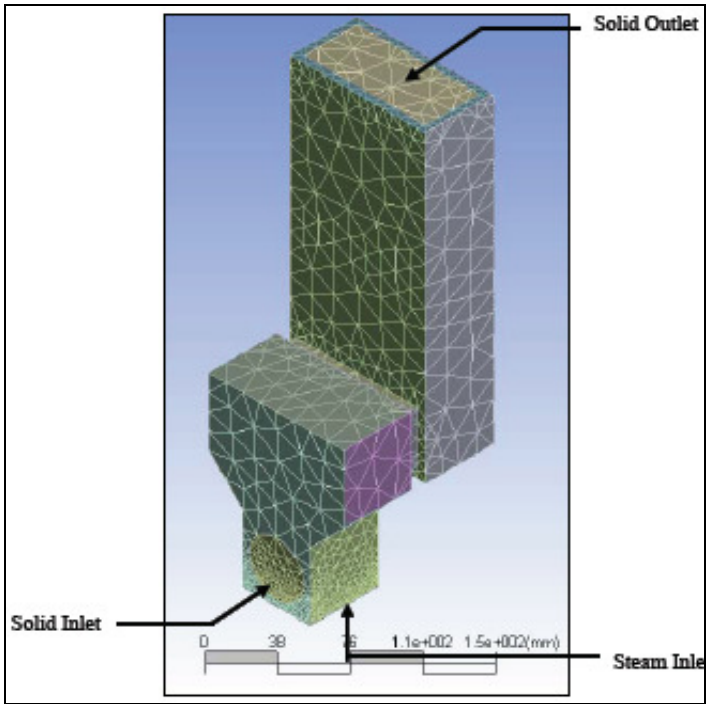

Figure B.2: Geometry of design 2 for CFBG internal parts

Figure B.3 and Figure B.4 shows the steam velocity streamlines for Design 1 and Design 2 respectively. From Figure B.3, it can be observed that uneven distribution of steam occurred in v-valve of Design 1. Same flowrate as in Design 2 is used in steam inlet 1, but the result shows that the steam tends to aggregate in one area, which is near to the solids inlet before it flows through the opening. This may be due to the pressure exerted by steam inlet 2. This can be confirmed in comparing the steam flow in Design 2 (Figure B.4) where the steam flow rate is same as in Design 1, at steam inlet 1.

Solids would not be transferred wholly to the riser if this phenomenon prevails. Steam flowing through inlet 2 also exhibits an unusual pattern. The additional steam flow at steam inlet 2 doesn't aid smooth transportation of solid from v-valve to the riser and it can be seen from Figure B.3 that it hinders the transfer process, due to the bypass of steam through the walls of the v-valve with less interaction with solids. Very low velocities observed throughout the riser section is a clear indication of the fact that the

secondary air through inlet 2 restricts the flow of steam at inlet 1, hindering the transport of solids from v-valve to the riser.

Figure B.4 shows even distribution of steam for Design 2. High velocity region seen at steam inlet may be due the mixing between solids and steam, leading to turbulence and higher velocity. A desired steam flow pattern is observed in Design 2 with smooth flow of steam covering the entire cross section of the v-valve as well as riser.

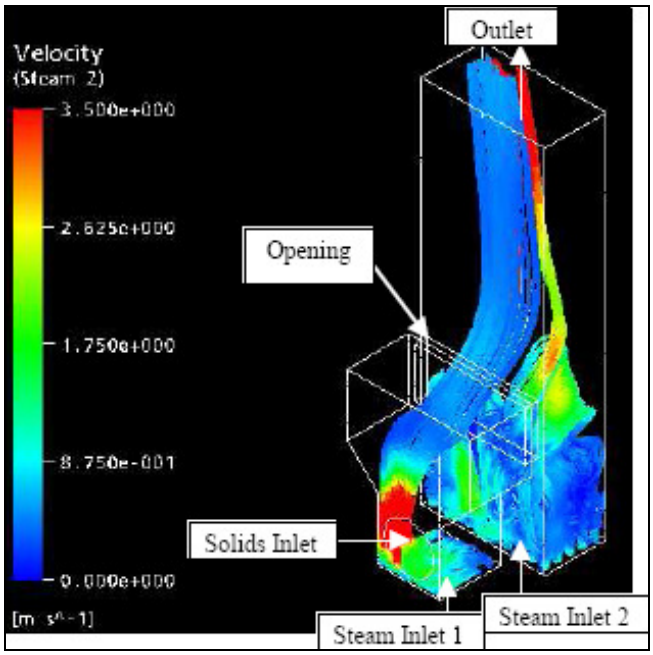

Figure B.3: Steam velocity streamlines for design 1

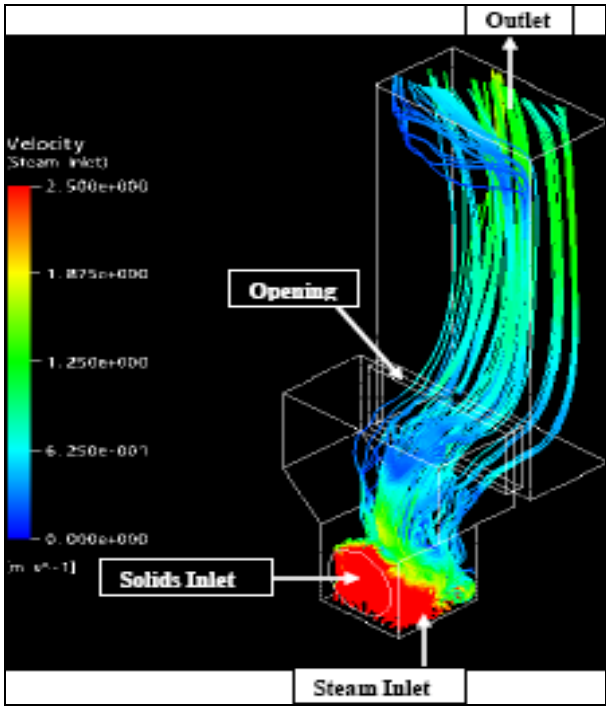

Figure B.4: Steam velocity streamlines for design 1

Figure B.5 and Figure B.6 shows the sand velocity vectors for Design 1 and Design 2. It can be seen that not all sand directly flows into riser through the opening; some of them will knock on the 'roof' or wall of v-valve before entering the riser. As a result, part of the energy carried by sand is loss due to collisions.

One can observe that the solids in Design 1 are leaking out from steam inlet 1 due to low pressure at that region, which validates the possibility of leakage. However this phenomenon maybe subsided when main bed aeration is initiated, thus full operation of CFBG should be modeled to study this behavior.

It can be seen from Figure B.5 that sand accumulations are likely to occur at the lower part of riser. Sand accumulation is not desirable, as it will disturb the solid circulation system and heat transfer between two compartments. However, from Figure B.6, there is no solid leakage from steam inlet and the solids can be transported without the need of secondary steam at inlet 2.

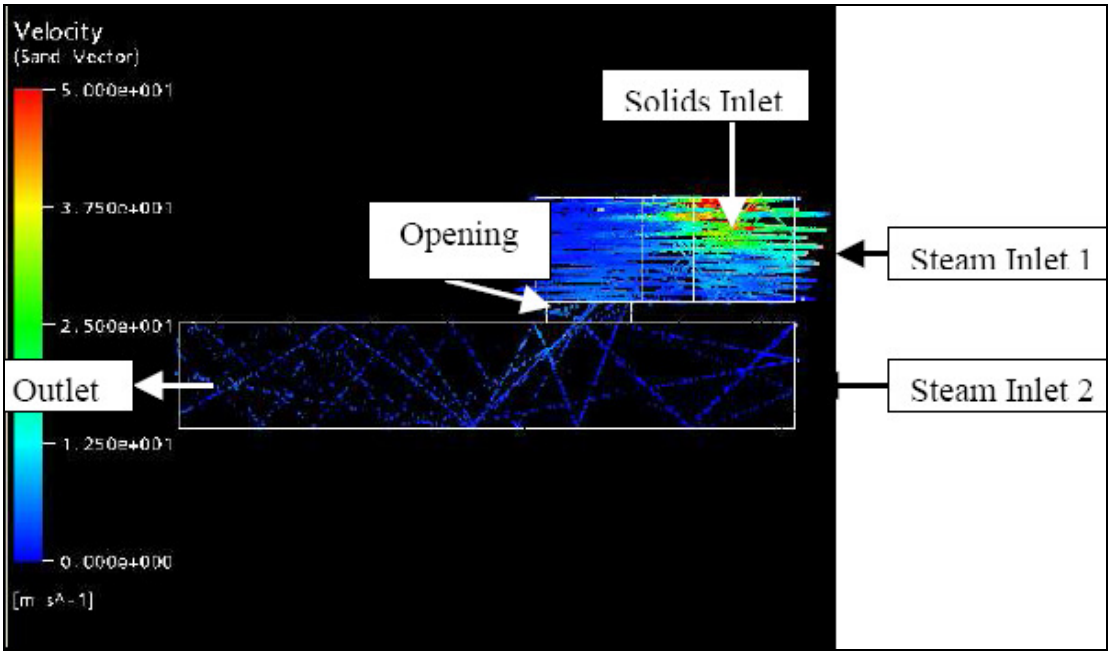

Figure B.5: Sand velocity vector for design 1

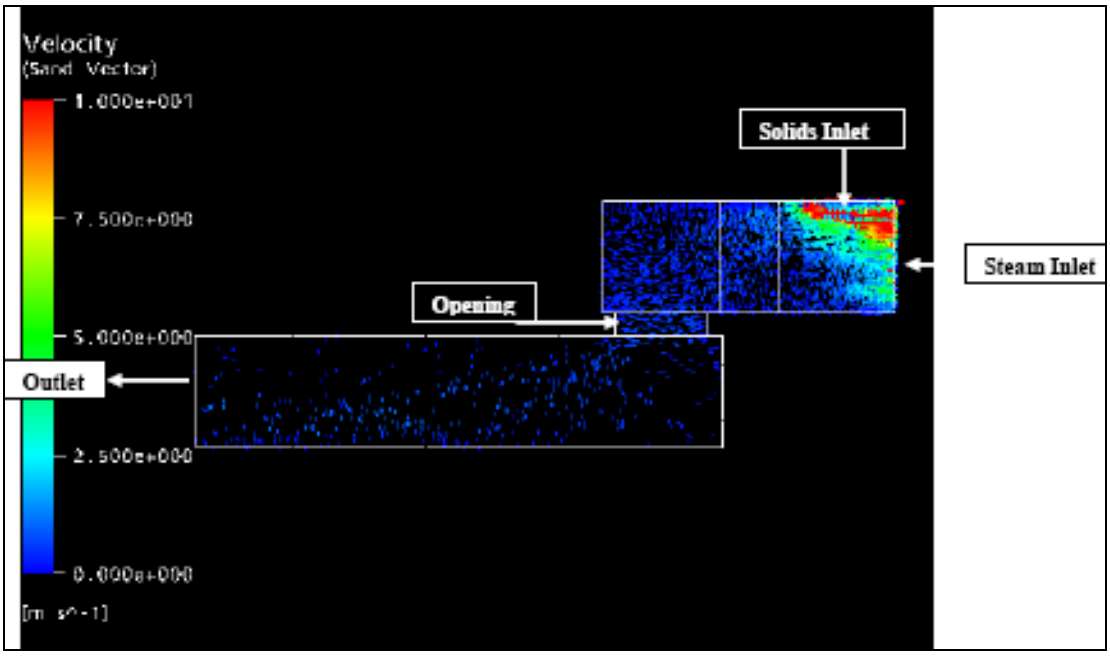

Figure B.6: Sand velocity vector for design 2

On the other hand, it can be observed that from Figure B.7 that the vortex of sand exists in v-valve. Sand vortices will induce longer sand mean residence times in v-valve and thus the contact time between the sand and steam will be longer. With longer contact time, more heat will be transferred from hot sand to the steam.

This phenomenon will lead to heat loss to the steam, which flows out from the riser will not have chance to transfer heat to the bed because the riser outlet is located above the bed height. In addition, sand vortex will provoke more rapid inter-particle collisions. Inter-particle collision is also one of the factors that will lead to heat loss.

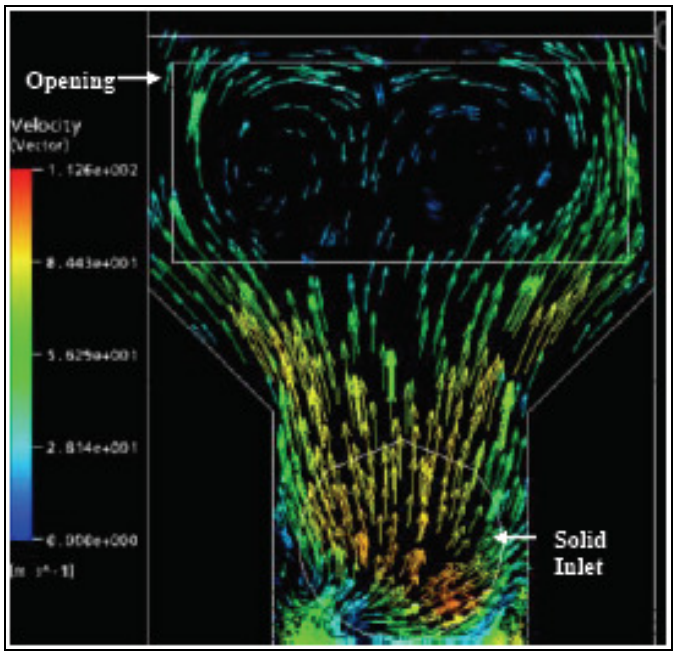

Figure B.7: Sand velocity vectors in v-valve

APPENDIX C PRELIMINARY NUMERICAL SIMULATION OF SINGLE COMPONENT AND BINARY MIXTURE SYSTEM IN CFBG

Figure C.1, C.2 and C.3 show the solids fraction contours at the gasifier at various superficial velocities applied on different drag model systems. For Syamlal O'Brien (1994) system, the numerical U_{mf} is determined to be 0.14 m/s by using bed expansion study. The bed height increases until it levels off at a steady-state bed height, as shown in Figure 3.

Static bed height (H_0) of 0.3m is determined at 0.10 m/s for Syamlal O'Brien (1994) system. With increasing gas superficial velocity, the initial bed height increases, with 4% and 11% relative increment at 0.14 m/s and 0.18 m/s gas flow respectively. Solid volume fractions of Wen and Yu system and Gidaspow system are as shown in Figure C.2 and C.3. Both systems are fluidized at 0.10 m/s, with significant bed height expansion at increasing flow velocity. Significant reduction in solid volume fraction can be observed in contours of various gas velocity models. The chaotic transient generation of bubble formation can be seen at higher velocity.

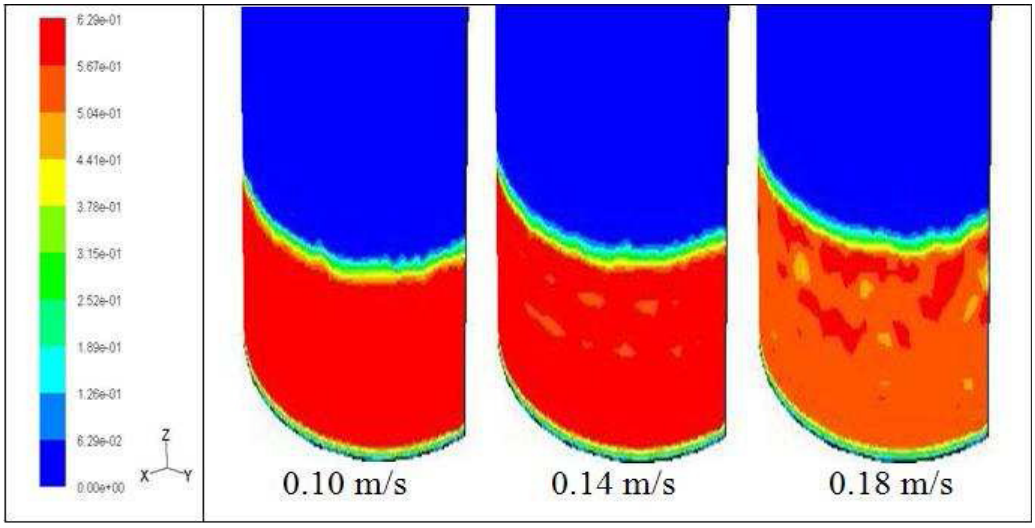

Figure C.1: Simulated single component Syamlal O'Brien model solids volume fraction profile at 3.0s (U =0.10- 0.18m/s)

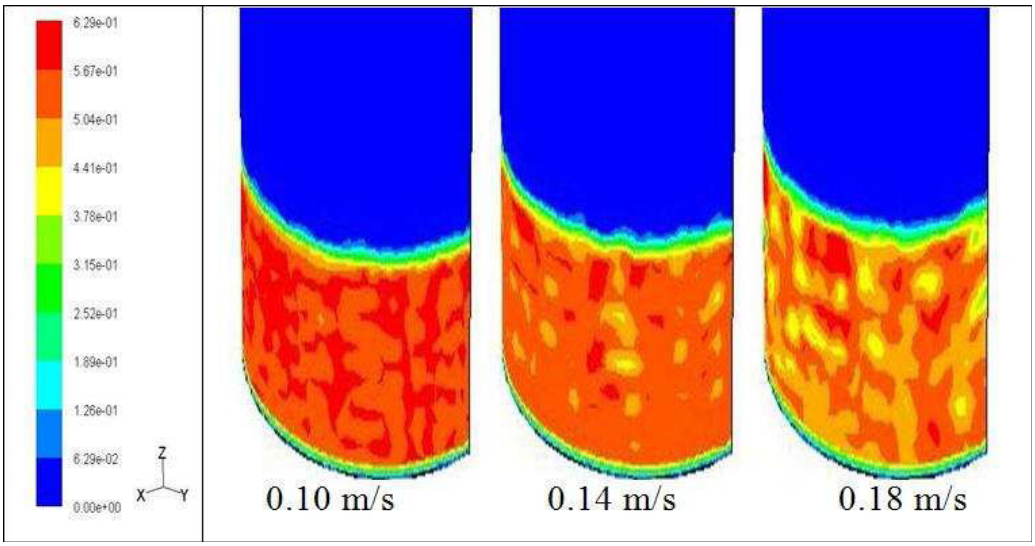

Figure C.2: Simulated single component Wen and Yu model solids volume fraction profile at 3.0s (U =0.10- 0.18m/s)

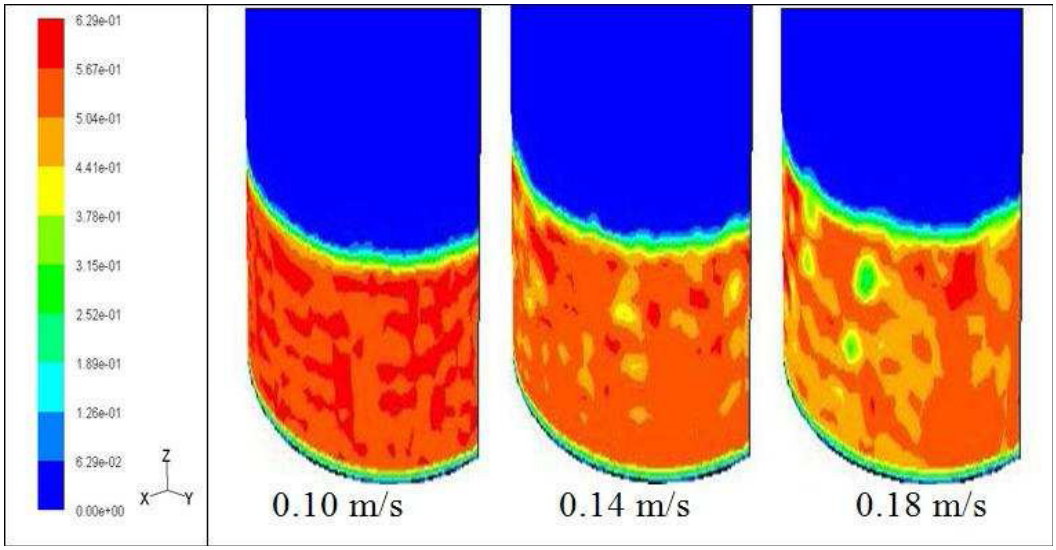

Figure C.3: Simulated single component Gidaspow model solids volume fraction profile at 3.0s (U =0.10- 0.18m/s)

Figure C.4 and C.5 show the palm shell fraction contour at the gasifier at various palm shell volume percentage mixed with sand. More homogeneous palm shell distribution is observed with higher palm shell volume percentage.

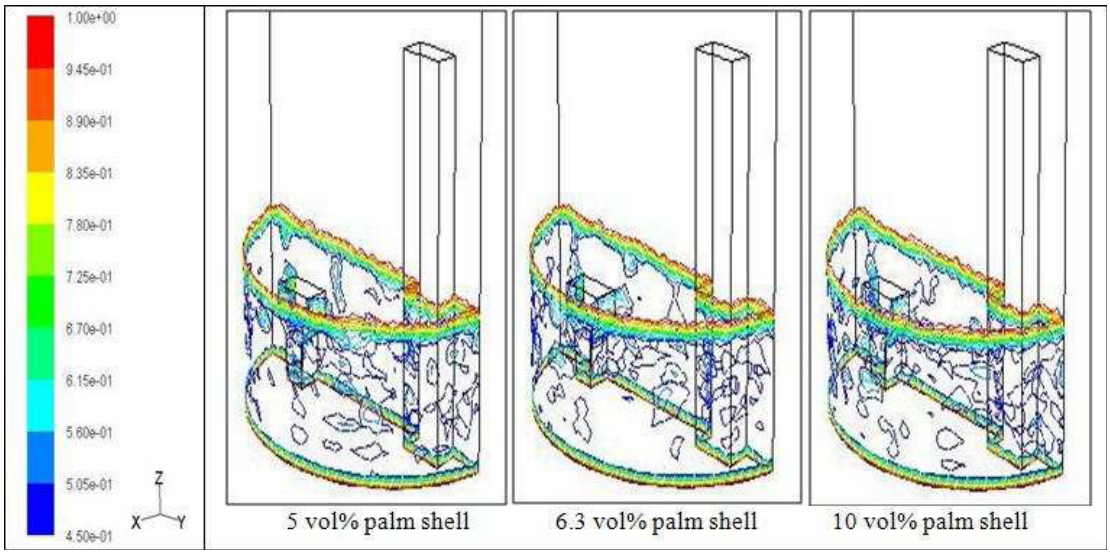

Figure C.4: Simulated bubble distribution profile in binary mixtures system at 5.0s (3D front view, 5, 6.3, 10 vol%, U =0.16 m/s)

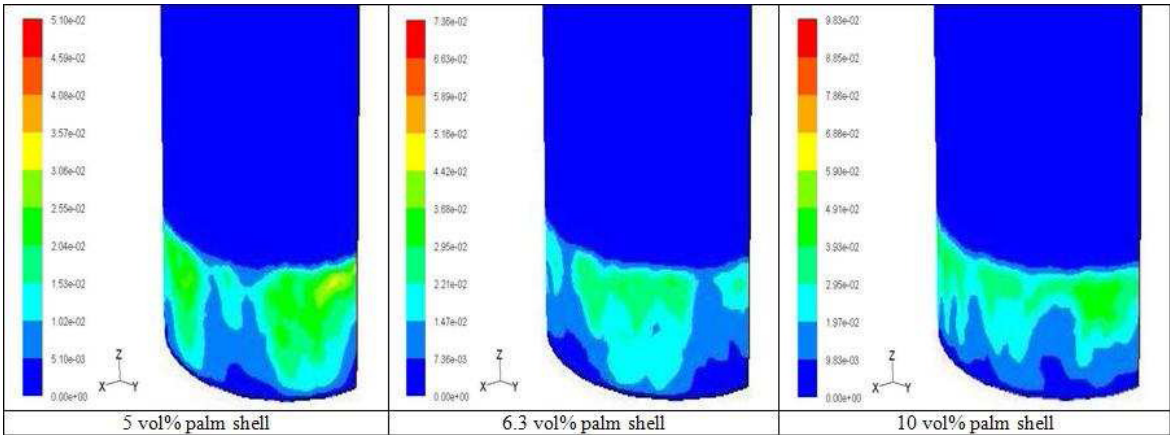

Figure C.5: Simulated palm shell distribution profile in binary mixture system at 5.0s (5, 6.3, 10 vol%, U = 0.16 m/s)